Government of **Western Australia**
Department of **Mines and Petroleum**

RECORD 2009/10

INTERPRETED BEDROCK GEOLOGY OF THE SOUTH YILGARN AND CENTRAL ALBANY-FRASER OROGEN, WESTERN AUSTRALIA

by
CV Spaggiari, S Bodorkos, M Barquero-Molina, IM Tyler, and MTD Wingate

Geological Survey of Western Australia

Government of Western Australia
Department of Mines and Petroleum

Record 2009/10

INTERPRETED BEDROCK GEOLOGY OF THE SOUTH YILGARN AND CENTRAL ALBANY–FRASER OROGEN, WESTERN AUSTRALIA

by
CV Spaggiari, S Bodorkos, M Barquero-Molina[1], IM Tyler, and MTD Wingate

[1] University of Texas, Austin, USA

Geological Survey of Western Australia

MINISTER FOR MINES AND PETROLEUM
Hon. Norman Moore MLC

DIRECTOR GENERAL, DEPARTMENT OF MINES AND PETROLEUM
Richard Sellers

EXECUTIVE DIRECTOR, GEOLOGICAL SURVEY OF WESTERN AUSTRALIA
Tim Griffin

REFERENCE
The recommended reference for this publication is:
Spaggiari, CV, Bodorkos, S, Barquero-Molina, M, Tyler, IM and Wingate, MTD 2009, Interpreted bedrock geology of the South Yilgarn and central Albany–Fraser Orogen, Western Australia: Geological Survey of Western Australia, Record 2009/10, 84p.

National Library of Australia Card Number and ISBN 978-1-74168-156-7 (PDF)

Grid references in this publication refer to the Geocentric Datum of Australia 1994 (GDA94). Locations mentioned in the text are referenced using Map Grid Australia (MGA) coordinates, Zones 50 and 51. All locations are quoted to at least the nearest 100 m.

Published 2009 by Geological Survey of Western Australia
This Record is published in digital format (PDF) and is available online at www.dmp.wa.gov.au/GSWApublications.
Laser-printed copies can be ordered from the Information Centre for the cost of printing and binding.

Further details of geological publications and maps produced by the Geological Survey of Western Australia are available from:
Information Centre
Department of Mines and Petroleum
100 Plain Street
EAST PERTH, WESTERN AUSTRALIA 6004
Telephone: +61 8 9222 3459 Facsimile: +61 8 9222 3444
www.dmp.wa.gov.au/GSWApublications

Contents

Appendix

Figures

Tables

Interpreted bedrock geology of the South Yilgarn and central Albany–Fraser Orogen, Western Australia

by

CV Spaggiari, S Bodorkos, M Barquero-Molina[1], IM Tyler, and MTD Wingate

Abstract

This Record is to accompany the interpreted bedrock geology map of the southern Yilgarn Craton and central Albany–Fraser Orogen region published in the geological exploration package, Geological Survey of Western Australia (2007), and reviews the geology of this region. It includes new geochronological results and structural observations, and discusses alterations made to previously published maps. Modifications to some tectonic boundaries and tectonic unit subdivisions have implications for understanding the crustal architecture and tectonic development of the southern margin of Western Australia. Understanding these features contributes to our understanding of the existing mineral deposits, and aids mineral exploration in this predominantly greenfields region.

The Albany–Fraser Orogen is here divided into a foreland component (the Northern Foreland) and a basement component, which is defined as the disparate crustal fragments affected by, and probably amalgamated by, c. 1345–1260 Ma Stage I tectonism (the Kepa Kurl Booya Province). The Albany–Fraser Orogen also includes the Recherche and Esperance Supersuites (formerly Recherche Granite and Esperance Granite), and various Mesoproterozoic cover rocks. The Kepa Kurl Booya Province is further divided into the Biranup Zone, the Fraser Zone (formerly the Fraser Complex), and the Nornalup Zone (formerly the Nornalup Complex).

The Munglinup Gneiss is reassessed as a reworked component of the southern Yilgarn Craton and is therefore included in the Northern Foreland. This is based on new and previously published geochronology that indicate it is dominated by granites of the same age as those within the Yilgarn Craton (c. 2660 Ma), the presence of remnants of greenstones, and a gradational strain and metamorphic boundary into the gneiss in the western-central Albany–Fraser Orogen. Within the Kepa Kurl Booya Province, the Biranup Zone is interpreted as an exotic terrane that is dominated by components with protoliths that formed between 1690–1660 Ma, their reworked counterparts (generally gneissic rocks), and Mesoproterozoic intrusions into these rocks. Specifically, this includes the Dalyup and Coramup Gneisses, but not the c. 1300 Ma Fraser Zone. The Fraser Zone is dominated by metamafic rocks and includes metagranitic and metasedimentary rocks that are here collectively named the Fraser Range Metamorphics.

The Biranup Zone is a significant remnant of middle crust at least 800 km long that is interpreted to have accreted onto the southern margin of the Yilgarn Craton during Stage I of the Albany–Fraser Orogeny, as there is no evidence of a c. 1690–1660 Ma event along this margin. Potential links between the Biranup Zone and the Fraser Range Metamorphics suggest formation of a magmatic island arc adjacent to the Biranup Zone between c. 1310–1300 Ma during convergence, prior to final collision of the West Australian Craton (southern Yilgarn Craton margin) and the Mawson Craton. The origin of the Biranup Zone is unknown, but possible correlatives occur within the western Gawler Craton (e.g. the Tunkillia Suite) and the southwestern Arunta Orogen (Warumpi Province).

KEYWORDS: Albany–Fraser Orogen, tectonic units, geochronology, interpreted bedrock geology, aeromagnetic data

---

[1] University of Texas, Austin, USA

Introduction

The South Yilgarn Geological Exploration Package, Geological Survey of Western Australia (GSWA) Record 2007/13, includes an interpreted bedrock geology (IBG) map suitable for printing at scales between 1:250 000 and 1:500 000 covering NEWDEGATE*, BREMER BAY, RAVENSTHORPE, HYDEN, LAKE JOHNSTON, ESPERANCE, and NORSEMAN (Figs 1 and 2). The map updates the Geological Survey of Western Australia 1:500 000 scale state map dataset and is largely based on recently acquired aeromagnetic data, its interpretation, and previous mapping. The IBG map omits Cenozoic cover sequences, such as the Plantagenet Group, in favour of the interpreted underlying units. This Record complements and documents this map. Its primary purpose is to provide a review of the geology of the Albany–Fraser Orogen, and that part of the southern Yilgarn Craton affected by it. This Record also presents new geochronological results and structural observations, and outlines and discusses changes made to previous maps (e.g. Myers, 1989; Myers, 1995a,b; Myers and Hocking, 1998). This includes some modifications to tectonic boundaries and tectonic subdivisions, and has implications for the understanding of the tectonic development of the southern margin of Western Australia. Understanding the nature of the tectonic units and their boundaries is important for exploration models, as has become apparent with the recently discovered gold province that extends for at least 250 km along the southeastern margin of the Yilgarn Craton and includes the 4.05 Moz Tropicana–Havana deposit (Doyle et al., 2008).

* Capitalized names refer to standard 1:250 000 map sheets unless otherwise indicated.

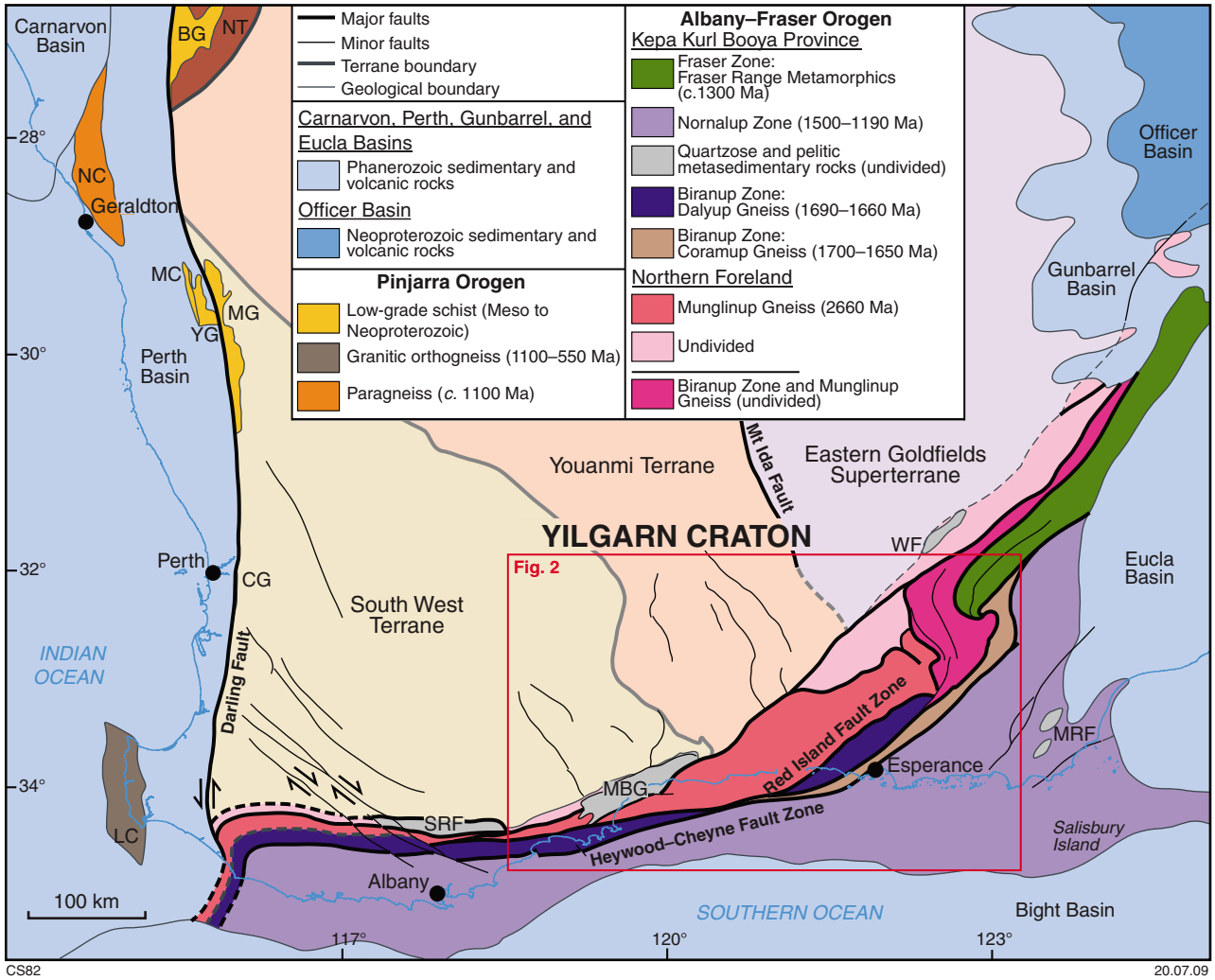

Figure 1. Geological map of southwestern Australia adapted from Geological Survey of Western Australia (2007), Tyler and Hocking (2001), and Fitzsimons and Buchan (2005). BG, Badgeradda Group; CG, Cardup Group; LC, Leeuwin Complex; MBG, Mount Barren Group; MC, Mullingarra Complex; MG, Moora Group; MRF, Mount Ragged Formation; NC, Northampton Complex; NT, Narryer Terrane; SRF, Stirling Range Formation; WF, Woodline Formation; YG, Yandanooka Group. The red box denotes the location of Figure 2.

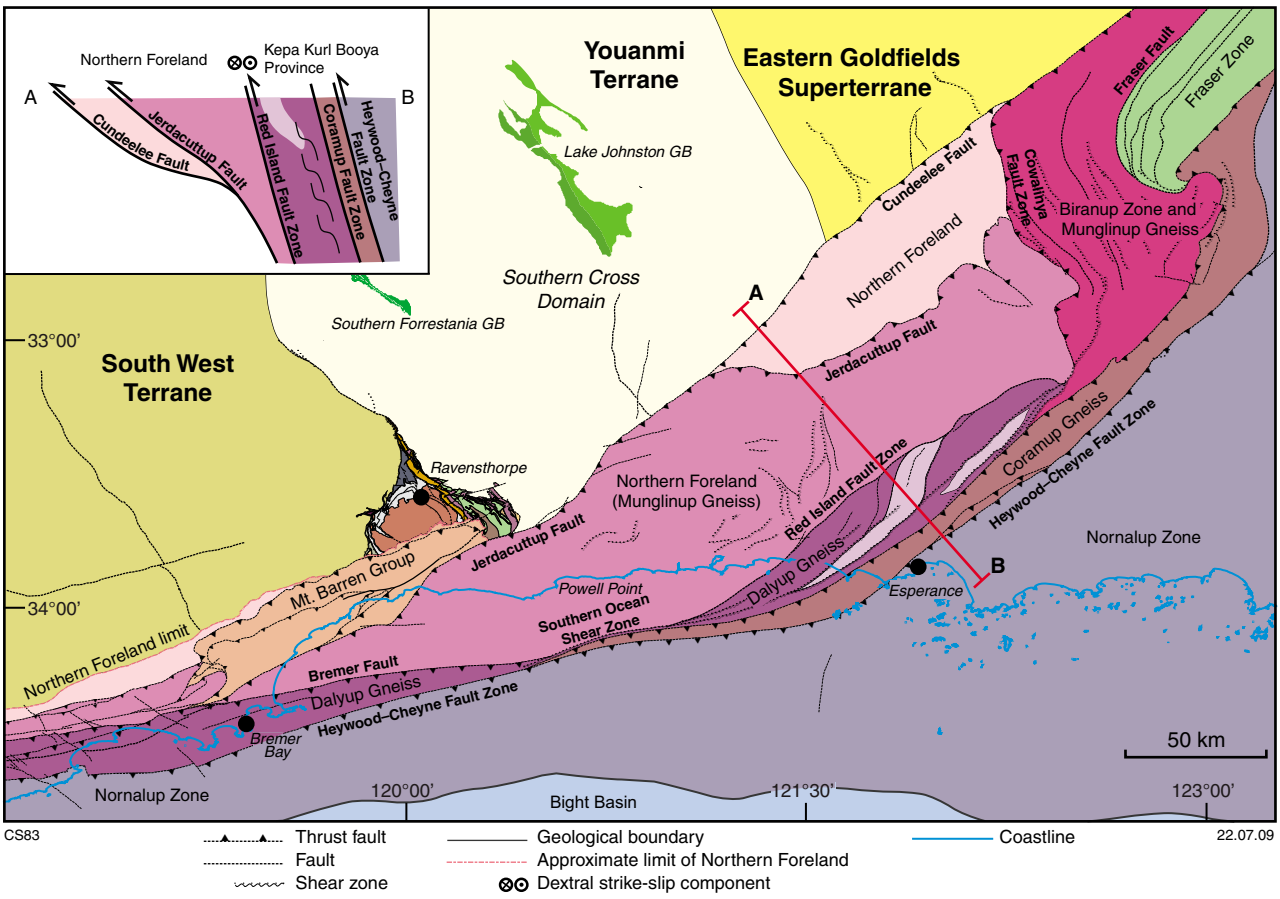

Figure 2. Simplified geological map of the Albany–Fraser Orogen and southern Yilgarn Craton extracted from the interpreted bedrock geology map (Geological Survey of Western Australia, 2007).

Methodology used to create the interpreted bedrock geology map

The IBG map was compiled in a GIS environment (ArcMap) to provide maximum spatial accuracy, and to facilitate the use of numerous datasets as layers. This allows interpretations of specific features to be made by directly comparing information from each dataset at specific locations, which not only improves the interpretation of individual features themselves, but also enhances our understanding of their signatures in each dataset.

Datasets and data sources — purpose and limitations

The datasets used in the compilation include:

- aeromagnetic data flown at 400 m line spacing or greater (government surveys);
- aeromagnetic data flown at less than 400 m line spacing (registered company surveys);
- radiometric data flown at 400 m line spacing, shown as ternary images where red = potassium, green = thorium, blue = uranium, black = none of these present, white = all of these present;
- gravity data (predominantly 11 × 11 km station grid government survey data);
- Landsat TM, mostly as RGB images with band combinations of 7:4:1 and 7:5:4;
- GSWA 1:100 000 Geological Series map sheets (where available);
- GSWA 1:250 000 Geological Series map sheets;
- GSWA 1:1 000 000 Geological Series map sheets;
- 2006 and 2007 fieldwork;
- U–Th–Pb Secondary Ionization Mass Spectrometry (SIMS) zircon geochronology undertaken on a Sensitive High Resolution Ionization Mass Spectrometer (SHRIMP)

Aeromagnetic data used for the images were reduced to pole to correct the positions of the anomalies. These data were then used to create the first vertical derivative images. First vertical derivative images were primarily used to trace the locations of geological features and aeromagnetic trendlines as close to the surface as possible. Structures such as folds and faults were interpreted from the aeromagnetic images by tracing out the aeromagnetic trendlines, and identifying truncations and discontinuities in them. Locations of major faults and geological boundaries were also interpreted from observations of major changes in magnetic character, particularly where they are sharp, and demagnetized zones. Most of the trendlines follow magnetic highs, but include some

linear lows. It should be noted that although the map is intended as a surface solid geology map, some of the geological features observed in the aeromagnetic images are subsurface (within bedrock), particularly where weathering or Cenozoic cover conceals their magnetic signature at or near the surface. Furthermore, if they represent features that dip, such as faults, then they may outcrop at a slightly different location to where the subsurface anomaly is located on the 2D image, that is, where the dipping magnetic feature would intersect the surface through the cover. Fold closures interpreted from the trendlines are limited to large-scale folds because the 400 m line spacing data provides a maximum of 80 to 100 m ground resolution. In cases where greater resolution data was available, for example, 200-m line spacing data, a maximum of 50 to 70 m ground resolution can be interpreted. Mafic dykes, where recognizable as such, have been mapped as a separate layer. It follows that some of the mafic dykes interpreted from the aeromagnetic images are under cover and may also be subsurface intrusions, i.e., not just covered by regolith.

Faults on the map are divided by type, where known, and as major or minor faults (denoted by line thickness). Major faults are defined as having greater length and more displacement than minor faults. For example, minor faults tend to have strike lengths on the order of 10s of kilometres (maximum about 50 km) and displacements of metre-scale up to a few kilometres, whereas major faults tend to have strike lengths on the order of 100s of kilometres and displacements greater than a few kilometres. Where magnetic anomalies are offset, the displacement direction (dextral or sinistral) is shown — this is apparent direction only (i.e. interpreted from 2D imagery) and should not be assumed to be strike-slip offset. Faults shown as interpreted are commonly under cover, but this is not always the case because the aeromagnetic images can sometimes show faults that are not obvious through outcrop. Many of the faults on the map are associated with magnetic lows, and in the southern Yilgarn Craton these commonly coincide with major quartz veins or large fractures, particularly through granites.

Remotely sensed surface datasets such as Landsat and radiometrics provide a means to interpret lithological contacts and, in conjunction with the geological maps, to determine lithologies. Because the surface datasets are georeferenced they also allow lithological contacts to be drawn with greater spatial accuracy than most of the geological maps because the mapping was done before the availability of orthophotography and, in the case of the GSWA 1:250 000 maps, before the availability of GPS. Ternary radiometric images have provided some information about differences in granitic rocks, particularly in the southern part of NEWDEGATE and northern part of BREMER BAY. However, because most of the project area is within the southern wheatbelt of Western Australia, and outcrop is sparse, the remotely sensed surface datasets have been of minimal use to this project.

The compilation of the IBG map was greatly facilitated by the GSWA 1:1 000 000 Geological Series maps (ALBANY and ESPERANCE), 1:250 000 Geological Series maps (NEWDEGATE, BREMER BAY, RAVENSTHORPE, HYDEN, LAKE JOHNSTON, ESPERANCE, and NORSEMAN), and 1:100 000 Geological Series maps (NORSEMAN, RAVENSTHORPE, and COCANARUP; including 1:100 000 maps in preparation on NORSEMAN). This mostly required simplifying and grouping of units suitable for the scale of the IBG map, and the original maps, in particular the 1:100 000 maps, should be used where more detailed information is required.

The geochronological study was undertaken following procedures described by Wingate et al. (2008a). Dates quoted in this Record are $^{207}Pb/^{206}Pb$ ages (corrected for common Pb using the ^{204}Pb-correction method; see Wingate et al. (2008a) for details) and were determined using the U–Th–Pb SIMS (SHRIMP) method on zircon crystals unless otherwise specified. The associated uncertainties are quoted at the 95% confidence level unless otherwise indicated. For further details about individual samples references to the individual reports are given in the text.

South Yilgarn Craton

This section provides a brief overview of the geology of the southern part of the Yilgarn Craton that is largely unaffected by the Proterozoic Albany–Fraser Orogeny, focusing on rocks within the project area. Rocks of the Yilgarn Craton that are clearly deformed and metamorphosed during the Albany–Fraser Orogeny make up the Northern Foreland (Figs 1 and 2; after Beeson et al., 1988; Myers, 1990a), which is discussed below in the Albany–Fraser Orogen section. The Albany–Fraser Orogen intersects several terranes of the Yilgarn Craton; the South West Terrane, the Southern Cross Domain of the Youanmi Terrane, and the Kalgoorlie, Kurnalpi, and Burtville Terranes of the Eastern Goldfields Superterrane (Figs 1 and 2). Deformation and metamorphism has largely obscured terrane boundary structures within the Northern Foreland, making them difficult to recognize. In addition, the amount of displacement on bounding thrust and strike-slip faults of the Albany–Fraser Orogen (e.g. Jerdacuttup Fault, Cundeelee Fault), is unknown. The terrane boundaries have also been partially obscured by Late Archean granitic magmatism.

The South West Terrane has been retained as a distinct terrane in the current scheme of Cassidy et al. (2006), but those authors state that additional work is required to characterize its components and define its boundary with the Youanmi Terrane. The South West Terrane is dominated by high-grade granitic gneisses, metasedimentary rocks, and meta-igneous rocks that were intruded by granite and pegmatite between 2.75 – 2.62 Ga, with the majority post-dating 2.69 Ga (Myers, 1993; Wilde et al., 1996; Nemchin and Pidgeon, 1997). Supracrustal sequences that range in age from 3.2 – 2.8 Ga are found in the Chittering, Jimperding, and Balingup metamorphic belts (Wilde et al., 1996). The Jimperding metamorphic belt is significant because it contains quartzite with a range of relatively old detrital zircons between 3.73 – 3.00 Ga (Wilde et al., 1996; Wilde, 2001; Wingate et al., 2008b). The main greenstone sequence in the western part of the terrane is the low-grade c. 2.72 – 2.67 Ga Saddleback Greenstone Belt near

Boddington (Wilde et al., 1996). There are several other exposures of undivided greenstones that mainly present as metamorphosed slivers within metagranitic rocks. Greenstone belts located within the project area are the Gibb Rock, Hyden (replaces East Hyden and South Hyden), Kalgarin, Mount Vernon, and Powder Puff Hill Greenstone Belts (see Chin et al., 1984 for descriptions). The Kalgarin, Mount Vernon, Hyden, and Powder Puff Hill Greenstone Belts are dominated by mafic granulite, and the latter two also contain minor metamorphosed iron formation. The Gibb Rock Greenstone Belt is dominated by mafic volcanic rocks and also includes metamorphosed iron formation.

The southern part of the Southern Cross Domain of the Youanmi Terrane comprises a mixture of moderately to strongly deformed Archean granitic gneisses, granodiorite and monzogranite, and generally less deformed younger plutons of low-Ca monzogranite. There are four major greenstone belts; the Forrestania Greenstone Belt, the Lake Johnston Greenstone Belt, and the Carlingup and Cocanarup Greenstone Belts of the Ravensthorpe area (Fig. 2; and described below). Both the southern part of the Southern Cross Domain and the South West Terrane have been intruded by mafic dykes of the Widgiemooltha, Gnowangerup–Fraser, Nindibillup, and Beenong Dyke Suites (see **Mafic dyke suites** below).

Forrestania Greenstone Belt

The Forrestania Greenstone Belt is situated north of Ravensthorpe, within the Southern Cross Domain of the Youanmi Terrane, and has been a locus for Ni–Cu sulfide exploration. The structure of the belt is dominated by a gently north plunging syncline, except in the south where the belt narrows and curves to a northwesterly trend, and aeromagnetic data indicate it is extensively sheared (Chin et al., 1984; Perring et al.,1995; Geological Survey of Western Australia, 2007). The syncline is interpreted to have formed during the first phase of deformation under amphibolite facies conditions (Chin et al., 1984). An axial planar cleavage that formed during this event is overprinted by a crenulation cleavage, which is interpreted to have formed during a second phase of deformation, accompanied by retrograde metamorphism (Chin et al., 1984).

The belt comprises a lower, 3–5 km thick succession of metamorphosed dominantly volcanic mafic and ultramafic rocks, interlayered with metamorphosed banded iron-formation and chert, overlain by an upper, 3–5 km thick succession of pelitic and psammitic schists (Chin et al., 1984; Perring et al., 1995). The lower succession contains at least four komatiite sequences with both Al-undepleted and Al-depleted komatiites (Perring et al., 1996). Detailed physical volcanology descriptions and geochemical analyses of the komatiite sequences are given in Perring et al. (1995) and Perring et al. (1996), respectively. Although an age of 2.9 Ga for the greenstones is reported in Perring et al. (1996), there does not seem to be any published geochronological data. The Forrestania Greenstone Belt is cut by mafic dykes of the four suites described below (see **Mafic dyke suites**), the oldest being the c. 2420 Ma Widgiemooltha Dyke Suite.

Lake Johnston Greenstone Belt

The Lake Johnston Greenstone Belt has a northwesterly trend and is situated approximately 100 km east of the Forrestania Greenstone Belt, within the Southern Cross Domain of the Youanmi Terrane. It comprises what were previously known as the Maggie Hays, Lake Hope, and East Tamar Greenstone Belts (Griffin, 1990). The belt is poorly exposed and its largest deposit, the Maggie Hays nickel sulfide prospect, has virtually no surface expression and was discovered 100–180 m below the surface (Clayton et al., 2005). Much of the western margin of the belt is bound by the Tay Fault, a major fault that extends through granitic rocks south of the belt that is truncated by the Mesoproterozoic Jerdacuttup Fault. Part of the eastern margin of the belt is bound by the northeast-dipping Koolyanobbing Fault. The southwestern side of the belt is folded into a northwest trending syncline and anticline pair (the Burmiester syncline and the Gordon anticline), with rocks belonging to the stratigraphically lowest unit, the Maggie Hays Formation, exposed in the anticline core (Gower and Bunting, 1976; Clayton et al., 2005). The greenstones have been metamorphosed to greenschist, or locally, amphibolite facies (Gower and Bunting, 1976).

Gower and Bunting (1976) divided the belt into three formations (listed in stratigraphic order); the Maggie Hays Formation, the Honman Formation, and the Glasse Formation. This excluded isolated greenstone xenoliths in granitic rocks to the west, which lie west of the Tay Fault. The Maggie Hays Formation consists of pillowed metabasalts, metamorphosed mafic and ultramafic intrusives (including layered gabbroic rocks), and minor metasedimentary rocks including metamorphosed banded iron-formation and volcanogenic metasedimentary rocks (Gower and Bunting, 1976). The Honman Formation consists of metamorphosed banded iron-formation, clastic metasedimentary rocks, metamorphosed ultramafic rocks (including komatiite), and minor felsic metavolcanic and metavolcaniclastic rocks (Gower and Bunting, 1976; Clayton et al., 2005). The Glasse Formation consists of metamorphosed mafic volcanic rocks, and metamorphosed mafic intrusive and ultramafic rocks (Gower and Bunting, 1976).

The ages of the greenstone sequences are not well constrained and the only geochronological data are SHRIMP U–Pb analyses by Wang et al. (1996), who dated felsic metavolcanic rocks from the Honman Formation, sampled at the Maggie Hays nickel sulfide prospect. A felsic metavolcanic rock from below the komatiite layer gave an age of 2921 ± 4 Ma, interpreted to be the age of extrusion, whereas a similar rock from above the komatiite layer gave a more complex result with three age groups of 2930 ± 3 (n=11), 2903 ± 5 (n=7), and 2856 ± 8 Ma (n=2). Zircons from the older 2930 ± 3 Ma group are interpreted as inherited and the age of 2903 ± 5 Ma is interpreted as the extrusion age (Wang et al., 1996). The younger age of 2856 ± 8 Ma is interpreted as either a late metamorphic event or being due to lead loss from the 2903 ± 5 Ma group (Wang et al., 1996). The Lake Johnston Greenstone Belt is cut by the Widgiemooltha, Gnowangerup–Fraser, and Beenong Dyke Suites (see **Mafic dyke suites**), including the large Jimberlana dyke, which is part of the c. 2420 Ma Widgiemooltha Dyke Suite.

Carlingup and Cocanarup Greenstone Belts and associated rocks

Two major greenstone belts and associated rocks are present in the Ravensthorpe area, adjacent to the southeastern part of the boundary between the South West and Youanmi Terranes. These are the Carlingup (formerly Ravensthorpe Range) and Cocanarup (formerly West River) Greenstone Belts (Thom et al., 1984; Witt, 1997). Witt (1997, 1998) defined the Cocanarup and Carlingup Greenstone Belts as separate terranes, along with the Ravensthorpe Terrane, which is now named the Ravensthorpe Suite (Geological Survey of Western Australia, 2007). The terrane nomenclature was abandoned because it was used to distinguish fault-bounded rock packages with lithological and structural differences, as opposed to different crustal entities. In addition, the location of the boundary between the South West and Youanmi Terranes is ambiguous and requires further investigation (Cassidy et al., 2006). At present it is placed along the western margin of the main exposures of the Cocanarup Greenstone Belt.

The Carlingup Greenstone Belt is the easternmost belt in the Ravensthorpe area. It is bounded to the east by predominantly west-dipping thrust faults, and to the west by the west-dipping Chidnup Fault, which separates it from the Cocanarup Greenstone Belt and Ravensthorpe Suite (Witt, 1997, 1998). To the south, the Carlingup and Cocanarup Greenstone Belts and the Ravensthorpe Suite are truncated by the Mesoproterozoic Jerdacuttup Fault, and partially overlain by the Paleoproterozoic Mount Barren Group (see **Mount Barren Group**, below). To the north, the Carlingup Greenstone Belt is truncated by Archean granitic rocks and a major, northwesterly trending unnamed fault. Witt (1997, 1998) suggested that the Cocanarup Greenstone Belt and Ravensthorpe Suite were thrust eastwards over the Carlingup Greenstone Belt, followed by formation of a major south-plunging synform (Beulah synform) during the Archean. This was followed by north–south compression to produce localized shear zones and folds. These structures are cut by a series of small, east-northeasterly trending faults with predominantly dextral offset interpreted to relate to the Mesoproterozoic Jerdacuttup Fault (Witt, 1997, 1998). All rocks in the Carlingup and Cocanarup Greenstone Belts and Ravensthorpe Suite were metamorphosed between 400°C and 600°C, and at approximately 2.5 kbar (Witt, 1998).

The descriptions of the lithological units below are summarized from Witt (1997, 1998), where more detailed lithological, structural, and metamorphic geology of the Ravensthorpe area can be found. Additional information can also be found in Thom et al. (1984). The Carlingup Greenstone Belt comprises metamorphosed mafic and ultramafic rocks, metasedimentary rocks (including banded iron-formation), and minor dacitic to rhyolitic metavolcanic rocks. These are divided into the Chester Formation (base), the Bandalup Ultramafics, the Maydon Basalt, and the Hatfield Formation (top). Unassigned units include felsic metavolcanic and metavolcaniclastic rocks, polymictic metaconglomerate, and metasandstone interbedded with oligomictic metaconglomerate. The latter is possibly part of the Paleoproterozoic Mount Barren Group. Zircons from rhyolite from the unassigned felsic metavolcanics gave a SHRIMP U–Pb age of 2958 ± 4 Ma (GSWA 112163; Nelson, 1995a). The Chester Formation is at least 750 m thick and consists of pelitic and psammitic rocks interbedded with thin layers of metachert and metamorphosed banded iron-formation, and minor metapsephite and metamorphosed felsic volcanic and volcaniclastic rocks. The Bandalup Ultramafics are 1.5 km thick and comprise a sequence of metamorphosed komatiites with minor high-Mg metabasalt and metagabbro, interlayered with thin units of metamorphosed banded iron-formation. The Maydon Basalt is 2 km thick and comprises a sequence of pillowed metabasalt with minor metadolerite and rare interflow metasedimentary rocks. The basalt is siliceous and has a high Mg content. The Hatfield Formation is at least 1 km thick and comprises fine-grained clastic metasedimentary rocks, minor dacitic metamorphosed volcanic and volcaniclastic rocks, and minor coarse-grained metaclastic rocks interbedded with pelitic rocks.

The Cocanarup Greenstone Belt comprises strongly deformed, amphibolite facies metasedimentary rocks, and mafic and ultramafic rocks including spinifex-textured komatiite. The northern part of the belt contains micaceous quartzite, quartz–muscovite schist, and quartz–feldspar–biotite–andalusite schist. These are interleaved with metamorphosed ultramafic rocks, minor amphibolite and mafic gneiss. The southern part of the belt is lithologically similar to the Chester Formation in the Carlingup Greenstone Belt and contains para-amphibolite and quartz–plagioclase–mica–garnet schist. Ultramafic rocks are not as abundant as in the north.

The Ravensthorpe Suite lies between the two greenstone belts and contains the Annabelle Volcanics and the Manyutup Tonalite. They are interpreted to be co-magmatic, based on field relationships and geochemical data. The only geochronological information is a SHRIMP U–Pb zircon age of 2966 ± 12 Ma for the tonalite reported in an abstract by Savage et al. (1996). This is within error of the 2958 ± 4 Ma age of the rhyolite from the Carlingup Greenstone Belt (GSWA 112163; Nelson, 1995a). The Annabelle Volcanics are stratigraphically complex and dominated by volcaniclastic rocks associated with minor lavas that consist predominantly of metamorphosed, calc-alkaline basalt (10–20%), andesite (50–70%), and dacite (20–30%). The Manyutup Tonalite is dominated by coarse-grained, equigranular biotite–hornblende tonalite, but also varies to dioritic and granodioritic compositions. Minor phases include quartz-diorite, microtonalite, hornblendite, and anorthositic gabbro.

The Cocanarup and Carlingup Greenstone Belts and Ravensthorpe Suite are cut by numerous mafic dykes belonging to the Gnowangerup–Fraser Dyke Suite, as well as those belonging to the Nindibillup and Beenong Dyke Suites (see **Mafic dyke suites**). Dykes from all three suites are particularly numerous just east of the Carlingup Greenstone Belt.

Mafic dyke suites

Dykes drawn on the IBG map are mostly interpreted from aeromagnetic datasets, which in some cases have a relatively coarse resolution so several dykes may appear as one linear anomaly. This only becomes obvious when higher resolution datasets are available. In reality the dykes are far more numerous and often form en echelon arrays or multiple intrusions that typically utilize fractures or pre-existing structures. For this reason, it is difficult to determine crosscutting relationships between dyke suites because it is not clear whether the termination of an individual dyke is a primary magmatic feature, or an overprinting and therefore crosscutting feature. Furthermore, magnetic anomalies of dykes that overlap are additive, both horizontally and vertically, which also inhibits determining cross-cutting relationships. Nonetheless, four suites of mafic dykes can be recognized within the project area based on orientation, magnetic character, and previous studies; the Widgiemooltha, Gnowangerup–Fraser, Nindibillup, and Beenong Dyke Suites (Fig. 3). Of these, the last two have previously been described locally (e.g. Isles and Cooke, 1990; Harris and Li, 1995) but are here newly recognized as more extensive suites.

Dykes belonging to the Widgiemooltha Dyke Suite trend east to east-northeast, are mostly 10–50 m wide, but can be up to 2 km wide, and have lateral extents up to hundreds of kilometres (Sofoulis, 1966; Myers, 1990b). The Binneringie dyke and the Jimberlana Norite are the largest intrusions of this suite. In general, dykes belonging to the Widgiemooltha Dyke Suite are composed of olivine gabbro and dolerite, and include cumulate textures and granophyric differentiates (Campbell et al., 1970; Elias and Bunting, 1982). An extension of the Binneringie dyke to the west has isotope-dilution thermal ionization mass spectrometry (IDTIMS) and ion microprobe (SHRIMP) U–Pb baddeleyite ages of 2418 ± 3 Ma and 2420 ± 7 Ma, respectively (Nemchin and Pidgeon, 1998). These ages are within uncertainty of Rb–Sr and Sm–Nd isochron ages of 2411 ± 52 and 2411 ± 55 Ma, respectively, for the Celebration dyke and Jimberlana Norite (Turek 1966; Fletcher et al., 1987). The baddeleyite ages reported above are slightly older than an IDTIMS baddeleyite age of 2410 ± 2 Ma, also from the Binneringie dyke (French et al., 2002), and precise SHRIMP baddeleyite and zircon ages of 2403 and 2407 Ma from the Jimberlana Norite (Wingate et al., unpublished data). Dykes belonging to the Widgiemooltha Dyke Suite crosscut Archean structures in the Yilgarn Craton but are cut by structures formed during the Mesoproterozoic Albany–Fraser Orogeny.

The Gnowangerup–Fraser Dyke Suite is one of the largest suites and extends across the southern and southeastern parts of the Yilgarn Craton. The suite is part of the c. 1210 Ma Marnda Moorn Large Igneous Province (Wingate et al., 2005). The suite includes northeasterly trending dykes from the eastern Albany–Fraser Orogen and southeastern Yilgarn Craton informally named the Fraser dykes, which appear to be continuous with those in the central Albany–Fraser Orogen and southern Yilgarn Craton. Dykes belonging to the Gnowangerup–Fraser Dyke Suite are mostly moderately to strongly magnetic. Their trend changes from dominantly east-northeast in the west, to northeast in the east (parallel to the craton margin; Fig. 3). In aeromagnetic images the dykes are visible as multiple intrusions, with the two dominant trends overlapping each other where they meet in the central Albany–Fraser Orogen and southern Yilgarn Craton margin. East of Ravensthorpe the dykes are particularly numerous (Fig. 3). Dykes belonging to the Gnowangerup–Fraser Dyke Suite typically consist of dolerite, gabbro, and minor quartz diorite locally (Wingate et al., 2005). Two dykes from the Gnowangerup–Fraser Dyke Suite have zircon ages of 1203 ± 15 Ma and c. 1238 Ma (Evans, 1999), and three others (in the Stirling Ranges) have zircon, baddeleyite, and zirconolite ages of 1215 ± 10, 1217 ± 39, and 1218 ± 3 Ma respectively (Rasmussen and Fletcher, 2004). A northeast-trending dyke exposed in the Victory Gold Mine at Kambalda yielded a baddeleyite age of 1212 ± 10 Ma (Fraser dyke; Wingate et al., 2000). This dyke has identical paleomagnetic directions to four dykes near Ravensthorpe, supporting the interpretation that the Fraser and Gnowangerup dykes are part of the same suite (Giddings, 1976; Pisarevsky et al., 2003; Wingate et al., 2005). Aeromagnetic images demonstrate that the Gnowangerup–Fraser Dyke Suite clearly crosscuts most major structures in the northeastern Albany–Fraser Orogen. However, to the south (within the Kepa Kurl Booya Province and most of the Munglinup Gneiss) dykes from this suite are not discernable in aeromagnetic images. This is because they are strongly deformed in these areas (Fig. 4c). In the western part of Newdegate (at approximately Zone 50, MGA 670100E 6284000N) the Gnowangerup–Fraser Dykes Suite appears to be cut by northeast trending minor faults, which suggests these faults post-date 1210 Ma.

The Nindibillup Dyke Suite is a new name defining a suite of east-southeasterly trending mafic dykes (Fig. 3). These dykes vary from strongly magnetic and extensive, some up to hundreds of kilometres long, to moderately or non-magnetic varieties that are less extensive. Three types are distinguished on the IBG map. The age of this dyke suite is unknown, but it clearly crosscuts major structures of the Albany–Fraser Orogen, which suggests it post-dates Stage II (1215–1140 Ma) of the Albany–Fraser Orogeny. The Nindibillup Dyke Suite may correlate with east-southeasterly trending dykes inferred to be of early Cambrian age in the western part of the Albany–Fraser Orogen based on paleomagnetic data (Harris and Li, 1995), but these dykes have not been directly dated. The composition of dykes belonging to the Nindibillup Dyke Suite is largely unknown, however exposures of east-southeast trending mafic dykes cutting granitic gneiss (Munglinup Gneiss) on the coast west of Quagi Beach contain a substantial portion of secondary amphibole (Fig. 4e,f). These dykes are undeformed but locally contain leucosomes and show back-veining that cuts the dykes and their granitic gneiss host, indicating intrusion conditions were hot. This suggests they may have formed during the late stages of Stage II of the Albany–Fraser Orogeny, perhaps between 1160–1140 Ma, after deformation along major structures that are cut by the dykes.

The Beenong Dyke Suite is a new name given to northwesterly trending dykes in the region (Fig. 3). These

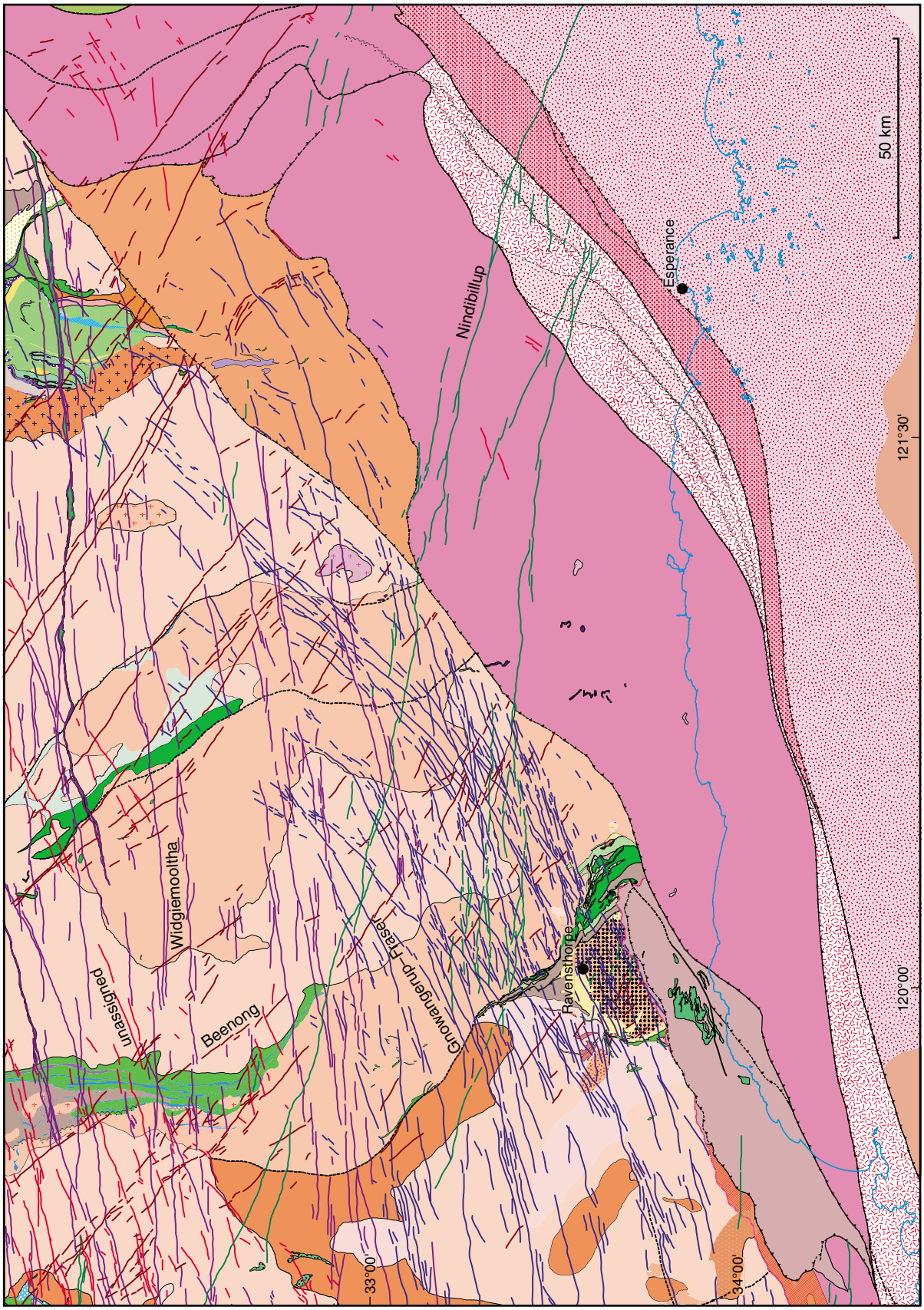

Figure 3. **Extract from the interpreted bedrock geology map (Geological Survey of Western Australia, 2007) showing major faults and the four mafic dyke suites. A representative from each suite is named. ENE-trending purple lines, Widgiemooltha Dyke Suite; NNE- to ENE-trending dark blue lines, Gnowangerup–Fraser Dyke Suite; ESE-trending green lines, Nindibillup Dyke Suite; SE-trending brown lines, Beenong Dyke Suite; red lines, undivided dykes. See Geological Survey of Western Australia (2007) for attribution of the units, which are too numerous to show here.**

dykes are mostly moderately magnetic and tend to be of relatively short length, especially compared to dykes of the Nindibillup Dyke Suite. Their age is unknown but they clearly crosscut structures in the Albany–Fraser Orogen. Their composition is also unknown. Although these dykes have the same trend as the c. 1210 Ma Boyagin dykes, which are part of the Marnda Moorn Large Igneous Province (Wingate et al., 2005), they are probably younger as they crosscut younger structures in the Kepa Kurl Booya Province near Bremer Bay.

Albany–Fraser Orogen

The southern and southeastern margins of the Yilgarn Craton were reworked during the Mesoproterozoic Albany–Fraser Orogeny, which took place in two stages; c. 1345–1260 Ma (Stage I) and c. 1215–1140 Ma (Stage II; Clark et al., 2000; Bodorkos and Clark, 2004a). Stage I of the orogeny is widely assumed to have been caused by the collision of the combined West Australian and North Australian Cratons and the Mawson Craton, whereas Stage II is interpreted to represent intracratonic reworking (e.g. Myers et al., 1996; Clark et al., 2000). Only part of the Albany–Fraser Orogen is exposed in Western Australia, and it is interpreted to be part of the larger, Australo–Antarctic Albany–Fraser–Wilkes Orogen that was linked prior to the breakup of Gondwana (Fig. 5; Fitzsimons, 2003). The Wilkes Land coast in East Antarctica is part of East Gondwana and has outcrops of ortho- and paragneisses that have similarities to the Nornalup and Biranup Zones of the Kepa Kurl Booya Province of the Albany–Fraser Orogen (Fitzsimons, 2003, and references therein). To the west, the Albany–Fraser Orogen is truncated by the late Meso- to Neoproterozoic Darling Fault Zone and Pinjarra Orogen. To the northeast, it is potentially contiguous with the Musgrave Complex (Myers et al., 1996).

Much of the eastern part of the Albany–Fraser Orogen in Western Australia is covered by the Officer, Gunbarrel, and Eucla Basins, which also overlie the Madura, Forrest, Waigen, and Coompana Complexes to the east (Figs 1 and 5). Very little is known about these tectonic elements because of the cover. The Coompana Complex (referred to as Coompana Block in South Australia; Flint and Daly, 1993) is linked to the western margin of the Gawler Craton but is entirely covered by younger basin rocks. The only basement rock available for observation from the Coompana Complex comes from the Mallabie 1 drillhole in South Australia, which intersected granitic gneiss at its base. Zircons from this gneiss have been dated by LA-ICPMS and gave an age of 1505 ± 7 Ma (Wade et al., 2007), which is unlike any known ages of granitic rocks from the Albany–Fraser Orogen. However, the presence of a late Mesoproterozoic thermal overprint shown by dating of the same drillcore (K–Ar hornblende and biotite ages of c. 1185 and 1159 Ma, respectively) does suggest a link to Stage II of the Albany–Fraser Orogeny (Drexel et al., 1993; Fitzsimons, 2003). The Madura, Forrest, and Waigen Complexes are interpreted to lie between the Nornalup Zone of the Albany–Fraser Orogen and the Coompana Complex (Shaw et al., 1996), but the only information available is from drillcore from south of Haig Cave, which intersects the Madura Complex. Zircons from a sample of amphibolite from this core returned a SHRIMP U–Pb age of 1415 ± 7 Ma, interpreted as the age of igneous crystallization of the protolith (GSWA 178070, depth interval 363.52 – 364.0 m; Nelson, 2005a). Zircons from unfoliated biotite microtonalite from the same core returned a SHRIMP U–Pb age of 1408 ± 7 Ma, interpreted as the age of igneous crystallization of the microtonalite (GSWA 178071, depth interval 611.8 – 612.5 m; Nelson, 2005b). This is within error of the interpreted igneous crystallization age of 1407 ± 7 Ma from zircons from foliated biotite tonalite gneiss taken from the same core (GSWA 178072, depth interval 637.6 – 640.0 m; Nelson, 2005c). These ages do suggest some differences in the basement between the Kepa Kurl Booya Province of the Albany–Fraser Orogen and the Coompana Complex, but because so little is known it is difficult to construct viable tectonic interpretations.

Lithotectonic subdivisions of the Albany–Fraser Orogen

The Albany–Fraser Orogen comprises several lithotectonic units, some of which have been modified in GSWA (2007) and in this Record. Understanding which tectonic elements constitute purely exotic terranes, which were part of the Yilgarn Craton, and which are a tectonic mixture of both is problematic and requires structural, metamorphic, geochemical, and importantly, geochronological work. Previously, the tectonic elements have been subdivided on the basis of differences in geophysical (largely aeromagnetic) signature and the structural style evident in such datasets (e.g. Beeson et al., 1988; Myers, 1990a; Whitaker, 1992, 1993; Fitzsimons, 2003). The recently acquired 400 m line-spacing government aeromagnetic data and increasing availability of high resolution company surveys have allowed a reassessment of these subdivisions, and revision of the positions of major faults that separate them. We have combined the geophysical analysis with targeted fieldwork and SHRIMP U–Pb zircon dating to aid the interpretation. We also present preliminary results from a detailed structural and metamorphic study (PhD being undertaken by M Barquero-Molina, University of Texas, Austin, USA) in the Bremer Bay area.

The Albany–Fraser Orogen is now divided into its foreland component (the Northern Foreland; Northern Domain of Beeson et al. (1988)), its pre-Stage I amalgamation basement components (the Kepa Kurl Booya Province; Central and Southern Domains of Beeson et al. (1988)), the Recherche and Esperance Supersuites (formerly Recherche Granite and Esperance Granite, Myers (1995b)), and various Mesoproterozoic cover rocks. The Kepa Kurl Booya Province is further divided into the Biranup Zone (formerly Biranup Complex), the Fraser Zone (formerly the Fraser Complex, Myers, 1985), and the Nornalup Zone (formerly the Nornalup Complex, Myers (1990a)). These, and the reasons for the changes, are described below.

The Northern Foreland

The Northern Foreland is defined as the portion of the Yilgarn Craton that is reworked by the Albany–Fraser Orogeny, reflecting its position northwards of the

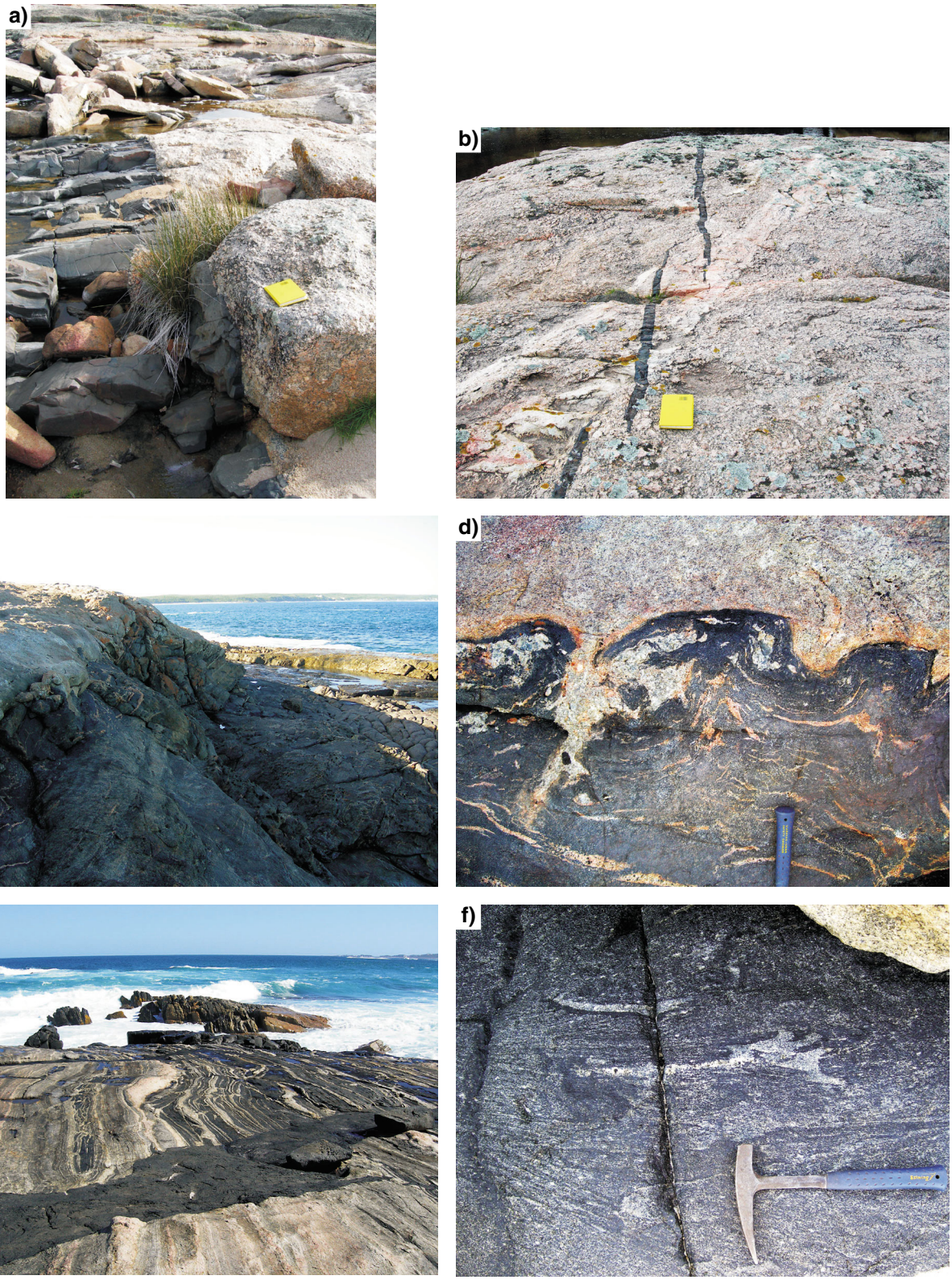

CS85

collisional orogenic belt (Figs 1 and 2). The Northern Foreland was originally documented in Myers (1990a) as 'the southern part of the Yilgarn Craton into which large numbers of dykes were emplaced subparallel with the orogen, and onto which thrust sheets of metasedimentary rocks were transported from the south.' (Myers, 1990a, p. 255). These metasedimentary rocks include the Stirling Range Formation and Mount Barren Group. The Munglinup Gneiss has previously been included in the Biranup Complex of Myers (1995b), but recent work indicates that much of it was originally part of the Yilgarn Craton, and it is therefore included in the Northern Foreland. It is interpreted as a higher grade, more strongly reworked component of the Northern Foreland, bound by major faults.

Reworking of the Yilgarn Craton in the Northern Foreland varied from moderate- to high-strain, ductile deformation under amphibolite- to granulite-facies metamorphic conditions (Munglinup Gneiss and southern part of the Mount Barren Group) to low- to moderate-strain, brittle to semi-brittle, greenschist to amphibolite conditions (Beeson et al., 1988; Myers, 1995a; Jones, 2006). The variation in conditions reflects generally lower strain and lower metamorphic grade with increasing distance from the orogen, or exhumation of shallower crustal levels of the Northern Foreland. In the Pallinup River section in the west, on Bremer Bay, Beeson et al. (1988) described an increase in deformation intensity from north to south, with progressive overprinting of Archean, regional north-northwest trending structures by Mesoproterozoic, Albany–Fraser-related, west-southwest trending, dextral shear zones and gneissic foliations. The northern limit of the Northern Foreland was defined by the presence of discontinuous and widely spaced shear zones (Beeson et al., 1988). Mafic dykes also show the effects of increased deformation intensity within the Northern Foreland from north to south (Beeson et al., 1988). In the north, magmatic textures and clear intrusive relationships are preserved, whereas towards the south, the dykes are metamorphosed and rotated parallel to the trend of the main, Albany–Fraser Orogeny related fabric. To the east, deformation intensity increases towards the Cundeelee Fault, which is a major fault separating Archean rocks from mixed Archean and Proterozoic rocks (Jones, 2006; Tyler and Hocking, 2006; Geological Survey of Western Australia, 2007).

Figure 4. (facing page) Photographs of mafic dykes. Notebook is 19 cm long: a) undeformed dolerite dyke cutting porphyritic syenogranite in the South West Terrane. The dykes trend 065 and are interpreted as belonging to the Gnowangerup–Fraser Dyke Suite. Gairdner River, off Wangup Road (Zone 51, MGA 687180E 6329649N); b) same location and dyke set as a), showing a smaller en echelon group of dykes cutting microgranite and porphyritic syenogranite; c) coarse amphibolite to mafic granulite gneiss observed as a 10–15 m wide dyke within leucocratic granitic gneiss (Munglinup Gneiss). The mafic gneiss is variable in grain size, locally contains garnet, and is locally banded. The dyke is interpreted as belonging to the Gnowangerup–Fraser Dyke Suite, but unlike those in a) and b) has been affected by Stage II of the Albany–Fraser Orogeny. Headland west of Quagi Beach (Zone 51, MGA 342323E 6254430N); d) irregular intrusive contact of the mafic dyke shown in c). The margins of the dyke show crenulate margins and extensive back-veining, which constitutes good evidence that the country rock gneisses were soft when the mafic magma intruded; e) undeformed mafic dyke cutting orthogneiss (Munglinup Gneiss) with deformed and metamorphosed coarse-grained mafic layers. The dyke trends 120 and is interpreted as belonging to the Nindibillup Dyke Suite. The deformed mafic layers are possibly part of the Gnowangerup–Fraser Dyke Suite, deformed during Stage II of the Albany–Fraser Orogeny. Headland west of Quagi Beach (Zone 51, MGA 340067E 6253344N); f) localized leucosomes in an amphibolite dyke, interpreted as belonging to the Nindibillup Dyke Suite, near that shown in e). Headland west of Quagi Beach (Zone 51, MGA 339642E 6253155N).

Munglinup Gneiss

The Munglinup Gneiss was first defined by Myers (1995b) as a gneissic unit derived from Archean granite, granodiorite, tonalite, and pegmatite within the Kepa Kurl Booya Province (formerly Biranup Complex). The Kepa Kurl Booya Province was interpreted as an allochthonous piece of Archean and Proterozoic crust that was accreted to the Yilgarn Craton during the Albany–Fraser Orogeny (Myers et al., 1996). In GSWA (2007) the Munglinup Gneiss is interpreted as reworked Yilgarn Craton and is therefore defined as part of the Northern Foreland. It represents the southernmost exposures of the craton within elongate, fault-bound packages of predominantly granitic gneiss, parallel to the craton margin (Figs 1 and 2). West of Ravensthorpe it is part of the Northern Domain of Beeson et al. (1988), where it is bound by the linked, south-dipping Boxwood Hill and Yungunup Pool Thrusts to the north, and the south-dipping Millers Point Thrust and Bremer Fault to the south. The thrusts are high-strain zones that locally contain leucosomes, and are interpreted as oblique thrust faults with a component of dextral strike-slip movement (Beeson et al., 1988). South of the Mount Barren Group (Fig. 2) the northern margin of the Munglinup Gneiss is bound by the Jerdacuttup Fault, which links to the Bremer Fault to the west, and is interpreted to form the northern edge of a separate fault-bound package to the east, with the Mount Barren Group as a separate thrust package inbetween the two fault-bound packages of Munglinup Gneiss.

The Jerdacuttup Fault has been interpreted as a major, south-dipping thrust that has also accommodated a component of dextral strike-slip movement and is partly responsible for exhuming the Munglinup Gneiss (Myers, 1990a; Witt, 1997, 1998). To the east, the Jerdacuttup Fault has a curved pattern, which suggests it is moderately to shallowly dipping in that region (see cross-section on Fig. 2). It is truncated by the Cowalinya Fault Zone to the east. The Cowalinya Fault Zone is the western margin of an extensively deformed package of rocks where the Munglinup Gneiss and rocks of the Biranup Zone in the Kepa Kurl Booya Province are indistinguishable. This package wraps around the southwestern end of the Fraser Zone, forming an 'S-bend'. To the south, the Munglinup

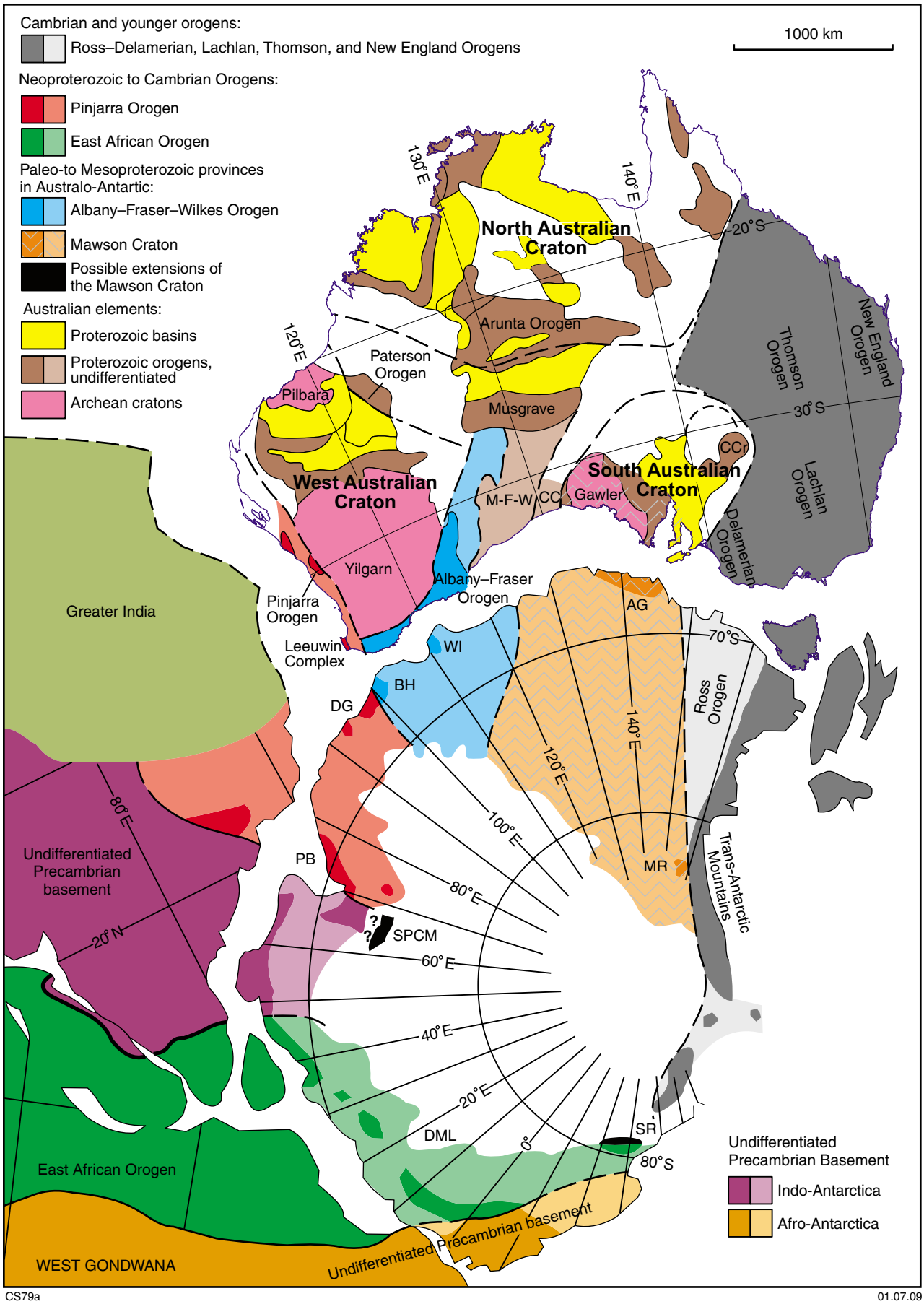

CS79a 01.07.09

Gneiss is bound by the Red Island Fault Zone, which is interpreted as the present-day expression of the suture between the craton margin and the Kepa Kurl Booya Province (Geological Survey of Western Australia, 2007). The Red Island Fault Zone links to the Southern Ocean Shear Zone to the west, which in turn is linked to the Bremer Fault futher west.

The Munglinup Gneiss comprises amphibolite to granulite facies orthogneisses, interlayered with lenses of metamorphosed mafic rocks, with minor banded metachert (jaspilite), amphibolitic schist, serpentinite, and metamorphosed ultramafic rocks, which are interpreted as remnants of Archean greenstone sequences (Thom et al., 1977; Beeson et al., 1988; Myers, 1990a). The orthogneisses were derived from Late Archean monzogranitic, monzodioritic, granodioritic, and tonalitic precursors (Nelson et al., 1995; Geological Survey of Western Australia, 2008). The oldest phase dated is a medium- to dark-grey, strongly foliated monzogranitic gneiss with well-developed differentiated layering from outcrops along the Pallinup River, west of Bremer Bay. It yielded a SHRIMP U–Pb zircon igneous crystallization age of 2681 ± 5 Ma (GSWA 184120; Figs 6a and 7a; Table A1; Bodorkos and Wingate, 2008a).

The most abundant phase in the Munglinup Gneiss is a leucocratic, mostly homogeneous, banded tonalitic to monzogranitic gneiss (Fig. 6b,c). This has been intruded by sheets of porphyritic monzodiorite (Fig. 6d). The monzodiorite appears to postdate the event responsible for the development of the gneissic foliation in the leucocratic banded tonalitic to monzogranitic gneiss, but both plutonic phases predate at least two episodes of folding. Zircons from the two phases at Powell Point give SHRIMP U–Pb ages for igneous crystallization (estimated using the upper concordia intercept of a discordia array) that are within error of each other (Fig. 7b,c). These are 2660 ± 13 Ma for the leucocratic tonalitic gneiss (GSWA 184128; Table A2) and 2658 ± 21 Ma for the prophyritic monzodiorite (GSWA 184127; Table A3) (Bodorkos and Wingate, 2008b,c). Previous dating of biotite-bearing monzogranitic gneiss from Powell Point (GSWA 83696A; Nelson, 1995b), with which GSWA 184128 is tentatively correlated, yielded a minimum age of 2595 ± 11 Ma for igneous crystallization of the precursor monzogranite, which is significantly younger than the age of 2660 ± 13 Ma for GSWA 184128. The c. 2660 Ma ages are consistent with a poorly constrained age of 2661 ± 5 Ma, interpreted to reflect igneous crystallization, from banded leucocratic granodioritic gneiss approximately 70 km northeast of Powell Point, on the Lort River (GSWA 184314; Figs 6e and 7d; Table A4; Bodorkos and Wingate, 2008d). Biotite tonalite gneiss on the Young River also gave a poorly constrained, minimum age of 2639 ± 37 Ma, interpreted as the igneous crystallization age of the precursor granite (Fig. 6c; GSWA 83702; Nelson, 1995c). Further north on the Young River a group of twelve zircons from biotite monzogranite gave an igneous crystallization age of 2631 ± 8 Ma (GSWA 83691; Nelson, 1995d). This may represent a slightly younger Late Archean phase within the Munglinup Gneiss.

The geochronological data indicate at least three phases of granitic magmatism at c. 2680, 2660, and 2630 Ma. These ages are comparable to typical Yilgarn Craton granite ages (Cassidy et al., 2006, and references therein) and support the interpretation that the granitic precursors to the orthogneisses were part of the Yilgarn Craton. Nelson et al. (1995) reported T_{DM} Nd model ages of 2930–2920 Ma for three monzogranitic gneisses from the Young River and Powell Point areas, which are comparable to the ages of felsic volcanic rocks in the Lake Johnston Greenstone Belt (2921 ± 4 Ma) and Carlingup Greenstone Belt (2958 ± 4 Ma), and the Manyutup Tonalite near Ravensthorpe (2966 ± 12 Ma; see **South Yilgarn Craton**, above), and hence compatible with a Yilgarn Craton source for these monzogranitic melts. Biotite monzogranitic gneiss from the Young River and Powell Point have ε_{Nd} values of -3.3, -2.5, and -2.4, suggesting a component of juvenile mantle material mixed with the crustal melt (Nelson et al., 1995). These isotopic data could therefore indicate partial derivation of the granitic precursors from Yilgarn Craton greenstones. This interpretation is further supported by the presence of isolated lenses of mafic and ultramafic rocks, including some with historic nickel deposits (e.g. Young River Nickel project, east of Ravensthorpe), which are interpreted as remnants of Archean greenstone that were intruded by the granitic precursors to the orthogneisses (Thom and Lipple, 1971; Thom et al., 1977; Geological Survey of Western Australia, 2007).

The Munglinup Gneiss includes at least one phase of granitic gneiss that has a Proterozoic protolith. Biotite granodioritic gneiss from near Bald Rock on the Lort River has an igneous crystallization age of 1299 ± 14 Ma (GSWA 83690; Nelson, 1995e). This age corresponds with Stage I of the Albany–Fraser Orogeny (1345–1260 Ma, Clark et al., 2000; Bodorkos and Clark, 2004a), but is the only data available that indicates its effect in the Munglinup Gneiss. It is also the only evidence of magmatism associated with the Recherche Supersuite (c. 1330–1280 Ma; Nelson et al., 1995) in the Northern Foreland. The orthogneiss in this area has differential layering, is well-lineated, and contains numerous mafic layers from mm- to cm-scale, some of which were probably mafic dykes (Fig. 6f,g). These contain folded felsic veins, as do the orthogneisses. Similar mafic horizons can be found throughout the Munglinup Gneiss and may

Figure 5. Crustal elements of easternmost Gondwana (modified from Fitzsimons, 2003; Tyler, 2005; and Geoscience Australia, 1998). Where paler and darker shades of the same colour are shown, the paler shade indicates large areas without outcrop where the crustal element is inferred. AG, Terre Adélie–King George V Land; BH, Bunger Hills; CC, Coompana Complex (concealed by the Officer and Eucla Basins); CCr, Curnamona Craton; DG, Denman Glacier region; DML, Dronning Maud Land; M–-F–W, Madura, Forrest, and Waigen Complexes (undivided; concealed by the Gunbarrel, Officer and Eucla Basins); MR, Miller Range; PB, Prydz Bay; SPCM, southern Prince Charles Mountains; SR, Shackleton Range; WI, Windmill Islands.

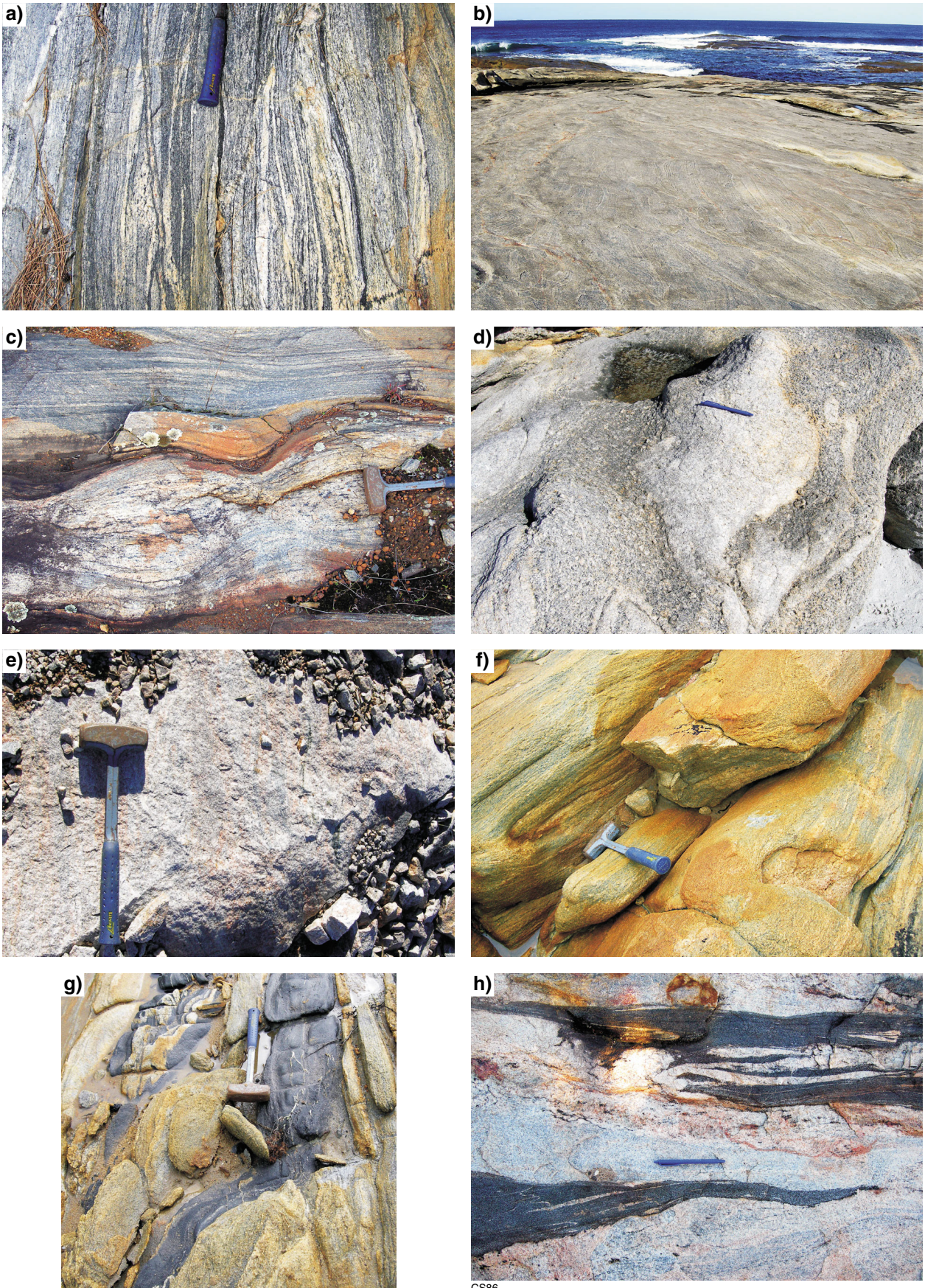

CS86

represent deformed remnants of the Gnowangerup–Fraser Dyke Suite, which intruded at c. 1210 Ma (Figs 4c–e and 6h).

Although the data are sparse, metamorphic ages recorded in the Munglinup Gneiss fall within the bracket for Stage II of the Albany–Fraser Orogeny (1215–1140 Ma; Clark et al., 2000). The leucocratic tonalitic gneiss from Powell Point yielded a group of eight analyses from within zircon grain edges and rims with very low Th/U (mostly < 0.15) that gave a weighted mean $^{207}Pb^*/^{206}Pb^*$ date of 1195 ± 17 Ma (Group 1; GSWA 184128; Fig. 7b; Table A2; Bodorkos and Wingate, 2008b). The Group 1 date of 1195 ± 17 Ma does not differ significantly from the lower intercept date of 1184 ± 170 Ma, yielded by the linear regression through the 16 analyses in Group 2 (c. 2660 Ma), so the discordia array is interpreted to reflect a dominant single episode of radiogenic-Pb loss from zircons formed during igneous crystallization of the precursor leucocratic tonalite. A Stage II age can also be determined from the slightly to strongly discordant analyses of the prophyritic monzodiorite at Powell Point. A linear regression through all 29 analyses (Table A3) defines a discordia chord with little excess scatter (MSWD = 3.1), and upper and lower concordia intercepts of 2658 ± 21 and 1149 ± 220 Ma, respectively (Fig. 7c). If the discordia chord mainly reflects a single episode of radiogenic-Pb loss from zircons formed during igneous crystallization of the monzodiorite, then the regression indicates that this episode took place at c. 1150 Ma. This is consistent with partial resetting of the U–Pb system in these zircons during granulite facies metamorphism associated with Stage II of the Albany–Fraser Orogeny.

The Munglinup Gneiss has been affected by at least three phases of large-scale folding, and is locally sheared and boudinaged. The metamorphic fabrics in the gneisses are commonly defined by assemblages that include magnetite, and therefore the megascale structures are well-defined in aeromagnetic imagery, particularly fold interference patterns (Fig. 8a,b). The fold patterns correspond to mesoscale structures in outcrop, where early hook folds (F_1) of gneissic banding in leucocratic tonalitic gneiss are refolded into approximately north trending, open to tight folds (F_2; Fig. 9a). These are refolded by east to northeasterly trending tight folds, which are parallel to the dominant trend of the orogen (F_3; Fig. 9b). The F_2 and F_3 folds are interpreted to correlate with the megascale refolded folds visible in the aeromagnetic imagery (Fig. 8a,b). These folds are cut by shears that locally contain leucosomes, which indicates this last phase of deformation took place at high temperatures, probably in the granulite facies (Figs 9b,c and 10). In outcrop, dextral shears trend predominantly east while sinistral shears trend predominantly northwest. Both post-date the folding and can be interpreted as conjugates, indicative of northwest–southeast compression (Fig. 9d). The Munglinup Gneiss is also locally boudinaged (Fig. 6c) but the timing of the boudinage with respect to the folding is not clear. The boudins mostly trend parallel to the orogen, and do not appear to be folded. This suggests they are relatively late and may relate to extension of the orogen in a northeast–southwest orientation, perpendicular to the conjugate shearing (Fig. 9d).

Given that the late stages of deformation appear to have been in the granulite facies it is likely that the shearing, and possibly the third phase of folding, which has the regional trend of the orogen, corresponds to Stage II of the Albany–Fraser Orogeny. This is supported by the high temperature metamorphic ages described above. The second phase of folding is more problematic with respect to its timing and could relate to either Stage I or II, or could be Late Archean. Its approximate northerly trend is consistent with Late Archean structures in the Yilgarn Craton, and may correlate with the regional D_4 event (D_2 in Swager (1997)) in the Eastern Goldfields Superterrane that post-dates 2660 Ma (Blewett and Czarnota, 2007). These folds are unlike those observed to the south within the Biranup Zone, e.g. in the Bremer Bay area (see **Dalyup Gneiss**, below), which further supports a Late Archean age. At Powell Point the early hook folds (F_1) and gneissic banding in the leucocratic tonalitic gneiss appear to pre-date intrusion of the prophyritic monzogranite at 2658 ± 21 Ma, and are therefore interpreted as Late Archean structures.

Figure 6. Photographs of the Munglinup Gneiss: a) medium- to dark-grey, strongly foliated monzogranitic gneiss with well-developed differentiated layering, Pallinup River, approximately 50 m from sample site GSWA 184120 (Zone 51, MGA 658763E 6191694N). The layering is isoclinally folded and offset by low-angle shears; b) typical exposure of Munglinup Gneiss, leucocratic banded tonalitic to monzogranitic gneiss at Munglinup Beach Headland on the South Coast (Zone 51, MGA 297801E 6248385N); c) boudinaged leucocratic banded tonalitic to monzogranitic gneiss at the Young River, east of Ravensthorpe (Zone 51, MGA 314944E 6235295N). This locality is likely to be representative of sample site of GSWA 83702, Nelson (1995c), which gave a minimum age of 2639 ± 37 Ma; d) porphyritic monzodiorite with rafts of leucocratic banded tonalitic gneiss, Powell Point, South Coast (Zone 51, MGA 274527E 6243949N); e) leucocratic banded tonalitic to monzogranitic gneiss at the Lort River (Zone 51, MGA 338711E 6274811N); f) well-lineated orthogneiss with differential layering within Munglinup Gneiss near Bald Rock, Lort River (Zone 51, MGA 349076E 6302425N). The photo shows breakage surfaces within the most homogeneous occurrence in the area, and was probably the sample site of GSWA 83690 (Nelson, 1995e), dated at 1299 ± 14 Ma; g) mafic lenses in orthogneiss within Munglinup Gneiss near Bald Rock; same location as f). The mafic lenses include folded leucosomes and may be remnant mafic dykes; h) mafic lenses in banded tonalitic to monzogranitic gneiss at the Lort River; same location as e). As in g) these mafic lenses include folded leucosomes.

Mount Barren Group

The Mount Barren Group consists of lower greenschist to upper amphibolite facies Proterozoic metasedimentary rocks that overlie the southern edge of the Yilgarn Craton for a strike length of about 120 km, from Bremer Bay to

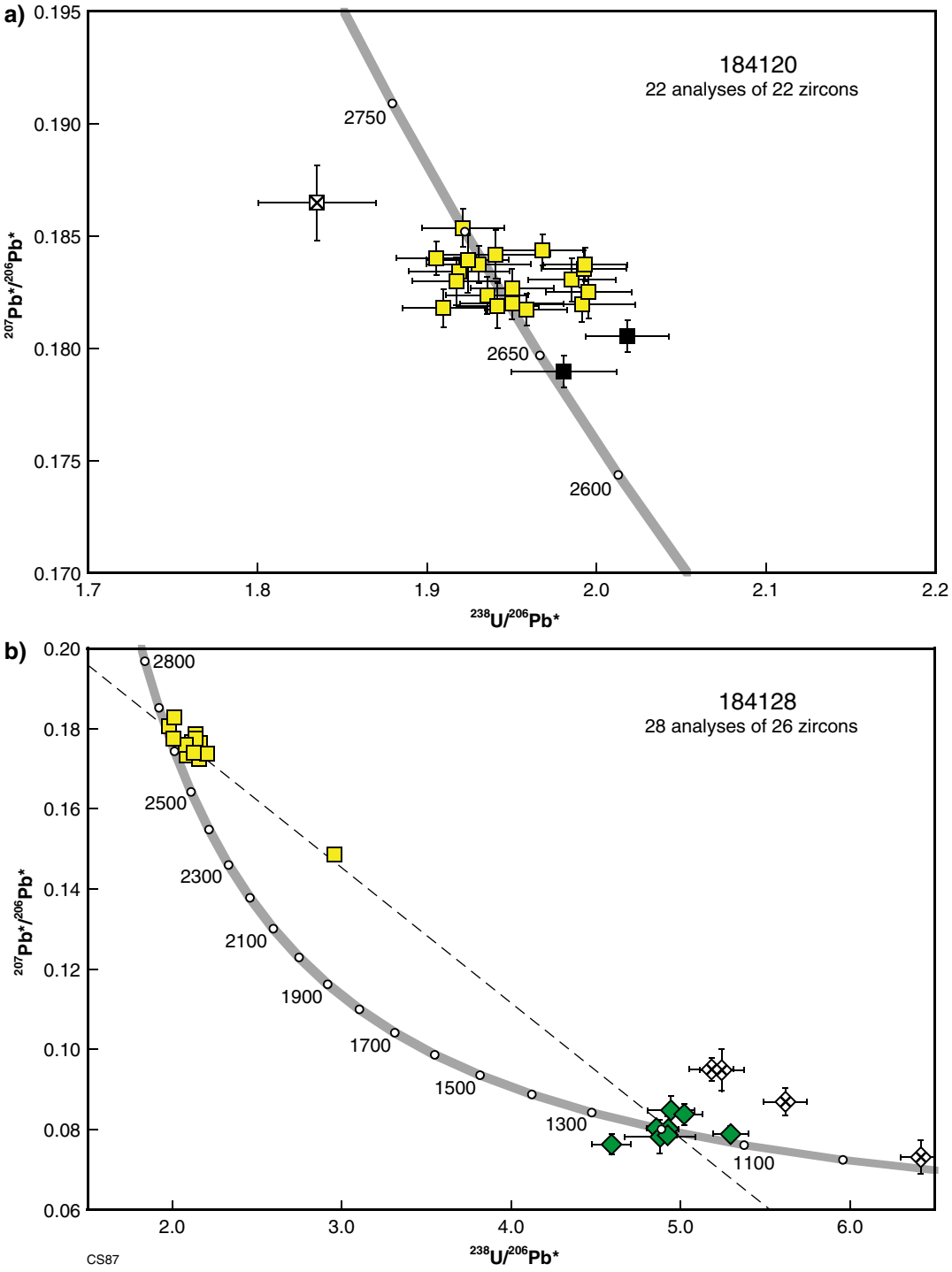

Figure 7. **a) U–Pb analytical data for sample GSWA 184120: monzogranitic gneiss, Pallinup River (Zone 51, MGA 658727E 6191757N). Yellow squares denote Group 1 (igneous crystallization); black squares denote Group 2 (affected by loss of radiogenic Pb); crossed square denotes Group 3 (affected by inaccurate common-Pb correction); b) U–Pb analytical data for sample GSWA 184128: leucocratic tonalitic gneiss, Powell Point (Zone 51, MGA 274332E 6243706N). Green diamonds denote Group 1 (high grade metamorphism); yellow squares denote Group 2 (igneous crystallization; affected by ancient loss of radiogenic Pb); crossed diamonds indicate ungrouped analyses (discordance >20% or f204 >3%). Dashed line depicts discordia chord defined by data in Group 2 only, with all other analyses excluded from the regression;**

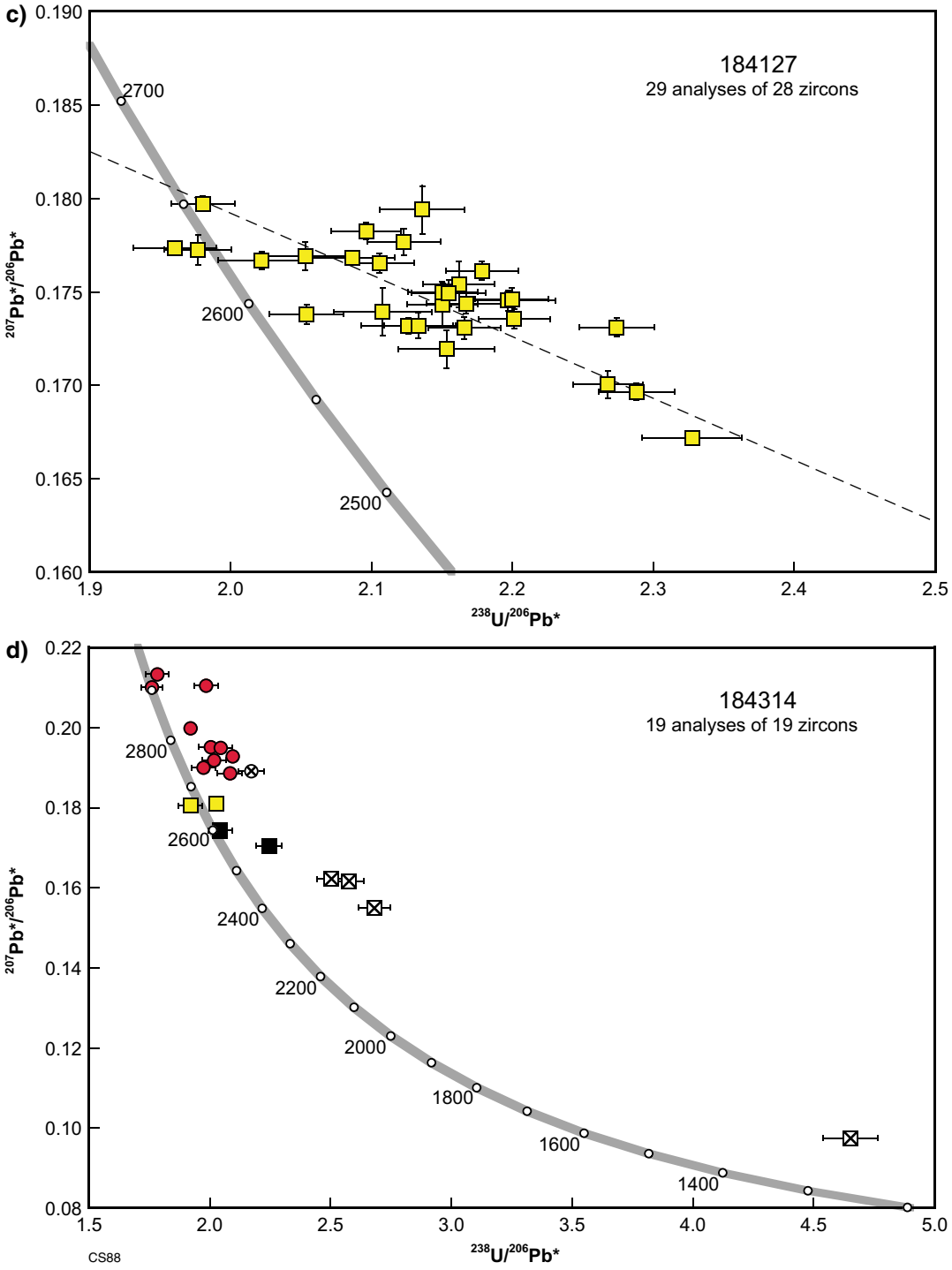

Figure 7. **c) U–Pb analytical data for sample GSWA 184127 (Zone 51, MGA 274527E 6243949N): porphyritic monzodiorite, Powell Point. Yellow squares denote Group 1 (igneous crystallization; subsequently affected by ancient loss of radiogenic Pb). Dashed line depicts discordia chord defined by data in Group 1. The upper concordia intercept is not significantly different from the date of 2650 ± 4 Ma (1σ) yielded by the oldest concordant analysis (25.1; Table A3), so the upper intercept date of 2658 ± 21 Ma is interpreted as the best estimate of the age of igneous crystallization of the monzodiorite; d) U–Pb analytical data for sample GSWA 184314: leucocratic granodioritic gneiss, Lort River – Ashdale Road (Zone 51, MGA 338711E 6274811N). Yellow squares denote Group 1 (igneous crystallization); red circles denote Group 2 (xenocrystic zircons; possibly affected by ancient loss of radiogenic Pb); black squares denote Group 3 (igneous zircons; affected by ancient loss of radiogenic Pb); crossed symbols (circle and squares) indicate ungrouped analyses of xenocrystic and igneous zircons, respectively (discordance >10%).**

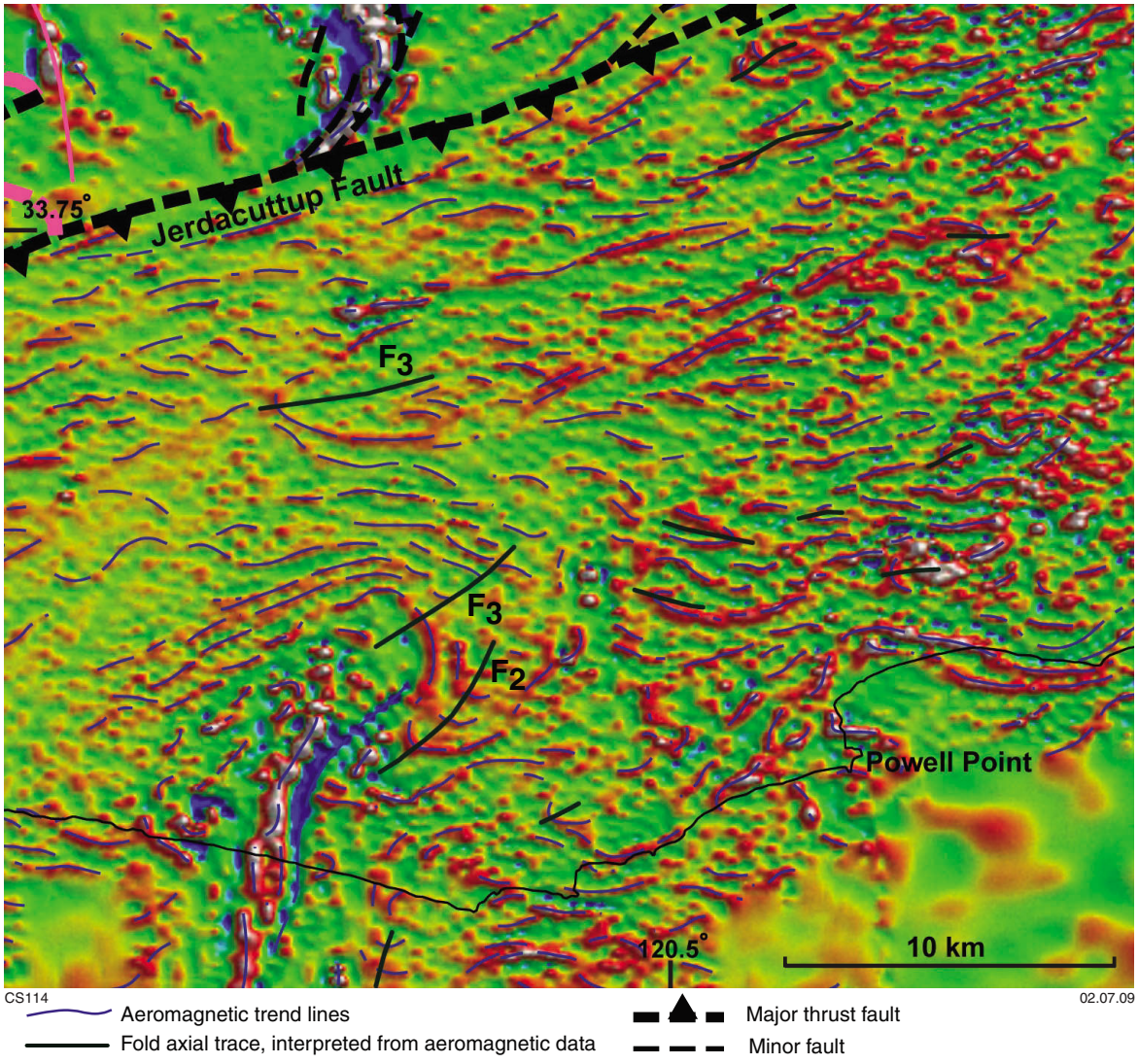

Figure 8. **a) Reduced to pole, first vertical derivative aeromagnetic image of part of the Munglinup Gneiss, southeast of Ravensthorpe, showing its magnetic character and a large-scale, refolded fold west of Powell Point. The fold generations are denoted F_2 and F_3, accordingly. The map features were extracted from the interpreted bedrock geology map in Geological Survey of Western Australia (2007);**

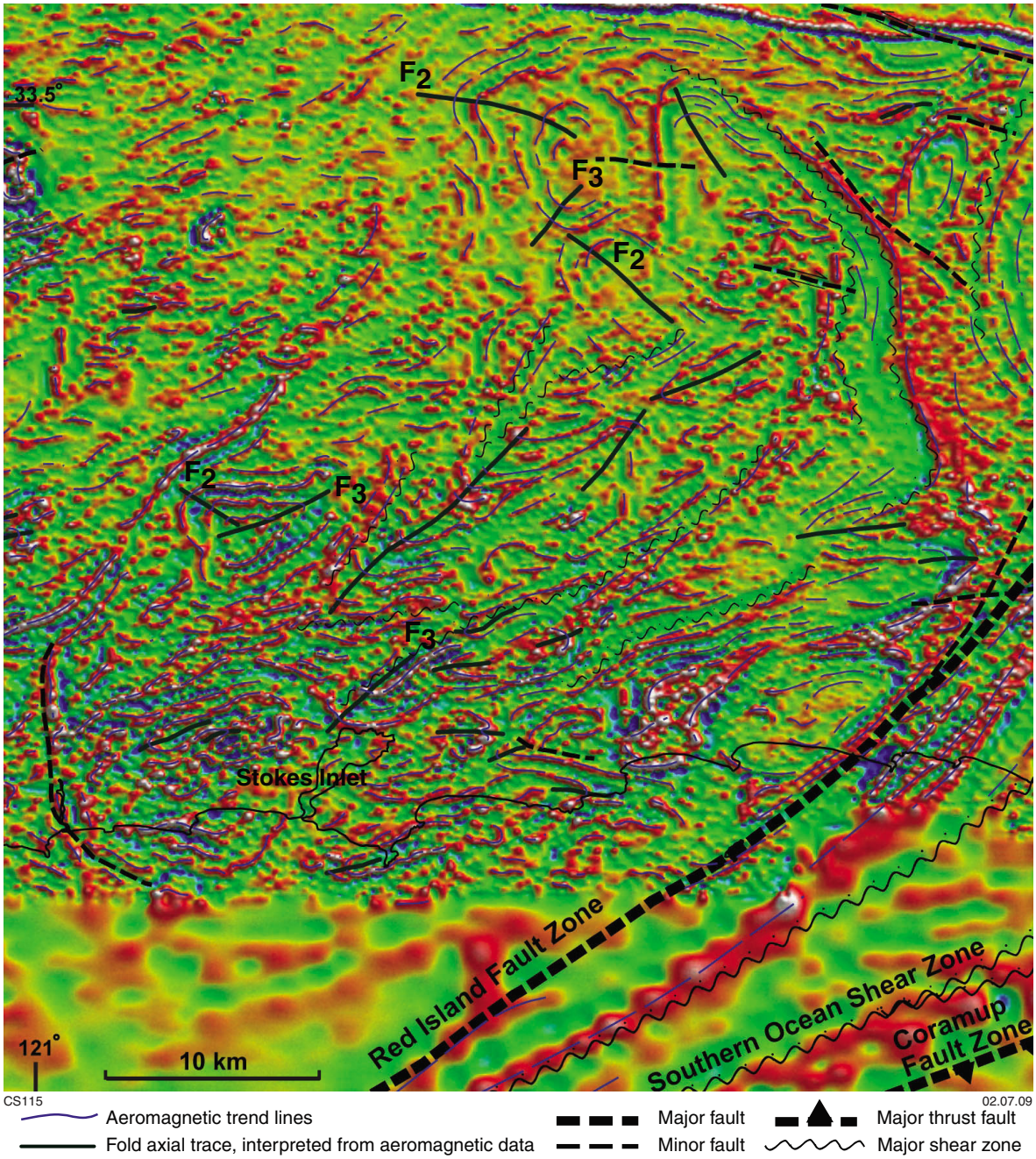

Figure 8. b) Same as a), showing interpreted refolded folds in the area around, and north of, Stokes Inlet. The Red Island Fault Zone separates the Munglinup Gneiss from the Biranup Zone of the Kepa Kurl Booya Province, which has a completely different magnetic character (see text for explanation).

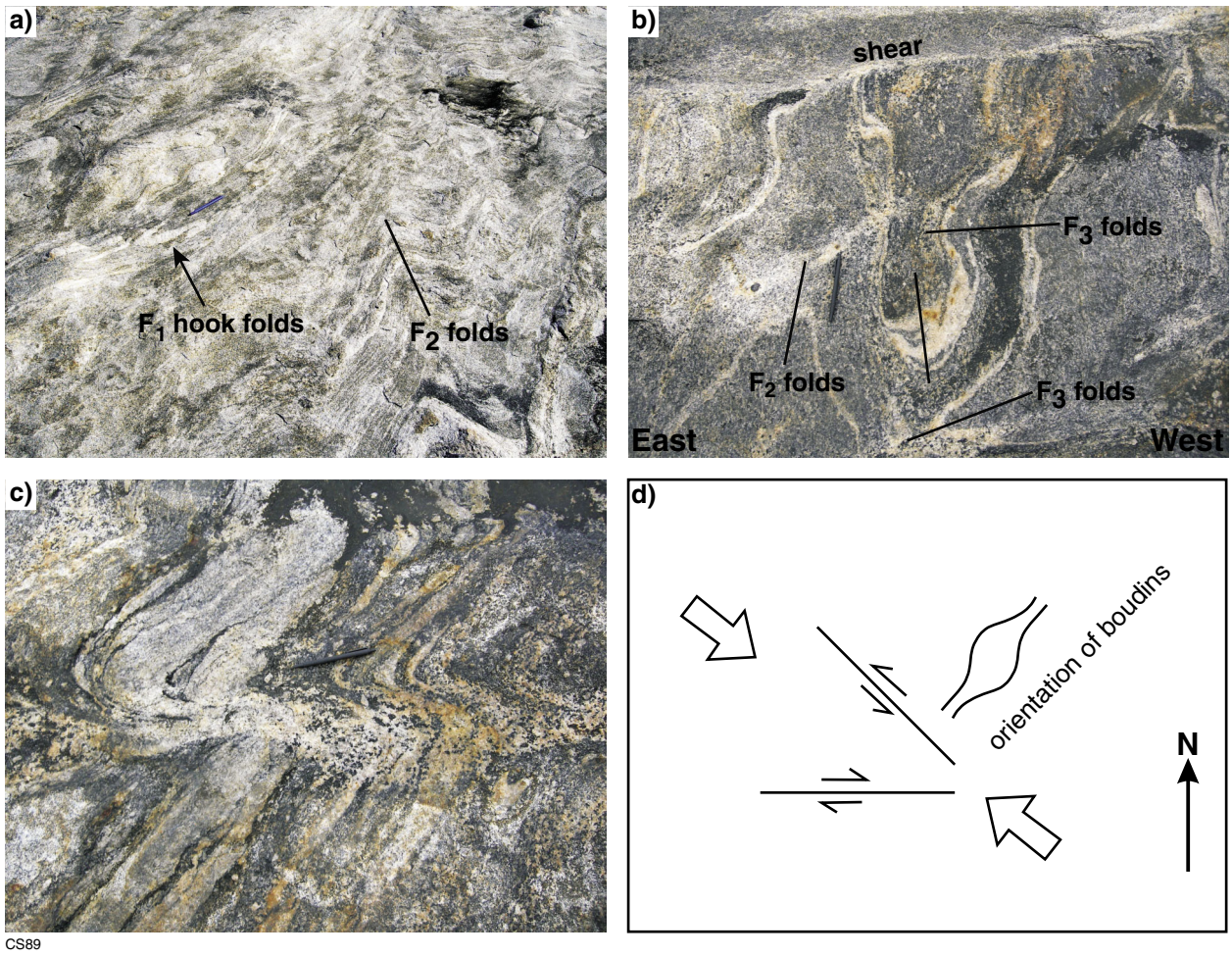

Figure 9. **Photographs and structural features of the Munglinup Gneiss: a) small-scale F_1 hook folds in banding of leucocratic gneiss, refolded by larger-scale, regional, north-trending F_2 folds; Powell Point (Zone 51, MGA 274527E 6243949N). The blue pen near the hook fold shows the scale; b) north trending tight to isoclinal F_2 folds refolded by east to east-northeast trending F_3 folds in both the leucocratic tonalitic gneiss and the porphyritic monzodiorite, Powell Point (Zone 51, MGA 274527E 6243949N). The black pen in the centre shows the scale; c) asymmetric, northeast trending F_3 folds cut by leucosome-filled shears. These folds are developed in both the leucocratic tonalitic gneiss and the porphyritic monzodiorite Powell Point (Zone 51, MGA 274527E 6243949N). The black pen in the centre shows the scale; d) interpretative sketch of conjugate shears indicating northwest–southeast compression, with boudinage indicating orthogonal extension during Stage II of the Albany–Fraser Orogeny. In this interpretation the shear cross-cutting F_3 folds in c) is an example of half of a conjugate pair.**

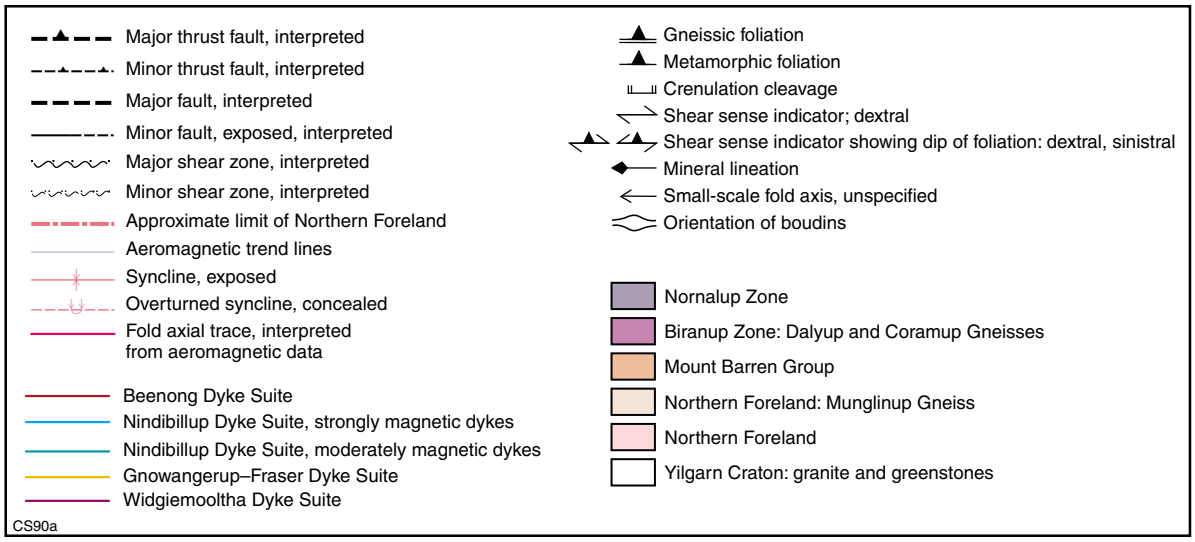

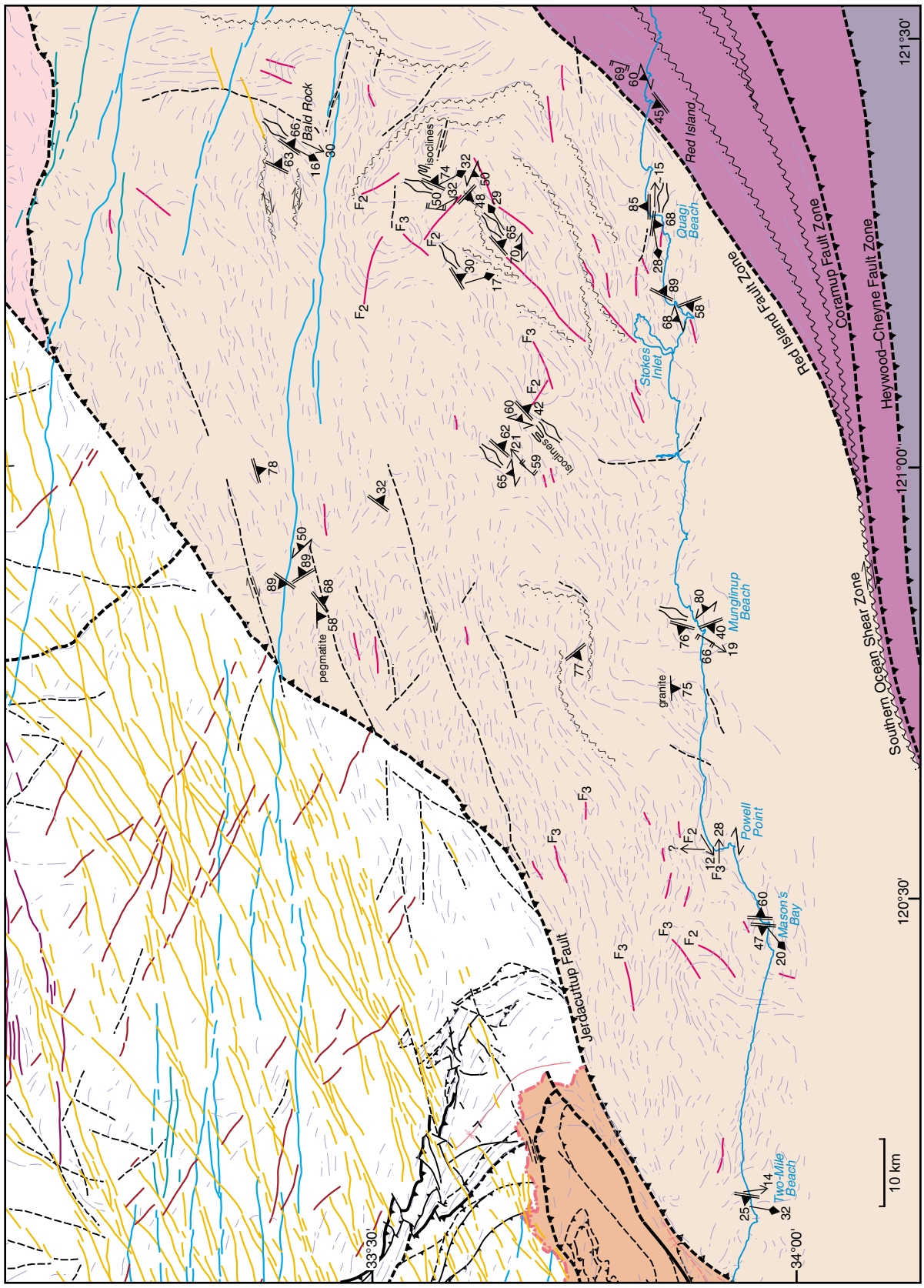

Figure 10. Extract from the interpreted bedrock geology map (Geological Survey of Western Australia, 2007) showing the major portion of the Munglinup Gneiss, overlain with field structural observations and interpretations (see legend on page 20).

east of Ravensthorpe (Fig. 2; Thom et al., 1977, 1984; Witt, 1997). It is divided into the Steere Formation, the Kundip Quartzite, and the Kybulup Schist (Thom and Chin, 1984; Thom et al., 1984). The Steere Formation is the lowermost unit and consists of a thin basal conglomerate with clasts of quartzite, chert, banded iron-formation, and felsic volcanic rocks, overlain by several metres of pebbly sandstone and 4 m of dolomitic limestone (Thom et al., 1977; Thom et al., 1984; Witt, 1997). At its type locality in the Western Steere River the Steere Formation has been interpreted as nonconformably overlying the Archean Manyutup Tonalite of the Yilgarn Craton (Thom et al., 1977; Thom et al., 1984); however Witt (1997) argued that the basal contact was a thrust fault. The Steere Formation does not appear to be laterally continuous, and may be representative of a restricted, coastal depositional environment (Witt, 1997).

The Kundip Quartzite consists predominantly of thickly bedded, pure quartzite that is interbedded with mica- and magnetite-bearing quartzites and mudstone, and minor thin lenses of metaconglomerate dominated by quartzite clasts (Fig. 11a; Thom et al., 1984; Witt, 1997; Vallini et al., 2005). At Barrens Beach thin muscovite-rich layers contain rare kyanite (Witt, 1997). The quartzite is well exposed in a series of prominent rocky peaks which shows its predominant southeasterly dip (Fig. 11b). Sedimentary structures such as cross-bedding and ripple marks are common (Witt, 1997) and suggest shallow near-shore marine to tidal sandflat conditions. The Kybulup Schist consists predominantly of thinly bedded pelitic and psammitic rocks that vary in metamorphic grade. Low-grade, mudstone-dominant rhythmites and shales that coarsen upwards to siltstone, and slates and phyllites are found in the northwest, while amphibolite-facies, kyanite-, staurolite-, and garnet-bearing schists are found in the southeast (Thom et al., 1984; Witt, 1997; Fitzsimons et al, 2005; Vallini et al., 2005). Witt (1997) described rare outcrops of dolomite and calc-silicate schist, which he interpreted as indicative of a facies variation within the Kybulup Schist, suggesting the presence of carbonate banks surrounded by deeper water sediments. Vallini et al. (2002, 2005) examined drill core of a low-grade section of the Mount Barren Group and described a 26 m thick phosphatic unit at the interface between the Kundip Quartzite and the Kybulup Schist. The unit is thinly bedded and consists of alternating medium- to coarse-grained sandstone and carbonaceous shale, and is enriched in phosphatic minerals, including xenotime, which has been used for dating (see **Geochronology of the Mount Barren Group**, below). The Mount Barren Group has been interpreted as a deltaic to shallow-marine sequence, with fluvial or fluvial-deltaic sediments represented by the Steere Formation, a delta-plain or upper delta-front represented by the Kundip Quartzite, and a lower delta-front, possibly with an upper prograding section, represented by the Kybulup Schist (Witt, 1998; Dawson et al., 2002; Vallini et al., 2002; 2005).

The Mount Barren Group hosts an approximately 300 m thick mafic intrusion named the Cowerdup Sill (Thom et al., 1977, 1984). Thom et al. (1977, 1984) described a strongly differentiated sequence of ultramafic rocks at the base, through to granophyre at the top, but Witt (1997) reported that the differentiation was difficult to see in the field, and that the sill consisted mainly of mafic granophyre with abundant quartz and local K-feldspar, with the typical assemblage being quartz–plagioclase–calcic-amphibole–chlorite(–K-feldspar–relict-clinopyroxene). The sill is broadly conformable with the Mount Barren Group but does cut the stratigraphy regionally (Thom and Chin, 1984; Witt, 1997).

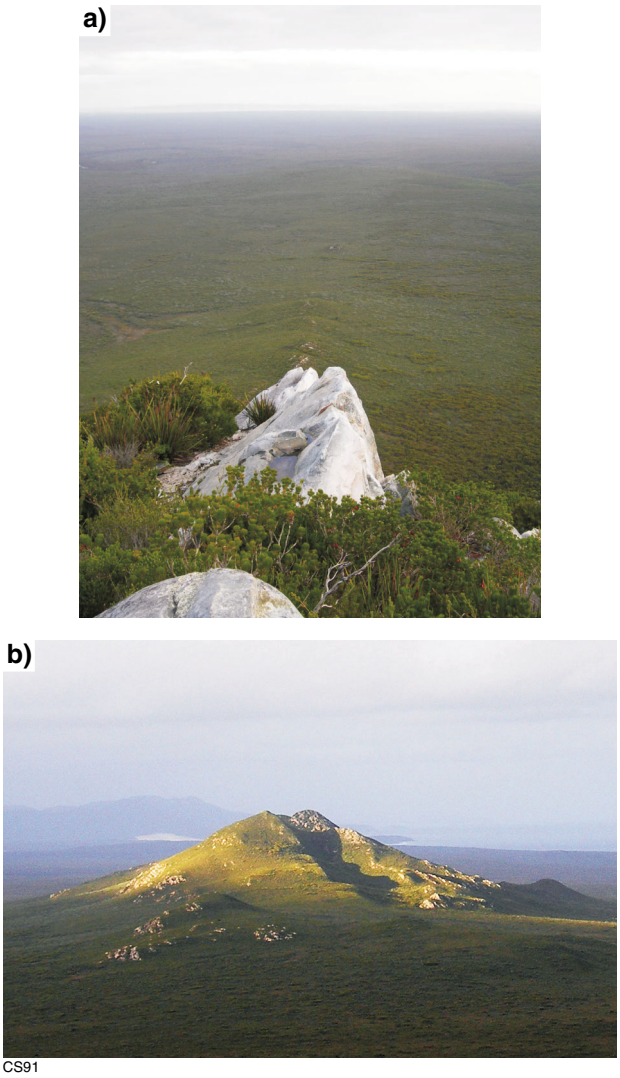

Figure 11. a) White quartzite of the Kundip Quartzite (Mount Barren Group) on the peak of West Mount Barren, looking southwest. The trace of the southeasterly dipping bed can be seen at the foot of the peak in the distance; b) view of Mount Bland looking northeast from West Mount Barren, showing the southeasterly dipping beds (from upper left to lower right in the photo) of the Kundip Quartzite (Mount Barren Group).

Structure and metamorphism of the Mount Barren Group

Most studies of the Mount Barren Group have concluded that it is a northwest vergent fold and thrust belt (e.g. Sofoulis, 1958; Thom et al., 1984; Myers, 1990a; Witt,

1998). The amount of overall displacement on thrust faults is unknown, and there is some debate about whether or not the Mount Barren Group is completely allochthonous (e.g. Witt, 1998; Dawson et al., 2002). Several stages of folding and associated fabrics have been recognized within the Mount Barren Group, with the highest degree of complexity in the higher grade rocks to the south and southeast (Witt, 1998; Wetherley, 1998; Dawson et al., 2003). Outcrops are dominated by south- to southeast-dipping foliations, and two principal cleavages have been correlated across the group (Fitzsimons and Buchan, 2005). These are S_1 and S_2 cleavages (S_2 and S_4 of Wetherley, 1998) that are axial planar to gently plunging, open to isoclinal folds (Dawson et al., 2003; Fitzsimons and Buchan, 2005). These structures are overprinted by upright kinks and folds associated with a weak, axial planar crenulation cleavage that developed at significantly shallower structural levels (S_5 of Wetherley, 1998; Dawson et al., 2003; Fitzsimons and Buchan, 2005).

Rocks of contrasting metamorphic grade are juxtaposed by major structures, such as the Hamersley Fault, placing higher grade rocks structurally above lower grade rocks (Witt, 1998; Wetherley, 1998; Fitzsimons and Buchan, 2005). The lower-grade, greenschist-facies rocks in the north and west typically contain sericite(–chlorite) assemblages, while the higher-grade, amphibolite-facies rocks in the southeast contain kyanite- and staurolite-assemblages, with peak metamorphic garnet, staurolite, and kyanite produced prior to or during D_2 deformation (Hollingsworth, 1996; Stephens, 1996; Wetherley, 1998). Pressure–temperature pseudosections and geothermobarometry indicate that the highest-grade assemblages formed at temperatures just above 600°C and pressures of around 8 kbar (Witt, 1998; Wetherley, 1998). The Cowerdup Sill contains equivalent assemblages of actinolite, chlorite, and saussuritized plagioclase in the low-grade rocks, and garnet, hornblende, plagioclase, and quartz in the high-grade rocks, which constrains the timing of intrusion as prior to D_2 (Witt, 1997; Wetherley, 1998). Abundant quartz veins that contain coarse-grained garnet–staurolite and locally kyanite selvedges indicate devolatilization and fluid flow, either before or during peak metamorphism (Hollingsworth, 1996; Wetherley, 1998).

Geochronology of the Mount Barren Group

SHRIMP U–Pb detrital zircon studies of the Mount Barren Group have shown that it has a maximum depositional age of c. 1700 Ma, and significant detrital zircon populations at c. 2663, 2645, 2291, 2246, 2018, 1857, 1803, and 1773 Ma (Fig. 12; Nelson, 1996a,b; Dawson et al., 2002; Hall et al., 2008). Vallini et al. (2002, 2005) dated authigenic xenotime overgrowths on zircon grains from a

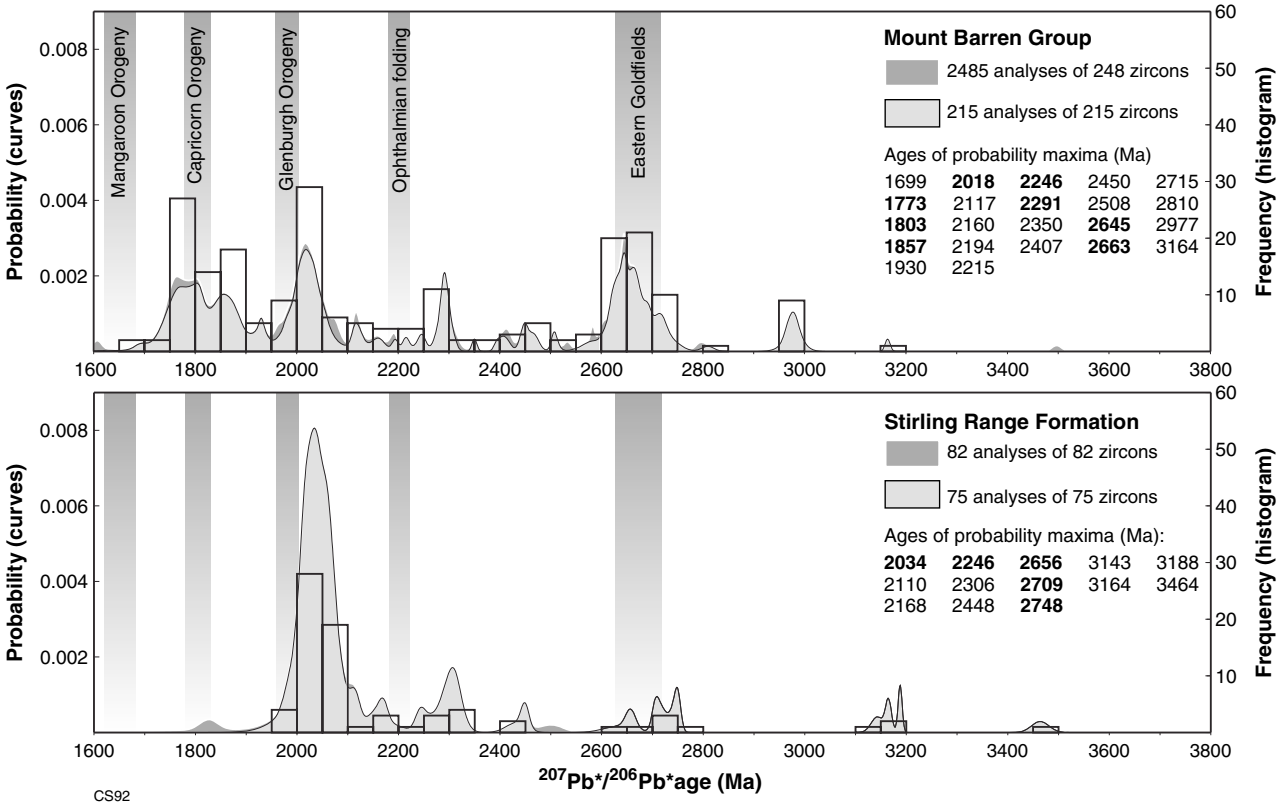

Figure 12. Probability density plots of SHRIMP U–Pb detrital zircon ages from the Mount Barren Group and Stirling Range Formation, overlain with the ages of zircon-forming events in the southern Yilgarn Craton and the Gascoyne Complex (after Hall et al., 2008). Black curves with pale grey fill, ages of probability maxima, and histograms (bin width 50 Ma) include only data with discordance <10% and f204 <1%, and exclude analyses affected by instability in the primary beam. White curves with dark grey fill include all data. Source data from Nelson (1996a,b), Dawson et al. (2002) and Rasmussen et al. (2002).

low grade phosphatic unit (described above) between the Kundip Quartzite and Kybulup Schist and obtained four age populations of 1693 ± 4, 1645 ± 3, 1578 ± 10, and 1481 ± 21 Ma. Xenotime within the low-grade phosphatic unit shows no evidence of Stage I or II metamorphism, and the unit is interpreted as a shielded, low-strain envelope because of its low permeability and porosity (Vallini et al., 2005). Based on detailed petrography and geochemistry Vallini et al. (2005) deduced a paragenetic sequence for the unit. The 1693 ± 4 Ma date was interpreted to date early diagenesis of unconsolidated sediments, and therefore is closest to the depositional age of the unit. The onset of burial, and a possible change to anerobic conditions, was interpreted to have commenced before c. 1654 Ma. The two younger age populations of 1578 ± 10 and 1481 ± 21 Ma were interpreted to reflect periods of hydrothermal xenotime growth post-dating quartz cementation, and may reflect further burial.

The Mount Barren Group may be part of a much broader group of sedimentary rocks deposited on or close to the southern and southeastern margin of the Yilgarn Craton during the Paleoproterozoic, but with variable provenance (Hall et al., 2008). Dawson et al. (2002) suggested that a detrital age population of c. 2645 Ma in the Mount Barren Group indicated that the Yilgarn Craton was not a sediment source, however magmatism of this age is evident in the Eastern Goldfields Superterrane (Hall et al., 2008, and references therein). The Stirling Range Formation, approximately 100 km west of the Mount Barren Group, consists of sub-greenschist to lower greenschist facies quartzite, shale, slate, and phyllite (Muhling and Brakel, 1985). It has a minimum age of 1800 ± 14 Ma, based on authigenic xenotime of probable diagenetic origin (Rasmussen et al., 2004). This suggests a somewhat older depositional age than that of the Mount Barren Group. It has been interpreted as a shallow-marine, tide-dominated succession (Cruse, 1991; Cruse and Harris, 1994). Detrital zircons and xenotime from the Stirling Range Formation indicate a maximum depositional age of 2016 ± 6 Ma (Rasmussen et al., 2002, 2004). Comparisons of probability plots of detrital zircon ages from the Mount Barren Group and Stirling Range Formation are inconclusive, and show both similarities and differences, but data for the Stirling Range Formation are not abundant (Fig. 12). The Woodline Formation is found approximately 350 km to the northeast of the Mount Barren Group, near and parallel to the Fraser Zone, and consists of lower greenschist facies mature sandstone interbedded with siltstone (Hall et al., 2008). Its detrital zircon age spectra are most similar to those of the Earaheedy Group on the northeastern margin of the Yilgarn Craton, and it has a maximum depositional age of 1737 ± 28 Ma, suggesting it may have been deposited at a similar time to the Mount Barren Group (Hall et al., 2008).

Dating of peak metamorphism from kyanite-bearing, amphibolite facies rocks of the Mount Barren Group yielded SHRIMP U–Pb ages of 1206 ± 6 and 1194 ± 8 Ma, for xenotime and monazite, respectively (Dawson et al., 2003). Dawson et al. (2003) interpreted these ages to represent c. 1205 Ma peak thermal metamorphism, statically overprinting the S_1 and S_2 foliations. This age led Dawson et al. (2003) to interpret the widespread intrusion of the c. 1210 Ma Gnowangerup–Fraser Dyke Suite to be the heat source for peak metamorphism during the early part of Stage II of the Albany–Fraser Orogeny. This interpretation is not consistent with the dominant ages of high-grade metamorphism within the adjacent Biranup Zone of the Kepa Kurl Booya Province, which indicate that granulite facies metamorphism took place at c. 1180 Ma (see **Kepa Kurl Booya Province**, below) and post-dated c. 1210 Ma mafic dyke emplacement, but could relate to an earlier, less extensive metamorphic event.

Kepa Kurl Booya Province

Myers (1990a) divided the Albany–Fraser Orogen into two major tectonic units; an inboard, intensely deformed component named the Biranup Complex, and an outboard component named the Nornalup Complex. In this definition the Biranup Complex contained what was later called the Munglinup Gneiss, Dalyup Gneiss, and Coramup Gniess (Myers, 1995b), as well as the Fraser Complex. In Myers (1995b) the c. 1300 Ma Fraser Complex was removed from the Biranup Complex. As stated above, in light of new data and interpretations the Biranup Complex is now renamed the Kepa Kurl Booya Province (with three subordinate units decribed below) and is defined as the crystalline basement of the Albany–Fraser Orogen, i.e. the disparate crustal fragments affected by, and probably amalgamated by, Stage I tectonism. It includes three major zones that contain rocks with different protolith ages and geological histories, together with the Recherche and Esperance Supersuites, and various Mesoproterozoic cover rocks. Rocks that cannot be grouped into any of these units are simply referred to as undivided Kepa Kurl Booya Province.

The three major tectonic units of the Kepa Kurl Booya Province are the Biranup Zone, the Fraser Zone (formerly the Fraser Complex, Doepel, 1973; Myers, 1985), and the Nornalup Zone (formerly the Nornalup Complex, Myers, 1990a). The Biranup Zone contains both the Dalyup Gneiss and the Coramup Gneiss, which are both dominated by orthogneisses with c. 1690–1660 Ma protolith ages. The Dalyup and Coramup Gneisses are combined in the one zone because of similarities in their geological histories and the difficulty of distinguishing them in outcrop (see below). The northeasterly trending Fraser Zone (Fig. 1) contains the c. 1300 Ma Fraser Range Metamorphics, which includes the metamafic rocks previously interpreted as a layered intrusion (i.e. the Fraser Complex of Myers, 1985), and strongly deformed, high-grade metasedimentary and metagranitic rocks. The Fraser Zone is bound by the Fraser Fault and the Coramup Fault Zone at its southwestern end (Figs 13 and 14) but its boundaries along strike to the northeast are less clear and are the subject of current work. The Nornalup Zone is the southernmost unit and includes the Mesoproterozoic Malcolm Gneiss and paragneissic rocks in the Albany region. In the eastern Albany–Fraser Orogen the Salisbury Gneiss and the Mount Ragged Formation were not deposited until after Stage I tectonism and are therefore interpreted as cover rocks overlying the Nornalup Zone. The Biranup and Nornalup Zones have been intruded by granitic rocks of the c. 1330–1280 Ma

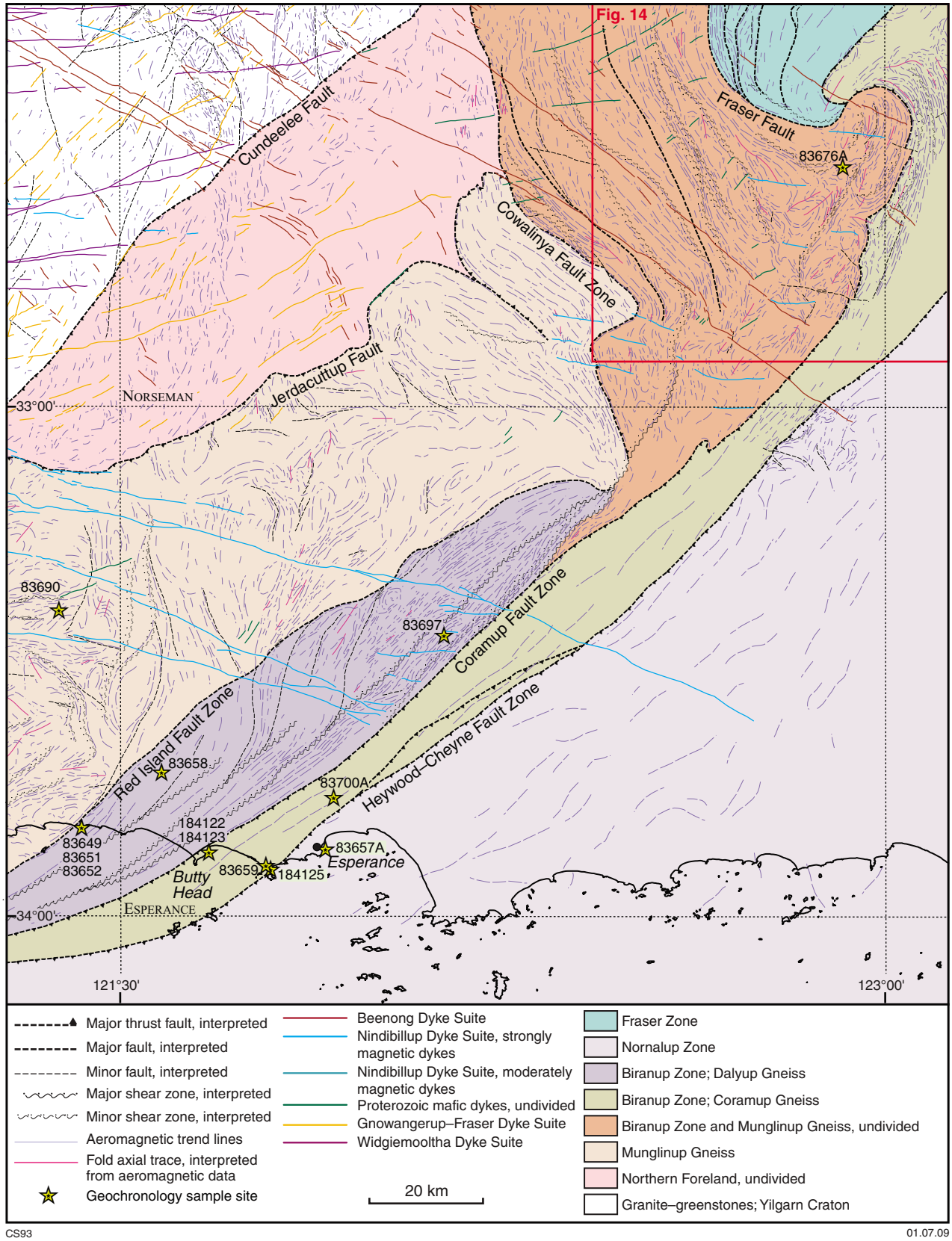

Figure 13. Structural map of Esperance, and part of Norseman, showing aeromagnetic trendlines, major and minor faults, and folds interpreted from the aeromagnetic data. The locations of geochronology samples are also shown. Extracted from the interpreted bedrock geology map in Geological Survey of Western Australia (2007).

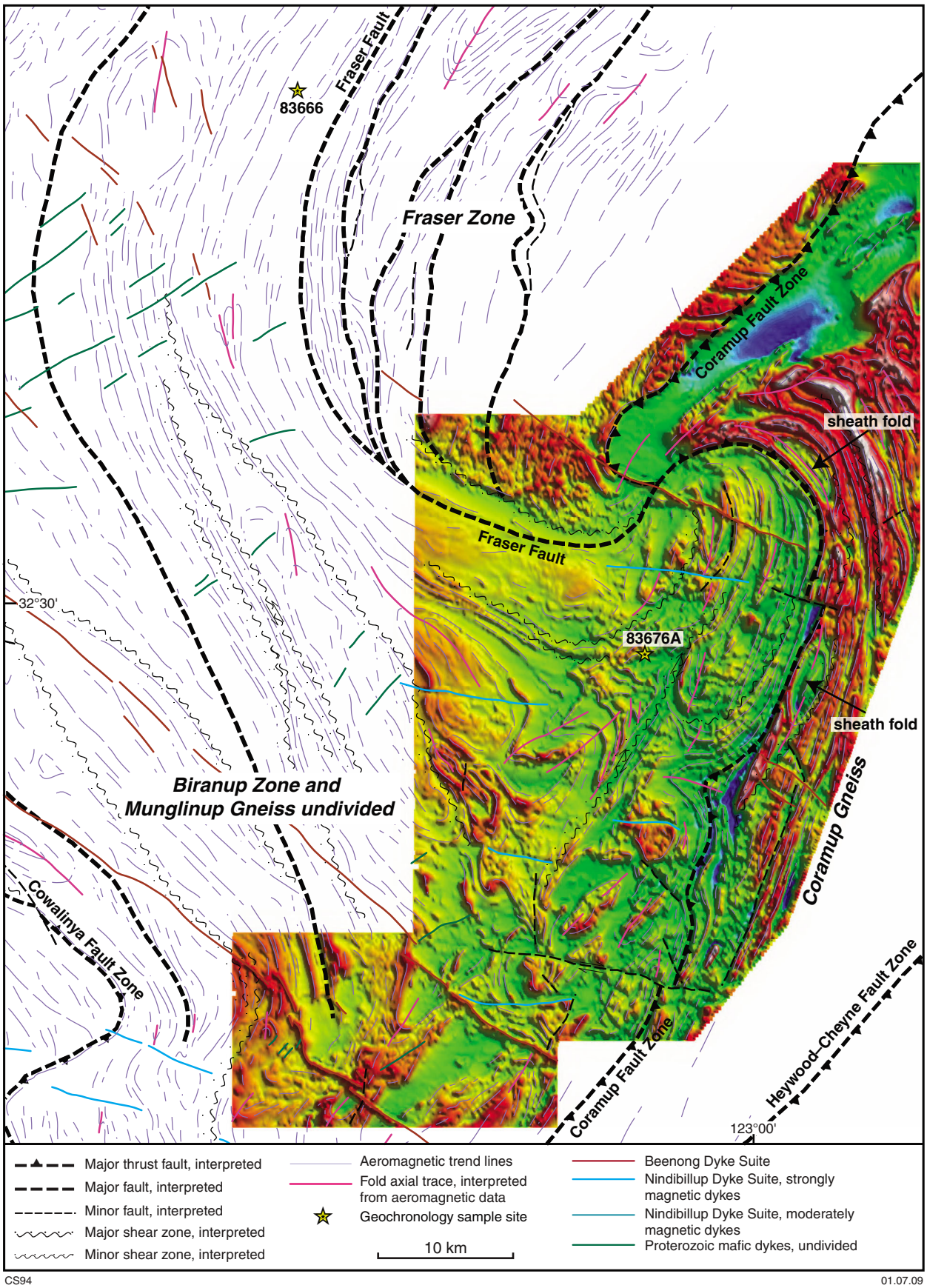
Fraser Fault
83666
Fraser Zone
Coramup Fault Zone
sheath fold
Fraser Fault
32°30'
83676A
sheath fold
Biranup Zone and
Munglinup Gneiss undivided
Coramup Gneiss
Cowalinya Fault Zone
Heywood–Cheyne Fault Zone
Coramup Fault Zone
123°00'
Major thrust fault, interpreted
Major fault, interpreted
Minor fault, interpreted
Major shear zone, interpreted
Minor shear zone, interpreted
Aeromagnetic trend lines
Fold axial trace, interpreted from aeromagnetic data
Geochronology sample site
10 km
Beenong Dyke Suite
Nindibillup Dyke Suite, strongly magnetic dykes
Nindibillup Dyke Suite, moderately magnetic dykes
Proterozoic mafic dykes, undivided
CS94
01.07.09

Recherche Supersuite (Nelson et al., 1995; Clark, 1999). Metagranitic rocks of c. 1330–1280 Ma age are also found in the Fraser Range Metamorphics in the Fraser Zone, but are not included in the Recherche Supersuite because the spatial relationships and tectonic setting in relation to the formation of the Nornalup and Biranup Zones prior to and during amalgamation are unclear, i.e. it is not known whether they represent the same magmatic event.

Biranup Zone

The Biranup Zone comprises a belt of mid-crustal rocks about 800 km long and (on average) 25 km wide, which wraps around the southern and southeastern margin of the Yilgarn Craton (Fig. 1). The main components of the Biranup Zone are the Dalyup and Coramup Gneisses, both of which are dominated by granitic rocks that have protolith ages between c. 1690–1660 Ma (Nelson et al., 1995; Bodorkos and Clark, 2004b; Geological Survey of Western Australia, 2008). Because of this, and the lack of evidence of any magmatic or tectonothermal event in the southern Yilgarn Craton at this time, the Biranup Zone is interpreted as an exotic terrane that was accreted to the southern Yilgarn Craton margin during Stage I of the Albany–Fraser Orogeny (cf. Nelson et al., 1995; Clark et al., 2000). The Dalyup and Coramup Gneisses are difficult to distinguish in outcrop and they are predominantly subdivided by the presence of paragneissic rocks in the latter. The Coramup Gneiss has previously been described as a ductile shear zone, and is a 10–20 km wide belt of strongly to intensely deformed, heterogeneous gneissic rocks (Figs 2, 13, and 14; Myers, 1995b; Bodorkos and Clark, 2004a,b; Geological Survey of Western Australia, 2007). These units were previously restricted to the eastern part of the Albany–Fraser Orogen but recent geochronological work has shown that rocks with protolith ages of c. 1680 Ma are present in the Bremer Bay area to the west (Geological Survey of Western Australia, 2008). These are assigned to the Dalyup Gneiss. Like the Munglinup Gneiss, rocks in the Biranup Zone have locally been intruded by granitic rocks at c. 1300 Ma (Recherche Supersuite; Nelson et al., 1995).

Biranup Zone rocks typically have a high magnetic signature, especially in the west (Fig. 15), and in the Bremer Bay area the Dalyup Gneiss has recorded magnetic susceptibility readings up to 42×10^{-3} SI units. The strong magnetic response appears to be primarily due to metamorphic magnetite within the granitic gneisses. The high-grade, Southdown magnetite iron-ore deposit is interpreted to lie within the Dalyup Gneiss in the Biranup Zone, and is located on a strong, linear magnetic high (Fig. 15).

Figure 14. Reduced to pole aeromagnetic image (Southern Fraser open file dataset) and structural interpretation of the southwestern end of the Fraser Zone. The image shows complex refolded folds in the Biranup Zone and Munglinup Gneiss, and high strain in the Coramup Gneiss, including interpreted large-scale sheath folds. The two geochronology sample sites shown are part of the Biranup Zone. Extracted from the interpreted bedrock geology map in Geological Survey of Western Australia (2007).

The Northern Foreland (Munglinup Gneiss) is separated from the Kepa Kurl Booya Province (Biranup Zone) by the Miller Point Thrust and the Bremer Fault to the west, which link to the Southern Ocean Shear Zone and Red Island Fault Zone to the east (Figs 2, 10, and 15; Thom and Chin, 1984; Beeson et al., 1988; Myers, 1989; Geological Survey of Western Australia, 2007). To the south, the Biranup Zone is separated from the Nornalup Zone by the Heywood – Cheyne Fault Zone. Within the Biranup Zone, the Coramup Fault Zone separates the Dalyup Gneiss from the Coramup Gneiss (Myers, 1995b; Bodorkos and Clark, 2004a,b). To the east, on Esperance, the aeromagnetic imagery shows a strongly linear pattern where the Dalyup Gneiss (and slivers of c. 1300 Ma Recherche Supersuite) are highly strained adjacent to the Coramup Fault Zone (Fig. 13). From approximately 110 km northeast of the coast, on Norseman, a complex zone of refolded folds and high strain zones is evident in the aeromagnetic imagery. At the northeastern end of this zone, the Coramup Fault Zone is folded up against the southeastern side of the Fraser Zone. Complexly interleaved Munglinup Gneiss and undivided rocks of the Biranup Zone wrap around the southwestern end of the Fraser Zone, bound by the Fraser Fault (Figs 13 and 14). Due to the structural complexity in this region, and similarity of rock types, it is difficult to distinguish Biranup Zone rocks from the Munglinup Gneiss, and they are therefore shown as undivided in the interpreted bedrock geology map (Geological Survey of Western Australia, 2007). These rocks are separated from the Northern Foreland (Munglinup Gneiss) by the Cowalinya Fault Zone, which links to the Cundeelee Fault to the north (Figs 2 and 13). It is likely that the Biranup Zone of the Kepa Kurl Booya Province extends to the northeast beyond the Ten Mile Rocks locality (GSWA 83666, Fig. 14), between the Yilgarn Craton and Fraser Zone. This is currently being investigated.

Dalyup Gneiss

The Dalyup Gneiss is the main component of the Biranup Zone and is composed of heterogeneous granitic rocks, and less abundant mafic rocks. Exposures are usually intensely deformed and metamorphosed up to granulite facies, with little preservation of original igneous textures. Rock types include granodioritic, monzogranitic, and syenogranitic gneisses, orthopyroxene-bearing granitic gneiss, quartz–magnetite gneiss, mafic gneiss, and amphibolite (Beeson et al., 1988; Nelson et al., 1995; Geological Survey of Western Australia, 2007).

Structure and metamorphism of the Dalyup Gneiss

The distinctly linear magnetic character of the Dalyup Gneiss in the western and central parts of the orogen is due to its shear-dominated structure, which includes multiple generations of coaxial, tight to isoclinal folds and dominantly high strain. This contrasts strongly with the magnetic character of the Munglinup Gneiss, which

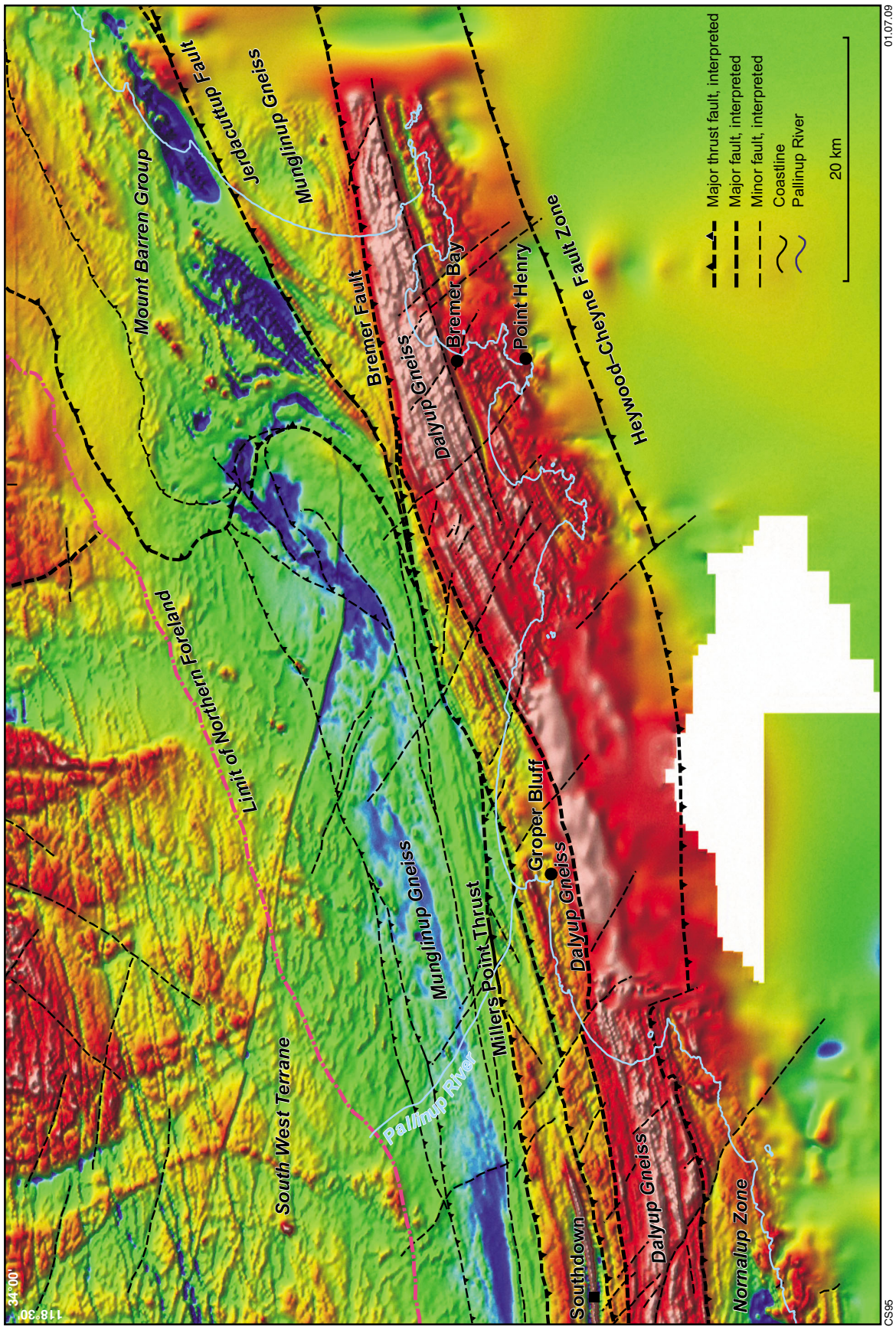

Figure 15. Reduced to pole aeromagnetic image (GSWA–GA dataset) of the northwestern part of Bremer Bay, with major structures and lithotectonic units labelled. Note the strong magnetic response of most of the Dalyup Gneiss in this region. The locality of the Pallinup River is shown, as well as the Southdown iron ore deposit, just near the western edge of Bremer Bay. Extracted from Geological Survey of Western Australia (2007).

has a well-developed refolded fold pattern cut by shears (Figs 8a,b and 10). The Coramup Gneiss has a similar, distinctly linear magnetic character but is interpreted to contain megascale sheath folds visible in 300 m line-spacing aeromagnetic data to the northeast (Fig. 14).

The Dalyup Gneiss is best exposed along the south coast, especially in the Bremer Bay region, the Pallinup River and estuary including Groper Bluff, and near Lake Gidong east of Quagi Beach (Figs 2, 10, and 13). While all of these areas exhibit high-strain, shear-dominated deformation, the Bremer Bay region is also characterized by large-scale boudinage, suggesting at least one extensional event. The Central Domain of Beeson et al. (1988) was defined along the Pallinup River and is dominated by rocks of the Dalyup Gneiss. Beeson et al. (1988) described granulite facies rocks comprising about 5% thin, discontinuous lenses of mafic granulite interlayered with 25% quartz–magnetite gneiss and 70% felsic granulite that underwent two phases of deformation. D_1 was only observed as a foliation in the hinges of D_2 folds, which are overturned to the north-northwest and have a well-developed west-southwesterly trending axial planar foliation defined by hornblende- and orthopyroxene-rich aggregates and biotite. The limbs of these folds are locally boudinaged. D_2 folds vary in style from shallowly plunging to the east-northeast or west-southwest to steeply plunging, or have highly curvilinear fold axes particularly towards the fault contact with the Northern Foreland (Miller Point Thrust and Bremer Fault). Adjacent to the fault the folds are rotated parallel to the mineral lineation (L_2), which is interpreted to reflect dextral transpression. D_2 is interpreted to have been accompanied by the formation of three sets of shear zones. The first set are small-scale, west-northwesterly trending sinistral and west-southwesterly trending dextral conjugate shears that are overprinted by a second set of small-scale northerly trending sinistral and west-northwesterly trending dextral conjugate shears that also overprint the D_2 folds and boudins. Both sets are associated with pegmatitic intrusions that infill tension gashes. The structural geometry suggests north-northwest compression. All D_2 structures were overprinted by a third set of small-scale, easterly trending sinistral shears that are more common towards to the south, and more brittle than the earlier structures (see Beeson et al. (1988) for more detail on the structure in this region).

In the Bremer Bay region the rocks are dominated by granulite-facies stromatic migmatites with lithologies that include tonalitic, granodioritic, dioritic, and orthopyroxene–clinopyroxene-bearing orthogneisses. The rocks display a complex structural history comprising up to three different phases of bidirectional boudinage, which alternate with phases of folding. Deformation was ductile and is interpreted to have taken place at mid-crustal levels. Different melts were generated and emplaced during all stages of ductile deformation and continued to migrate through the country rock after deformation ceased. Despite the abundance of partial melting, the structures show consistent orientations, geometries, and superposed relationships that can be traced for up to 12 km.

A prevalent fabric is defined by alternating leucosomes and melanosomes, and is parallel to the main compositional layering. Formation of this fabric is the earliest event recorded in this region, although locally it is observed to be axial planar to early isoclinal folds (F_1) of centimetre-wide leucosome bands. This fabric and the early folds were subsequently boudinaged, and refolded, as described below.

1. First bidirectional extension phase: small, centimetre to decimetre blocky boudins of mafic-rich layers parallel to the dominant migmatitic fabric are present throughout the entire Bremer Bay area (Fig. 16a). These boudins formed concurrently with two orthogonal directions, northwest–southeast and northeast–southwest. Leucosomes (former melt) are localized in the neck areas of these small boudins, and intermittently along the boudinaged layers.

2. Open to isoclinal, upright to recumbent folds (F_2): these fold the migmatitic foliation and the boudinaged mafic layers described above (Fig. 16b). The folds range from a few centimetres to a metre in amplitude, plunge shallowly to moderately (from 3° to nearly 40°) to the southwest, and are common throughout the Bremer Bay area.

3. Second bidirectional extension phase: intermediate-scale (less than a metre to a few metres in scale) boudins are found throughout the Bremer Bay area. The migmatitic foliation, open to isoclinally folded mafic square boudins, and locally, compositional layering, have all been boudinaged during this phase (Fig. 16c). As in the first extensional phase, these boudins formed in two orthogonal orientations, northwest–southeast and northeast–southwest, which show no crosscutting relationships. These boudins are also consistent in style and overall size throughout. Leucosomes are commonly observed concentrated in the necks of the boudins.

4. Regional, km-scale, asymmetric, northwest-verging, southwest-plunging overturned folds (F_3): These regional-scale folds have long shallow limbs and are found throughout the Bremer Bay area. They can be traced in areas where a northeast-striking and moderately to steeply southeast-dipping migmatitc foliation is exposed (corresponding to steeply dipping overturned limbs of the folds) to areas where a northwest-striking or shallowly southwest- to south-dipping migmatitc foliation is exposed (corresponding to upright, shallow-dipping limbs of the folds).

5. Third bidirectional extension phase: Large, decametre-sized boudins of the migmatitic foliation and compositional layering, oriented in orthogonal northwest–southeast and northeast–southwest directions, are present in the Bremer Bay area (Fig. 16d). They are visible only in areas that have a northwest-trending, shallow southwest-dipping migmatitic foliation, and not on the steeply dipping overturned limbs of the regional folds. As observed for the boudins of the two previous extension phases, former melts have intruded in the neck areas of these two sets of boudins.

Discrete shear zones and shear bands in a variety of orientations are observed at all scales, from 20 cm to many metres in length and centimetres to metres in

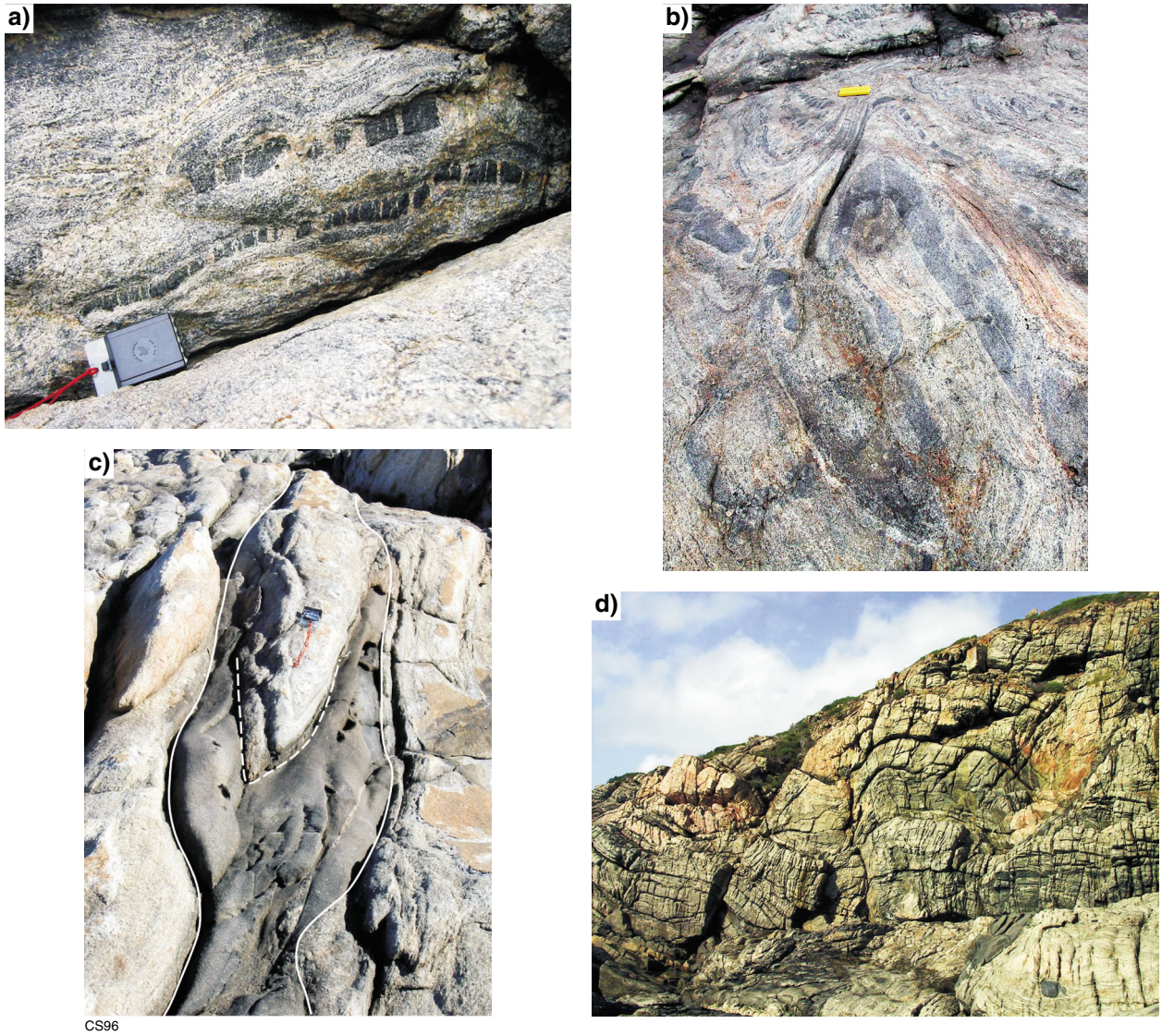

Figure 16. Structures in the Dalyup Gneiss, Biranup Zone, in the Bremer Bay region: a) early, small, square, northwesterly trending boudins of a mafic layer (first extensional phase; Zone 50, MGA 720770E 6187950N). The compass showing the scale is 10 cm long; b) open to tight D_2 folds of the dominant gneissic fabric folding early small, square to rectangular, northwesterly trending boudins of mafic layers. The hinge lines trend northeast and plunge shallowly to the southwest. The notebook showing the scale is 20 cm long. Fisheries Bay Headland (Zone 50, MGA 720855E 6187740N); c) northeast–southwest-trending boudin of a metre-wide mafic layer parallel to the main migmatitic foliation (outlined by the solid white line), which contains a tight fold of the migmatitic foliation (hinge area outlined by the dashed white line) at Banky Beach Headland. The compass showing the scale is 10 cm long (Zone 50, MGA 720765E 6187913N); d) large-scale (decametre), northwesterly trending boudins of the gneissic fabric bounded by discrete shear surfaces, Fisheries Bay Headland (third extensional phase; Zone 50, MGA 720763E 6187910N).

width. Pegmatitic material is commonly segregated along these zones and shows sharp to diffuse contacts with the country rock. Some zones show folds formed due to back rotation as described by Harris et al. (2002) and Harris (2003). Cross-cutting pegmatitic dykes vary from green plagioclase-rich, to pyroxene and white feldspar-rich, to pink K-feldspar rich compositions, with the latter typically the youngest. These late cross-cutting pegmatites occur as sets of very well-defined, close to orthogonal intrusions that strike northeast and northwest, and cut all other structures.

East of Bremer Bay, between the Red Island Shear Zone and the Coramup Fault Zone (near Lake Gidong, east of Quagi Beach, Figs 2 and 10), the Dalyup Gneiss contains heterogeneous granitic, granodioritic, and mafic phases that are strongly deformed and metamorphosed to upper amphibolite or granulite facies (Fig. 17a,b). Some of the mafic rocks appear to be remnants of mafic dykes (Fig. 17c,d). The orientations of the gneissic layering and various fold generations and associated fabrics are variable, but mostly trend north-northeast, parallel to the regional trend shown in the aeromagnetic images (Figs 10 and 13). Some of these folds are cut by mylonitic, dextral shear zones (Fig. 17e,f). Unlike in the Bremer Bay area, there are no well-developed boudins of any scale, which suggests a significant difference in kinematics. These rocks are interpreted to represent part of a mid-crustal shear zone, bound by major faults, such as the Red Island Shear Zone, which exhumed and juxtaposed them against the Northern Foreland (Munglinup Gneiss) (Figs 2, 10, and 13).

Geochronology of the Dalyup Gneiss

New SHRIMP U–Pb dating of zircons from the Dalyup Gneiss in the central Albany–Fraser Orogen has constrained granitic protolith ages to c. 1680 Ma. These ages are within uncertainty of the less precise SHRIMP U–Pb zircon dates reported in Nelson et al. (1995; see also Geological Survey of Western Australia, 2008), with the exception of GSWA 83652, which yielded a younger age of 1634 ± 26 Ma, based on a small population of 10 analyses of 6 zircons (Fig. 13). The dating by Nelson et al. (1995) showed that c. 1700 to 1600 Ma granitic precursors to gneissic rocks occur in the eastern-central part of the Kepa Kurl Booya Province. The samples yielded ages of 1671 ± 16 Ma (biotite–hornblende monzogranitic gneiss, GSWA 83651), 1692 ± 22 Ma (hornblende–biotite granodioritic gneiss, GSWA 83658), 1670 ± 15 Ma (garnet–biotite monzogranitic gneiss, GSWA 83666), and 1695 ± 16 Ma (hornblende syenogranite, GSWA 83676A; Figs 13, 14, and 18). The results imply that the Dalyup Gneiss extends northeast from the coast near Esperance, and around the southwestern end of the Fraser Zone (Fig. 14). Whether it extends the entire length of the northwestern edge of the Fraser Zone (i.e. between the Fraser Zone and the Yilgarn Craton) is unknown, but given the location of GSWA 83666 this is probable. The new dating presented here shows that the Dalyup Gneiss also extends at least as far west as the Bremer Bay region (Fig. 15).

Sample results and interpretations from recent dating are presented below. The results not only constrain the protolith ages, but also the timing of high-grade metamorphism, which mostly occurred at c. 1180 Ma, during Stage II of the Albany–Fraser Orogeny (1215–1140 Ma; Clark et al., 2000). The c. 1180 Ma age is within error of three other published dates, described below. Black et al. (1992) conducted SHRIMP U–Pb analysis on zircons from a granulite facies, quartz–plagioclase–orthopyroxene–hornblende pegmatite from Groper Bluff (Fig. 15), west of Bremer Bay, which intruded the host felsic gneiss at an early stage of its structural history. The low uranium contents of the pegmatite zircons led Black et al. (1992) to present the $^{206}Pb^*/^{238}U$ date of 1196 ± 8 Ma as the most robust (and precise) estimate of the igneous crystallization age, but the data indicate a slight degree of reverse discordance in their results, and we regard the less precise $^{207}Pb^*/^{206}Pb^*$ date of 1165 ± 28 Ma as a more conservative estimate of the crystallization age of the pegmatite. That date is also similar to the SHRIMP U–Pb zircon date of 1187 ± 12 Ma from a late-stage, folded pegmatite from west of Esperance (south of Lake Gidong), interpreted as the age of crystallization of the pegmatite (GSWA 83649; Fig. 13; Nelson, 1995f). Although the exact location of the pegmatite is unknown a field sketch shows that it is similar to the pegmatite shown in Figure 17a, and has experienced the same major folding episode as the host rocks, most likely during Stage II, and possibly not long after its intrusion (Fig. 19). Other evidence of Stage II deformation in the Dalyup Gneiss comes from two SHRIMP U–Pb zircon rim analyses from granulite facies, isoclinally folded, hornblende syenogranitic gneiss from the structurally complex region southwest of the Fraser Zone (GSWA 83676A; Fig. 14; Nelson, 1995g). The rim gave a $^{207}Pb^*/^{206}Pb^*$ mean age of 1184 ± 12 Ma, interpreted as a metamorphic age (Nelson, 1995g).

Rocks dated in the Bremer Bay area include orthopyroxene–clinopyroxene orthogneiss, granodioritic gneiss, and granodioritic and leucocratic pegmatites from boudin necks (Table 1). Orthopyroxene–clinopyroxene-bearing orthogneiss with well-developed differentiated layering from Fisheries Bay headland yielded a SHRIMP U–Pb zircon igneous crystallization age of 1680 ± 7 Ma (GSWA 184311; Figs 20a and 21a; Table A5; Bodorkos and Wingate, 2008e). The orthogneiss has been affected by the third extensional phase that produced large-scale boudinage (Fig. 16d), and the boudin necks are filled by abundant coarse-grained leucocratic granodiorite, of which GSWA 184310 (Bodorkos and Wingate, 2008f) is representative (Fig. 20b). The leucocratic granodiorite (GSWA 184310; Figs 20b and 21b; Table A6) has a granuloblastic texture with plagioclase crystals up to 8 mm in length, and comprises approximately 55% quartz, 35% plagioclase, 5% K-feldspar, 5% biotite, and accessory sulfide minerals and zircon (Bodorkos and Wingate, 2008f). Zircons from this sample are up to 800 μm long, with aspect ratios up to 3:1, and display a wide range of cathodoluminescence (CL) emission patterns. Cores with very low CL emission and either concentric zoning or chaotic structure are common, as are conformable rims with bright CL emission and oscillatory zoning. The sample yielded a weighted mean date of 1178 ± 3 Ma from 29 analyses of 22 zircons, characterized by a wide range of crystal morphologies (cores and rims), CL emissions

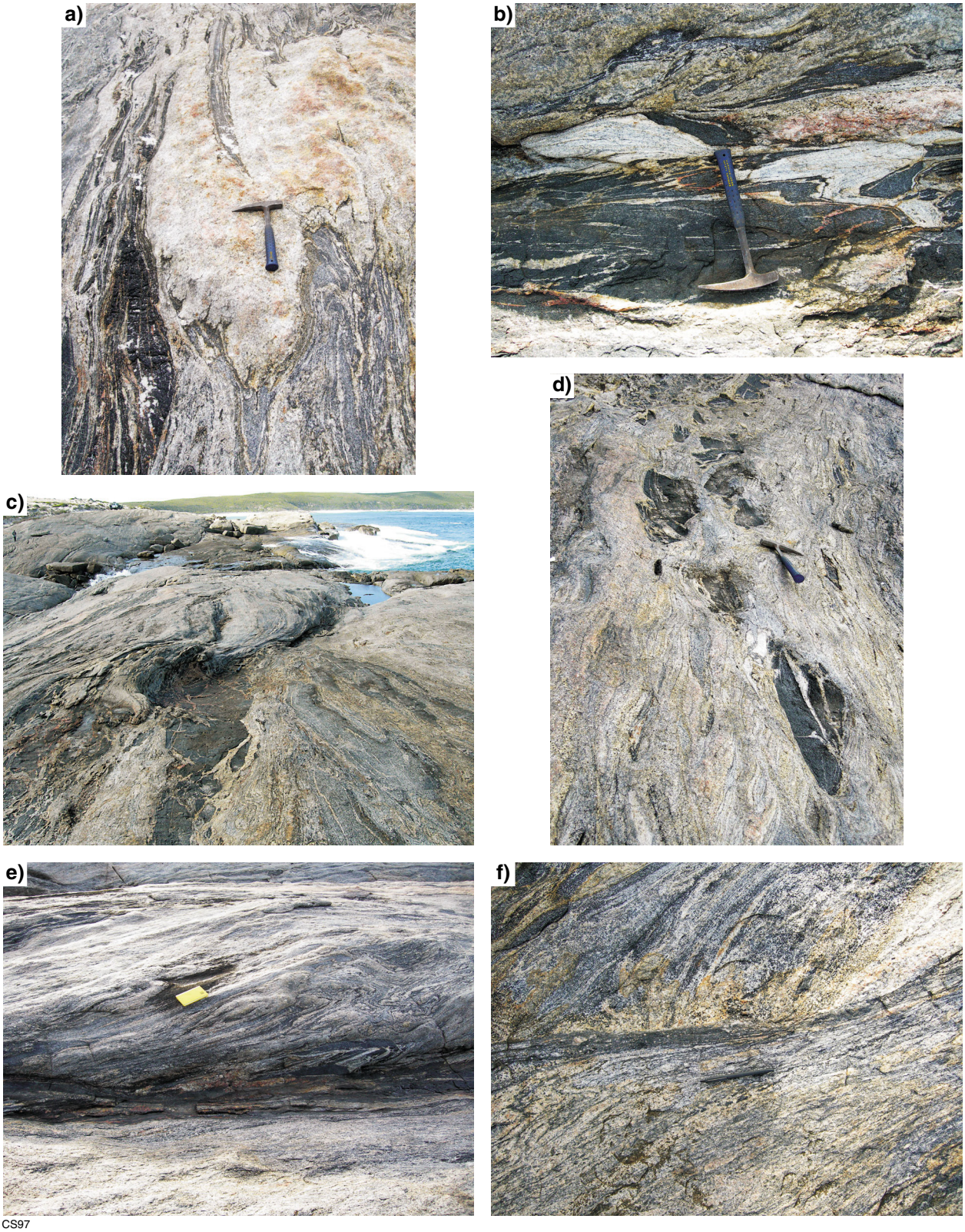

Figure 17. Photographs of the Dalyup Gneiss, Biranup Zone, east of the Red Island Fault Zone, coastal headland south of Lake Gidong (Zone 51, MGA 354671E 6255801N): a) complex heterogeneous phase relationships of granitic gneiss, mafic gneiss, and intrusive folded pegmatite; b) heterogeneity and strong deformation of granitic and mafic gneisses; c) inferred mafic dyke remnant in heterogeneous granitic and mafic gneiss. The dyke is cut by a dextral shear, close to where the hammer is in the centre of the photo. Note also the person in the upper left corner for scale of the exposure; d) inferred mafic dyke remnants in strongly deformed granitic gneiss; e) mylonite zone with dextral shear sense cutting gneissic fabric and earlier folds; f) detail of mylonite zone with dextral shear sense cutting gneissic fabric and earlier folds.

Table 1. Summary of geochronology and related structures in the Bremer Bay area

Locality	*Sample*	*Lithology*	*Age (Ma)*	*Interpretation*	*Deformation event*	*Relationship to other samples*
Fisheries Bay headland	GSWA 184311	Orthopyroxene–clinopyroxene-bearing orthogneiss	1680 ± 7	Igneous crystallization age of protolith	–	Host to GSWA 184310
Short Beach headland	GSWA 184312	Granodioritic gneiss	1689 ± 11	Igneous crystallization age of protolith	–	Host to GSWA 184326
Point Henry	GSWA 184119	Leucocratic monzogranitic gneiss	1670 ± 12	Minimum age of igneous crystallization of protolith	–	Host to GSWA 184307
Short Beach headland	GSWA 184312	Granodioritic gneiss	1154 ± 25	High-grade metamorphism	Within uncertainty of second and third extensional phases	Host to GSWA 184326
Point Henry	GSWA 184119	Leucocratic monzogranitic gneiss	1178 ± 4	High-grade metamorphism	Within uncertainty of second and third extensional phases	Host to GSWA 184307
Point Henry	GSWA 184307	Pegmatitic granodiorite	1187 ± 5	Igneous crystallization age of protolith	M-scale, NE-trending boudins formed during the second phase of extension	Intrudes GSWA 184119 in boudin neck
Point Henry	GSWA 184307	Pegmatitic granodiorite	1172 ± 16	High-grade metamorphism	M-scale, NE-trending boudins formed during the second phase of extension	Intrudes GSWA 184119 in boudin neck
Fisheries Bay headland	GSWA 184310	Leucocratic granodiorite	1178 ± 3	Both igneous crystallization age of granodiorite and high-grade metamorphism	Dm-scale, NW-trending boudins formed during the third phase of extension	Intrudes GSWA 184311 in boudin neck
Short Beach headland	GSWA 184326	Pegmatitic leucogranite	1148 ± 9	Igneous crystallization age of protolith	M-scale, NE-trending boudins formed during the second phase of extension, but interpreted to be a later intrusion	Intrudes GSWA 184312 in boudin neck; within uncertainty of high-grade metamorphism date in host

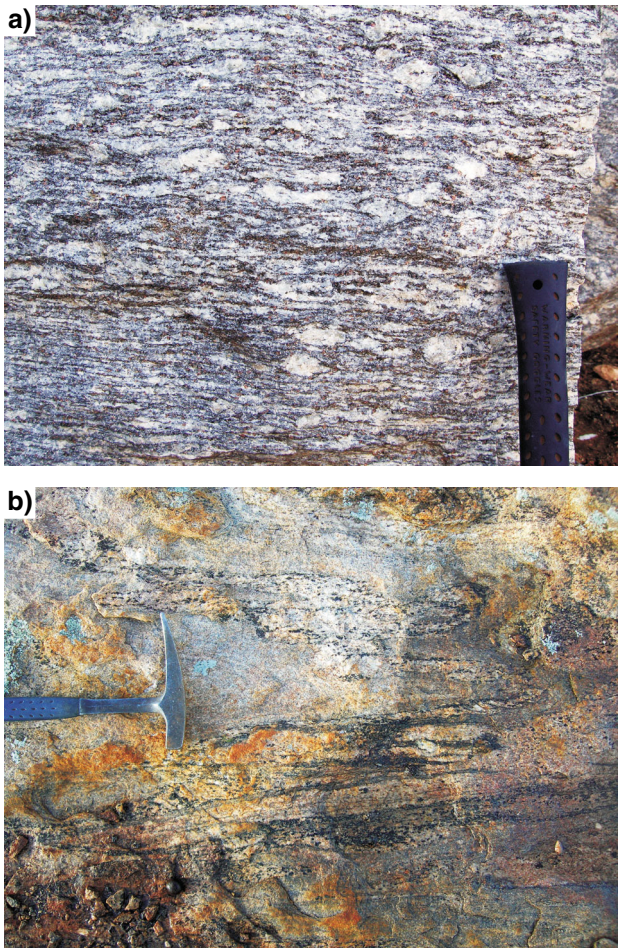

CS98

Figure 18. **(above) Previously dated Dalyup Gneiss, Biranup Zone: a) banded and strongly foliated garnet–biotite metamonzogranite, representative of GSWA 83666; Garnet Ice dimension stone quarry near Ten Mile Rocks (Zone 51, MGA 468777E 6450787N). Photograph courtesy of Mark Pawley; b) banded orthogneiss with sparse small to medium K-feldspar phenocrysts representative of GSWA 83676A. The main foliation is axial planar to the isoclinal folds of early leucosome and layering. North of Mount Andrew, Mount Andrew Track (Zone 51, MGA 491769E 6400828N).**

CS99

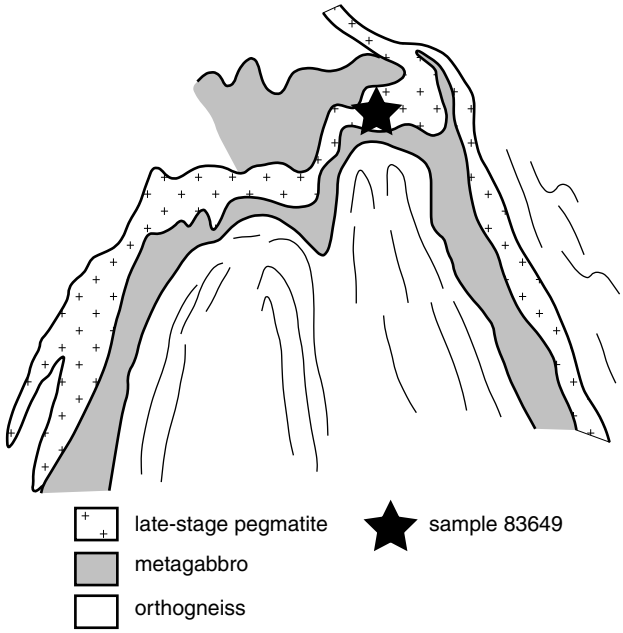

Figure 19. **(right) Field notebook sketch of late-stage pegmatite sample site GSWA 83649, Dalyup Gneiss, coastal headland south of Lake Gidong. Sketch traced from D Nelson's notebook, drawn on 28 March 1990. The exact location of the outcrop is unknown, and no scale was given. The photograph shows the what is inferred to be a similar outcrop from the same headland (Zone 51, MGA 354671E 6255801N, see also Fig. 17). The hammer is resting on the late-stage pegmatite.**

(very high to very low, with and without oscillatory zoning), uranium contents (55–2402 ppm), and Th/U ratios (0.03–2.12). The diversity of the constituent zircons suggests that this date should be interpreted as both an igneous crystallization age for the granodiorite, and the best estimate of the age of broadly synchronous high-grade metamorphism (Bodorkos and Wingate, 2008f). It is also the best estimate for the age of the third phase of extension related to the large-scale, bi-directional boudinage.

Granodioritic gneiss at Short Beach headland yielded a SHRIMP U–Pb zircon igneous crystallization age of 1689 ± 11 Ma, which is within error of the orthopyroxene–clinopyroxene orthogneiss at Fisheries Bay headland (GSWA 184312; Figs 20c and 21c; Table A7; Bodorkos and Wingate, 2008g). The granodioritic gneiss is medium-grained, seriate to locally porphyritic, and strongly foliated and hosts layers of mafic granulite that probably represent the remnants of an early dyke suite. Both rock types have been affected by medium-scale boudinage related to the second extensional phase. These boudins are northwesterly trending, and their necks are filled by coarse-grained, little-deformed leucogranite, of which GSWA 184326 (Bodorkos and Wingate, 2008h) is representative. The host rock GSWA 184312 also yielded a date of 1154 ± 25 Ma from zircon rims and discrete grains (Group 2, Table A7), which is interpreted as the best estimate of the age of high-grade metamorphism. The four zircon core analyses in Group 3 (Table A7), which yielded dates of 2510–1747 Ma, are interpreted to be of xenocrystic zircons physically entrained by the granodioritic magma prior to igneous crystallization (Bodorkos and Wingate, 2008g).

The pegmatitic leucogranite (GSWA 184326) is from a boudin neck within a foliated mafic granulite (Fig. 20d), which in turn is hosted by strongly foliated granodioritic gneiss of which GSWA 184312 (Bodorkos and Wingate, 2008g) is representative. The pegmatite comprises approximately 55% plagioclase, 20% microcline, 10% quartz, 10% hornblende, 3–5% biotite, and accessory opaque oxide minerals and zircon (Bodorkos and Wingate, 2008h). SHRIMP U–Pb analysis of zircon rims and discrete grains yielded a date of 1148 ± 9 Ma, which is interpreted as the age of igneous crystallization of the leucogranite (Group 1; Fig. 21d; Table A8). The age of 1154 ± 25 Ma for the high-grade metamorphic event from the granodioritic gneiss (GSWA 184312; Bodorkos and Wingate, 2008g) is indistinguishable from the igneous crystallization age of 1148 ± 9 Ma inferred for the leucogranite within the boudin neck, although the unmetamorphosed character of the leucogranite suggests that the formation of the northeast-trending boudin necks post-dated high-grade metamorphism of the host rocks. Analysis of zircon cores yielded a date of 1664 ± 12 Ma (Group 3; Fig. 21d; Table A8) and is interpreted as the age of igneous crystallization of a dominant xenocrystic zircon component physically entrained by the leucogranitic magma prior to igneous crystallization (Bodorkos and Wingate, 2008h). This age is slightly younger than the igneous crystallization age of 1689 ± 10 Ma determined for the host granodioritic gneiss (GSWA 184312; Bodorkos and Wingate, 2008g). This suggests that either minor ancient loss of radiogenic Pb is widespread in the leucogranite-hosted xenocrysts, or that the xenocrysts entrained by the leucogranite were not derived directly from its current host rocks (Bodorkos and Wingate, 2008h).

South of Bremer Bay, at Point Henry (Fig. 15) leucocratic monzogranitic gneiss contains elongate lenses (up to five metres wide) of medium- to coarse-grained and gneissic mafic granulite as medium-scale, northeasterly trending boudins that are orthogonal to those at Short Beach, and the boudin necks are filled by very coarse-grained, little-deformed granodiorite, of which GSWA 184307 (Fig. 20e) is representative. Boudinage of the mafic granulite is asymmetric, indicating dextral extensional shear, and intrafolial isoclinal folds are developed in the adjacent monzogranitic gneiss (Fig. 20f,g). Patches of pegmatitic granodiorite occur within both the gneiss and the mafic granulite, and all structures, fabrics, and rock types are affected by localized development of tight, mesoscopic folds. SHRIMP U–Pb zircon dating of the leucocratic monzogranitic gneiss yielded a minimum age for igneous crystallization of the monzogranitic precursor of 1670 ± 12 Ma (GSWA 184119; Fig. 21e; Table A9; Bodorkos and Wingate, 2008i). The eight analyses in Group 1 are characterized by a high degree of internal scatter (MSWD = 2.4), possibly due to minor ancient loss of radiogenic Pb from some of the zircons that yielded $^{207}Pb^*/^{206}Pb^*$ dates at the younger end of the spectrum. Consequently, the date of 1670 ± 12 Ma for Group 1 is interpreted as a minimum age. The date of 1178 ± 4 Ma for the 14 analyses in Group 2 is interpreted as the age of the high-grade metamorphic event responsible for zircon rim growth (Bodorkos and Wingate, 2008i).

SHRIMP U–Pb zircon dating of the pegmatitic granodiorite (Fig. 20e; GSWA 184307) from a boudin neck at Point Henry related to the second extensional phase yielded an igneous crystallization age of 1187 ± 5 Ma, interpreted from the 10 zircon core analyses in Group 1 (Fig. 21f; Table A10; Bodorkos and Wingate, 2008j). A date of 1172 ± 16 Ma for the 16 analyses in Group 2 is interpreted as the age of a high-grade metamorphic event responsible for the formation of thick rims mantling magmatic zircon cores, and also new growth of discrete zircons. The date of 1172 ± 16 Ma attributed to high-grade metamorphism of the pegmatitic granodiorite is indistinguishable from the date of 1178 ± 4 Ma ascribed to high-grade metamorphism of the host monzogranitic gneiss (GSWA 184119). This indicates that both igneous phases were metamorphosed during the same tectonothermal event (Bodorkos and Wingate, 2008j).

All dates of high temperature metamorphism and crystallization of pegmatitic material within boudin necks in the Bremer Bay region are within uncertainty of 1182–1179 Ma, with the exception of the pegmatitic leucogranite from Short Beach headland (GSWA 184326). As explained above, this pegmatitic leucogranite may have formed after the high grade metamorphism of the host rocks, possibly as a late intrusion into a pre-existing, second extensional phase boudin neck as the 1148 ± 9 Ma age is younger than those of the second and third phases dated elsewhere. The dating of the leucocratic material from boudin necks related to the second and third extensional phases at Point Henry and Fisheries Bay headland, respectively, shows

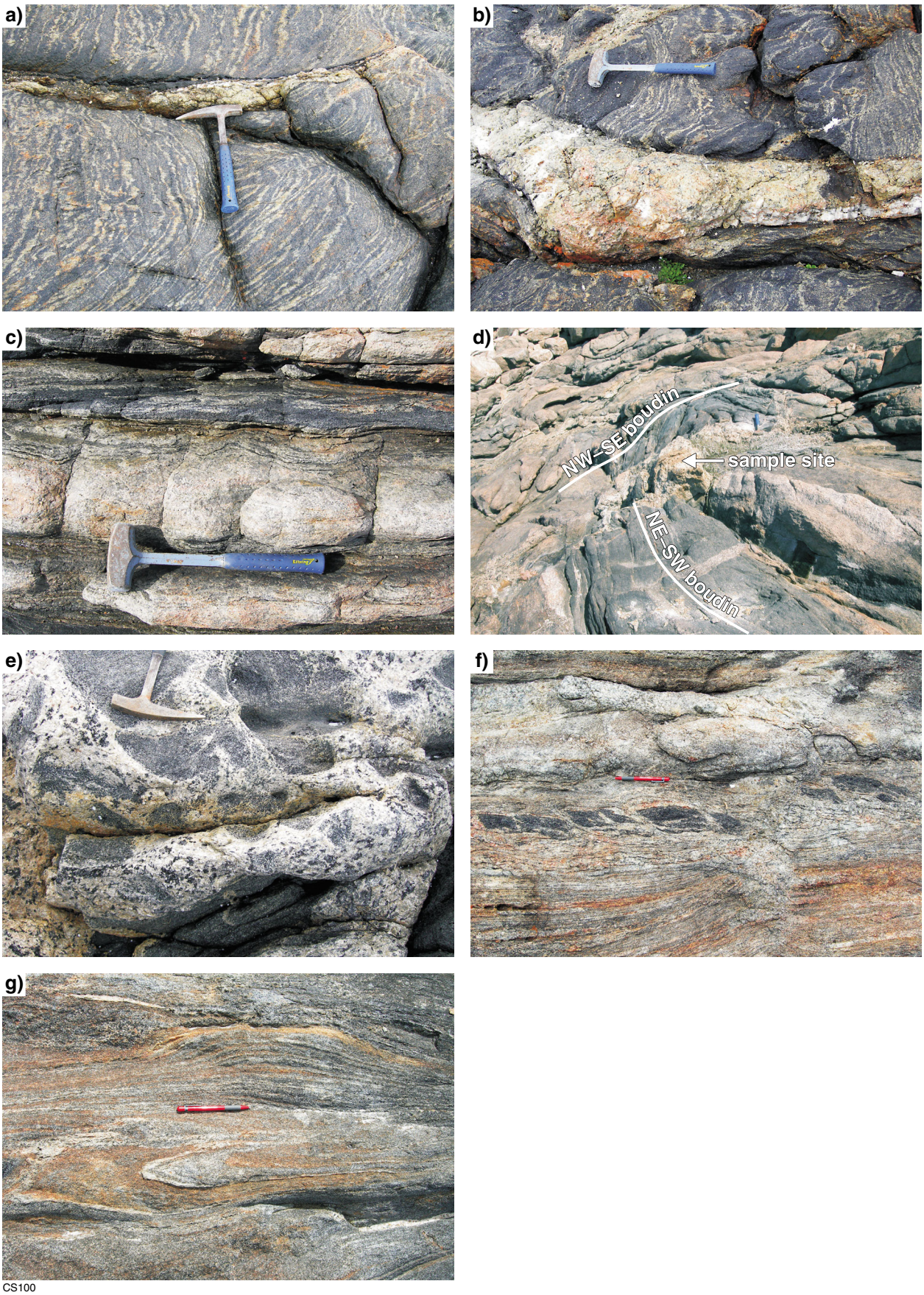

CS100

that intrusion of this material and extension occurred between c. 1190 and 1180 Ma, coincident with the high-grade metamorphism (Table 1). This indicates that the large-scale, regional F_3 folding event, (that is bracketed by the second and third extensional phases) also occurred at this time, but the first extensional phase and first two folding events are older. All U–Pb zircon metamorphic dates obtained from the Bremer Bay area correspond to Stage II of the Albany–Fraser Orogeny (Clark et al., 2000). No evidence of metamorphism relating to Stage I of the Albany–Fraser Orogeny was identified, which suggests that all three phases of extension and folding occurred during Stage II.

Crustal evolution of the Dalyup Gneiss

Black et al. (1992) interpreted early crustal formation to have taken place in the Dalyup Gneiss (Central Domain of Beeson et al. (1988)) at c. 3110 Ma. This was based on poorly constrained dates of inherited zircon in two samples (pegmatite and felsic gneiss) from Groper Bluff and the nearby Pallinup Estuary (Fig. 15), but Sm–Nd model ages from these rocks is consistent with this interpretation (Black et al., 1992). In contrast, early crustal formation of the western Nornalup Zone (Southern Domain of Beeson et al. (1988)) was interpreted to have taken place at c. 2.25 Ga (T_{DM}), based on Sm–Nd model ages of three samples, and supported by data from Fletcher et al. (1983). Sm–Nd T_{dm} model ages reported from the Biranup Zone are 2210 Ma and 2310 Ma (GSWA 83651 and GSWA 83666, respectively; Nelson et al., 1995). A Recherche Supersuite granite within the Biranup Zone yields a T_{dm} model age of 2070 Ma (GSWA 83697; Nelson et al., 1995).

Only four xenocrystic zircons have been found in the precursor rocks to the Dalyup Gneiss in the current geochronology study, and none in that of Nelson et al. (1995). Therefore it is difficult to independently assess the significance of the Sm–Nd model ages of Black et al. (1992) and Nelson et al. (1995), although the four xenocrystic zircons are Paleoproterozoic and do fit with the model ages of Nelson et al. (1995) (see above; granodioritic gneiss from Short Beach headland, GSWA 184312). Our U–Pb data, and that of Nelson et al. (1995), indicate that the igneous precursors to the Dalyup Gneiss formed via magmatic crystallization between 1690–1660 Ma. However, the Sm–Nd data most likely indicate that the precursors had some crustal contamination from older, Paleoproterozoic sources, or are products of mixing of different source rocks (see also Nelson et al., 1995). This is supported by negative ε_{Nd} values of -5.0, -4.0, and -3.8 for the three samples listed above (Nelson et al., 1995), and -15.8, -15.4, and -18.3 for the c. 1190 Ma felsic gneiss and pegmatite reported in Black et al. (1992). These data indicate a substantial component of crustal contamination during formation of the igneous precursors.

Figure 20. Photographs of dating sites of the Dalyup Gneiss, Bremer Bay region: a) orthopyroxene–clinopyroxene orthogneiss from Fisheries Bay headland. The layering in the orthogneiss has a strike of 140, diping 45° to the southwest, parallel to the stretching direction of large-scale boudins in this area. Sample GSWA 184311 was taken 1.5 m from here (Zone 50, MGA 720773E 6187931N); b) coarse-grained, leucocratic granodiorite from a large-scale boudin neck in orthopyroxene–clinopyroxene orthogneiss (as in (a)) from Fisheries Bay headland. Sample site GSWA 184310 (Zone 50, MGA 720773E 6187931N); c) typical boudinaged granodioritic gneiss at Short Beach headland, where sample GSWA 184312 was collected (Zone 50, MGA 720437E 6186221N). The sample was taken from the leucocratic layer in the centre of the photo, above the sledge hammer; d) pegmatitic leucogranite intruded into the neck of an intermediate-size (~2 m) northeasterly trending boudin in a mafic gneiss layer within granodioritic gneiss at Short Beach northern headland, where sample GSWA 184326 was collected (Zone 50, MGA 720546E 6186078N). Northwesterly trending boudins of the same mafic layer and migmatitic fabric in the granodiorite gneiss are interpreted as coeval; e) very coarse-grained pegmatitic granodiorite in the neck of a medium-scale boudin within mafic granulite and monzogranitic gneiss at Point Henry (Zone 50, MGA 719139E 6181985N). The granodiorite is representative of sample GSWA 184307; f) asymmetric boudinage of mafic granulite in monzogranitic gneiss. The latter is representative of sample GSWA 184119, collected at Point Henry (Zone 50, MGA 719139E 6181985N); g) intrafolial folds in monzogranitic gneiss, representative of sample GSWA 184119, collected at Point Henry (Zone 50, MGA 719139E 6181985N).

Coramup Gneiss

The Coramup Gneiss is separated from the Dalyup Gneiss by the Coramup Fault Zone, and from the Nornalup Zone to the southeast by the Heywood–Cheyne Fault Zone (Figs 2, 13, and 14; Myers, 1995b; Bodorkos and Clark, 2004a,b; Geological Survey of Western Australia, 2007). Unlike the Dalyup Gneiss, the Coramup Gneiss contains both orthogneisses and paragneisses. The Coramup Gneiss is poorly exposed and most work has focused on the coastal exposures west of Esperance. Rock types include finely layered granitic to granodioritic gneiss, tonalitic gneiss (including a pyroxene-bearing variety), lenses and boudins of metamorphosed mafic rocks, quartz-rich psammite, minor migmatitic metapelite, and rare, thin boudins of calc-silicate rocks (Bodorkos and Clark, 2004a,b). The Coramup Gneiss has been described as a zone of high strain rocks (Bodorkos and Clark, 2004a,b) and this evidently continues northeast of the coast where sheath folds can be interpreted in the aeromagnetic images (Fig. 14). In outcrop these rocks are metagranite L-tectonites with a strong rodding fabric defined by quartz and biotite, and aligned K-feldspar (Fig. 22a,b).

Structure and metamorphism of the Coramup Gneiss

Exposures of the Coramup Gneiss on the coast west of Esperance have yielded detailed information about their structural and metamorphic history (Bodorkos and Clark, 2004a,b). During Stage I of the Albany–Fraser Orogeny

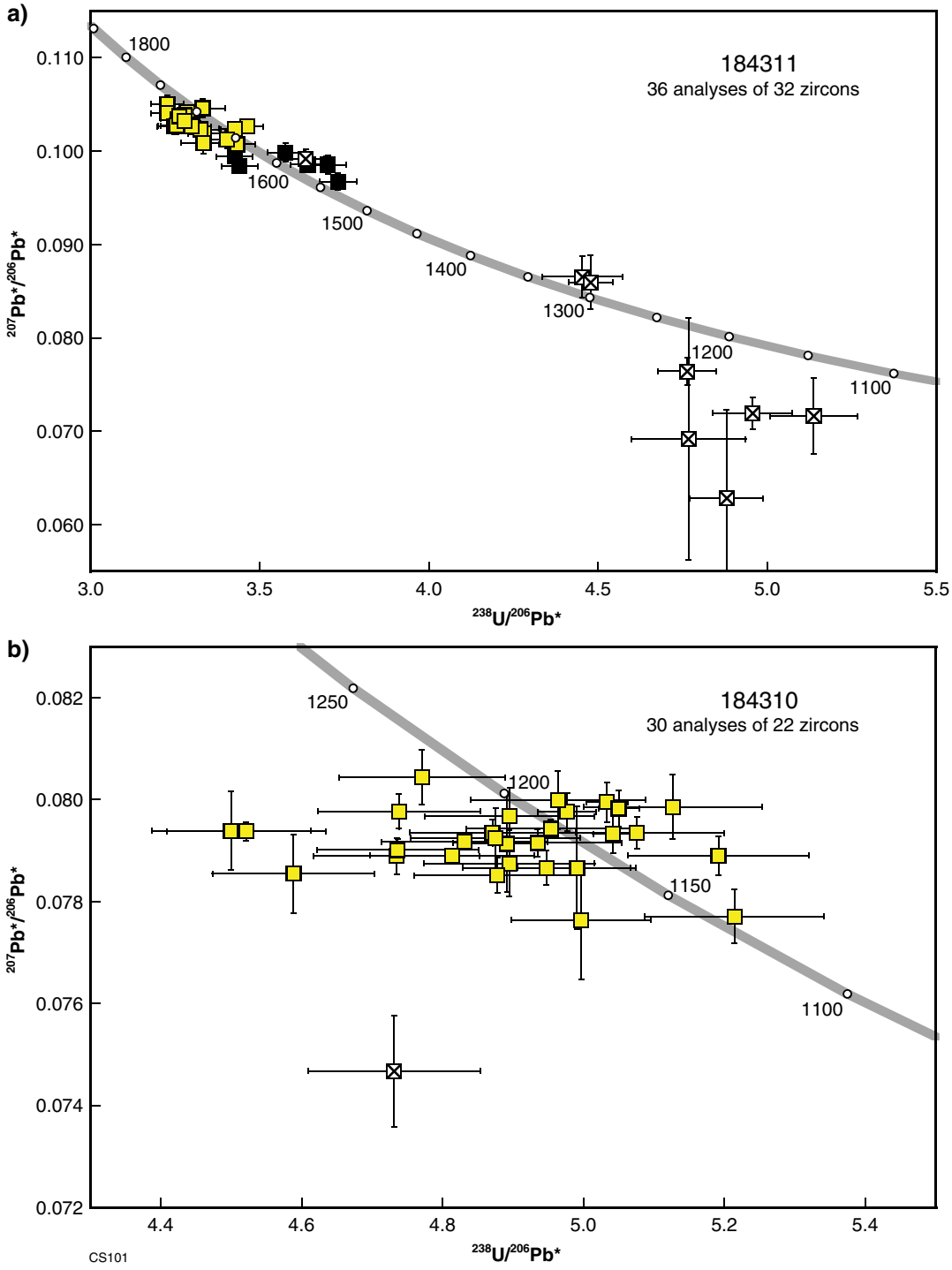

Figure 21. a) U–Pb analytical data for sample GSWA 184311: orthopyroxene–clinopyroxene orthogneiss, Fisheries Bay headland (Zone 50, MGA 720773E 6187931N). Yellow squares denote Group 1 (igneous crystallization); black squares denote Group 2 (affected by ancient loss of radiogenic Pb); crossed squares indicate ungrouped analyses (f204 > 0.6% or discordance <–10%); b) U–Pb analytical data for sample GSWA 184310: leucocratic granodiorite, Fisheries Bay headland (Zone 50, MGA 720773E 6187931N). Yellow squares denote Group 1 (igneous crystallization and high-grade metamorphism); crossed square indicates ungrouped analysis (discordance <–15%);

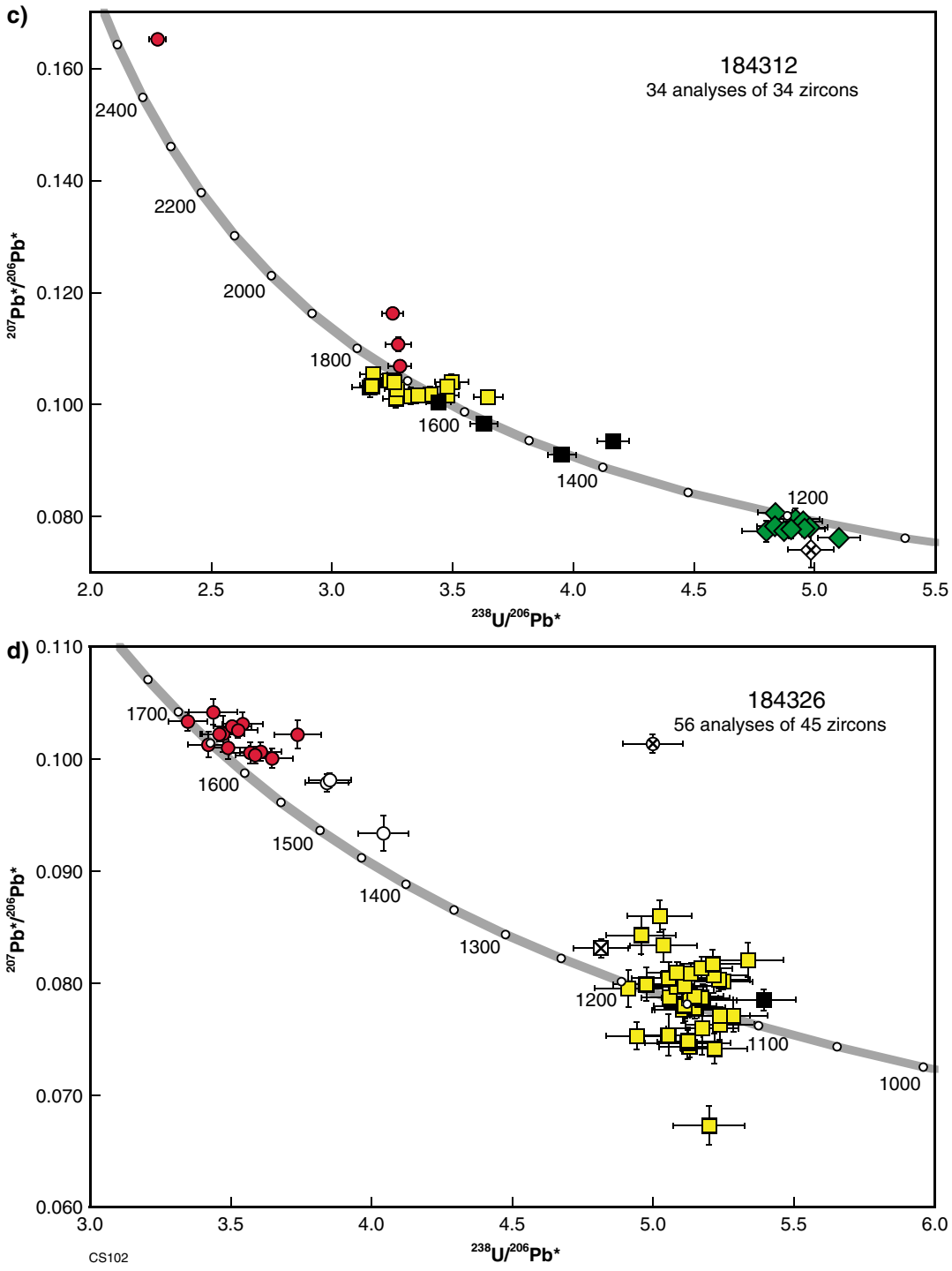

Figure 21. c) U–Pb analytical data for sample GSWA 184312: granodioritic gneiss, Short Beach headland (Zone 50, MGA 720437E 6186221N). Yellow squares denote Group 1 (igneous crystallization); green diamonds denote Group 2 (high-grade metamorphism); red circles denote Group 3 (xenocrystic zircons); black squares denote Group 4 (magmatic zircons affected by ancient loss of radiogenic Pb); crossed diamond indicates ungrouped analysis (*f*204 >1%); d) U–Pb analytical data for sample GSWA 184326: pegmatitic leucogranite, Short Beach headland (Zone 50, MGA 720546E 6186078N). Yellow squares denote Group 1 (igneous crystallization); black square denotes Group 2 (magmatic zircon affected by radiogenic Pb loss); red circles denote Group 3 (dominant xenocrystic component); white circles denote Group 4 (xenocrystic zircons affected by loss of radiogenic Pb loss); crossed circle denotes ungrouped xenocrystic core (discordance >10%); crossed squares denotes core-rim overlap;

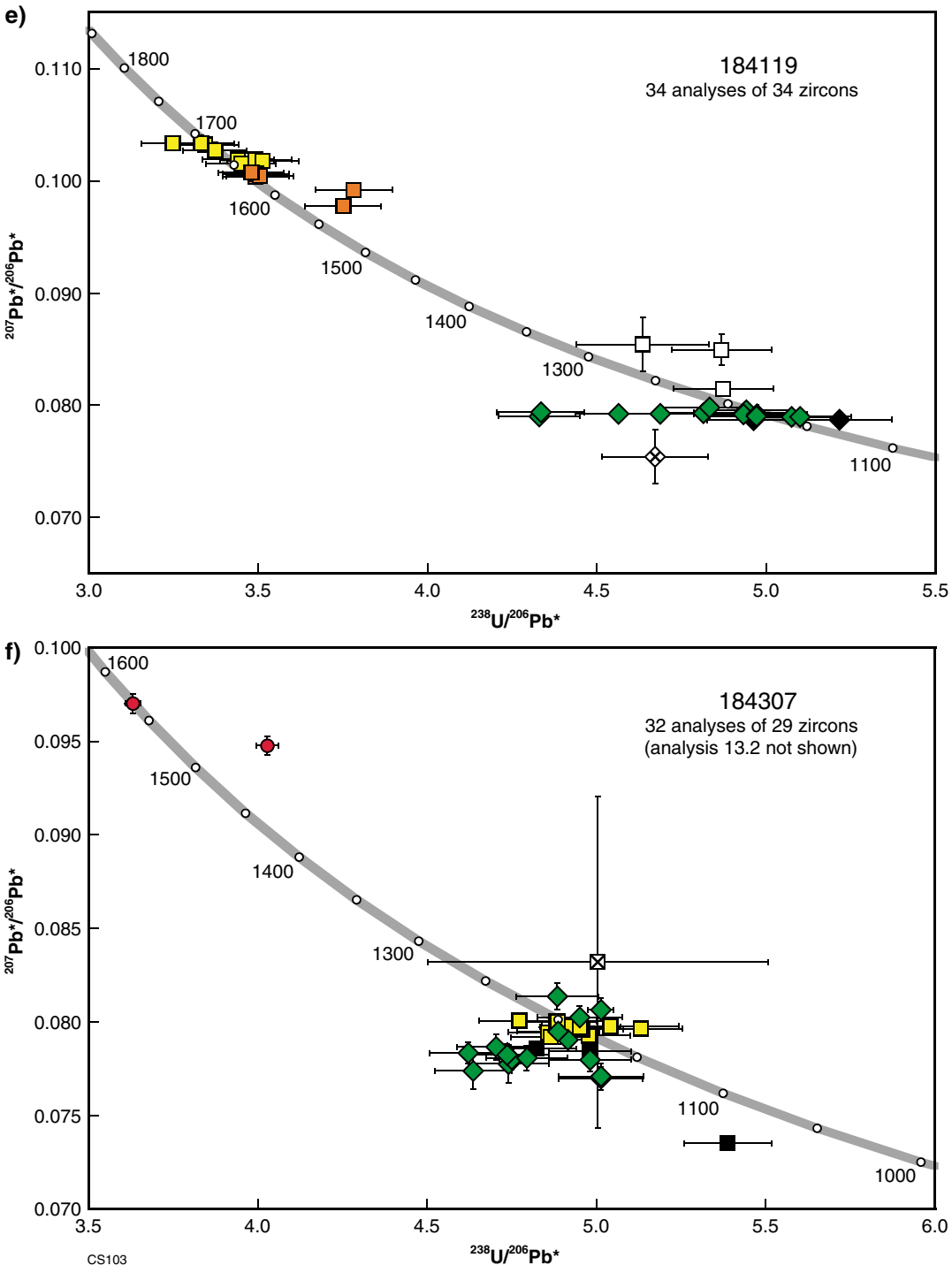

Figure 21. e) U–Pb analytical data for sample GSWA 184119: monzogranitic gneiss, Point Henry (Zone 50, MGA 719139E 6181985N). Yellow squares denote Group 1 (magmatic zircon cores); green diamonds denote Group 2 (metamorphic zircon rims); orange squares denote Group 3 (magmatic zircons affected by minor ancient loss of radiogenic Pb); white squares denote Group 4 (magmatic zircons recrystallized during high-grade metamorphism); black diamonds denote Group 5 (metamorphic zircon rims affected by loss of radiogenic Pb); crossed diamond indicates ungrouped analysis (f204 >2%); f) U–Pb analytical data for sample GSWA 184307: pegmatitic granodiorite, Point Henry (Zone 50, MGA 719234E 6182133N). Yellow squares denote Group 1 (igneous crystallization); green diamonds denote Group 2 (high grade metamorphism); red circles denote Group 3 (xenocrystic cores); black squares denote Group 4 (igneous crystallization; affected by ancient loss of radiogenic Pb); crossed square indicates ungrouped analysis (f204 >3%).

(1345–1260 Ma; Clark et al., 2000) the Coramup Gneiss underwent three stages of high-grade metamorphism, with the first stage interpreted to have taken place at c. 1300 Ma, recording peak conditions of 800–850°C and 5–7 kbar and formation of a subhorizontal gneissosity during extension (Bodorkos and Clark, 2004a,b). The second stage, interpreted to have taken place at c. 1290 Ma, recorded similar temperatures but higher pressures (about 10 kbar) during burial and recrystallization, and transposition of the gneissosity into southeast-dipping shear zones. This was accompanied by tight, recumbent, asymmetrical folding indicating northwest-vergent thrusting (Bodorkos and Clark, 2004a,b). These two stages were followed by decompression recording temperatures of 700–800°C and pressures of 7–8 kbar, and the subsequent intrusion of Recherche Supersuite sills at 1290–1280 Ma (Nelson et al., 1995; Bodorkos and Clark, 2004a,b).

High temperature, moderate- to low-pressure metamorphism (750–800°C and 5–6 kbar) and the formation of steeply southeast-dipping dextral shear zones, a shallowly southwest-plunging mineral lineation, and northwest-vergent folding took place during Stage II of the Albany–Fraser Orogeny (1215–1140 Ma; Clark et al., 2000; Bodorkos and Clark, 2004a,b). This is constrained by the emplacement of a syn-kinematic pegmatite at 1168 ± 12 Ma (Bodorkos and Clark, 2004b). Late, sinistral mylonite zones and psuedotachylites are correlated with similar structures in the eastern Nornalup Zone that postdate intrusion of the c. 1140 Ma Esperance Granite (Nelson et al., 1995; Bodorkos and Clark, 2004a).

Geochronology of the Coramup Gneiss

Previous SHRIMP U–Pb dating of the Coramup Gneiss indicated that the igneous precursor of garnet-bearing tonalitic gneiss near Butty Head (Fig. 13) has a poorly constrained igneous crystallization age in the range 1700–1600 Ma (Bodorkos and Clark, 2004b), equivalent to previously reported ages for the Dalyup Gneiss (Nelson et al., 1995). A syn-D_2 pegmatite, also from near Butty Head, gave a well-constrained date of 1168 ± 12 Ma from both zircon cores and rims (Bodorkos and Clark, 2004b), which is similar to the c. 1180 Ma age of metamorphism in the Dalyup Gneiss.

New SHRIMP U–Pb zircon dating of rocks from near Butty Head (Plum Pudding Rocks, GSWA 184123) has yielded an igneous crystallization age of 1688 ± 12 Ma from zircon cores from a garnet-bearing monzogranitic gneiss, confirming the presence of precursor rocks of the same age as those in other parts of the Biranup Zone (Figs 22c and 23a; Table A11; Bodorkos and Wingate, 2008k). The monzogranitic gneiss is adjacent to metapelitic rocks that are interlayered at 1–10 m-scale with metamorphosed quartz sandstone (Fig. 22d), of which GSWA 184122 is representative (Bodorkos and Wingate, 2008l). The metasedimentary rocks contain small-scale intrafolial folds and an axial planar fabric that is absent in the monzogranitic gneiss, which suggests that the precursor monzogranite intruded the protoliths of the metasedimentary rocks, but the relative timing relationships are not clear. All rocks and fabrics were deformed by mesoscopic to macroscopic upright tight folds that plunge gently to the northeast and southwest. The garnet-bearing monzogranitic gneiss (GSWA 184123) has a well-developed differentiated layering defined by alternating biotite-rich folia and quartzofeldspathic lamellae. The overall texture is granuloblastic; consistent with recrystallization under upper amphibolite to granulite facies conditions (Bodorkos and Wingate, 2008k). Analysis of zircon rims from this sample yielded a date of 1224 ± 9 Ma, which is interpreted as the age of the high-grade metamorphic event responsible for rim growth (Bodorkos and Wingate, 2008k).

The metamorphosed quartz sandstone (GSWA 184122) contains approximately 85% quartz, and subordinate plagioclase, biotite, and garnet and has a coarse granuloblastic texture consistent with upper amphibolite to granulite facies metamorphism (Bodorkos and Wingate, 2008l). The date of 1757 ± 39 Ma (1σ) for the single analysis (Fig. 23b; Table A12) in Group 2 is interpreted as the age of the youngest detrital zircon core, and therefore constitutes a maximum age for deposition of the precursor quartz sandstone. The 36 core analyses in Group 3 have $^{207}Pb^*/^{206}Pb^*$ dates that define significant age components (based on three or more data points) at c. 2650, c. 2623, c. 2357, c. 2263, and c. 2031 Ma, and several minor components spanning the range 3392–2102 Ma (Fig. 23c). These are interpreted as the ages of zircon-bearing rocks in the detrital source region(s) of the precursor quartz sandstone. The date of 1225 ± 7 Ma for the 11 rim analyses in Group 1 is interpreted as the age of the high-grade metamorphic event responsible for zircon rim growth in the metamorphosed quartz sandstone. The 16 analyses in Group 4 are interpreted as zircon rims grown during metamorphism and affected by minor ancient loss of radiogenic Pb. The date of 1196 ± 7 Ma defined by the 16 analyses constitutes a maximum age for the Pb-loss event, which may have been related to the c. 1170 Ma tectonothermal event (i.e. the syn-D_2 pegmatite) documented at this locality by Bodorkos and Clark (2004a,b).

The igneous crystallization age of 1688 ± 12 Ma for the precursor of the garnet-bearing monzogranitic gneiss provides an independent constraint for the minimum age for deposition of the precursor quartz sandstone it is interpreted to intrude (GSWA 184122). In addition, the date of 1224 ± 9 Ma ascribed to high-grade metamorphism of the precursor monzogranite is indistinguishable from the date of 1225 ± 7 Ma attributed to high-grade metamorphism of the precursor quartz sandstone (GSWA 184122; Fig. 23b; Table A12; Bodorkos and Wingate, 2008l). This indicates that both rocks were metamorphosed during the same tectonothermal event, which corresponds to Stage II of the Albany–Fraser Orogeny (Clark et al., 2000). Bodorkos and Clark (2004a,b) inferred a c. 1300 Ma granulite-facies metamorphic event during Stage I of the Albany–Fraser Orogeny, prior to a higher-pressure event that they correlated with similarly-styled metamorphism in the Fraser Zone at c. 1290 Ma, but the U–Pb SHRIMP results presented here show no evidence for c. 1300 Ma zircon rim growth due to metamorphism in these rocks. This suggests that Stage I of the Albany–Fraser Orogeny in the Coramup Gneiss involved granitic plutonism and the

CS104

development of strong gneissic fabrics, but not the partial melting event inferred by Bodorkos and Clark (2004a,b). Instead, it seems likely that high-temperature, moderate- to low-pressure metamorphism in the Coramup Gneiss took place early in Stage II, and overprinting upright structures were developed during the later stages of the same orogenic event, at c. 1180 Ma.

At Observatory Point, west of Esperance, sheets of homogeneous foliated leucogranite (Fig. 22e) are interlayered with dark grey, coarse-grained, orthopyroxene-bearing dioritic gneiss with a granuloblastic texture and well-developed differentiated layering consistent with recrystallization under granulite-facies conditions, of which GSWA 184125 is representative (Figs 13 and 22f,g). The foliated leucogranite has not undergone the same degree of deformation as the dioritic gneiss, and is intrusive into it. Both rock types are cross-cut by pegmatitic segregations. The dioritic gneiss is interpreted to occur as a south-southeasterly dipping thrust sheet between two layers of the foliated leucogranite, all within the footwall of the Heywood–Cheyne Fault Zone.

The foliated leucogranite comprises perthitic alkali feldspar, oligoclase, and quartz, with accessory biotite, heavily oxidized hypersthene, garnet, zircon, apatite, and magnetite (Nelson, 1995h). It yielded a SHRIMP U–Pb zircon age of 1288 ± 12 Ma, interpreted as the igneous crystallization age of the precursor granite (GSWA 83659; Nelson, 1995h). This is consistent with a distinguishably older igneous crystallization age of 1322 ± 11 Ma for the dioritic gneiss that it intrudes (GSWA 184125; Fig. 23d; Table A12; Bodorkos and Wingate, 2008m). Thirteen analyses of zircon rims within the orthopyroxene-bearing dioritic gneiss yielded a date of 1195 ± 4 Ma, interpreted as the age of the high-grade metamorphism (Group 2 in Fig. 23d; Table A12; Bodorkos and Wingate, 2008m).

Figure 22. Photographs of the Coramup Gneiss, Biranup Zone: a) metagranite L-tectonite with strong rodding in zone of large-scale sheath folds. At this locality the rodding lineation plunges 67° towards 091. Old Telegraph Track (Zone 51, MGA 506467E 6410544N); b) metagranite L-tectonite with strong rodding defined by stretched quartz and biotite. K-feldspar crystals are also aligned. At this locality the rodding lineation plunges 4° towards 192. East of Mount Andrew (Zone 51, MGA 502814E 6389122N). Photograph courtesy of Mark Pawley; c) sample site of dark-grey, coarse-grained garnet-bearing monzogranitic gneiss with well-developed differential layering at Plum Pudding Rocks (GSWA 184123; Zone 51, MGA 377419E 6251030N); d) pale grey, coarse-grained and garnet-bearing metamorphosed quartz sandstone representative of GSWA 184122, Plum Pudding Rocks (Zone 51, MGA 377419E 6251030N); e) south-southeasterly dipping sheet of foliated leucogranite representative of GSWA 83659 (Nelson, 1995h) below dioritic gneiss, separated by a layer of pegmatitic leucosome. Observatory Point (Zone 51, MGA 388659E 6247378N); f) view of sample site GSWA 184125 within south-southeasterly dipping layers of dark grey, orthopyroxene-bearing dioritic gneiss. Observatory Point (Zone 51, MGA 388659E 6247378N); g) detail of sample site GSWA 184125 showing the dark grey, orthopyroxene-bearing dioritic gneiss dated. Observatory Point (Zone 51, MGA 388659E 6247378N).

In summary, the geochronological data show that the Coramup Gneiss consists of older metasedimentary and metagranitic rocks that have ages comparable to other rocks in the Biranup Zone, and are therefore interpreted to be part of the same c. 1690–1660 Ma tectonic unit. These rocks have been metamorphosed up to granulite facies conditions and intruded by the Recherche Supersuite during Stage I of the Albany–Fraser Orogeny, with subsequent high temperature metamorphism during Stage II. These events are also similar to those recorded in the adjacent Dalyup Gneiss.

Fraser Zone

The Fraser Zone is a newly defined unit in the Kepa Kurl Booya Province within the eastern Albany–Fraser Orogen (Fig. 1) that contains metamafic rocks that were previously assigned to the Fraser Complex of Doepel (1973) and Myers (1985), as well as interlayered lenses of metagranitic and metasedimentary rocks that were previously assigned as undivided Biranup Complex (now Kepa Kurl Booya Province; Tyler and Hocking, 2008). Collectively, these are here named the Fraser Range Metamorphics because of similarities in their ages and metamorphic and structural histories (see below). Only the southwestern corner of the Fraser Zone is represented in the interpreted bedrock geology of the South Yilgarn Geological Exploration Package (GSWA, 2007). The extents of the Fraser Zone are currently being investigated but in the southwest it is bound by the Fraser Fault and the Coramup Fault Zone (Figs 13 and 14). The southeastern margin of the Fraser Zone and contact with the Nornalup Zone is not as clearly defined and is largely obscured by younger cover rocks of the Eucla Basin (Fig. 1). However, it has also been interpreted as a faulted contact, largely based on differences in metamorphic grade (Coramup Fault Zone; Myers, 1985; Clark, 1999).

The Fraser Zone is dominated by high-grade mafic and gabbroic rocks that have a strong, distinct geophysical signature in both aeromagnetic and gravity data (Fig. 24). Most of the northern part of the Fraser Zone is obscured by younger rocks of the Eucla Basin but the geophysical data show that it is an approximately 425 km long, northeasterly trending, fault-bounded unit that is up to 50 km wide.

The Fraser Complex: previous interpretations

The Fraser Complex was previously named as a metamorphic complex after the Fraser Range in Doepel (1973), and early work is referred to in Doepel and Lowry (1970) and Doepel (1975). In Doepel (1973) the metagranitic rocks were included with the metamafic rocks and the Fraser Complex was interpreted as an upfaulted

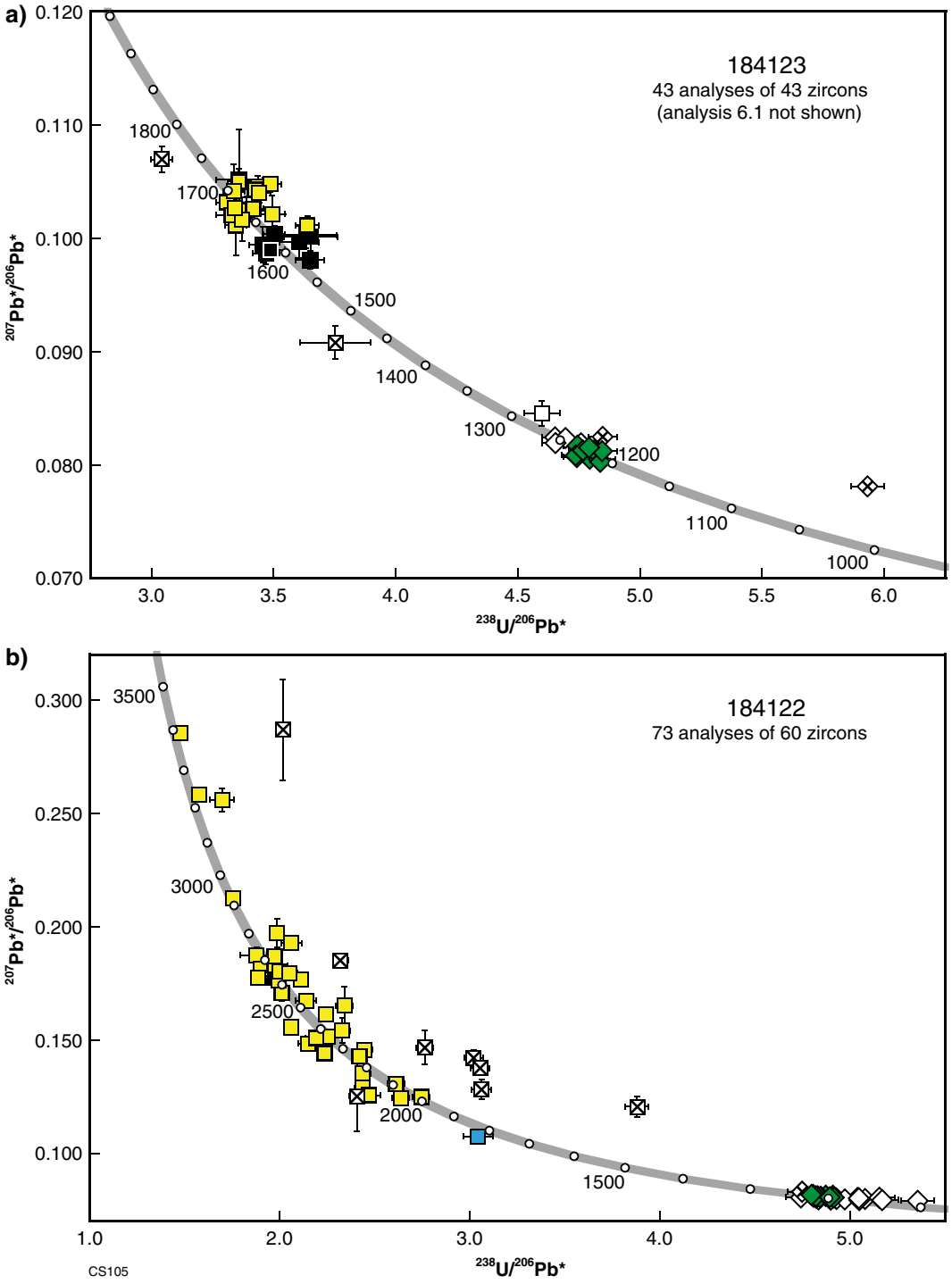

Figure 23. **a) U–Pb analytical data for sample GSWA 184123: garnet-bearing monzogranitic gneiss, Plum Pudding Rocks (Zone 51, MGA 377419E 6251030N). Yellow squares denote Group 1 (igneous zircon cores); green diamonds denote Group 2 (metamorphic zircon rims); black squares denote Group 3 (igneous zircon cores affected by minor ancient loss of radiogenic Pb); white square denotes Group 4 (igneous zircon core affected by recrystallization); white diamonds denote Group 5 (metamorphic zircon rims with minor core-rim overlap); crossed squares and diamonds indicate ungrouped analyses (primary beam instability, or discordance <–5% or >5%); b) U–Pb analytical data for sample GSWA 184122: metamorphosed quartz sandstone, Plum Pudding Rocks (Zone 51, MGA 377419E 6251030N). Green diamonds denote Group 1 (metamorphic zircon rims); blue square denotes Group 2 (youngest detrital zircon core); yellow squares denote Group 3 (older detrital zircon cores affected by minor ancient loss of radiogenic Pb); white diamonds denote Group 4 (metamorphic zircon rims affected by minor ancient loss of radiogenic Pb); crossed diamond denotes Group 5 (core-rim overlap); crossed squares indicate ungrouped analyses (discordance <–10% or >10%);**

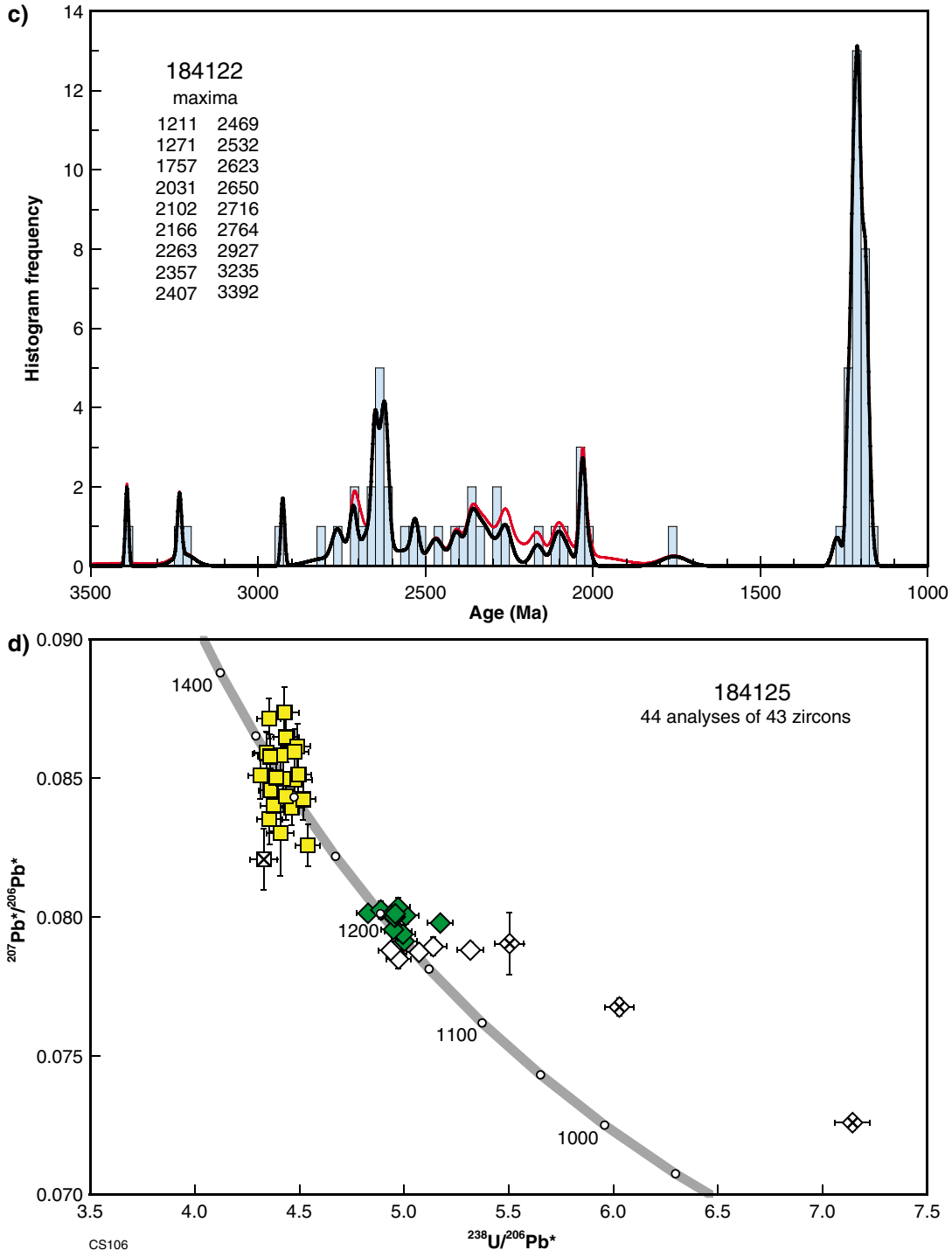

Figure 23. **c) probability density diagram and frequency histogram for sample GSWA 184122: metamorphosed quartz sandstone, Plum Pudding Rocks (Zone 51, MGA 377419E 6251030N). Heavy curve, maxima values, and frequency histogram (bin width 25 Ma) include only data with discordance <10% (66 analyses of 55 zircons). Light curve includes all data (73 analyses of 60 zircons); d) U–Pb analytical data for sample GSWA 184125: orthopyroxene-bearing dioritic gneiss, Observatory Point (Zone 51, MGA 388659E 6247378N). Yellow squares denote Group 1 (igneous zircon cores); green diamonds denote Group 2 (metamorphic zircon rims); white diamonds denote Group 3 (metamorphic zircon rims affected by minor ancient loss of radiogenic Pb); crossed squares and diamonds indicate ungrouped core and rim analyses respectively (discordance <–5% or >5%).**

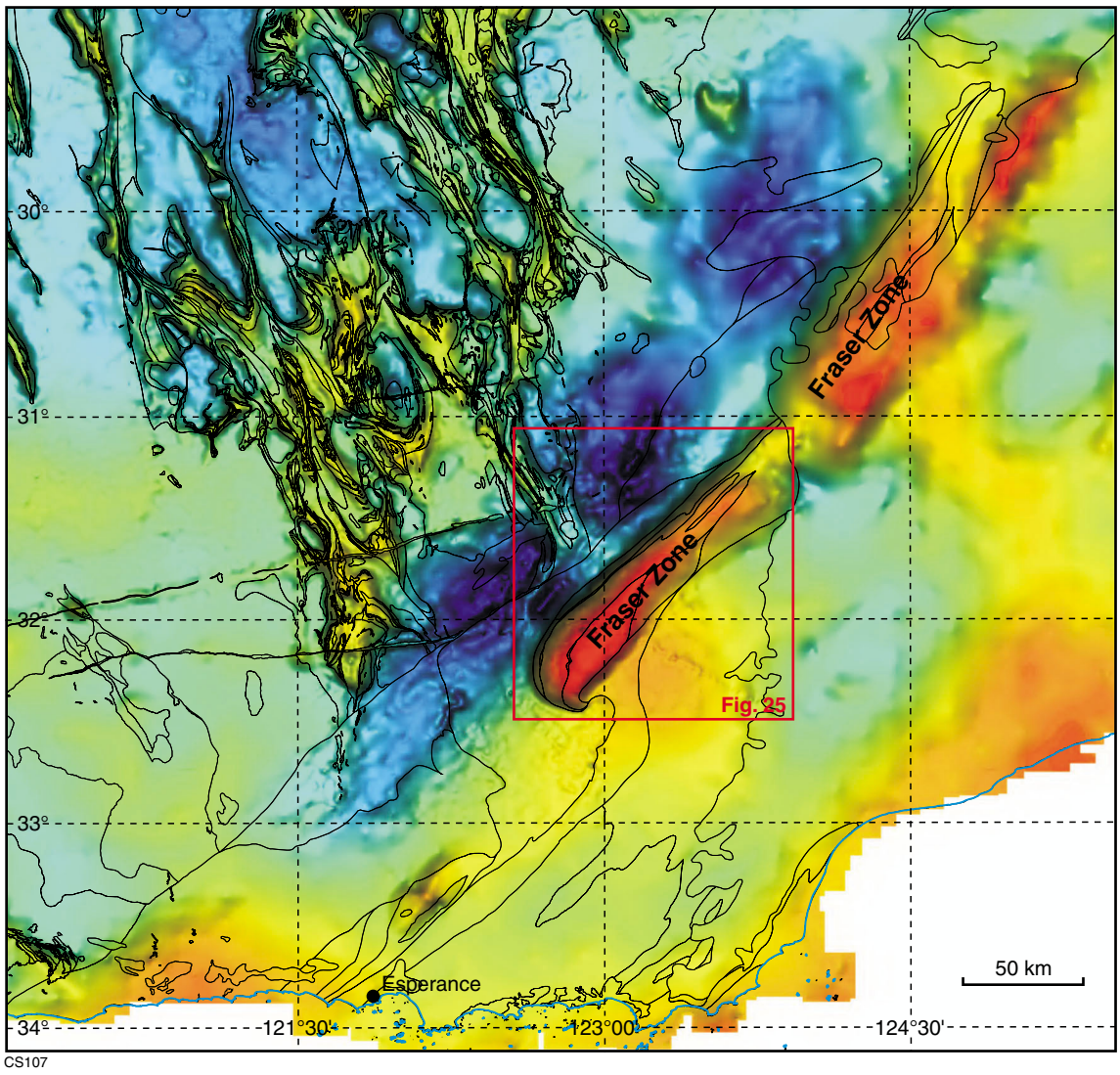

Figure 24. Gravity image (government dataset) showing the eastern part of the central Albany–Fraser Orogen, Eastern Goldfields Superterrane and southeastern Youanmi Terrane with geology polygon outlines from Tyler and Hocking (2008) overlain. The Fraser Zone and Fraser Range Metamorphics are mostly defined by the gravity high in red.

wedge of a lower crustal layer. Doepel and Lowry (1970) interpreted the mafic granulites as mainly mafic intrusive rocks, whereas Wilson (1969a) and Bunting et al. (1976) interpreted them as dominantly derived from mafic extrusive rocks, supported by the presence of inferred amygdales and relict pillows and thin interlayered bands of quartzite.

The first tectonic subdivisions of the Fraser Complex and surrounding rocks were drawn in Bunting et al. (1976), where a transition zone of reworked Archean rocks was delineated along the southeast margin of the Yilgarn Craton, bounded by the northeasterly trending Western Gneiss and Granite Zone consisting of Proterozoic igneous and metamorphic rocks with no recognizable remnants of the Yilgarn Craton. This was separated from the Fraser Complex by the Fraser Fault.

Myers (1985) interpreted the mafic rocks of the Fraser Complex to represent part of a large layered intrusion, and as such its previous stratigraphic name (the Fraser Complex) defined it as an igneous complex. Condie and Myers (1999) argued that it was unlikely that the units were part of a single stratiform intrusion, and interpreted the complex as representing remnants of multiple oceanic magmatic arcs. They argued that trace element data indicated a subduction-related source for the mafic magmas. Given the ambiguity of its tectonic setting the names Fraser Zone and Fraser Range Metamorphics are preferred.

Fraser Range Metamorphics

Myers (1985) divided the Fraser Complex into five structurally interlayered units (Fig. 25). These are now part of the Fraser Range Metamorphics within the Fraser Zone. The five units of Myers (1985) are garnet amphibolite (interpreted as metagabbro) with thin layers of metamorphosed ultramafic rocks, metamelanogabbro,

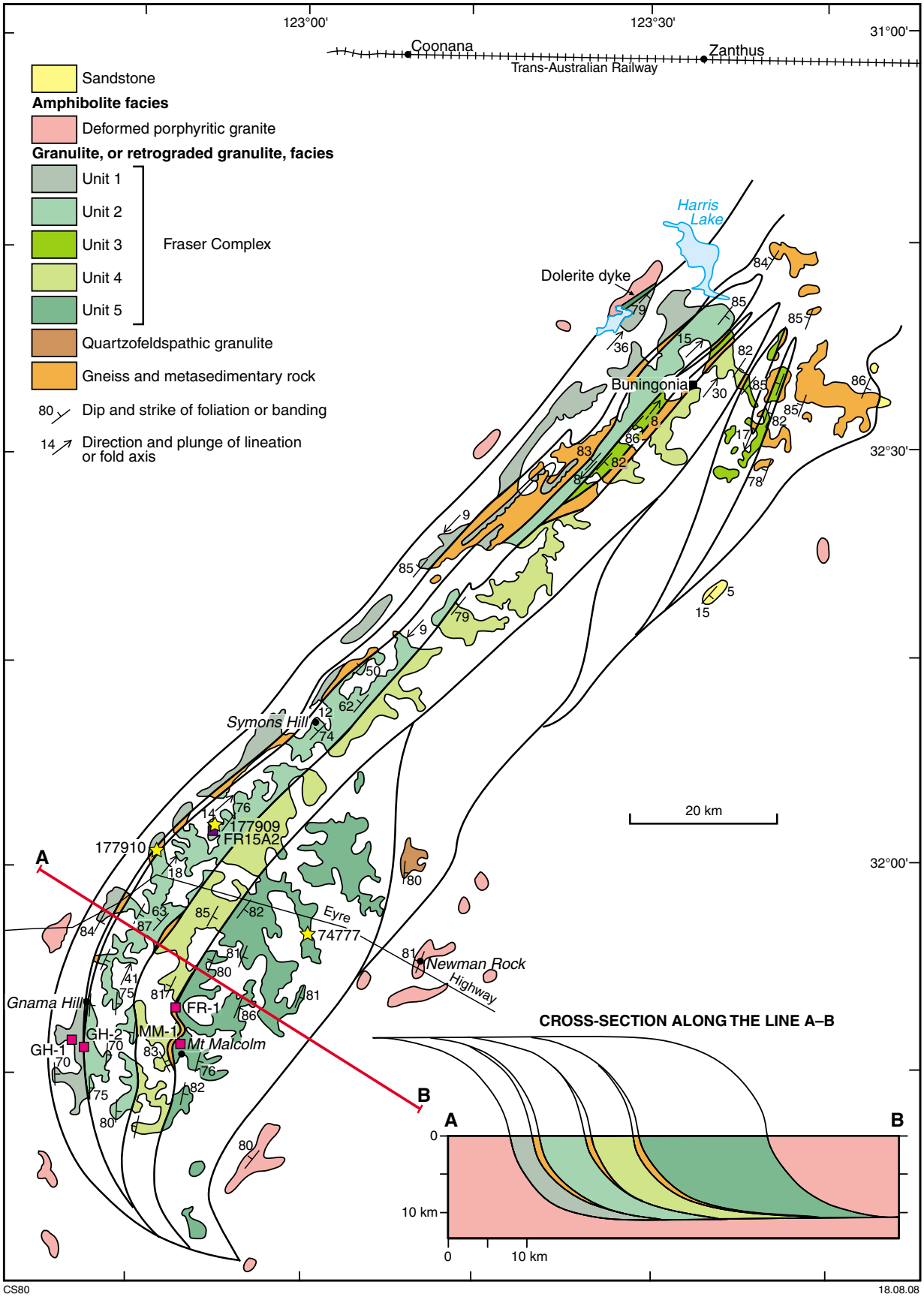

Figure 25. Geological map of the southern part of the Fraser Zone (previously the Fraser Complex) with schematic cross-section (after Myers, 1985). GSWA sample sites are marked with yellow stars, sample sites of Clark et al. (1999) are marked with pink boxes, and sample site FR15A2 of De Waele and Pisarevsky (2008) is marked with a purple box.

metaleucogabbro, and meta-anorthosite (Unit 1), pyroxene granulite interpreted as derived from gabbro or norite (Units 2 and 4), meta-leucogabbro, meta-anorthosite, minor metagabbro and meta-melanogabbro (Unit 3), and metagabbro or olivine gabbronorite, much of which is gradational from strongly foliated pyroxene granulite into undeformed two-pyroxene gabbros with well-preserved igneous textures (Unit 5; Fig. 26a; Myers, 1985; Fletcher et al., 1991; Clark et al., 1999). Unit 5 is in the eastern part of the Fraser Zone and is less deformed and metamorphosed than the other units (Wilson, 1969b; Myers, 1985). The five units are interpreted to be structurally interlayered with relatively thin fault slivers of quartzofeldspathic gneiss, metasedimentary gneiss, quartzite, metagranite, and pegmatite (Fig. 26b,c; Wilson, 1969c; Doepel and Lowry, 1970; Myers, 1985; Clark et al., 1999). Some of the metagranite and pegmatite is intrusive into the mafic rocks but is also deformed and metamorphosed (Myers, 1985; Clark et al., 1999).

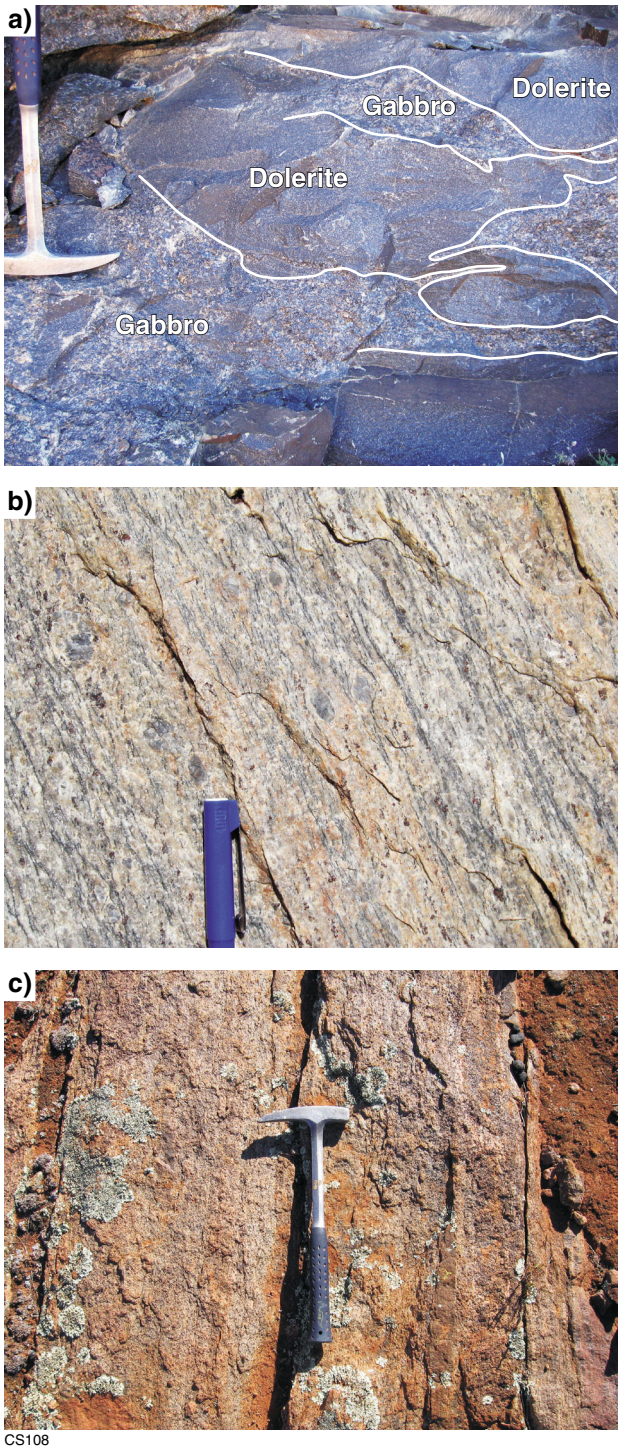

The Fraser Range Metamorphics are dominated by a northeasterly trending, steeply northwesterly to southeasterly dipping, pervasive foliation and northeasterly or southwesterly, moderately plunging mineral lineations and fold axes (Myers, 1985; Clark et al., 1999). The boundaries between the units are interpreted to be major thrust faults that interleaved thin slivers of basement gneiss and metasedimentary rocks with the mafic rocks, with the Fraser Fault as the leading, northwest-verging thrust (Fig. 25; Myers, 1985). Wilson (1969a) interpreted both sinistral and reverse sense movement on the Fraser Fault placing the Fraser Range Metamorphics northwards over the Western Gneiss and Granite Zone described in Bunting et al. (1976). In the northwest (as shown in Fig. 25, southwest of Harris Lake), the Fraser Fault has been described as an approximately 2 km wide zone of shearing containing schistose or mylonitic rocks retrogressed from granulite to amphibolite facies that include metagabbro, quartzofeldspathic gneiss, and amphibolite-banded gneiss (Myers, 1985).

Within the Fraser Range Metamorphics in the southern part of the Fraser Zone Clark et al. (1999) defined three phases of deformation (D_1–D_3), two phases of metamorphism (M_1–M_2) and four episodes of recrystallization (M_{1a}–M_{2b}) (Fig. 25; Table 2). Isoclinally folded leucosomes and destruction of M_{1b} disequilibrium textures in high-strain zones show that M_{2a} occurred under lower temperature conditions than $M_{1a/b}$. Pyroxene granulites of Unit 1 were retrogressed to garnet(–clinopyroxene) amphibolites (Myers, 1985; Fletcher et al., 1991) during D_2/M_{2a}, but show evidence of increased pressure relative to M_1, attributed to burial of the Fraser Range Metamorphics,

Figure 26. Photographs of the Fraser Range Metamorphics: a) metagabbro with megacrystic feldspars, localized garnet within feldspar and coarse groundmass intruding metadolerite. The contacts between the two phases have lobate and wisp-like form, some of which are annotated in the photo. This is Unit 5 in Myers (1985). Fraser Range Black dimension stone quarry (Zone 51, MGA 502080E 6447098N). Photograph courtesy of Mark Pawley; b) garnet-rich banded orthogneiss. Large K-feldspar porphyroclasts indicate reverse shear sense with top to the southeast. Nearby shears offsetting leucosome indicate the same shear sense. This is within Unit 2 in Myers (1985). Fantasia dimension stone quarry and GSWA 177909 sample site (Zone 51, MGA 491256E 6465549N). Photograph courtesy of Mark Pawley; c) paragneiss sliver locally interlayered with mafic amphibolite. Paragneiss includes psammitic layers that are quartz- and garnet-rich, pelitic layers with garnet and sillimanite, and bands of leucosome. This is within Unit 2 in Myers (1985). Gnamma Hill (Zone 51, MGA 471675E 6440359N). Photograph courtesy of Mark Pawley.

Table 2. Summary of geological events affecting the southern Fraser Range Metamorphics (after Clark et al., 1999)

Age (c. Ma)	*Geological event*	*Deformation event*	*Structural elements*	*Metamorphic event*	*Peak mineral assemblage*[(a)]	*P–T estimate*
≤1388	Deposition of sediments					
1345–1313	Initial Stage I thickening in the eastern Albany–Fraser Orogen					
1313–1301	?Extension, intrusion of Fraser Metamorphics gabbro + charnockite	D_1	Formation of pervasive gneissic ± migmatitic layering (S_1)	M_{1a}	(i) Cpx–Opx–Ol–Pl±Sp (ii) Grt–Sp–Sil–Pl–Qtz	≥ 800°C, 600–700 MPa
1301–1293	Near-isobaric cooling			M_{1b}	(i) Cpx–Opx–Pl–Qtz±Sp (ii) Grt–Crd–Sil–Pl–Qtz	~750°C, 600–700 MPa
1293–1288	Crustal thickening, granite intrusion + retrogression	D_2	Layer-parallel dextral shearing localized along unit boundaries (S_1/S_2)	M_{2a}	(i) Grt–Cpx–Hbl–Pl–Qtz	650°C, 800–1000MPa
1288–1260[(b)]	Exhumation of the Fraser Metamorphics	D_3	Retrograde shearing localized to western boundary of Unit 1	M_{2b}	(i) Ep–Amph–Pl–Qtz	500°C, 400 MPa

NOTES: (a) Peak assemblages are those used in P–T calculations: (i) denotes peak assemblage in metabasic rocks; (ii) denotes peak assemblage in metasedimentary rocks
(b) Based on cooling ages from Bunting et al. (1976), Baksi and Wilson (1980) and Fletcher et al. (1991)

crustal thickening, and tectonic interleaving (Clark, 1999; Clark et al., 1999). Exhumation of the Fraser Range Metamorphics along the western margin (Fraser Fault) is attributed to D_3, marked by development of mylonitic rocks and retrogression from granulite facies to amphibolite-greenschist assemblages (Myers, 1985; Clark et al., 1999).

Geochronology of the Fraser Range Metamorphics

Published U–Pb SHRIMP zircon dating has focused on the better exposed, southern part of the Fraser Range Metamorphics (Clark et al., 1999; De Waele and Pisarevsky, 2008; Figs 24 and 25), and does not include the northern part as erroneously reported by De Waele and Pisarevsky (2008). Older Rb–Sr and Sm–Nd isotopic studies have also mostly focused on the southern region but are generally broader and include rocks from the region between the Fraser Zone and the Yilgarn Craton (Arriens and Lambert, 1969; Bunting et al., 1976; Fletcher et al., 1991). The Rb–Sr and Sm–Nd model ages indicated poorly constrained, mixed ages of c. 1330–1300 Ma for the Fraser Range Metamorphics. The best constraint on the age of igneous crystallization of the metagabbro from Unit 5 is a Sm–Nd isochron age of 1291 ± 21 Ma (MSWD=0.25), derived from orthopyroxene, clinopyroxene, olivine, and plagioclase from a sample of olivine gabbronorite (GSWA 74777; Fig. 25; Fletcher et al., 1991). This sample comes from approximately 1.3 km north-northeast of the Fraser Range Black dimension stone quarry (Fig. 26a), and is most likely the same rock unit. The same sample provided a biotite–whole-rock Rb–Sr age of 1268 ± 20 Ma interpreted as the timing of cooling below the blocking temperature for biotite in this rock (Fletcher et al., 1991). Pyroxene-bearing mafic granulite from Unit 2 yielded a SHRIMP U–Pb age of 1291 ± 8 Ma, based on nine analyses of seven zircons (3 cores and 6 rims, FR15A1, Fig. 25; De Waele and Pisarevsky, 2008). The cluster of core and rim analyses was interpreted as the igneous crystallization age of the gabbroic protolith.

Orthopyroxene–hornblende orthogneiss (charnockite) that forms a large lens near Mt Malcolm has a SHRIMP U–Pb zircon age of 1301 ± 6 Ma, interpreted as the age of igneous crystallization (sample MM–1; Fig. 25; Clark et al., 1999). This provides a minimum age for the metagabbroic rocks of Unit 5 that it intrudes, which occurred during formation of the first fabric (M_{1a}/D_1, Table 2; Clark et al., 1999). Orthopyroxene-bearing orthogneiss just north of Mt Malcolm yielded a SHRIMP U–Pb zircon age of 1293 ± 9 Ma, which is also interpreted as an igneous crystallization age (sample FR–1, Fig. 25; Clark et al., 1999). The age is within error of sample MM–1, but the intrusion is interpreted as post-D_1 and pre-D_2 (Clark et al., 1999). Monzogranite gneiss from the Fantasia dimension stone quarry yielded a SHRIMP U–Pb zircon age of 1287 ± 14 Ma, interpreted as a minimum age for igneous crystallization of the monzogranite precursor of the gneiss (GSWA 177909l Figs 25 and 26b; Wingate and Bodorkos, 2007a).

The ages are all within error of each other and suggest these granitic precursors are all part of the same suite. De Waele and Pisarevsky (2008) reported younger ages of 1280 ± 10 Ma and 1250 ± 23 Ma (the latter being uncorrected for common Pb) for granitic gneisses southwest of Symons Hill (Fig. 25), but these are poorly constrained and may not be geologically meaningful. Alternatively, they could be part of a slightly younger suite of granitic rocks such as that represented by an aplite dyke that intrudes the mafic granulite of Unit 1, which yielded a SHRIMP U–Pb zircon age of 1288 ± 12 Ma, interpreted as the age of igneous crystallization (sample GH–1; Fig. 25; Clark et al., 1999). The dyke is interpreted to have intruded shortly after M_{2a} retrogression (Table 2; Clark et al., 1999).

Paragneiss is exposed at Gnamma Hill as a thin sliver between Units 1 and 2 (Figs 25 and 26c; Myers, 1985). Quartzofeldspathic gneiss from this locality is garnet-rich, and contains minor sillimanite, cordierite, and biotite, and has a composite S_1/S_2 foliation related to M_1 and M_2 (sample GH–2; Fig. 25; Clark et al., 1999). Sample GH–2 yielded a slightly reverse discordant zircon population with an age of 1388 ± 12 Ma (SHRIMP U–Pb, 11 analyses), interpreted as detrital grains sourced from a proximal, homogeneous igneous source (Clark et al., 1999). This was further interpreted to possibly reflect a volcanogenic sequence that formed prior to the Stage I collision event of the Albany–Fraser Orogeny (Clark et al., 1999). Strongly foliated quartz metasandstone, interlayered with amphibolite and pyroxene mafic granulite, between Units 1 and 2 (GSWA 177910; Fig. 25) yielded a maximum depositional age of 1466 ± 17 Ma (SHRIMP U–Pb, 4 analyses of zircon cores; Wingate and Bodorkos, 2007b). The sample also yielded significant detrital population maxima at c. 1582, 1640, 1680 Ma, and a minor component at c. 2651 Ma (27 analyses of 26 zircon cores). This is in contrast to the tight population of 1388 ± 12 Ma in sample GH–2 of Clark et al. (1999), albeit from a small dataset, and indicates different source rocks, possibly including the Biranup Zone. Analysis of 21 zircon rims in quartz metasandstone GSWA 177910 yielded a metamorphic age of 1304 ± 7 Ma (Wingate and Bodorkos, 2007b). This age is within error of the igneous crystallization ages of the precursors to the granitic gneisses in the Fraser Range Metamorphics.

Rare zircons, interpreted as xenocrystic, from granitic gneisses about 2.5 km south of Symons Hill (Fig. 25) have poorly constrained Paleoproterozoic ages of 1876 ± 44, 1814 ± 134, 1738 ± 28, 1674 ± 22, and 1665 ± 96 Ma, the youngest two of which are similar to ages of the Dalyup and Coramup Gneisses (i.e. the Biranup Zone; De Waele and Pisarevsky, 2008). As there are no other known source rocks of this age in the vicinity, this suggests that source region(s) of the Symons Hill granitic rocks included either protoliths of the Biranup Zone, or recycled components of it. Quartz metasandstone to the southwest contains detrital zircons of similar age (GSWA 177910; Wingate and Bodorkos, 2007b), so it is possible that the slivers of paragneiss in the Fraser Range Metamorphics may have provided zircons recycled from the Biranup Zone, assuming they were deposited prior to granite intrusion. Alternatively, the zircons could have come from much further afield.

The geochronological data presented here indicate a short time span for igneous crystallization, granulite-facies

metamorphism, localized retrogression, and cooling (cf. Fletcher et al., 1991; Clark et al., 1999). The only reliable age for metamorphism is 1304 ± 7 Ma from zircon rims from quartz metasandstone (GSWA 177910), which is within error of the interpreted syn-M_{1a}/D_1 intrusion age of 1301 ± 6 Ma of the charnockitic orthogneiss (sample MM–1). This also fits with intrusion of post-D_1, pre-D_2 orthopyroxene-bearing orthogneiss (sample FR–1) slightly later at 1293 ± 9 Ma. If the age of 1291 ± 8 Ma for the pyroxene-bearing mafic granulite of Unit 2 (sample FR15A1) truly reflects igneous crystallization of its gabbroic precursor, as postulated by De Waele and Pisarevsky (2008), then this suggests a very tight age bracket with 1299 Ma being a maximum age for Unit 2 gabbro intrusion. This would have been followed by granulite-facies metamorphism commencing within 2 million years (based on the metamorphic age of the quartz sandstone), or within 4 million years (based on interpretation of the charnockite intruding syn-M_{1a}/D_1), and assuming the calculated errors are geologically meaningful. A more likely explanation is that the zircons analyzed in the pyroxene-bearing mafic granulite (sample FR15A1 of De Waele and Pisarevsky, 2008) indicate a metamorphic age, rather than an igneous crystallization age of the protolith, or a mixed age of the two. The CL image of the zircons (fig. 5b in De Waele and Pisarevsky, 2008) show them to be mostly homogeneous, with no indication of sector zoning typical of magmatic zircon, and De Waele and Pisarevsky (2008) interpret the rims of the grains, which make up part of the concordia age, to have grown during metamorphism. A 1291 ± 8 Ma metamorphic age for this sample would be more consistent with the ages reported for the 1301 ± 6 Ma syn-M_{1a}/D_1 charnockitic orthogneiss intrusion (sample MM–1) and the 1304 ± 7 Ma metamorphic rims from the quartz metasandstone (GSWA 177910).

All of the geochronological data indicate tectonothermal activity during Stage I of the Albany–Fraser Orogeny, with no evidence of Stage II. The preservation of pre-1250 Ma Rb–Sr cooling ages (Bunting et al., 1976; Fletcher et al., 1991) also indicate a lack of Stage II activity.

Nornalup Zone

The Nornalup Zone is the southern- and eastern-most of the lithotectonic units comprising the Albany–Fraser Orogen in Western Australia (Fig. 1). It is separated from the Biranup Zone by the Heywood–Cheyne Fault Zone, and extends from the Darling Fault in the west to at least as far as the Fraser Zone in the east, where it becomes obscured by Eocene sandstones and siltstones of the Eucla Basin (Hocking, 1990; Myers, 1995b; Geological Survey of Western Australia, 2007). The Nornalup Zone may extend offshore (Fig. 1), but its extent is difficult to determine because of the voluminous Recherche and Esperance Supersuites. Only a small part of the Nornalup Zone was included in GSWA (2007), and no new mapping or analytical work was carried out.

The Nornalup Zone consists of the Malcolm Gneiss in the eastern Nornalup Zone, and paragneisses in the western Nornalup Zone in the Albany region (Myers, 1995b; Clark, 1999). The Salisbury Gneiss and the Mount Ragged Formation constitute Mesoproterozoic cover rocks that overlie the Nornalup Zone, but are included in this section because of their geographic position. The oldest unit exposed is the Malcolm Gneiss, which is dominated by siliciclastic metasedimentary rocks and orthogneiss, and includes mafic amphibolitic schist, quartzofeldspathic gneiss, minor calc-silicate rocks, and intrusions of the c. 1330–1280 Ma Recherche Supersuite (Nelson et al., 1995; Clark, 1999). The metasedimentary rocks consist dominantly of muscovite–biotite psammites and quartzite, with subordinate garnet–biotite–sillimanite pelitic rocks that are locally migmatitic (Clark, 1999). A maximum depositional age for the protolith of the metasedimentary gneiss is defined by a detrital zircon population of 1560 ± 40 Ma (n=10) from near Point Malcolm (GSWA 112128; Nelson, 1995i). This sample also included a population of five analyses that gave an age of 1807 ± 35 Ma, and single grains with ages of 2033 ± 10 Ma (1σ), 2175 ± 13 Ma (1σ), and 2734 ± 14 Ma (1σ). Low-pressure, high-temperature metamorphism (4–5 kbar, 750–800°C) of the Malcolm Gneiss was accompanied by the intrusion of monzogranite and granodiorite of the Recherche Supersuite at 1330 ± 14 Ma (Poison Creek; GSWA 83662; Nelson, 1995j) and 1314 ± 21 Ma (Israelite Bay; GSWA 83663; Nelson, 1995k) during Stage I of the Albany–Fraser Orogeny (Clark et al., 2000). This was followed by formation of northwesterly verging folds, which were cut by an aplite dyke that has a SHRIMP U–Pb zircon age of 1313 ± 16 Ma (Clark et al., 2000). Metadolerite dykes also cut the regional foliation in the Malcolm Gneiss (Clark, 1999).

Paragneiss in the western Nornalup Zone is less abundant and includes garnet–sillimanite migmatitic rocks and quartzites (Clark, 1995; Love, 1999). Migmatitic rocks from two localities near Albany (Fig. 1) contain detrital zircons with ages of 1750–1720 Ma, have a maximum depositional age of c. 1360 Ma (Whalehead Rock; Love, 1999), and were metamorphosed at 1314 ± 5 Ma (Whalehead Rock; Love, 1999) and 1304 ± 3 Ma (Ledge Point; Clark, 1995). This constrains the depositional age of the Whalehead Rock paragneiss to between c. 1360 and 1310 Ma, and the first episode of metamorphism to Stage I (Fitzsimons and Buchan, 2005). Early deformation of the western Nornalup Zone is characterized by recumbent folding with an associated flat-lying compositional layering, which was transposed by a northeasterly trending subvertical foliation associated with northwest-directed thrusting and dextral transpression (Duebendorfer, 2002; Fitzsimons and Buchan, 2005).

Stage I tectonism culminated with thrusting of the Nornalup Zone over the Biranup Zone along the Heywood–Cheyne Fault Zone, and stitching of the Biranup Zone by late-stage (1300–1280 Ma) Recherche Supersuite plutons (Clark et al., 1999, 2000; Bodorkos and Clark, 2004b). This was followed by deposition of the Mount Ragged Formation (Fig. 1). The Mount Ragged Formation is found to the northwest of the Malcolm Gneiss and comprises upper greenschist to lower amphibolite facies, massive grey quartzites, muscovite quartzites, and sporadic thin layers of pelitic rocks (Clark, 1999). The mature quartzose sediments are interpreted to have been

deposited in shallow intracratonic basins (Clark et al., 2000). SHRIMP U-Pb analysis identified an older detrital zircon component (seven analyses) with a weighted mean age of 1783 ± 12 Ma, and a maximum depositional age is defined by a separate population (12 analyses) with an age of 1321 ± 24 Ma. This is consistent with local derivation from the unconformably underlying Recherche Supersuite, and in conjunction with the angular relationship between the Mount Ragged Formation and the complexly deformed gneissic rocks that it overlies, it suggests that the eastern Nornalup Zone was uplifted and eroded between Stages I and II of the Albany–Fraser Orogeny (Clark et al., 2000). Such an interpretation is supported by amphibolite facies metamorphism (4–5 kbar, 550°C) and the growth of 1154 ± 15 Ma rutile in the Mount Ragged Formation, which shows that these rocks were buried and metamorphosed during Stage II (Clark et al., 2000).

A similar origin and setting is likely for deposition of the pelitic protoliths of the Salisbury Gneiss (Bodorkos and Clark, 2004b). The Salisbury Gneiss is exposed on a series of islands offshore to the southeast of Esperance (Fig. 1). It is separated from the Malcolm Gneiss to the northwest by the Rodona Fault (Myers, 1995b; Clark et al., 2000). On Salisbury Island the Salisbury Gneiss comprises pelitic gneisses and mafic granulite, porphyritic granitic gneiss, and two-pyroxene metagabbro that is undeformed in its core but amphibolitic at its margins (Clark, 1999). Migmatitic pelitic gneiss contains mesosomes of biotite–sillimanite–garnet–cordierite–feldspar–quartz(–spinel), and leucosomes are K-feldspar-rich with localized garnet(–cordierite). These gneisses record granulite facies metamorphic conditions of approximately 800°C and >5 kbar (Clark, 1999; Clark et al., 2000). The depositional age of the Salisbury Gneiss is unknown, but a lack of evidence for Stage I metamorphism suggests deposition may have post-dated it, and that the unit is distinct from the Malcolm Gneiss (Clark, 1999). Migmatitic leucosome derived from partial melting of the pelitic gneiss yielded SHRIMP U–Pb zircon ages of 1214 ± 8 (18 core analyses) and 1182 ± 13 Ma (six rim analyses) (Clark et al., 2000). The older age is interpreted to date crystallization of the leucosome, and the younger age is interpreted as having formed during decompression from peak metamorphic conditions (Clark et al., 2000), potentially in response to the emplacement of the widespread Gnowangerup Dyke Suite (Wingate et al., 2000). These ages record Stage II metamorphism in the southeastern-most exposed part of the Nornalup Zone.

In the late stages of Stage II of the Albany–Fraser Orogeny the western Nornalup Zone was intruded by the voluminous porphyritic Burnside Granite between 1190–1170 Ma (Black et al., 1992), triggering growth of new metamorphic zircon at 1169 ± 7 Ma in its pelitic host rocks (Clark, 1995). Stage II tectonism in the eastern Nornalup Zone produced syntectonic pegmatite within spaced, northeasterly trending ductile shear zones with dip-slip kinematics in the Malcolm Gneiss and Recherche Supersuite (Clark et al., 2000). In the Malcolm Gneiss, one such pegmatite yielded a SHRIMP U–Pb monazite age of 1165 ± 5 Ma. This was interpreted as the age of crystallization of the pegmatite, the age of shearing related to thrusting of the Salisbury Gneiss to the northwest along the Rodona Fault, and the age of related deformation in the Mount Ragged Formation (Clark et al., 2000). The end of Stage II tectonism in the eastern Nornalup Complex was marked by the intrusion of the porphyritic Esperance Supersuite (Myers, 1995b; Nelson et al., 1995). Late felsic dykes that intrude the Mount Ragged Formation are probably the same age (Myers, 1995b; Clark, 1999).

Recherche and Esperance Supersuites

The c. 1330–1280 Ma Recherche Supersuite (formerly Recherche Granite of Myers, 1995b; Nelson et al., 1995; Clark, 1999) and the c. 1140 Ma Esperance Supersuite (formerly Esperance Granite of Myers, 1995b; Nelson et al., 1995) mark two major magmatic events that coincide with Stages I and II of the Albany–Fraser Orogeny, respectively (Clark et al, 2000). Igneous rocks belonging to the Recherche Supersuite are generally metamorphosed to amphibolite or granulite conditions, have a gneissic fabric, and may include syn-magmatic mafic dykes (Myers, 1995b; Nelson et al., 1995). Deformation and metamorphism occurred either during Stage I or II, or both (Nelson et al., 1995; Clark et al., 2000). Igneous rocks belonging to the Esperance Supersuite are generally metamorphosed to greenschist to amphibolite conditions and are generally less pervasively deformed, but may locally contain a foliation or be mylonitic (Myers, 1995b; Nelson et al., 1995). Deformation and metamorphism occurred during the later stages of Stage II (Nelson et al., 1995; Clark et al., 2000).

The Recherche Supersuite was originally defined as part of the Nornalup Zone, where it is most extensive (Myers, 1995b). It includes granitic gneissic rocks that Myers (1995b) divided into even-grained and porphyritic units. Clark (1999) recognized two distinct varieties in the eastern Nornalup Zone, with the majority consisting of biotite–hornblende monzogranite gneiss that has rare calc-silicate boudins (e.g. GSWA 83662 from Poison Creek, dated at 1330 ± 14 Ma; Nelson, 1995j). The other variety is a peraluminous, garnet-bearing granodiorite gneiss that does not contain hornblende (e.g. GSWA 83663 from Israelite Bay, dated at 1314 ± 21 Ma; Nelson, 1995k). The Recherche Supersuite contains syn-plutonic mafic dykes that show extensive back-veining and disaggregation by the granite, and hybrid zones that indicate magma mingling (Myers, 1995b; Clark, 1999). These rocks are intruded by equigranular granitic and aplitic dykes, one of which yielded a SHRIMP U–Pb igneous crystallization age of 1313 ± 16 Ma (Clark et al., 2000). Granitic rocks belonging to the Recherche Supersuite are much less abundant in the western Nornalup Complex, which is dominated by Stage II granitic rocks (Fitzsimons and Buchan, 2005). Orthopyroxene-bearing orthogneiss from Whalehead Rock near Albany (Fig. 1) is pervasively foliated and contains trains of mafic enclaves (enderbitic granite of Pidgeon, 1990; Fitzsimons and Buchan, 2005). It has a U–Pb zircon age of 1289 ± 10 Ma, determined via conventional isotope-dilution thermal ionization mass spectrometry, and this is interpreted as an igneous crystallization age. Tonalitic gneiss from the same

locality yielded SHRIMP U–Pb zircon ages of 1302 ± 7 and 1296 ± 10 Ma, similarly interpreted as igneous crystallization ages (Love, 1999).

Recherche Supersuite meta-igneous rocks are also interpreted to occur in the Biranup Zone, and within the Munglinup Gneiss of the Northern Foreland. This assumes a spatial connection between the Kepa Kurl Booya Province and Northern Foreland, and between the Nornalup and Biranup Zones. The former is rather tenuous, and is based solely on the one example of Recherche Supersuite biotite granodioritic gneiss from near Bald Rock, which has an igneous crystallization age of 1299 ± 14 Ma (see **Geochronology of the Munglinup Gneiss**, above, Figs 10 and 13; GSWA 83690; Nelson, 1995e). If the spatial connection is assumed the occurrences of the Recherche Supersuite stitch the Biranup Zone with the Nornalup Zone, and the Kepa Kurl Booya Province with the Northern Foreland during Stage I of the Albany–Fraser Orogeny.

Recherche Supersuite meta-igneous rocks dated in the Biranup Zone are biotite monzogranitic gneiss from Mount Burdett (GSWA 83697; Nelson, 1995l), hornblende–biotite syenogranite gneiss from Coramup Hill (GSWA 83700A; Nelson, 1995m), and foliated leucogranite from Observatory Point (GSWA 83659; Nelson, 1995h; Myers, 1995b; Fig. 13). The biotite monzogranitic gneiss from Mount Burdett is found within a large, strongly deformed, fault slice within the Dalyup Gneiss (Geological Survey of Western Australia, 2007) and yielded a SHRIMP U–Pb zircon igneous crystallization age of 1299 ± 18 Ma (GSWA 83697; Nelson, 1995l). Both the hornblende–biotite syenogranite gneiss from Coramup Hill (GSWA 83700A; Nelson, 1995m) and the foliated leucogranite from Observatory Point (GSWA 83659; Nelson, 1995h) occur within the Coramup Gneiss (Fig. 13). The Coramup Hill orthogneiss (GSWA 83700A) yielded a SHRIMP U–Pb zircon age of 1283 ± 13 Ma, interpreted as the age of igneous crystallization of the precursor. The orthogneiss is strongly foliated and is interpreted to have been metamorphosed up to granulite facies, then retrogressed to amphibolite facies conditions (Nelson, 1995m). Foliated leucogranite from Observatory Point (GSWA 83659) yielded a SHRIMP U–Pb zircon age of 1288 ± 12 Ma, interpreted as the igneous crystallization age of the precursor granite (Nelson, 1995h; see also **Geochronology of the Coramup Gneiss**, above). These ages are slightly younger than those of the Recherche Supersuite metagranitic rocks within the Nornalup Zone, but the date of 1314 ± 21 Ma (GSWA 83663; Nelson, 1995k) from the granodiorite gneiss from Israelite Bay is within error.

The Esperance Supersuite represents magmatism associated with the late stages of Stage II of the Albany–Fraser Orogeny, at c. 1140 Ma (Nelson et al., 1995; Clark et al., 2000). The Esperance Granite of Myers (1995b) was defined by relatively undeformed, low metamorphic grade granitic rocks that intrude the Recherche Supersuite and was based on dating from Wireless Hill (GSWA 83657A; Nelson, 1995n), Balladonia Rock (GSWA 83667; Nelson, 1995o), and pegmatite south of Lake Gidong within the Dalyup Gneiss (GSWA 83652; Nelson, 1995e). The latter is excluded from the Esperance Supersuite because it is strongly deformed and yielded a SHRIMP U–Pb age of 1187 ± 12 Ma, similar to high grade metamorphic ages recorded in the Dalyup Gneiss (see **Geochronology of the Dalyup Gneiss**, above and Fig. 19).

Unmetamorphosed, porphyritic biotite granite sampled at Balladonia Rock in the northwestern part of the eastern Nornalup Zone has an imprecise SHRIMP U–Pb zircon age (based on five analyses) of 1135 ± 56 Ma, interpreted as the age of igneous crystallization (GSWA 83667; Nelson, 1995o). A similar, imprecise age was obtained from unmetamorphosed, porphyritic biotite monzogranite quarried from Wireless Hill in Esperance (GSWA 83657A, Nelson, 1995n) collected from Esperance Harbour jetty, which yielded a SHRIMP U–Pb zircon age of 1138 ± 38 Ma, interpreted as a minimum age of igneous crystallization of the monzogranite. The spatial extent of the Esperance Supersuite across the Albany–Fraser Orogen is not well constrained and it is presently confined to the Nornalup Zone.

Discussion and summary

This Record and GSWA (2007) review the geology of the southernmost part of the Yilgarn Craton and the central Albany–Fraser Orogen, and reinterpret the spatial and age relationships of the lithotectonic units of the latter, largely based on new geophysical and geochronological data. This sets the framework to reassess the crustal architecture and tectonic evolution, although there is still uncertainty about many aspects of the different units. In particular, there is much scope for:

1) new geochemical work to help understand protolith formation, relationships between lithotectonic units, and tectonic setting;
2) further geochronological work to help better constrain the timing of metamorphism in each unit, as well as continuing to constrain protolith ages and extents of the units;
3) more detailed structural analysis to help better constrain the structural evolution of each unit, and the kinematic history and timing of movement on the large faults that separate them; and
4) P–T–t analysis to help better constrain any differences in metamorphic evolution between the lithotectonic units, and differences across major faults.

All of these aspects are required to help understand the spatial relationships of the units over time, which is vital for understanding the tectonic setting and geodynamics. Further uncertainty arises because only part of the Orogen — effectively one side of it — is preserved, and exposure is limited. However, that part which is preserved has strongly contrasting rock properties that are well displayed in aeromagnetic imagery, which allows extrapolations from observed geology to be made and highlights features that are otherwise not visible. The high magnetite content concentrated in the fabric of the granulite facies rocks clearly outlines structures such as refolded folds and shears, even with data as coarse as 400 m line-spacing (e.g. Fig. 8). This has helped to determine the structural character and extent of the lithotectonic units.

The crustal architecture of the orogen appears to be dominated by craton-vergent (northwesterly) thrust faults and folds (mostly defined as F_2/D_2) at all scales, and to a lesser extent dextral shear zones (e.g. Myers, 1985; Beeson et al., 1988; Myers, 1990a, 1995b; Witt, 1998; Wetherley, 1998; Clark et al., 2000; Bodorkos and Clark, 2004b; Geological Survey of Western Australia, 2007). This has been interpreted to reflect a largely compressional regime during both Stages I and II. However, extension also appears to have played a part, with some of the best evidence for this being the major boudin structures in the Bremer Bay area. Extensional structures are often more subtle and can be difficult to define when overprinted by compressional ones, and may be more widespread than currently recognized.

Lithotectonic units of the Albany–Fraser Orogen

The major lithotectonic units of the Albany–Fraser Orogen are here defined as the Northern Foreland, which is the reworked component of the southern Yilgarn Craton (including the Munglinup Gneiss), and the Kepa Kurl Booya Province, which is defined as the disparate crustal fragments affected by, and probably amalgamated by, Stage I tectonism. The Kepa Kurl Booya Province is divided into three major tectonic zones, plus the Recherche and Esperance Supersuites, and various Mesoproterozoic cover rocks (Figs 1 and 27). The three major tectonic zones are the c. 1690–1660 Ma Biranup Zone (which includes the Dalyup and Coramup Gneisses), the Fraser Zone (which includes the c. 1300 Ma Fraser Range Metamorphics), and the c. 1500–1300 Ma Nornalup Zone (which includes the Malcolm Gneiss and some of the gneissic rocks in the Albany region). The c. 1330–1280 Ma Recherche and c. 1140 Ma Esperance Supersuites are most voluminous within the Nornalup Zone.

The Northern Foreland is defined as those parts of the southern Yilgarn Craton that were affected by deformation associated with the collision of the Mawson Craton, and the intracratonic deformation that followed (i.e. Stages I and II of the Albany–Fraser Orogeny). In contrast, the Biranup Zone of the Kepa Kurl Booya Province has protolith ages of c. 1690–1660 Ma, with most dated at c. 1680 Ma. As there is no evidence of a magmatic or tectonothermal event in the southern Yilgarn Craton at this time, the Biranup Zone is interpreted as an exotic terrane that was wedged between the Yilgarn Craton and the Nornalup Zone during the collision (cf. Nelson et al., 1995; Clark et al., 2000). The only potential evidence of its presence in other lithotectonic units is in rare xenocrystic and detrital zircons from slivers of metagranite and quartz metasandstone from the Fraser Range Metamorphics (GSWA 177910, Wingate and Bodorkos, 2007b; De Waele and Pisarevsky, 2008). The Dalyup Gneiss has been interpreted as a possible source for detrital zircons with ages of 1750–1720 Ma analyzed by Clark (1995) in paragneiss from the western Nornalup Zone (Fitzsimons, 2003; Fitzsimons and Buchan, 2005), but it is now clear that these zircons are older than the Dalyup Gneiss. An alternative source might have been from rocks associated with the c. 1740–1690 Ma Kimban Orogeny in the Gawler Craton (Betts and Giles, 2006, and references therein; Payne et al., 2008).

If xenocrystic and detrital zircons in the Fraser Range Metamorphics were sourced from the Biranup Zone they indicate a spatial relationship between it and the Fraser Zone after 1466 ± 17 Ma (the maximum depositional age of the metamorphosed quartz sandstone, Wingate and Bodorkos, 2007b) and at c. 1300 Ma, when the metagranite intruded the gabbroic rocks of the Fraser Range Metamorphics. This implies that at least part of the Biranup Zone, or potentially supracrustal rocks associated with it, had been uplifted and eroded by this time and were adjacent to the Fraser Zone during its formation. Alternatively, the xenocrystic and detrital zircons within the Fraser Range Metamorphics could be far-travelled detritus, possibly sourced from the Capricorn Orogen, which contains rocks formed during the 1680–1620 Ma Mangaroon Orogeny (Sheppard et al., 2005). This would indicate that the Fraser Zone was adjacent to the Yilgarn Craton at c. 1300 Ma.

The post-1560 Ma Nornalup Zone is dominated by meta-igneous and granitic rocks of the Recherche and Esperance Supersuites, with the Malcolm Gneiss in the eastern Nornalup Zone being the only pre- or syn-Stage I unit providing any evidence of its origin. Granitic rocks loosely referred to as '?c. 1450 Ma' in Myers (1995b) have not been directly dated and it is not clear what they represent. The maximum depositional age for the protolith of the paragneiss in the Malcolm Gneiss is 1560 ± 40 Ma (n=10), from near Point Malcolm (GSWA 112128; Nelson, 1995i). These rocks were metamorphosed during intrusion of Recherche Supersuite granitic rocks at 1330 ± 14 Ma (GSWA 83662; Nelson, 1995j) and 1314 ± 21 Ma (GSWA 83663; Nelson, 1995k). The older age provides a minimum age for deposition of the Malcolm Gneiss protolith. Paragneiss at Whalehead Rock in the western Nornalup Zone was deposited between 1360–1310 Ma (Love, 1999; Fitzsimons and Buchan, 2005). If the precursors to the Malcolm Gneiss and Whalehead Rock paragneisses are about the same age it is possible that deposition of both units occurred just prior to, or during the very early stages of, Stage I of the Albany–Fraser Orogen. This would restrict all rocks in the Nornalup Zone as having formed during the Albany–Fraser Orogeny, or just prior to it, but much more data are needed to decipher this. It is also possible that the older rocks (proto-Malcolm Gneiss) of the Nornalup Zone formed part of a post-1560 Ma passive margin of the Mawson Craton, and that these rocks were not affected by tectonism until Stage I of the Albany–Fraser Orogeny. However, as stated above (see **Albany–Fraser Orogen**, above), it is not clear what influence the Madura, Waigen, Forrest, and Coompana Complexes may have had, and it is possible that the proto-Malcolm Gneiss was derived from one of these entities.

Tectonic history of the Albany–Fraser Orogen

The Albany–Fraser Orogeny has been divided into two stages of tectonothermal activity, based on geochronological, structural, and petrographic relationships

(Clark et al., 2000). Clark et al. (2000) attributed Stage I tectonism to c. 1345–1260 Ma convergence and collision of the West Australian – North Australian Craton and the Mawson Craton (Fitzsimons, 2003), with the Nornalup Zone interpreted as the western margin of the latter (Bodorkos and Clark, 2004b). Collision is interpreted to have occurred during Stage I owing to the presence of 'stitching plutons' of the Recherche Supersuite across the orogen (Fig. 27), although the evidence for this in the Northern Foreland is tenuous (see **Recherche and Esperance Supersuites**, above). Stage II tectonic activity is interpreted as c. 1215–1140 Ma intracratonic reactivation during assembly of the Rodinia supercontinent (Clark et al., 2000; Fitzsimons, 2003). It should be noted that unequivocal evidence for high-grade metamorphism during Stage I occurs only in the Fraser Range Metamorphics (Fraser Zone) and the Nornalup Zone, whereas during Stage II high-grade metamorphism appears to have been more focused into the Northern Foreland (Munglinup Gneiss) and the Biranup Zone (Dalyup and Coramup Gneisses; excluding Biranup Zone inboard of the Fraser Zone), based on SHRIMP U–Pb zircon geochronology. The Nornalup Zone also contains evidence of overprinting of Stage I assemblages by Stage II high grade metamorphism (Clark et al., 2000), but no Stage II metamorphic ages have been reported for the Fraser Range Metamorphics (Fraser Zone). This is supported by pre-1250 Ma Rb–Sr cooling ages (Bunting et al., 1976; Fletcher et al., 1991).

Sampling bias and almost exclusive use of the SHRIMP U–Pb zircon dating technique may be factors, but one would expect some preservation of zircon growth from Stage I granulite facies metamorphism. Another possibility is that Stage I did not reach high enough temperatures for long enough for significant zircon growth within the units where such data are lacking. This suggests that the inboard part of the eastern Albany–Fraser Orogen was a locus for high temperature tectonism during Stage I, but escaped high temperature reworking during Stage II, whereas the Northern Foreland (Munglinup Gneiss and Mount Barren Group) and Biranup Zone (Dalyup Gneiss and Coramup Gneisses; excluding Biranup Zone inboard of the Fraser Zone) were the locus for high temperature reworking during Stage II (Fig. 28). However, it is feasible that some displacement of crustal material has occurred in the relatively thinner, central Albany–Fraser Orogen that may have contained evidence of Stage I high temperature metamorphism, possibly during the Stage II extensional (or ?transtensional) events evident in the large-scale boudinage of the orthogneisses in the Bremer Bay area.

Stage I (c. 1345–1260 Ma)

Stage I marks the time when all of the lithotectonic units of the orogen underwent either tectonothermal or magmatic activity synchronously (Fig. 27). This is taken as the best estimate of the timing of suturing of the Kepa Kurl Booya Province onto the Yilgarn Craton margin primarily via northwest–directed thrusting (cf. Myers et al., 1996; Clark et al., 2000; Bodorkos and Clark, 2004b). However, one of the problems with understanding the tectonic history of the orogen as a whole is understanding the spatial relationships between the different lithotectonic units over time. This is particularly difficult for the early parts of their histories. The paleogeographic arrangement of the lithotectonic units prior to amalgamation is largely unknown, so any interpreted tectonic links and settings are speculative. If we accept that the Biranup Zone was an exotic terrane whose protolith formation was independent of the Albany–Fraser Orogeny, then the question arises as to how it became part of the Kepa Kurl Booya Province, and whether the Kepa Kurl Booya Province formed a complete entity prior to collision with the Yilgarn Craton?

The presence of 1690–1660 Ma detrital and xenocrystic zircons, albeit scant, in metasedimentary and metagranitic rocks within the Fraser Range Metamorphics suggests that the Biranup Zone may have been linked to the Fraser Zone at c. 1300 Ma. If the Fraser Range Metamorphics represent one or more remnant arcs, as suggested by Condie and Myers (1999), then it is possible that this arc developed adjacent to the Biranup Zone, either prior to, during, or after collision with the craton margin (Fig. 29). Much more work is needed to resolve questions such as this, particularly on the extent of the Biranup Zone in the eastern Albany–Fraser Orogen, and on the kinematics of major structures separating the lithotectonic units to establish what displacements have occurred.

The Biranup Zone appears to have been caught within the convergent zone between the West Australian – North Australian Craton and the Mawson Craton during Stage I (cf. Nelson et al., 1995). Bodorkos and Clark (2004b) suggested that subduction during convergence dipped to the southeast, because of the record of pre-1313 Ma magmatic and tectonothermal activity within the Nornalup Zone (Mawson Craton; Fig. 29a). Continued convergence would have resulted in collision of the Biranup Zone with the Nornalup Zone, potentially triggering a readjustment of the subduction zone causing it to step back towards the West Australian – North Australian Craton (southern Yilgarn) margin (Fig. 29b). Inferred transform faults along which the Biranup Zone may have migrated could have provided zones of weakness to facilitate this. This would have been coincident with early Stage I deformation in the Nornalup Zone, such as formation of northwesterly verging folds that are cut by an aplite dyke with a SHRIMP U–Pb zircon age of 1313 ± 16 Ma (Clark et al., 2000). Continued retreat of the subduction zone towards the West Australian – North Australian Craton (southern Yilgarn) margin would have extended the Biranup Zone and allowed formation of a magmatic arc, producing the Fraser Range Metamorphics (Fig. 29c). Continued convergence would result in final collision of the West Australian – North Australian Craton and the Mawson Craton, probably between c. 1300–1280 Ma. This is based on the age of intrusion of biotite granodioritic gneiss at 1299 ± 14 Ma (GSWA 83690; Nelson, 1995e) into the Northern Foreland, stitching of the Biranup and Nornalup Zones by late-stage (1300–1280 Ma) Recherche Supersuite plutons (Clark et al., 1999, 2000; Bodorkos and Clark, 2004b), and thrusting of the Nornalup Zone over the Biranup and Fraser Zones along the Heywood – Cheyne Fault Zone. This is also the timing of crustal thickening and high pressure and temperature metamorphism of the Fraser Range Metamorphics (Clark et al., 1999).

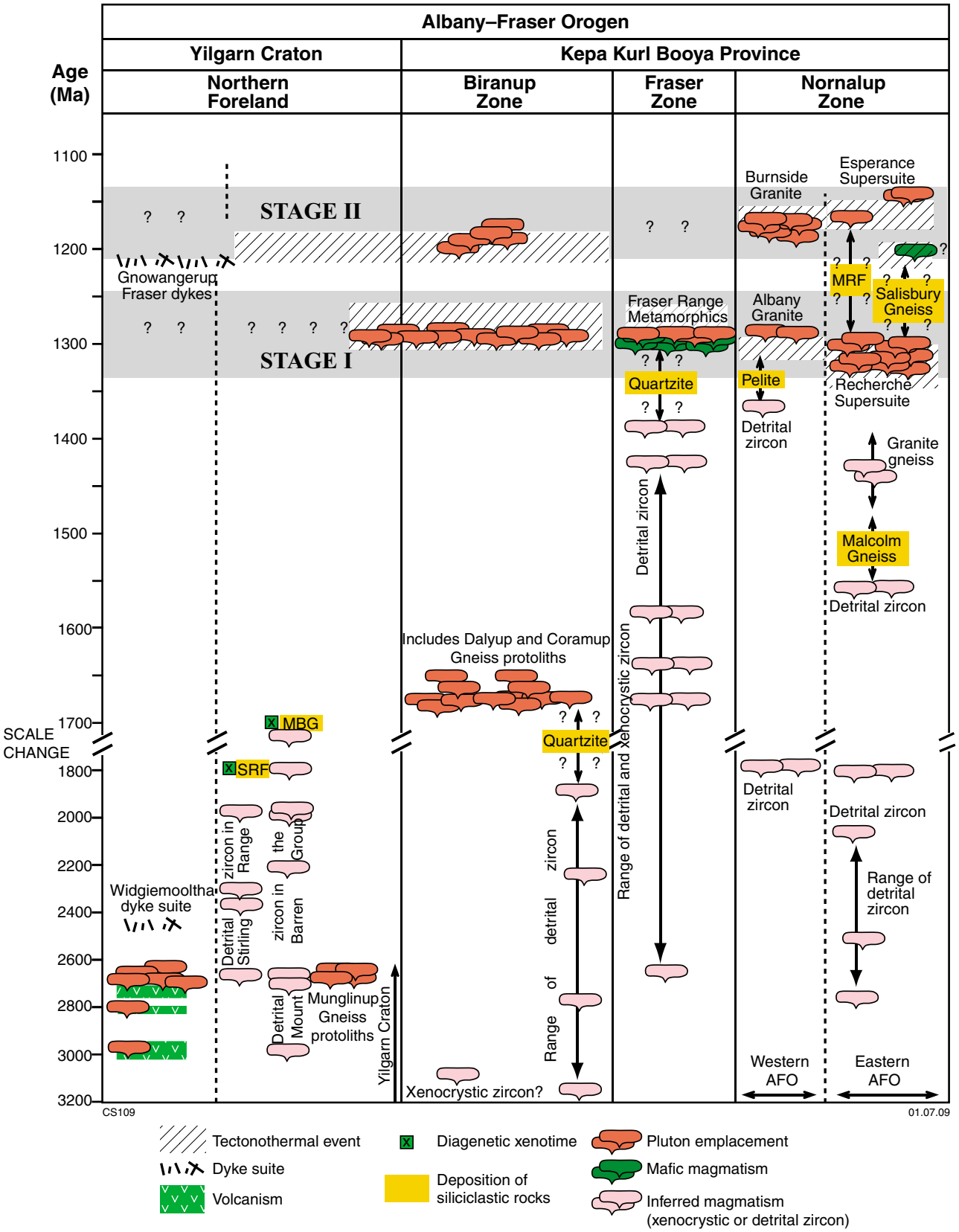

Figure 27. Time-space plot showing age relationships between the Northern Foreland, Biranup Zone, Fraser Zone and Nornalup Zone (modified from Fitzsimons and Buchan, 2005; see text for age data references). AFO=Albany–Fraser Orogen; SRF=Stirling Range Formation; MBG=Mount Barren Group; MRF=Mount Ragged Formation.

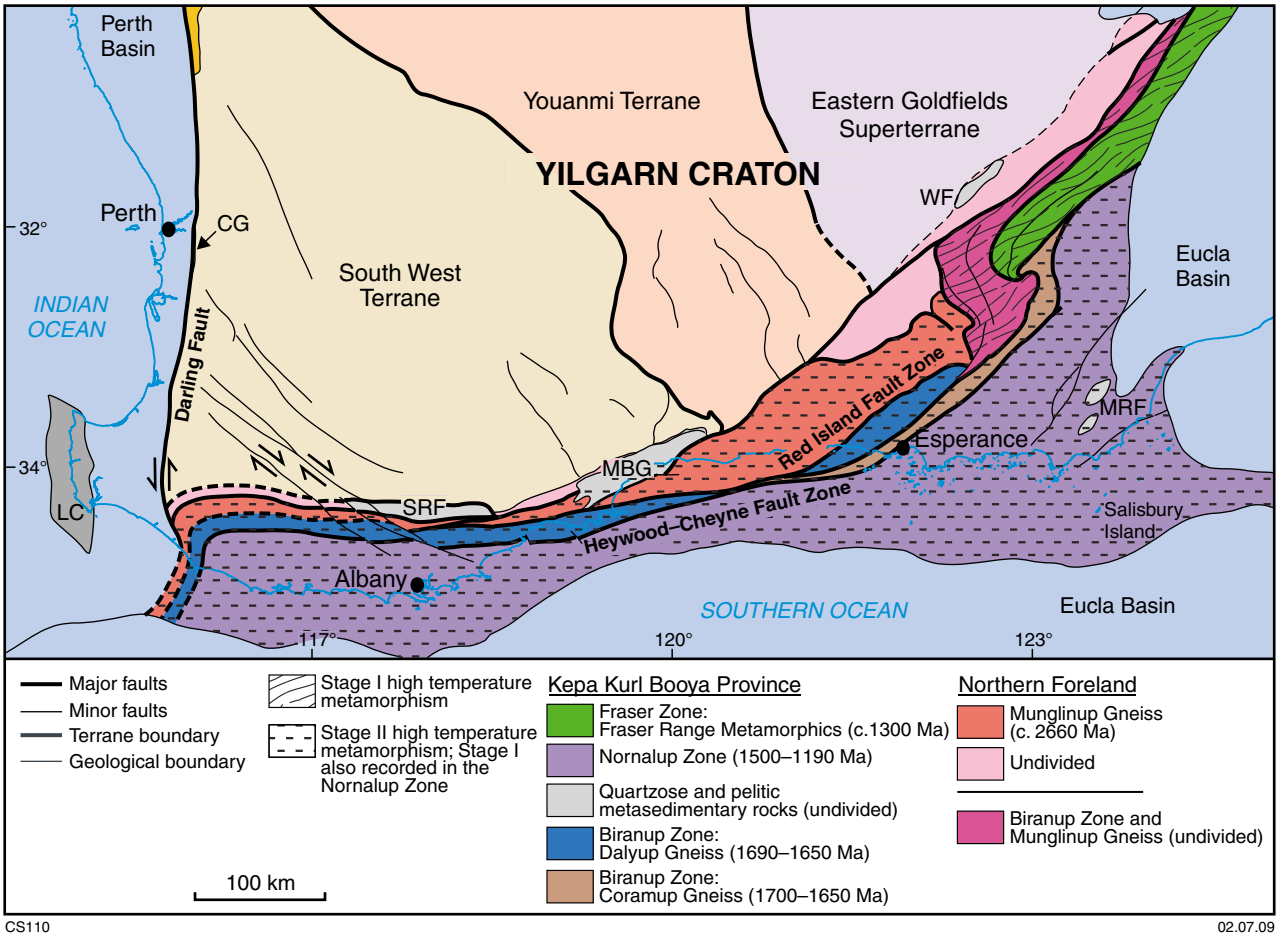

Figure 28. Geological map of the Albany–Fraser Orogen showing where high temperature metamorphism during Stages I and II is evident, as defined by SHRIMP U–Pb zircon geochronology. Note that both Stages I and II are recorded in the Nornalup Zone. CG, Cardup Group; LC, Leeuwin Complex; MBG, Mount Barren Group; MRF, Mount Ragged Formation; SRF, Stirling Range Formation; WF, Woodline Formation. Adapted from Geological Survey of Western Australia (2007), Tyler and Hocking (2001), and Fitzsimons and Buchan (2005).

Stage II (c. 1215–1140 Ma)

During the period between Stages I and II (c. 1260–1215 Ma) the sedimentary protoliths of the Mount Ragged Formation and the Salisbury Gneiss were deposited into shallow intracratonic basins, probably during extension of the collision-thickened crust (Clark et al., 2000; Bodorkos and Clark, 2004b). If we accept that Stage I marks the collision and stitching of the West Australian – North Australian Craton and the Mawson Craton, then Stage II must represent repeated intracontinental reworking of the orogen over approximately 75 million years at high temperatures (amphibolite to granulite) on a major scale. This would have modified the crustal architecture of the orogen significantly.

The commencement of Stage II was marked by high temperature metamorphism of the Salisbury Gniess in the eastern Nornalup Zone and the Coramup Gneiss in the Biranup Zone between c. 1225–1215 Ma (Clark et al., 2000; Bodorkos and Wingate, 2008k, l). The metamorphic dates of c. 1225 Ma recorded in the Coramup Gneiss suggest Stage II may have commenced slightly earlier than previously proposed by Clark et al. (2000). This was followed by the widespread emplacement of the c. 1210 Ma Gnowangerup–Fraser Dyke Suite (Clark et al., 2000; Wingate et al., 2000; Wingate et al., 2005). Intrusions of the Gnowangerup–Fraser Dyke Suite appear to be particularly dense around the southern to southeastern Yilgarn Craton margin, probably because the dykes are not readily recognizable in aeromagnetic images within the Northern Foreland and Kepa Kurl Booya Province due to metamorphism and deformation during Stage II (see Fig. 4). The Gnowangerup–Fraser Dyke Suite are part of the c. 1210 Ma Marnda Moorn large igneous province, which comprises several other dyke suites concentrated around the margins of the Yilgarn Craton, as well as some within it (Wingate, 2007). The orientation of the Gnowangerup–Fraser Dyke Suite subparallel to the regional trend of the Albany–Fraser Orogen suggests emplacement into zones of weakness formed during tectonic loading leading to downwards flexure of the craton margin, during Stage II of the Albany–Fraser Orogeny (Wingate et al., 2000). This interpretation is consistent with inferred broadly northwest–southeast stress directions (e.g. Beeson et al., 1988; Myers, 1990a,

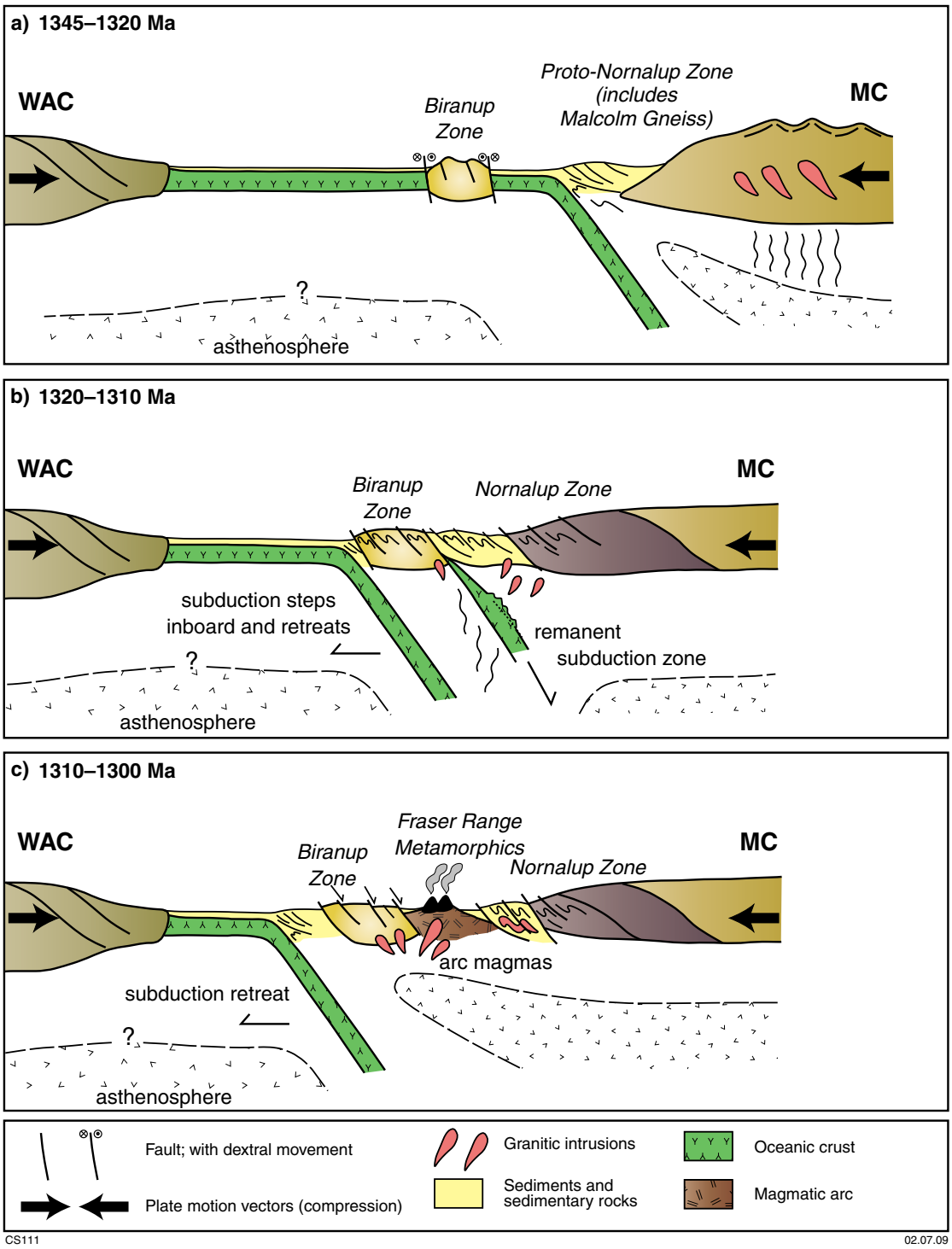

Figure 29. **Tectonic cartoons of the pre-collision part of Stage I of the Albany–Fraser Orogeny, modified from Bodorkos and Clark (2004b). Note that the Mawson Craton (MC) could include the Madura, Forrest, Waigen or Coompana Complexes. The combined North Australian–West Australian Craton is shown as WAC: a) southeast-dipping subduction during convergence of the WAC and MC, with the exotic Biranup Zone situated along inferred transform faults within the intervening ocean. Southeast-dipping subduction would have produced the early high temperature and low pressure metamorphism in the Malcolm Gneiss and early Recherche Supersuite intrusions in the Nornalup Zone (Clark et al., 2000); b) continued convergence resulting in collision of the Biranup Zone with the Nornalup Zone, potentially triggering a readjustment of the subduction zone causing it to step back towards the WAC. Inferred transform faults along which the Biranup Zone may have migrated could have provided zones of weakness to facilitate the change in subduction position. Early northwesterly verging folds cut by aplitic dykes were produced at this time (Clark et al., 2000); c) retreat of the subduction zone towards the WAC margin caused extension of the Biranup Zone and allowed formation of a magmatic arc, producing the Fraser Range Metamorphics. Collision of the WAC and MC is interpreted to occur shortly afterwards.**

1995b; Witt, 1998; Clark et al., 2000), and the presence of numerous fractures and faults visible in aeromagnetic images that are subparallel to the dykes.

High temperature metamorphism during Stage II appears to have been most widespread at c. 1180 Ma, with rocks in the Northern Foreland (Munglinup Gneiss and Mount Barren Group), the Biranup Zone (both Dalyup and Coramup Gneisses), and the Nornalup Zone (Salisbury Gneiss) affected (see respective geochronology sections above for details). The Dalyup Gneiss in the Bremer Bay area appears to have been dominated by both boudinage and extension and northwest-vergent folding at this time, whereas to the east on the coast near Lake Gidong (east of Quagi Beach, Fig. 10) it was dominated by shearing. Further to the east, at Butty Head (Fig. 13) the Coramup Gneiss is interpreted to record upright folding at about this time, or just after it (Bodorkos and Clark, 2004b). This suggests major differences in structural style and kinematics along the strike of the orogen, and within different units. High temperature metamorphism re-occurred between c. 1170–1150 Ma in the Biranup Zone, but was probably less extensive, and possibly also occurred in the Munglinup Gneiss, but more data are need to confirm this. At approximately the same time thrusting along the Rodona Fault and deformation of the Mount Ragged Formation in the eastern Nornalup Zone are also interpreted to have taken place (Clark et al., 2000), along with intrusion of the Burnside Granite and related metamorphism of the host pelitic rocks in the western Nornalup Zone (Clark, 1995).

From the geochronological data it is evident that high temperature metamorphism and associated deformation was widespread during Stage II. However, in most cases it is difficult to assign particular structures to Stages I or II without the facility to date specific fabrics or cross-cutting elements. At Bremer Bay, high temperature metamorphism and intermediate- and large-scale boudinage relating to the second and third phases of extension, respectively, occurred during Stage II at c. 1180 Ma, and bracket the large-scale northwest-vergent F_3 folding event (see **Dalyup Gneiss**, above). Stage II metamorphism has also been constrained in the Mount Barren Group, where Dawson et al. (2003) interpreted xenotime and monazite ages of 1206 ± 6 and 1194 ± 8 Ma, respectively, to record static overprinting of peak D_2 assemblages that were assumed to have formed during Stage I. However, no geochronological evidence of Stage I metamorphism or deformation in the Mount Barren Group has been found, and it is also possible that the northwest-vergent, asymmetric folding associated with the D_2 fabrics occurred during Stage II. Beeson et al. (1988) also defined similar, northwest-vergent, asymmetric D_2 folds within the Biranup Zone (their Central Domain), but these structures have not been dated. All of these areas share a similarity in the dominant northwest-vergent fold style, and the available geochronology suggests that this folding may have occurred synchronously during Stage II. If this is the case it would indicate that the northwest-vergent folding post-dated collision of the Biranup Zone with the Northern Foreland, which contains the Mount Barren Group. Alternatively, the similarity in fold style may just be a function of a long-lived, northwest–southeast, dominantly compressional stress regime, and the folding could have been diachronous. Major, lithotectonic unit-bounding faults, such as the Red Island Shear Zone, mostly cross-cut the main structures and fabrics and must have been active during the late stages of Stage II. They are also likely to be the main structures along which the high grade rocks were exhumed.

Major structures in the Albany–Fraser Orogen

The northern limit of the Northern Foreland is generally marked by a gradual increase in deformation intensity and metamorphic grade towards the orogen (Beeson et al., 1988; Jones, 2006). Major faults such as the Jerdacuttup and Cundeelee Faults generally mark sharp contacts between rocks with different metamorphic grade and deformation intensity within the Northern Foreland, and have been interpreted to have either thrust or transpressional kinematic histories (Myers, 1995a,b), although poor exposure makes this difficult to assess (Fig. 2). The Jerdacuttup Fault juxtaposes granulite facies, multiply deformed rocks of the Munglinup Gneiss against greenschist to amphibolite facies rocks of the Yilgarn Craton and the Northern Foreland. In the central Albany–Fraser Orogen it is interpreted to be the major structure along which mid-crustal rocks of the Northern Foreland (Munglinup Gneiss) were exhumed during the late stages of Stage II of the Albany–Fraser Orogeny, post-dating c. 1180 Ma granulite-facies metamorphism, and may have had an extensional geometry initially. Significant extension during Stage II of the Albany–Fraser Orogeny is evident in Biranup Zone rocks in the west (e.g. at Bremer Bay) where leucosomes formed in the necks of boudins indicate extension at c. 1180 Ma (see **Geochronology of the Biranup Zone**, above). Boudinage on this scale is not evident in Biranup Zone rocks to the east (near Esperance). This suggests a potential link between extensional exhumation of the Munglinup Gneiss, and extension of the western part of the Biranup Zone.

Unlike the Northern Foreland and Yilgarn Craton, the contact between the Northern Foreland and the c. 1690–1660 Ma Biranup Zone is sharp and is marked by major structures such as the Red Island Fault Zone and the Bremer Fault (Fig. 2). Again, these structures are interpreted to have formed during the late stages of Stage II of the Albany–Fraser Orogeny, post-dating c. 1180 Ma granulite-facies metamorphism, but are probably reworked structures that initially formed during Stage I collision. Kinematics are difficult to determine as the major faults do not crop out, and rocks on both sides have reached granulite facies during Stage II. In the Pallinup River area to the west, Beeson et al. (1988) interpreted ductile dextral transpression along the contact (Millers Point Thrust, which links to the Bremer Fault) overprinted by a more brittle episode of sinistral shearing. Further outboard, the contact between the Biranup Zone and the Nornalup Zone is marked by the Heywood–Cheyne Fault Zone, a major structure interpreted to link the Heywood Fault where it was mapped in the east (Clark, 1999; Bodorkos and Clark, 2004b) with a major fault to the west that cuts through Cheyne Bay, just north of Cape Riche where rocks

of the Nornalup Zone have been mapped (Fitzsimons and Buchan, 2005). Linking large structures across the Southern Ocean between exposures in the west to those in the east (Fig. 2) is problematic, because the higher resolution aeromagnetic data does not continue offshore (e.g. Fig. 8b). However, broad-scale magnetic anomalies are visible and the interpreted structures are based on existing geochronological and lithological data of onshore rocks.

Most of the major structures in the Albany–Fraser Orogen have been interpreted as north to northwesterly verging thrusts, usually with a component of dextral transpression (e.g. Myers, 1989; Witt, 1998; Wetherley, 1998; Clark et al., 2000; Fitzsimons and Buchan, 2005). The aeromagnetic imagery shows that the continuation of the Coramup Gneiss adjacent to the Coramup Fault Zone from the coast to the northeast is intensely sheared and contains large-scale sheath folds (Fig. 14). The presence of L-tectonites within these zones (Fig. 22a,b) indicates a substantial flattening component during shearing, which suggests northwesterly-directed compression. These structures are clearly folded about northeasterly trending fold axes, forming the 'S-bend' at the southwestern end of the Fraser Zone (Fig. 14). This geometry may indicate a component of late sinistral shear within this part of the orogen. Late, sinistral shearing has also been recognized in the Coramup Gneiss and western parts of the orogen (Beeson et al., 1988; Harris, 1995; Bodorkos and Clark, 2004b). Alternatively, it may have been produced by ongoing compression, possibly with a slight change in stress orientation, resulting in folding of the thrust surfaces after they had locked up.

Late, northwesterly trending brittle faults with apparent dextral sense cut through all units of the Albany–Fraser Orogen and the southern Yilgarn Craton. The age of these structures is unknown, but they appear to be part of the same set of faults that controlled deposition of the Permian to Cretaceous sediments in the Collie Basin to the north (Wilson, 1990), so are relatively young. Aeromagnetic imagery also shows a significant set of northeasterly trending brittle faults and fractures that are abundant within the southern Yilgarn Craton, but not the Albany–Fraser Orogen.

Geometry of the southern margin of the Yilgarn Craton

The east- to northeasterly trending Albany–Fraser Orogen truncates the entire southern margin of the Yilgarn Craton, including the South West Terrane, the Youanmi Terrane, and the Eastern Goldfields Superterrane (Fig. 1; Cassidy et al., 2006). These terranes are dominated by northwesterly trending structures, including their domain and terrane boundaries. The boundary between the South West and Youanmi Terranes is poorly defined (Cassidy et al., 2006), and at present is drawn along the western edge of the Carlingup and Cocanarup Greenstone Belts near Ravensthorpe. The terrane boundary follows a major fault that extends northwest from the northern tip of the greenstone belts, but further work, in particular geochronology, is needed to test whether a terrane distinction can be made. In contrast, the terrane boundary between the Youanmi Terrane and the Eastern Goldfields Superterrane is well marked by the Ida Fault (Swager, 1997), which is coincident with a sharp change from older to younger Sm–Nd model ages from west to east (Figs 2 and 30; Cassidy et al., 2002; Champion and Cassidy, 2007). However, the southern extension of this terrane boundary is not so clear because the Ida Fault is intruded by voluminous late Archean granitic rocks, and the Sm–Nd data are sparse. South of the Cundeelee Fault, within the Northern Foreland of the Albany–Fraser Orogen, the terrane boundaries are reworked and cryptic, and difficult to detect without extensive robust geochemical and geochronological data. In the southern Fraser area (Figs 13 and 14) the large 'S-bend' is coincident with the craton margin where combined Munglinup Gneiss and undifferentiated Biranup Zone rocks wrap around the southwestern end of the Fraser Zone. This could be due to the original margin geometry that existed prior to the collision of the Albany–Fraser Orogen. It is also possible that the Youanmi Terrane and the Eastern Goldfields Superterrane boundary may have been coincident with this margin geometry, and that the Youanmi Terrane extended further south, perhaps as a promontory. Deformation due to the collision of the Mawson Craton, and reworking during Stage II of the Albany–Fraser Orogeny, probably with a late component of sinistral strike-slip offset, would then have modified this geometry as is evident by the intense shearing, formation of refolded folds (e.g. Fig. 14), and interleaving of the craton margin, Biranup Zone, and Fraser Zone.

Origin of the Biranup Zone

The 1690–1660 Ma Biranup Zone, including the Coramup and Dalyup Gneisses, comprises a large piece of exotic middle crust sandwiched between the southern Yilgarn Craton margin and the Fraser and Nornalup Zones (Figs 1 and 2). It appears unlikely to have formed in situ, as there is no evidence of tectonothermal activity in adjacent lithotectonic units at that time (cf. Nelson et al., 1995). Therefore the question arises, where did it come from? Considering known sources preserved within the Australian continent two possibilities stand out: the western Gawler Craton and the southern Arunta Orogen (Fig. 5; Spaggiari et al., 2008). Both of these contain granitic rocks of the same age, but more information is required to constrain these hypotheses, which are clearly speculative. If the western Gawler Craton is a possible source then we have to understand what the roles of the Madura, Forrest, Waigen, and Coompana Complexes were, as these entities presently lie between the Albany–Fraser Orogen and the western Gawler Craton (Fig. 5). This is problematic because the basement rocks are entirely obscured by Phanerozoic cover, and the only information comes from sparse drillcore (see **Albany–Fraser Orogen** above). Extracting a large piece of crust (i.e. the Biranup Zone protoliths) from the present-day western Gawler Craton margin and juxtaposing it along the southern edge of the Yilgarn Craton involves reconciling all of these entities into their current configuration. However, if we consider the reconstruction of Betts et al. (2008) then this becomes feasible (Fig. 31). In these reconstructions the southern Arunta Orogen (Warumpi Province) and

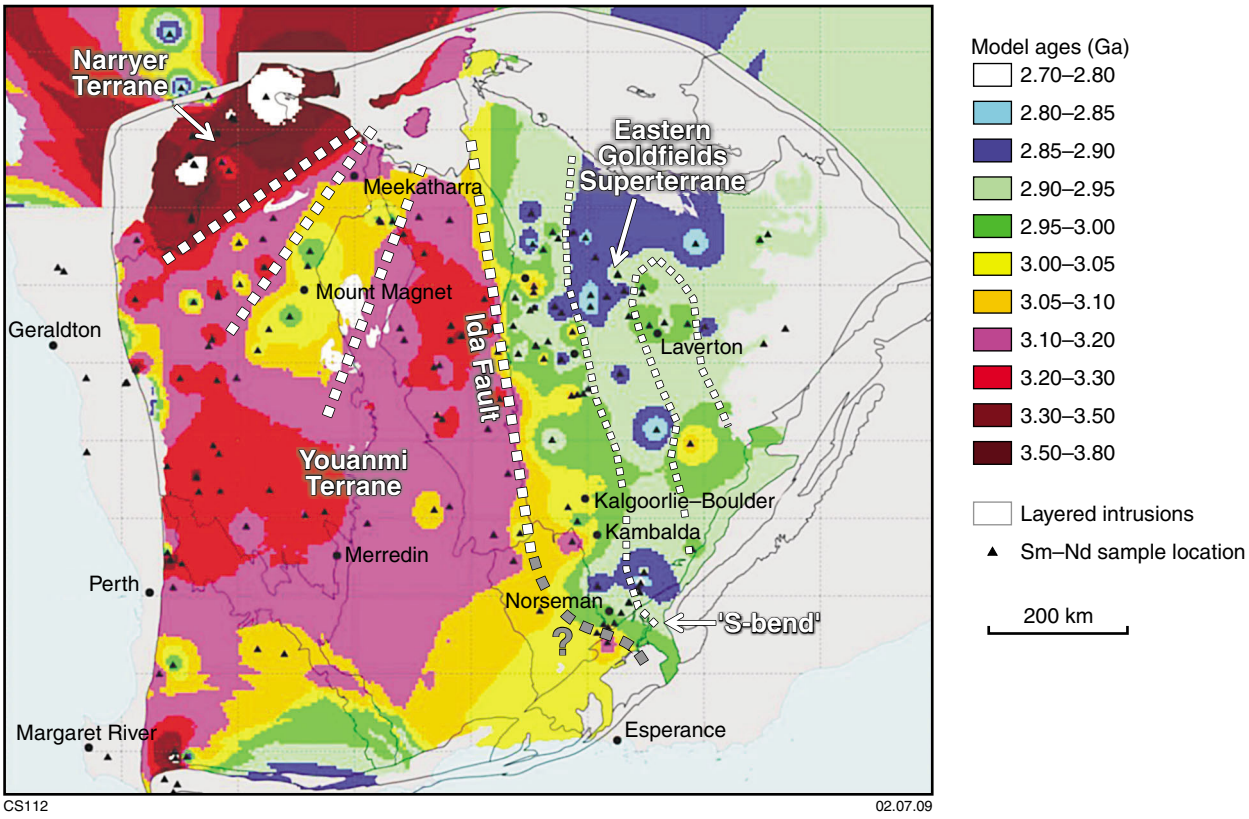

Figure 30. Sm–Nd model ages map of the Yilgarn Craton, showing the boundary between the Youanmi Terrane and Eastern Goldfields Superterrane, and the Ida Fault and its interpreted continuation to the south (after Champion and Cassidy, 2007).

part of the western Gawler Craton (Fowler Terrane) are situated along-strike from each other, behind the Mawson Craton, which includes the Archean nucleus of the Gawler Craton and is interpreted to have collided with the North Australian Craton (NAC) during the 1740–1690 Ma Kimban Orogeny. The Warumpi Province and Fowler Terrane contain rocks of comparable age to the Biranup Zone protoliths and may have been originally linked (Fig. 31). Episodic magmatism occurred during 1740–1640 Ma in the western Gawler Craton and includes emplacement of the Ifould and Tunkillia Suites, which have been interpreted to have arc-like geochemical signatures (Betts et al., 2008 and references therein). The 1690–1670 Ma Tunkillia Suite (Teasdale, 1997; Ferris and Schwartz, 2004; Fanning et al., 2007) matches the protolith ages of the Biranup Zone but its inferred subduction-related setting is disputed by Payne et al. (2006), who suggest a late- to post-tectonic setting related to the Kimban Orogeny instead.

The Warumpi Province is the south-westernmost part of the Arunta Orogen and contains metamorphic rocks with igneous and sedimentary protolith ages dated between 1690–1600 Ma (Scrimgeour et al., 2005). It contains voluminous high–K alkaline felsic intrusive and extrusive rocks that are interpreted as a magmatic arc that formed outboard of the NAC between 1690–1670 Ma, during a period of south-dipping subduction known as the Argilke Event that followed a long period of north-dipping subduction along the southern margin of the NAC (Fig. 32a; Scrimgeour et al., 2005; Close et al., 2006; Betts and Giles, 2006). Although clearly speculative, it is possible that the Biranup Zone protoliths formed at this time as part of the same complex.

Clearly distinct from the NAC, the Warumpi Province is interpreted as exotic (Scrimgeour et al., 2005; Close et al., 2006). It comprises rocks with younger and less evolved isotopic signatures, and younger protoliths that lack NAC inheritance. There is also no record of felsic magmatism of Warumpi Province age within the adjoining Aileron Complex of the NAC (Scrimgeour et al., 2005; Close et al., 2006). ε_{Nd} values between -2.64 and -1.29 suggest the Warumpi Province arc magmas intruded a fragment of pre-existing crust (Close et al., 2006). Although the data are sparse, similar conclusions can be drawn for the protoliths of the Biranup Zone (see **Crustal formation of the Dalyup Gneiss** above).

During the period 1660–1650 Ma a fore-arc sedimentary sequence interlayered with mafic rocks was deposited and subsequently metamorphosed at high temperatures and pressures (Yaya Metamorphic Complex) during the Liebig Orogeny, between 1640–1635 Ma (Scrimgeour et al., 2005; Close et al., 2006). The Liebig Orogeny marked the oblique accretion of the Warumpi Province to the NAC southern margin, with the subsequent development of the Central Australian Suture and associated bimodal

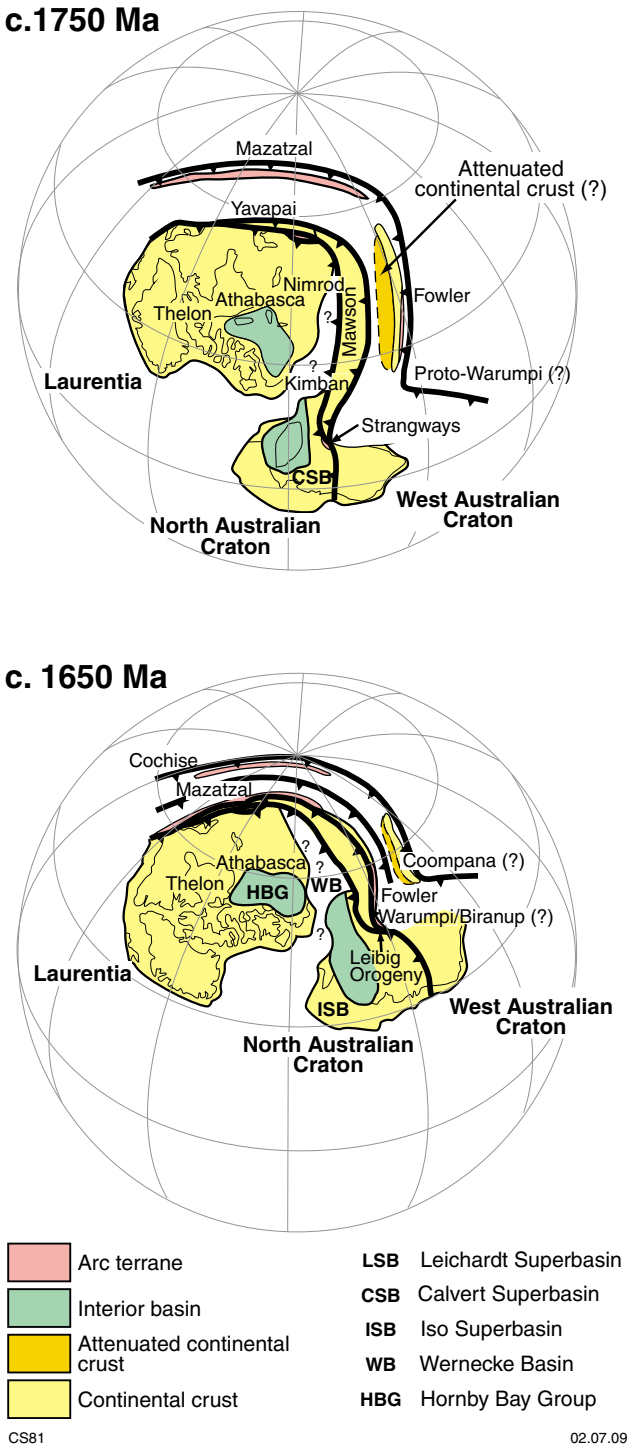

Figure 31. Reconstructions of Australia and Laurentia at c. 1750 and c.1650 Ma. The Biranup Zone is added as a possible part of the Warumpi Province that was subsequently rifted before being caught in the c. 1300 Ma Stage I collision of the Albany–Fraser Orogen (modified from Betts et al., 2008).

magmatism and formation of layered intrusions (Fig. 32b) (Scrimgeour et al., 2005; Close et al., 2006). It is possible that at this time the 'back-end' of the Warumpi Province rifted off as south-dipping subduction ceased due to the accretion of the Warumpi Province onto the NAC, and stepped outboard, possibly as a renewed north-dipping subduction zone beneath the rifted fragment. In this model this fragment would eventually become the Biranup Zone. The Liebig Orogeny was followed by a period of extension between 1630–1610 Ma that resulted in rapid exhumation of the deeply buried forearc sequence (Yaya Metamorphic Complex) and deposition of another sedimentary package (Fig. 32c) (Iwuputaka Metamorphic Complex; Close et al., 2006). Extension may have been caused by roll-back of the renewed subduction zone, allowing further displacement of the rifted fragment. This is consistent with the models of Betts et al. (2008) who argue that the NAC plate margin successively stepped out to the south behind various fragments as they were accreted.

This model assumes that the rifted fragment (Biranup Zone) was displaced southwestwards (present coordinates) and was affected by the postulated 52° clockwise rotation of the combined South Australian – Mawson Craton broadly at c. 1400 Ma (Giles et al., 2004), prior to Stage I of the Albany–Fraser Orogeny, when it eventually collided with the southern margin of the Yilgarn Craton. During the Albany–Fraser Orogeny the Biranup Zone was deformed, metamorphosed, and intruded by granitic magmas; all of which would have significantly changed its shape and volume. As described above, the Fraser Zone may have formed adjacent to the Biranup Zone prior to Stage I collision.

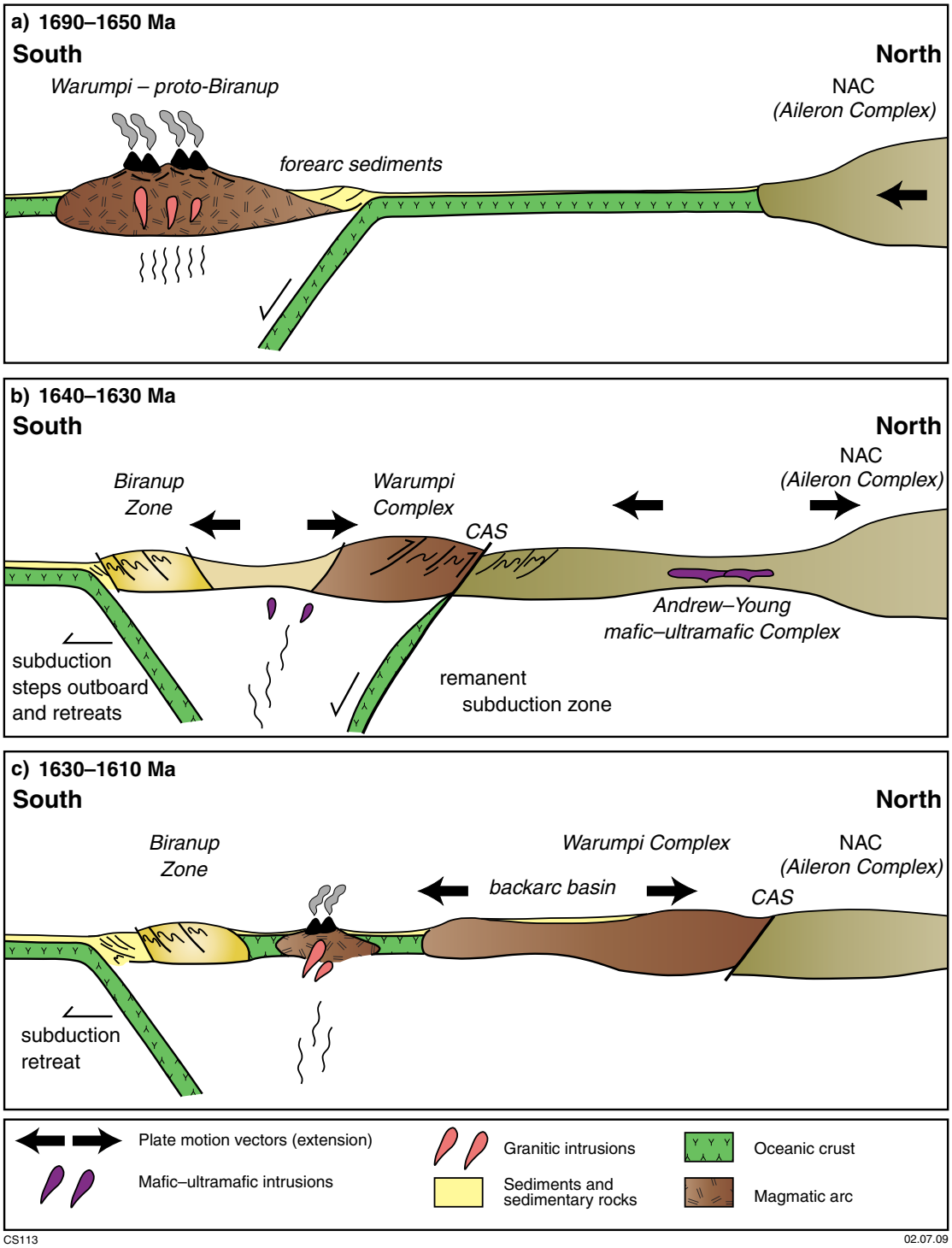

Figure 32. Tectonic cartoons showing the evolution of the Warumpi Province and the Biranup Zone protoliths (modified from presentation by Close et al. (2006): a) during the period 1690–1650 Ma south-dipping subduction produced a magmatic arc containing voluminous high–K alkaline felsic intrusive and extrusive rocks outboard of the North Australian Craton (NAC). These are interpreted as the protoliths for the Warumpi Province and the Biranup Zone. The fore-arc sedimentary rocks are the protoliths of the Yaya Metamorphic Complex; b) during the period 1640–1630 Ma oblique accretion of the Warumpi Province to the NAC southern margin produced the Central Australian Suture (CAS), associated bimodal magmatism and formation of layered intrusions during the Leibig Orogeny. At this time the 'back-end' of the Warumpi Province is interpreted to have rifted off as south-dipping subduction ceased and stepped outboard as a renewed north-dipping subduction zone; c) during the period 1630–1610 Ma the Biranup Zone is completely detached from the Warumpi Province as the north-dipping subduction zone retreats. A new arc and backarc basin form, within which the Iwuputaka sediments are deposited.

References

Arriens, PA and Lambert, IB 1969, On the age and strontium isotopic geochemistry of granulite-facies rocks from the Fraser Range, Western Australia, and the Musgrave Ranges, Central Australia: Special publication of the Geological Society of Australia, 2, p. 377–388.

Beeson, J, Delor, CP and Harris, LB 1988, A structural and metamorphic traverse across the Albany Mobile Belt, Western Australia: Precambrian Research, v. 40/41, p. 117–136.

Betts, PG and Giles, D 2006, The 1800–1100 Ma tectonic evolution of Australia: Precambrian Research, v. 144, p. 92–125.

Betts, PG, Giles, D and Schaefer, BF 2008, Comparing 1800–1600 Ma accretionary and basin processes in Australia and Laurentia: Possible geographic connections in Columbia: Precambrian Research, v. 166, p. 81–92.

Black, LP, Harris, LB and Delor, CP 1992, Reworking of Archaean and Early Proterozoic components during a progressive, Middle Proterozoic tectonothermal event in the Albany Mobile Belt, Western Australia: Precambrian Research, v. 59, p. 95–123.

Blewett, RS and Czarnota, K 2007, Diversity of structurally controlled gold through time and space of the central Eastern Goldfields Superterrane — a field guide: Geological Survey of Western Australia, Record 2007/19, 65p.

Bodorkos, S and Clark, DJ 2004a, Evolution of a crustal-scale transpressive shear zone in the Albany Fraser Orogen, SW Australia: 1. P–T conditions of Mesoproterozoic metamorphism in the Coramup Gneiss: Journal of Metamorphic Geology, v. 22, p. 691–711.

Bodorkos, S and Clark, DJ 2004b, Evolution of a crustal-scale transpressive shear zone in the Albany Fraser Orogen, SW Australia: 2. Tectonic history of the Coramup Gneiss and a kinematic framework for Mesoproterozoic collision of the West Australian and Mawson cratons: Journal of Metamorphic Geology, v. 22, p. 713–731.

Bodorkos, S and Wingate, MTD 2008a, 184120: monzogranitic gneiss, Pallinup River; Geochronology dataset 700, *in* Compilation of geochronology data, 2008 update: Geological Survey of Western Australia.

Bodorkos, S and Wingate, MTD 2008b, 184128: leucocratic tonalitic gneiss, Powell Point; Geochronology dataset 705, *in* Compilation of geochronology data, 2008 update: Geological Survey of Western Australia.

Bodorkos, S and Wingate, MTD 2008c, 184127: porphyritic monzodiorite, Powell Point; Geochronology dataset 704, *in* Compilation of geochronology data, 2008 update: Geological Survey of Western Australia.

Bodorkos, S and Wingate, MTD 2008d, 184314: leucocratic tonalitic gneiss, Lort River; Geochronology dataset 710, *in* Compilation of geochronology data, 2008 update: Geological Survey of Western Australia.

Bodorkos, S and Wingate, MTD 2008e, 184311: orthopyroxene-clinopyroxene orthogneiss, Fisheries Bay headland; Geochronology dataset 708, *in* Compilation of geochronology data, 2008 update: Geological Survey of Western Australia.

Bodorkos, S and Wingate, MTD,2008f, 184310: leucocratic granodiorite, Fisheries Bay headland; Geochronology dataset 707, *in* Compilation of geochronology data, 2008 update: Geological Survey of Western Australia.

Bodorkos, S and Wingate, MTD 2008g, 184312: granodioritic gneiss, Short Beach headland; Geochronology dataset 709, *in* Compilation of geochronology data, 2008 update: Geological Survey of Western Australia.

Bodorkos, S and Wingate, MTD 2008h, 184326: pegmatitic leucogranite, Short Beach headland; Geochronology dataset 711, *in* Compilation of geochronology data, 2008 update: Geological Survey of Western Australia.

Bodorkos, S and Wingate, MTD 2008i, 184119: monzogranitic gneiss, Point Henry; Geochronology dataset 699, *in* Compilation of geochronology data, 2008 update: Geological Survey of Western Australia.

Bodorkos, S and Wingate, MTD 2008j, 184307: pegmatitic granodiorite, Point Henry; Geochronology dataset 706, *in* Compilation of geochronology data, 2008 update: Geological Survey of Western Australia.

Bodorkos, S and Wingate, MTD 2008k, 184123: garnet-bearing monzogranitic gneiss, Plum Pudding Rocks; Geochronology dataset 702, *in* Compilation of geochronology data, 2008 update: Geological Survey of Western Australia.

Bodorkos, S and Wingate, MTD 2008l, 184122: metamorphosed quartz sandstone, Plum Pudding Rocks; Geochronology dataset 701, *in* Compilation of geochronology data, 2008 update: Geological Survey of Western Australia.

Bodorkos, S and Wingate, MTD 2008m, 184125: orthopyroxene-bearing dioritic gneiss, Observatory Point; Geochronology dataset 703, *in* Compilation of geochronology data, 2008 update: Geological Survey of Western Australia.

Bunting, JA, de Laeter, JR and Libby, WG 1976, Tectonic subdivisions and geochronology of the northeastern part of the Albany–Fraser Province, Western Australia: Geological Survey of Western Australia, Annual Report 1975, p. 117–126.

Campbell, IH, McCall, GJH and Tyrwhitt, DS 1970, The Jimberlana norite, Western Australia – a smaller analogue of the Great Dyke of Rhodesia: Geological Magazine, v. 107, p. 1–12.

Cassidy, KF, Champion, DC, Krapež, B, Barley, ME, Brown, SJA, Blewett, RS, Groenewald, PB and Tyler, IM 2006, A revised geological framework for the Yilgarn Craton: Geological Survey of Western Australia, Record 2006/8.

Cassidy, KF, Champion, DC, McNaughton, NJ, Fletcher, IR, Whitaker, AJ, Bastrakova, IV and Budd, AR 2002, Characterisation and metallogenic significance of Archean granitoids of the Yilgarn Craton, Western Australia: Amira International Limited, AMIRA project no. P482/MERIWA Project M281, Report no. 222 (unpublished).

Champion, DC and Cassidy, KF 2007, An overview of the Yilgarn Craton and its crustal evolution, *in* Proceedings of Geoconferences (WA) Inc. Kalgoorlie '07 Conference *edited by* FP Bierlein and CM Knox-Robinson: Geoscience Australia, Record 2007/14, p. 8–13.

Chin, RJ, Hickman, AH and Thom, R 1984, Hyden, W.A.: Geological Survey of Western Australia 1:250 000 Geological Series Explanatory Notes, 21p.

Clark, DJ 1999, Thermo-tectonic evolution of the Albany–Fraser Orogen, Western Australia: University of New South Wales, Australia, PhD thesis (unpublished).

Clark, DJ, Hensen, BJ and Kinny, PD 2000, Geochronological constraints for a two-stage history of the Albany–Fraser Orogen, Western Australia: Precambrian Research, v. 102, p. 155–183.

Clark, DJ, Kinny, PD, Post, NJ and Hensen, BJ 1999, Relationships between magmatism, metamorphism and deformation in the Fraser Complex, Western Australia: constraints from new SHRIMP U–Pb zircon geochronology: Australian Journal of Earth Sciences, v. 46, p. 923–932.

Clark, WC 1995, Granite petrogenesis, metamorphism and geochronology of the western Albany–Fraser Orogen, Albany, Western Australia: Curtin University of Technology, Australia, BSc (Honours) thesis (unpublished).

Clayton, W, Stott, C and Mazzucchelli, RH 2005, Maggie Hays nickel mineralization, Lake Johnston district, Western Australia, *in* Source Regolith expression of Australian ore systems; a compilation of exploration case histories with conceptual dispersion, process and exploration models *edited by* CRM Butt, IDM Robertson, KM Scott, and M Cornelius: Cooperative Research Centre for

Landscape Environments and Mineral Exploration (CRC LEME), CSIRO Exploration and Mining, Bentley, West. Aust., Australia, p. 109–111.

Close, DF, Scrimgeour, IR and Edgoose, CJ 2006, Evolution and mineral potential of the Paleoproterozoic Warumpi Province: Geoscience Australia, Record 2006/16, p. 9–10.

Condie, KC and Myers, JS 1999, Mesoproterozoic Fraser Complex: geochemical evidence for multiple subduction-related sources of lower crustal rocks in the Albany–Fraser Orogen, Western Australia: Australian Journal of Earth Sciences, v. 46, p. 875–882.

Cruse, T 1991, The sedimentology, depositional environment and Ediacaran fauna of Mondurup and Barnett Peaks, Stirling Range Formation, Western Australia: University of Western Australia, BSc (Honours) thesis (unpublished).

Cruse, T and Harris, LB 1994, Ediacaran fossils from the Stirling Range Formation, Western Australia: Precambrian Research, v. 67, p. 1–10.

Dawson, GC, Krapež, B, Fletcher, IR, McNaughton, NJ and Rasmussen, B, 2002, Did late Paleoproterozoic assembly of proto-Australia involve collision between the Pilbara, Yilgarn and Gawler Cratons? Geochronological evidence from the Mount Barren Group in the Albany–Fraser Orogen of Western Australia: Precambrian Research, v. 118, p. 195–220.

Dawson, GC, Krapež, B, Fletcher, IR, McNaughton, NJ and Rasmussen, B 2002, 1.2 Ga thermal metamorphism in the Albany–Fraser Orogen of Western Australia: consequence of colision or regional heating by dyke swarms?:Journal of the Geological Society, London, v. 160, p. 29–37.

De Waele, B and Pisarevsky, SA 2008, Geochronology, paleomagnetism and magnetic fabric of metamorphic rocks in the northeast Fraser Belt, Western Australia: Australian Journal of Earth Sciences, v. 55, p. 605–621.

Doepel, JJG 1973, Explanatory notes on the Norseman 1:250 000 Geological Sheet, Western Australia: Geological Survey of Western Australia, Record 1970/9, 57p.

Doepel, JJG 1975, Albany–Fraser Province, *in* The Geology of Western Australia: Geological Survey of Western Australia, Memoir 2, p. 94–102.

Doepel, JJG and Lowry, DC 1970, Zanthus, W.A.: Geological Survey of Western Australia, 1:250 000 Geological Series Explanatory Notes, 19p.

Doyle, M., Kendall, B., Gibbs, D and Kent, M 2008, Tropicana Deposit: a new gold province in Western Australia: Geological Society of Australia, Abstracts, v. 89, p. 85.

Drexel, JF, Preiss, WV and Parker, AJ 1993, The Geology of South Australia: The Precambrian, Vol. 1, Geological Survey of South Australia, Bulletin 54, 242p.

Duebendorfer, EM 2002, Regional correlation of Mesoproterozoic structures and deformational events in the Albany–Fraser Orogen, Western Australia: Precambrian Research, v. 116, 129–154.

Elias, M and Bunting, JA 1982, Wiluna, W.A.: Geological Survey of Western Australia 1:250 000 Geological Series Explanatory Notes, 20p.

Evans, T 1999, Extent and nature of the 1.2 Ga Wheatbelt dyke swarm, Yilgarn Craton, Western Australia: University of Western Australia, Australia, BSc (Honours) thesis (unpublished).

Fanning, CM, Reid, AJ and Teale, GS 2007, A geochronological framework for the Gawler Craton, South Australia: Bulletin 55, Geological Survey, Primary Industries and Resources, South Australia, 258p.

Ferris, GM and Schwartz, M 2004, Definition of the Tunkillia Suite, western Gawler Craton: MESA Journal, Department of Primary Industries and Resources South Australia, Adelaide, v. 34, p. 32–41.

Fitzsimons, ICW 2003, Proterozoic basement provinces of southern and southwestern Australia, and their correlation with Antarctica, *in* Supercontinent assembly and breakup *edited by* M Yoshida, BF Windley, and S Dasgupta: Geological Society, London, Special Publications, v. 206, p. 93–130.

Fitzsimons, ICW and Buchan, C 2005, Geology of the western Albany–Fraser Orogen, Western Australia — a field guide: Geological Survey of Western Australia, Record 2005/11, 32p.

Fitzsimons, ICW, Kinny, PD, Wetherley, S and Hollingsworth, DA 2005, Bulk chemical controls on metamorphic monazite growth in pelitic schists and implications for U–Pb age data: Journal of Metamorphic Geology, v. 23, 261–277.

Fletcher, IR, Libby, WG and Rosman, KJR 1987, Sm–Nd dating of the 2411 Ma Jimberlana dyke, Yilgarn Block, Western Australia: Australian Journal of Earth Sciences, v. 34, p. 523–525.

Fletcher, IR, Myers, JS and Ahmat, AL 1991, Isotopic evidence on the age and origin of the Fraser Complex, Western Australia: a sample of Mid-Proterozoic lower crust: Chemical Geology, v. 87, p. 197–216.

Fletcher, IR, Wilde, SA, Libby, WG and Rossman, KJR 1983, Sm–Nd model ages from across the margins of the Archean Yilgarn Block, Western Australia, II; southwest transect into the Proterozoic Albany–Fraser Province: Journal of the Geological Society of Australia, v. 30, p. 333–340.

Flint, RB and Daly SJ, 1993, Coompana Block, *in* The Geology of South Australia *edited* by JF Drexel, WV Preiss and AJ Parker: The Precambrian, Vol. 1, Geological Survey of South Australia, Bulletin 54, p. 168–169.

French JE, Heaman LM and Chacko T 2002, Feasibility of chemical U–Th–total Pb baddeleyite dating by electron microprobe: Chemical Geology, v. 188, p. 85–104.

Geological Survey of Western Australia 2007, South Yilgarn Geological Exploration Package: Geological Survey of Western Australia Record 2007/13.

Geological Survey of Western Australia 2008, Compilation of geochronology data, 2008 update: Geological Survey of Western Australia.

Geoscience Australia 1998, Australian Crustal Elements Map: dataset, viewed December 2008, <http://www.ga.gov.au/meta/ANZCW0703002384.html>.

Giddings, JW 1976, Precambrian palaeomagnetism in Australia I: Basic dykes and volcanics from the Yilgarn Block: Tectonophysics, v. 30, p. 91–108.

Giles, D, Betts, PG and Lister, GS 2004, 1.8–1.5-Ga links between the North and South Australian Cratons and the Early–Middle Proterozoic configuration of Australia: Tectonophysics, v. 380, p. 27–41.

Gower, CF and Bunting, JA 1976, Lake Johnston, W.A.: Geological Survey of Western Australia 1:250 000 Geological Series Explanatory Notes, 27p.

Griffin, TJ 1990, Southern Cross Province, *in* Geology and mineral resources of Western Australia: Geological Survey of Western Australia, Memoir 3, p. 60–77.

Hall, CE, Jones, SA and Bodorkos, S 2008, Sedimentology, structure and SHRIMP zircon provenance of the Woodline Formation, Western Australia: implications for the tectonic setting of the West Australian Craton during the Paleoproterozoic: Precambrian Research, v. 162, p. 577–598.

Harris, LB 1995, Correlation between the Albany, Fraser and Darling Mobile Belts of Western Australia and Mirnyy to Windmill Islands in the East Antarctic Shield: Implications for Proterozoic Gondwanaland reconstructions: Memoir of the Geological Society of India, v. 34, p. 47–71.

Harris, LB 2003, Folding in high-grade rocks due to back-rotation between shear zones: Journal of Structural Geology, v. 25, p. 223–240.

Harris, LB, Koyi, HA and Fossen, H 2002, Mechanisms for folding of high-grade rocks in extensional tectonic settings: Earth-Science Reviews, v. 59, p. 163–210.

Harris, LB and Li, Z-X 1995, Palaeomagnetic dating and tectonic significance of dolerite intrusions in the Albany Mobile Belt, Western Australia: Earth and Science Planetary Letters, v. 131, p. 143–164.

Hocking, RM 1990, Bremer Basin, *in* Geology and Mineral Resources of Western Australia: Geological Survey of Western Australia, Memoir 3, p. 561–563.

Hollingsworth, DA 1996, Veining, metasomatism and metamorphism of metapelites of the Mount Barren Group at West Beach, Western Australia: Curtin University of Technology, BSc (Honours) thesis (unpublished).

Isles, DJ and Cooke, AC 1990, Spatial associations between post-cratonisation dykes and gold deposits in the Yilgarn Block, Western Australia, *in* Mafic Dykes and Emplacement Mechanisms *edited by* Parker, Rickwood, and Tucker: Balkema, Rotterdam, ISBN 906191 158 3, p. 157–162.

Jones, SA 2006, Mesoproterozoic Albany–Fraser Orogen-related deformation along the southeastern margin of the Yilgarn Craton: Australian Journal of Earth Sciences, v. 53, p. 213–234.

Love, GJ 1999, A study of wall-rock contamination in a tonalitic gneiss from King Point, near Albany, Western Australia: Curtin University of Technology, BSc (Honours) thesis (unpublished).

Muhling, PC and Brakel, AT 1985, Mount Barker–Albany, W.A.: Geological Survey of Western Australia 1:250 000 Geological Series Explanatory Notes, 21p.

Myers, JS 1985, The Fraser Complex — a major layered intrusion in Western Australia: Geological Survey of Western Australia, Report 14, p. 57–66.

Myers, JS 1989, Albany, W.A.: Geological Survey of Western Australia, 1:1 000 000 Geological Series.

Myers, JS, 1990a, Albany–Fraser Orogen, *in* Geology and mineral resources of Western Australia: Geological Survey of Western Australia, Memoir 3, p. 255–263.

Myers, JS 1990b, Mafic dyke swarms, *in* Geology and mineral resources of Western Australia: Geological Survey of Western Australia, Memoir 3, p. 126.

Myers, JS 1993, Precambrian history of the West Australian Craton and adjacent orogens: Annual Review of Earth and Planetary Sciences, v. 21, p. 453–485.

Myers, JS 1995a, Geology of the Albany 1:1 000 000 sheet: Geological Survey of Western Australia, 1:1 000 000 Geological Series Explanatory Notes, 10p.

Myers, JS 1995b, Geology of the Esperance 1:1 000 000 sheet: Geological Survey of Western Australia, 1:1 000 000 Geological Series Explanatory Notes, 10p.

Myers, JS and Hocking, RM 1998, Geological map of Western Australia, 1:2 500 000 scale (13th edition): Geological Survey of Western Australia.

Myers, JS, Shaw, RD and Tyler, IM 1996, Tectonic evolution of Proterozoic Australia: Tectonics, v. 15, p. 1431–1446.

Nelson, DR 1995a, 112163: rhyolite, Bandalup, *in* Compilation of SHRIMP U–Pb zircon geochronology data, 1995: Geological Survey of Western Australia, Record 1995/3, p. 82–84.

Nelson, DR 1995b, 83696A: biotite monzogranite gneiss, Powell Point, *in* Compilation of SHRIMP U–Pb zircon geochronology data, 1994: Geological Survey of Western Australia, Record 1995/3, p. 23–25.

Nelson, DR 1995c, 83702: biotite tonalite gneiss, south of Young River, *in* Compilation of SHRIMP U–Pb zircon geochronology data, 1994: Geological Survey of Western Australia, Record 1995/3, p. 19–22.

Nelson, DR 1995d, 83691: biotite monzogranite gneiss, north of Young River, *in* Compilation of SHRIMP U–Pb zircon geochronology data, 1994: Geological Survey of Western Australia, Record 1995/3, p. 12–14.

Nelson, DR 1995e, 83690: biotite granodiorite gneiss, Bald Rock, *in* Compilation of SHRIMP U–Pb zircon geochronology data, 1994: Geological Survey of Western Australia, Record 1995/3, p. 26–29.

Nelson, DR 1995f, 83649: granite pegmatite, Lake Gidong Headland, *in* Compilation of SHRIMP U–Pb zircon geochronology data, 1994: Geological Survey of Western Australia, Record 1995/3, p. 33–36.

Nelson, DR 1995g, 83676A: hornblende syenogranite gneiss, Mount Andrew, *in* Compilation of SHRIMP U–Pb zircon geochronology data, 1994: Geological Survey of Western Australia, Record 1995/3, p. 49–52.

Nelson, DR 1995h, 83659: recrystallised leucogranite, Observatory Point, *in* Compilation of SHRIMP U–Pb zircon geochronology data, 1994: Geological Survey of Western Australia, Record 1995/3, p. 59–62.

Nelson, DR 1995i, 112128: muscovite–biotite–sillimanite paragneiss, Point Malcolm, *in* Compilation of SHRIMP U–Pb zircon geochronology data, 1994: Geological Survey of Western Australia, Record 1995/3, p. 78–81.

Nelson, DR 1995j, 83662: biotite–hornblende monzogranite gneiss, Poison Creek, *in* Compilation of SHRIMP U–Pb zircon geochronology data, 1994: Geological Survey of Western Australia, Record 1995/3, p. 67–70.

Nelson, DR 1995k, 83663: granodiorite gneiss, Israelite Bay, *in* Compilation of SHRIMP U–Pb zircon geochronology data, 1994: Geological Survey of Western Australia, Record 1995/3, p. 75–77.

Nelson, DR 1995l, 83697: biotite monzogranite gneiss, Mount Burdett, *in* Compilation of SHRIMP U–Pb zircon geochronology data, 1994: Geological Survey of Western Australia Record 1995/3, p. 56–58.

Nelson, DR 1995m, 83700A: hornblende–biotite syenogranite gneiss, Coramup Hill Quarry, *in* Compilation of SHRIMP U–Pb zircon geochronology data, 1994: Geological Survey of Western Australia, Record 1995/3, p. 53–55.

Nelson, DR 1995n, 83657A: porphyritic biotite monzogranite, Esperance Harbour jetty, *in* Compilation of SHRIMP U–Pb zircon geochronology data, 1994: Geological Survey of Western Australia, Record 1995/3, p. 63–66.

Nelson, DR 1995o, 83667: porphyritic biotite granite, Balladonia Rock, *in* Compilation of SHRIMP U–Pb zircon geochronology data, 1994: Geological Survey of Western Australia, Record 1995/3, p. 71–74.

Nelson, DR 1996a, 112168: fine-grained sandstone, No Tree Hill, *in* Compilation of SHRIMP U–Pb zircon geochronology data, 1996: Geological Survey of Western Australia, Record 1996/5, p. 80–83.

Nelson, DR 1996b, 112170: metasandstone, Barrens Beach, *in* Compilation of SHRIMP U–Pb zircon geochronology data, 1996: Geological Survey of Western Australia, Record 1996/5, p. 84–86.

Nelson, DR 2005a, 178070: amphibolite, south of Haig Cave; Geochronology dataset 596, *in* Compilation of geochronology data, 2008 update: Geological Survey of Western Australia.

Nelson, DR 2005b, 178071: biotite microtonalite, south of Haig Cave; Geochronology dataset 597, *in* Compilation of geochronology data, 2008 update: Geological Survey of Western Australia.

Nelson, DR 2005c, 178072: tonalitic gneiss, south of Haig Cave; Geochronology dataset 5987, *in* Compilation of geochronology data, 2008 update: Geological Survey of Western Australia.

Nelson, DR, Myers, JS and Nutman, AP 1995, Chronology and evolution of the Middle Proterozoic Albany–Fraser Orogen, Western Australia: Australian Journal of Earth Sciences, v. 42, p. 481–495.

Nemchin, AA and Pidgeon, RT 1997, Evolution of the Darling Range Batholith, Yilgarn Craton, Western Australia: a SHRIMP zircon study: Journal of Petrology, v. 38, p. 625–649.

Nemchin, AA and Pidgeon, RT 1998, Precise conventional and SHRIMP baddeleyite U–Pb age for the Binneringie Dyke, near Narrogin, Western Australia: Australian Journal of Earth Sciences, v. 45, p. 673–675.

Payne, JL, Barovich, K and Hand, M 2006, On the tectonic setting of the magmatic suite previously known as the 'Arc-like Tunkillia/Ifould': Geological Society of Australia Abstracts, p. 82.

Payne, JL, Hand, M, Barovich, K and Wade, BP 2008, Temporal constraints on the timing of high-grade metamorphism in the northern Gawler Craton: implications for the assembly of the Australian Proterozoic: Australian Journal of Earth Sciences, v. 55, p. 623–641.

Perring, CS, Barmes, SJ and Hill, RET 1995, The physical volcanology of Archean komatiite sequences from Forrestania, Southern Cross Province, Western Australia: Lithos, v. 34, p. 189–207.

Perring, CS, Barmes, SJ and Hill, RET 1996, The geochemistry of komatiites from Forrestania, Southern Cross Province, Western Australia: Evidence for crustal contamination: Lithos, v. 37, p. 181–197.

Pidgeon, RT 1990, Timing of plutonism in the Proterozoic Albany Mobile Belt, southwestern Australia: Precambrian Research, v. 47, p. 157–167.

Pisarevsky, SA, Wingate, MTD and Harris, LB 2003, Late Mesoproterozoic (ca 1.2 Ga) paleomagnetism of the Albany–Fraser Orogen: no pre-Rodinia Australia–Laurentia connection: Geophysical Journal International, v. 155, p. F6–F11.

Rasmussen, B, Bengston, S, Fletcher, IR and McNaughton, NJ 2002, Discoidal impressions and trace-like fossils more than 1200 million years old: Science, v. 296, p. 1112–1115.

Rasmussen, B and Fletcher, IR 2004, Zirconolite: A new U–Pb chronometer for mafic igneous rocks: Geology, v. 39, p. 785–788.

Rasmussen, B, Fletcher, IR, Bengston, S and McNaughton, NJ 2004, SHRIMP U–Pb dating of diagenetic xenotime in the Stirling Range Formation, Western Australia: 1.8 billion year minimum age for the Stirling biota: Precambrian Research, v. 133, p. 329–337.

Savage, MD, Barley, ME and McNaughton, NJ 1996, SHRIMP U–Pb dating of 2.95 to 3.0 Ga intermediate to silicic rocks in the southern Yellowdine Terrane, Yilgarn Craton: Geological Society of Australia Abstracts, v. 41, p. 376.

Scrimgeour, IR, Kinny, PD, Close, DF and Edgoose, CJ 2005, High–T granulites and polymetamorphism in the southern Arunta Region, central Australia: Evidence for a 1.64 Ga accretional event: Precambrian Research, v. 142, p. 1–27.

Shaw, RD, Wellman, P, Gunn, P, Whitaker, AJ, Tarlowski, C and Morse, M 1996, Guide to using the Australian Crustal Elements Map: Australian Geological Survey Organisation, Record 1996/30, 44p.

Sheppard, S, Occhipinti, SA and Nelson, DR 2005. Intracontinental reworking in the Capricorn Orogen, Western Australia: the 1680–1620 Mangaroon Orogeny: Australian Journal of Earth Sciences, v. 52, p. 443–460.

Sofoulis, J 1958, The geology of the Phillips River Goldfield, W.A.: Geological Survey of Western Australia, Bulletin 110, 240p.

Sofoulis, J 1965, Widgiemooltha, W.A.: Western Australia Geological Survey, 1:250 000 Geological Series Explanatory Notes, 40p.

Spaggiari, CV, Bodorkos, S, Tyler, IM and Barquero-Molina, M 2008, The c. 1680 Ma Dalyup Gneiss of the Albany–Fraser Orogen, Western Australia: What is it, and where did it come from?: Geological Society of Australia, Abstracts, v. 89, p. 232–233.

Stephens, JR 1996, Structural and metamorphic evolution of the East Mount Barren area, Albany–Fraser Orogen, Western Australia: Curtin University, Perth, Honours thesis (unpublished).

Swager, CP 1997, Tectono-stratigraphy of Late Archean greenstone terranes in the southern Eastern Goldfields, Western Australia: Precambrian Research, v. 83, p. 11–42.

Teasdale, J 1997, Methods for understanding poorly exposed terranes: The interpretative geology and tectonothermal evolution of the western Gawler Craton: The University of Adelaide, Adelaide, PhD thesis (unpublished).

Thom, R and Chin, RJ 1984, Bremer Bay, W.A.: Geological Survey of Western Australia, 1:250 000 Geological Series Explanatory Notes, 20p.

Thom, R, Chin, RJ and Hickman, AH 1984, Newdegate, W.A.: Geological Survey of Western Australia,1:250 000 Geological Series Explanatory Notes, 24 p.

Thom, R and Lipple, SL 1971, Ravensthorpe, WA Sheet SI 51-05: Geological Survey of Western Australia, 1:250 000 Geological Series.

Thom, R, Lipple, SL and Sanders, CC 1977, Ravensthorpe, W.A.: Geological Survey of Western Australia,1:250 000 Geological Series Explanatory Notes, 40p.

Turek, A 1966, Rubidium–strontium isotopic studies in the Kalgoorlie–Norseman area, Western Australia: Australian National University, Canberra, PhD thesis (unpublished).

Tyler, IM 2005, Australia: Proterozoic, *in* Encyclopedia of Geology *edited by* RC Selley, LRM Cocks and IR Plimer: Elsevier, Oxford, v. 1, p. 208–221.

Tyler, IM and Hocking, RM (compilers) 2001, Tectonic units of Western Australia, 1:2 500 000: Geological Survey of Western Australia.

Tyler, IM and Hocking, RM (compilers) 2006, Interpreted bedrock geology of Western Australia, 1:500 000: Geological Survey of Western Australia.

Tyler, IM and Hocking, RM (compilers) 2008, Update of interpreted bedrock geology of Western Australia, 1:500 000: Geological Survey of Western Australia.

Vallini, DA, Rasmussen, B, Krapež, B, Fletcher, IR and McNaughton, NJ 2002, Obtaining diagenetic ages from metamorphosed sedimentary rocks: U–Pb dating of unusually coarse xenotime cement in phosphatic sandstone: Geology, v. 30, p. 1083–1086.

Vallini, DA, Rasmussen, B, Krapež, B, Fletcher, IR and McNaughton, NJ 2005, Microtextures, geochemistry and geochronology of authigenic xenotime constraining the cementation history of a Paleoproterozoic metasedimentary sequence: Sedimentology, v. 52, p. 101–122.

Wade, BP, Payne, JL, Hand, M and Barovich, KM 2007, Petrogenesis of ca 1.50 Ga granitic gneiss of the Coompana Block: filling the 'magmatic gap' of Mesoproterozoic Australia: Australian Journal of Earth Sciences, v. 54, p. 1089–1102.

Wang, Q, Schiøtte, L and Campbell, IH 1996, Geochronological constraints on the age of komatiites and nickel mineralisation in the Lake Johnston Greenstone Belt, Yilgarn Craton, Western Australia: Australian Journal of Earth Sciences, v. 43, p. 381–385.

Wetherley, S 1998, Tectonic evolution of the Mount Barren Group, Albany–Fraser Province, Western Australia: University of Western Australia, PhD thesis (unpublished).

Whitaker, AJ 1992, Albany Magnetic and Gravity Interpretation (1:1 000 000 scale map): Bureau of Mineral Resources, Geology and Geophysics, Canberra.

Whitaker, AJ 1993, Esperance Magnetic and Gravity Interpretation (1:1 000 000 scale map): Australian Geological Survey Organisation, Canberra.

Wilde, SA 2001, Jimperding and Chittering metamorphic belts, southwestern Yilgarn Craton, Western Australia — a field guide: Geological Survey of Western Australia, Record 2001/12, 24p.

Wilde, SA, Middleton, MF and Evans, BJ 1996, Terrane accretion in the southwest Yilgarn Craton: evidence from a deep seismic crustal profile: Precambrian Research, v. 78, p. 179–196.

Wilson, AC 1990, Collie Basin, *in* Geology and mineral resources of Western Australia: Geological Survey of Western Australia, Memoir 3, p. 525–531.

Wilson, AF 1969a, Granulite terrains and their tectonic setting and relationship to associated metamorphic rocks in Australia: Geological Society of Australia Special Publication No 2, p. 243–258.

Wilson, AF 1969b, Some structural, geochemical and economic aspects of the metamorphosed East Fraser Gabbro and associated pyroxene granulites of the Fraser Range, Western Australia: Indian Mineralogist, v. 10, p. 46–66.

Wilson, AF 1969c, The pyroxene granulites and associated gabbros of the Fraser Range, Western Australia, and their economic significance: Australian Institute of Mining and Metallurgy, Proceedings v. 231, p. 47–57.

Wingate, MTD 2007, Proterozoic mafic dykes in the Yilgarn Craton, *in* Proceedings of Geoconferences (WA) Inc. Kalgoorlie '07 Conference *edited by* FP Bierlein and CM Knox-Robinson: Geoscience Australia Record 2007/14, p. 80–83.

Wingate, MTD and Bodorkos, S 2007a, 177909: monzogranite gneiss, Yardilla Bore; Geochronology dataset 659, *in* Compilation of geochronology data, 2008 update: Geological Survey of Western Australia.

Wingate, MTD and Bodorkos, S 2007b, 177910: metamorphosed quartz sandstone, Peter's Dam; Geochronology dataset 660, *in* Compilation of geochronology data, 2008 update: Geological Survey of Western Australia.

Wingate, MTD, Campbell, IH and Harris, LB 2000, SHRIMP baddeleyite age for the Fraser Dyke Swarm, southeast Yilgarn Craton, Western Australia: Australian Journal of Earth Sciences, v. 47, p. 309–313.

Wingate, MTD, Morris, PA, Pirajno, F and Pidgeon, RT 2005, Two Large Igneous Provinces in late Mesoproterozoic Australia: Geological Society of Australia Abstracts, v. 81, p. 151.

Wingate, MTD, Kirkland, CL and Bodorkos, S 2008a, Introduction to geochronology data released in 2008: Compilation of geochronology data, 2008 update, Geological Survey of Western Australia.

Wingate, MTD, Kirkland, CL and Bodorkos, S 2008b, 177904: quartzite, Windmill Hill; Geochronology dataset 740, *in* Compilation of geochronology data, 2008 update: Geological Survey of Western Australia.

Witt, WK 1997, Geology of the Ravensthorpe and Cocanarup 1:100 000 sheets: Geological Survey of Western Australia, 1:100 000 Geological Series Explanatory Notes, 26p.

Witt, WK 1998, Geology and mineral resources of the Ravensthorpe and Cocanarup 1:100 000 sheets: Geological Survey of Western Australia, Report 54, 152p.

Appendix

U–Th–Pb Secondary Ionization Mass Spectrometry zircon analytical data

Table A1. Ion microprobe analytical results for zircons from sample 184120: monzogranitic gneiss, Pallinup River

Grp no.	Spot no.	Grain .spot	^{238}U (ppm)	^{232}Th (ppm)	$^{232}Th/^{238}U$	f204 (%)	$^{238}U/^{206}Pb$ ±1σ	$^{207}Pb/^{206}Pb$ ±1σ	$^{238}U/^{206}Pb^*$ ±1σ	$^{207}Pb^*/^{206}Pb^*$ ±1σ	$^{238}U/^{206}Pb^*$ date (Ma) ±1σ	$^{207}Pb^*/^{206}Pb^*$ date (Ma) ±1σ	Disc (%)
1	9	9.1	138	142	1.06	0.089	1.920 ± 0.024	0.18616 ± 0.00086	1.921 ± 0.024	0.18537 ± 0.00091	2701 ± 28	2701 ± 8	0.0
1	13	13.1	222	177	0.83	0.035	1.967 ± 0.024	0.18468 ± 0.00069	1.968 ± 0.024	0.18437 ± 0.00071	2648 ± 26	2693 ± 6	1.6
1	7	7.1	92	62	0.70	0.086	1.939 ± 0.032	0.18495 ± 0.00108	1.941 ± 0.032	0.18419 ± 0.00134	2679 ± 37	2691 ± 12	0.4
1	11	11.1	171	185	1.12	0.144	1.903 ± 0.024	0.18531 ± 0.00075	1.906 ± 0.024	0.18402 ± 0.00082	2719 ± 27	2689 ± 7	–1.1
1	15	15.1	146	116	0.82	0.016	1.924 ± 0.024	0.18408 ± 0.00147	1.924 ± 0.024	0.18394 ± 0.00149	2698 ± 28	2689 ± 13	–0.3
1	6	6.1	153	108	0.73	0.070	1.929 ± 0.031	0.18436 ± 0.00083	1.931 ± 0.031	0.18374 ± 0.00093	2691 ± 35	2687 ± 8	–0.1
1	20	20.1	199	141	0.73	0.049	1.992 ± 0.025	0.18417 ± 0.00076	1.993 ± 0.025	0.18373 ± 0.00079	2621 ± 27	2687 ± 7	2.5
1	19	19.1	165	125	0.78	0.095	1.991 ± 0.025	0.18439 ± 0.00081	1.993 ± 0.025	0.18354 ± 0.00089	2622 ± 27	2685 ± 8	2.4
1	2	2.1	277	256	0.95	0.055	1.918 ± 0.030	0.18392 ± 0.00062	1.919 ± 0.030	0.18343 ± 0.00064	2704 ± 34	2684 ± 6	–0.7
1	10	10.1	110	78	0.74	0.145	1.983 ± 0.026	0.18435 ± 0.00098	1.986 ± 0.026	0.18305 ± 0.00123	2629 ± 28	2681 ± 11	1.9
1	16	16.1	91	86	0.97	0.085	1.916 ± 0.026	0.18375 ± 0.00106	1.917 ± 0.026	0.18300 ± 0.00116	2706 ± 30	2680 ± 10	–1.0
1	8	8.1	134	85	0.66	0.118	1.948 ± 0.025	0.18373 ± 0.00085	1.950 ± 0.025	0.18267 ± 0.00089	2668 ± 28	2677 ± 8	0.3
1	12	12.1	130	97	0.77	0.106	1.993 ± 0.025	0.18345 ± 0.00117	1.995 ± 0.025	0.18250 ± 0.00121	2619 ± 27	2676 ± 11	2.1
1	17	17.1	150	104	0.71	0.158	1.932 ± 0.024	0.18377 ± 0.00084	1.936 ± 0.024	0.18236 ± 0.00106	2685 ± 28	2674 ± 10	–0.4
1	1	1.1	226	165	0.75	0.048	1.949 ± 0.031	0.18243 ± 0.00069	1.950 ± 0.031	0.18200 ± 0.00073	2668 ± 34	2671 ± 7	0.1
1	5	5.1	188	132	0.72	0.088	1.990 ± 0.031	0.18274 ± 0.00076	1.992 ± 0.031	0.18195 ± 0.00083	2623 ± 34	2671 ± 8	1.8
1	21	21.1	177	138	0.81	–0.015	1.942 ± 0.024	0.18177 ± 0.00101	1.942 ± 0.024	0.18190 ± 0.00101	2678 ± 27	2670 ± 9	–0.3
1	22	22.1	148	120	0.83	0.082	1.908 ± 0.024	0.18252 ± 0.00085	1.910 ± 0.024	0.18179 ± 0.00091	2714 ± 28	2669 ± 8	–1.7
1	14	14.1	197	133	0.70	0.118	1.957 ± 0.024	0.18277 ± 0.00071	1.959 ± 0.024	0.18172 ± 0.00081	2659 ± 27	2669 ± 7	0.4
2	18	18.1	216	120	0.57	0.104	2.016 ± 0.025	0.18147 ± 0.00070	2.018 ± 0.025	0.18054 ± 0.00078	2594 ± 26	2658 ± 7	2.4
2	3	3.1	201	111	0.57	0.128	1.978 ± 0.031	0.18011 ± 0.00072	1.981 ± 0.031	0.17896 ± 0.00079	2635 ± 34	2643 ± 7	0.3
3	4	4.1	39	14	0.38	–0.227	1.839 ± 0.035	0.18445 ± 0.00167	1.835 ± 0.035	0.18648 ± 0.00200	2804 ± 43	2711 ± 18	–3.4

Table A2. Ion microprobe analytical results for zircons from sample 184128: leucocratic tonalitic gneiss, Powell Point

Grp no.	Spot no.	Grain .spot	^{238}U (ppm)	^{232}Th (ppm)	$^{232}Th/^{238}U$	f204 (%)	$^{238}U/^{206}Pb$ ±1σ	$^{207}Pb/^{206}Pb$ ±1σ	$^{238}U/^{206}Pb^*$ ±1σ	$^{207}Pb^*/^{206}Pb^*$ ±1σ	$^{238}U/^{206}Pb^*$ date (Ma) ±1σ	$^{207}Pb^*/^{206}Pb^*$ date (Ma) ±1σ	Disc (%)
1	21	20.1	10	0	0.04	2.599	4.815 ± 0.137	0.10700 ± 0.00363	4.944 ± 0.151	0.08488 ± 0.01036	1188 ± 33	1313 ± 237	9.5
1	19	18.1	17	13	0.79	2.293	4.907 ± 0.110	0.10333 ± 0.00271	5.022 ± 0.126	0.08385 ± 0.00978	1171 ± 27	1289 ± 227	9.2
1	18	17.1	604	88	0.15	0.037	4.856 ± 0.057	0.08076 ± 0.00038	4.858 ± 0.057	0.08044 ± 0.00044	1207 ± 13	1208 ± 11	0.1
1	28	14.2	695	20	0.03	0.000	4.928 ± 0.060	0.08025 ± 0.00037	4.928 ± 0.060	0.08025 ± 0.00037	1191 ± 13	1203 ± 9	1.0
1	25	24.1	31	1	0.02	0.523	5.267 ± 0.105	0.08338 ± 0.00188	5.295 ± 0.107	0.07896 ± 0.00341	1115 ± 21	1171 ± 86	4.8
1	27	26.1	673	85	0.13	0.084	4.920 ± 0.057	0.07937 ± 0.00041	4.924 ± 0.057	0.07866 ± 0.00047	1192 ± 13	1164 ± 12	–2.4
1	14	13.1	7	0	0.02	2.629	4.750 ± 0.209	0.10039 ± 0.00420	4.879 ± 0.227	0.07822 ± 0.01341	1202 ± 51	1152 ± 340	–4.3
1	5	5.1	15	1	0.04	1.885	4.505 ± 0.113	0.09219 ± 0.00250	4.592 ± 0.122	0.07633 ± 0.00824	1270 ± 31	1104 ± 216	–15.1
2	15	14.1	206	152	0.76	0.029	2.012 ± 0.025	0.18318 ± 0.00109	2.013 ± 0.025	0.18292 ± 0.00112	2600 ± 26	2679 ± 10	3.0
2	11	11.1	65	32	0.51	0.177	1.977 ± 0.028	0.18229 ± 0.00127	1.981 ± 0.028	0.18072 ± 0.00147	2634 ± 31	2659 ± 13	0.9
2	13	12.2	281	173	0.63	0.176	2.135 ± 0.027	0.18008 ± 0.00102	2.139 ± 0.027	0.17851 ± 0.00107	2473 ± 26	2639 ± 10	6.3
2	12	12.1	932	133	0.15	0.002	2.009 ± 0.023	0.17757 ± 0.00037	2.009 ± 0.023	0.17755 ± 0.00037	2605 ± 25	2630 ± 3	1.0
2	8	8.1	546	152	0.29	0.023	2.137 ± 0.023	0.17774 ± 0.00047	2.137 ± 0.023	0.17753 ± 0.00048	2474 ± 23	2630 ± 5	5.9
2	6	6.1	197	71	0.37	0.035	2.118 ± 0.033	0.17693 ± 0.00076	2.119 ± 0.033	0.17662 ± 0.00080	2492 ± 33	2621 ± 8	4.9
2	17	16.1	126	41	0.33	0.024	2.163 ± 0.028	0.17662 ± 0.00108	2.163 ± 0.028	0.17640 ± 0.00116	2450 ± 26	2619 ± 11	6.5
2	10	10.1	786	141	0.19	0.012	2.079 ± 0.024	0.17603 ± 0.00048	2.080 ± 0.024	0.17593 ± 0.00049	2531 ± 24	2615 ± 5	3.2
2	16	15.1	240	84	0.36	0.102	2.083 ± 0.034	0.17630 ± 0.00132	2.085 ± 0.034	0.17539 ± 0.00136	2526 ± 34	2610 ± 13	3.2
2	2	2.1	923	128	0.14	0.007	2.127 ± 0.033	0.17412 ± 0.00035	2.127 ± 0.033	0.17406 ± 0.00035	2484 ± 32	2597 ± 3	4.4
2	1	1.1	742	223	0.31	0.030	2.129 ± 0.032	0.17420 ± 0.00039	2.130 ± 0.032	0.17393 ± 0.00040	2481 ± 31	2596 ± 4	4.4
2	24	23.1	105	41	0.41	0.023	2.204 ± 0.033	0.17410 ± 0.00126	2.205 ± 0.033	0.17390 ± 0.00129	2411 ± 30	2596 ± 12	7.1
2	3	3.1	581	134	0.24	0.052	2.085 ± 0.032	0.17414 ± 0.00042	2.086 ± 0.032	0.17367 ± 0.00044	2525 ± 32	2593 ± 4	2.7
2	4	4.1	587	107	0.19	0.032	2.084 ± 0.035	0.17365 ± 0.00042	2.084 ± 0.035	0.17336 ± 0.00044	2526 ± 35	2590 ± 4	2.5
2	23	22.1	590	128	0.22	0.027	2.158 ± 0.025	0.17273 ± 0.00048	2.158 ± 0.025	0.17249 ± 0.00049	2454 ± 24	2582 ± 5	4.9
2	20	19.1	341	264	0.80	0.108	2.955 ± 0.037	0.14971 ± 0.00060	2.958 ± 0.037	0.14875 ± 0.00068	1877 ± 21	2332 ± 8	19.5
D	26	25.1	19	77	4.08	14.580	5.483 ± 0.122	0.19541 ± 0.00416	6.418 ± 0.302	0.07316 ± 0.03521	933 ± 41	1019 ± 975	8.4
D	7	7.1	17	63	3.76	6.611	5.247 ± 0.128	0.14340 ± 0.00344	5.618 ± 0.167	0.08700 ± 0.01477	1056 ± 29	1360 ± 327	22.4
D	9	9.1	12	0	0.02	–0.274	5.197 ± 0.131	0.09272 ± 0.00294	5.183 ± 0.131	0.09507 ± 0.00320	1137 ± 26	1530 ± 63	25.6
D	22	21.1	12	37	3.07	1.900	5.144 ± 0.131	0.11123 ± 0.00522	5.244 ± 0.142	0.09489 ± 0.00943	1125 ± 28	1526 ± 187	26.3

Table A3. Ion microprobe analytical results for zircons from sample 184127: porphyritic monzodiorite, Powell Point

Grp no.	Spot no.	Grain .spot	^{238}U (ppm)	^{232}Th (ppm)	$^{232}Th/^{238}U$	f204 (%)	$^{238}U/^{206}Pb$ ±1σ	$^{207}Pb/^{206}Pb$ ±1σ	$^{238}U/^{206}Pb^*$ ±1σ	$^{207}Pb^*/^{206}Pb^*$ ±1σ	$^{238}U/^{206}Pb^*$ date (Ma) ±1σ	$^{207}Pb^*/^{206}Pb^*$ date (Ma) ±1σ	Disc (%)
1	26	25.1	730	1536	2.17	0.005	1.980 ± 0.023	0.17977 ± 0.00040	1.981 ± 0.023	0.17972 ± 0.00040	2635 ± 25	2650 ± 4	0.6
1	19	18.1	73	20	0.28	0.263	2.131 ± 0.030	0.18174 ± 0.00128	2.136 ± 0.030	0.17939 ± 0.00154	2475 ± 29	2647 ± 14	6.5
1	22	21.1	594	432	0.75	0.014	2.096 ± 0.025	0.17838 ± 0.00044	2.096 ± 0.025	0.17825 ± 0.00044	2514 ± 25	2637 ± 4	4.6
1	24	23.1	223	326	1.51	0.066	2.122 ± 0.026	0.17825 ± 0.00071	2.123 ± 0.026	0.17766 ± 0.00076	2488 ± 25	2631 ± 7	5.4
1	6	6.1	1955	4146	2.19	0.008	1.961 ± 0.029	0.17742 ± 0.00024	1.961 ± 0.029	0.17736 ± 0.00024	2657 ± 33	2628 ± 2	–1.1
1	8	8.1	147	100	0.71	0.040	1.976 ± 0.024	0.17759 ± 0.00081	1.977 ± 0.024	0.17724 ± 0.00085	2639 ± 26	2627 ± 8	–0.5
1	3	3.1	371	243	0.68	0.026	2.052 ± 0.031	0.17714 ± 0.00074	2.053 ± 0.031	0.17691 ± 0.00075	2558 ± 32	2624 ± 7	2.5
1	14	13.1	714	736	1.07	0.020	2.086 ± 0.030	0.17702 ± 0.00038	2.087 ± 0.030	0.17684 ± 0.00038	2524 ± 30	2623 ± 4	3.8
1	1	1.1	478	279	0.60	0.030	2.021 ± 0.031	0.17695 ± 0.00047	2.022 ± 0.031	0.17669 ± 0.00049	2590 ± 33	2622 ± 5	1.2
1	28	27.1	431	269	0.65	–0.016	2.106 ± 0.025	0.17640 ± 0.00051	2.106 ± 0.025	0.17654 ± 0.00053	2505 ± 24	2621 ± 5	4.4
1	18	17.1	490	63	0.13	0.086	2.177 ± 0.025	0.17688 ± 0.00049	2.178 ± 0.025	0.17612 ± 0.00051	2435 ± 24	2617 ± 5	6.9
1	16	15.1	417	583	1.44	0.034	2.161 ± 0.025	0.17572 ± 0.00122	2.162 ± 0.025	0.17542 ± 0.00123	2451 ± 24	2610 ± 12	6.1
1	20	19.1	565	394	0.72	0.053	2.149 ± 0.025	0.17546 ± 0.00045	2.151 ± 0.025	0.17499 ± 0.00048	2462 ± 24	2606 ± 5	5.5
1	29	28.1	231	262	1.17	0.091	2.153 ± 0.026	0.17574 ± 0.00069	2.155 ± 0.026	0.17492 ± 0.00072	2457 ± 25	2605 ± 7	5.7
1	10	9.1	283	138	0.50	–0.020	2.200 ± 0.026	0.17442 ± 0.00061	2.200 ± 0.026	0.17459 ± 0.00062	2416 ± 24	2602 ± 6	7.2
1	5	5.1	368	240	0.67	0.066	2.195 ± 0.034	0.17512 ± 0.00054	2.197 ± 0.034	0.17453 ± 0.00059	2418 ± 31	2602 ± 6	7.0
1	13	12.1	437	177	0.42	0.030	2.166 ± 0.028	0.17464 ± 0.00053	2.167 ± 0.028	0.17437 ± 0.00058	2446 ± 26	2600 ± 6	5.9
1	11	10.1	413	301	0.75	0.022	2.150 ± 0.025	0.17452 ± 0.00123	2.150 ± 0.025	0.17432 ± 0.00124	2462 ± 24	2600 ± 12	5.3
1	7	7.1	116	81	0.72	0.236	2.103 ± 0.035	0.17604 ± 0.00125	2.108 ± 0.035	0.17393 ± 0.00144	2503 ± 34	2596 ± 14	3.6
1	15	14.1	699	184	0.27	0.015	2.054 ± 0.026	0.17394 ± 0.00052	2.054 ± 0.026	0.17381 ± 0.00053	2557 ± 27	2595 ± 5	1.4
1	12	11.1	752	8	0.01	–0.015	2.202 ± 0.025	0.17342 ± 0.00050	2.201 ± 0.025	0.17355 ± 0.00051	2414 ± 23	2592 ± 5	6.9
1	23	22.1	897	40	0.05	0.026	2.133 ± 0.024	0.17343 ± 0.00068	2.133 ± 0.024	0.17319 ± 0.00069	2478 ± 24	2589 ± 7	4.3
1	2	2.1	558	114	0.21	0.044	2.125 ± 0.033	0.17358 ± 0.00043	2.126 ± 0.033	0.17318 ± 0.00045	2485 ± 32	2589 ± 4	4.0
1	25	24.1	517	190	0.38	0.021	2.273 ± 0.027	0.17329 ± 0.00049	2.274 ± 0.027	0.17311 ± 0.00050	2350 ± 23	2588 ± 5	9.2
1	27	26.1	301	231	0.80	0.011	2.166 ± 0.026	0.17317 ± 0.00060	2.166 ± 0.026	0.17307 ± 0.00061	2447 ± 24	2588 ± 6	5.4
1	4	4.1	915	46	0.05	0.012	2.153 ± 0.034	0.17204 ± 0.00101	2.153 ± 0.034	0.17193 ± 0.00101	2459 ± 32	2577 ± 10	4.6
1	9	8.2	839	106	0.13	0.004	2.268 ± 0.025	0.17007 ± 0.00071	2.268 ± 0.025	0.17004 ± 0.00071	2355 ± 21	2558 ± 7	7.9
1	21	20.1	550	221	0.42	0.032	2.287 ± 0.027	0.16994 ± 0.00046	2.288 ± 0.027	0.16965 ± 0.00048	2337 ± 23	2554 ± 5	8.5
1	17	16.1	873	36	0.04	0.009	2.327 ± 0.035	0.16727 ± 0.00036	2.328 ± 0.035	0.16719 ± 0.00037	2304 ± 29	2530 ± 4	8.9

Table A4. Ion microprobe analytical results for zircons from sample 184314: leucocratic granodioritic gneiss, Lort River – Ashdale Road

Grp no.	Spot no.	Grain .spot	^{238}U (ppm)	^{232}Th (ppm)	$^{232}Th/^{238}U$	f204 (%)	$^{238}U/^{206}Pb$ ±1σ	$^{207}Pb/^{206}Pb$ ±1σ	$^{238}U/^{206}Pb^*$ ±1σ	$^{207}Pb^*/^{206}Pb^*$ ±1σ	$^{238}U/^{206}Pb^*$ date (Ma) ±1σ	$^{207}Pb^*/^{206}Pb^*$ date (Ma) ±1σ	Disc (%)
1	3	3.1	217	146	0.69	0.021	2.027 ± 0.024	0.18114 ± 0.00059	2.028 ± 0.024	0.18095 ± 0.00060	2584 ± 25	2662 ± 6	2.9
1	6	6.1	153	60	0.41	0.007	1.920 ± 0.049	0.18050 ± 0.00105	1.920 ± 0.049	0.18043 ± 0.00107	2703 ± 57	2657 ± 10	–1.7
2	4	4.1	719	382	0.55	0.014	1.783 ± 0.047	0.21342 ± 0.00087	1.783 ± 0.047	0.21330 ± 0.00087	2870 ± 61	2931 ± 7	2.1
2	15	15.1	352	325	0.95	0.017	1.984 ± 0.049	0.21062 ± 0.00047	1.984 ± 0.049	0.21047 ± 0.00048	2631 ± 54	2909 ± 4	9.6
2	8	8.1	91	67	0.76	0.038	1.760 ± 0.043	0.21039 ± 0.00078	1.760 ± 0.043	0.21005 ± 0.00082	2900 ± 58	2906 ± 6	0.2
2	2	2.1	236	81	0.35	0.046	1.920 ± 0.013	0.20015 ± 0.00104	1.921 ± 0.013	0.19975 ± 0.00105	2702 ± 15	2824 ± 9	4.3
2	14	14.1	224	191	0.88	0.019	2.004 ± 0.049	0.19526 ± 0.00083	2.004 ± 0.049	0.19510 ± 0.00085	2609 ± 53	2786 ± 7	6.3
2	12	12.1	297	154	0.54	0.020	2.044 ± 0.050	0.19515 ± 0.00053	2.044 ± 0.050	0.19497 ± 0.00053	2567 ± 52	2785 ± 4	7.8
2	1	1.1	109	31	0.29	0.052	2.094 ± 0.018	0.19326 ± 0.00105	2.095 ± 0.018	0.19280 ± 0.00110	2515 ± 18	2766 ± 9	9.1
2	9	9.1	407	247	0.63	0.014	2.017 ± 0.049	0.19194 ± 0.00037	2.018 ± 0.049	0.19182 ± 0.00037	2595 ± 52	2758 ± 3	5.9
2	11	11.1	946	635	0.69	0.009	1.974 ± 0.048	0.19006 ± 0.00051	1.974 ± 0.048	0.18998 ± 0.00051	2642 ± 53	2742 ± 4	3.6
2	5	5.1	305	151	0.51	0.037	2.082 ± 0.051	0.18889 ± 0.00133	2.083 ± 0.051	0.18856 ± 0.00134	2527 ± 51	2730 ± 12	7.4
3	7	7.1	271	134	0.51	0.023	2.043 ± 0.050	0.17457 ± 0.00045	2.044 ± 0.050	0.17437 ± 0.00046	2568 ± 52	2600 ± 4	1.2
3	17	17.1	1101	124	0.12	0.016	2.244 ± 0.054	0.17062 ± 0.00042	2.245 ± 0.054	0.17048 ± 0.00042	2375 ± 48	2562 ± 4	7.3
D	13	13.1	467	182	0.40	0.026	2.170 ± 0.054	0.18928 ± 0.00045	2.171 ± 0.054	0.18905 ± 0.00046	2442 ± 51	2734 ± 4	10.7
D	19	19.1	941	88	0.10	0.131	2.500 ± 0.061	0.16332 ± 0.00141	2.503 ± 0.061	0.16215 ± 0.00142	2167 ± 45	2478 ± 15	12.6
D	16	16.1	1767	65	0.04	0.005	2.577 ± 0.062	0.16172 ± 0.00043	2.577 ± 0.062	0.16168 ± 0.00043	2114 ± 44	2473 ± 4	14.5
D	18	18.1	2055	244	0.12	0.017	2.681 ± 0.065	0.15508 ± 0.00050	2.681 ± 0.065	0.15493 ± 0.00050	2043 ± 43	2401 ± 6	14.9
D	10	10.1	706	83	0.12	0.012	4.651 ± 0.114	0.09754 ± 0.00028	4.652 ± 0.114	0.09743 ± 0.00030	1255 ± 28	1576 ± 6	20.3

Table A5. Ion microprobe analytical results for zircons from sample 184311: orthopyroxene–clinopyroxene orthogneiss, Fisheries Bay headland

Grp no.	Spot no.	Grain .spot	^{238}U (ppm)	^{232}Th (ppm)	$^{232}Th/^{238}U$	f204 (%)	$^{238}U/^{206}Pb$ ±1σ	$^{207}Pb/^{206}Pb$ ±1σ	$^{238}U/^{206}Pb^*$ ±1σ	$^{207}Pb^*/^{206}Pb^*$ ±1σ	$^{238}U/^{206}Pb^*$ date (Ma) ±1σ	$^{207}Pb^*/^{206}Pb^*$ date (Ma) ±1σ	Disc (%)
1	20	16.1	108	74	0.71	–0.132	3.230 ± 0.048	0.10387 ± 0.00096	3.226 ± 0.048	0.10501 ± 0.00115	1741 ± 23	1715 ± 20	–1.5
1	18	14.1	104	59	0.59	–0.010	3.331 ± 0.067	0.10448 ± 0.00099	3.330 ± 0.067	0.10457 ± 0.00099	1693 ± 30	1707 ± 17	0.8
1	14	10.1	167	138	0.86	0.062	3.285 ± 0.046	0.10466 ± 0.00074	3.287 ± 0.046	0.10412 ± 0.00077	1712 ± 21	1699 ± 14	–0.8
1	26	22.1	188	112	0.61	–0.026	3.228 ± 0.049	0.10379 ± 0.00074	3.227 ± 0.049	0.10401 ± 0.00076	1740 ± 23	1697 ± 13	–2.6
1	24	20.1	137	109	0.83	0.131	3.274 ± 0.047	0.10494 ± 0.00087	3.278 ± 0.048	0.10380 ± 0.00088	1716 ± 22	1693 ± 16	–1.4
1	35	31.1	195	166	0.88	–0.034	3.263 ± 0.049	0.10347 ± 0.00068	3.261 ± 0.049	0.10376 ± 0.00070	1724 ± 23	1692 ± 12	–1.9
1	16	12.1	132	102	0.80	0.048	3.271 ± 0.049	0.10410 ± 0.00089	3.272 ± 0.049	0.10369 ± 0.00100	1719 ± 23	1691 ± 18	–1.6
1	33	29.1	108	67	0.64	0.005	3.255 ± 0.048	0.10346 ± 0.00103	3.255 ± 0.048	0.10341 ± 0.00116	1727 ± 22	1686 ± 21	–2.4
1	36	32.1	139	126	0.94	–0.053	3.278 ± 0.047	0.10269 ± 0.00080	3.276 ± 0.047	0.10315 ± 0.00080	1717 ± 22	1682 ± 14	–2.1
1	17	13.1	122	100	0.85	0.170	3.290 ± 0.048	0.10431 ± 0.00106	3.296 ± 0.049	0.10284 ± 0.00114	1708 ± 22	1676 ± 20	–1.9
1	21	17.1	140	87	0.65	0.037	3.293 ± 0.048	0.10315 ± 0.00089	3.294 ± 0.048	0.10282 ± 0.00096	1709 ± 22	1676 ± 17	–2.0
1	34	30.1	133	111	0.87	0.038	3.254 ± 0.047	0.10304 ± 0.00082	3.255 ± 0.047	0.10271 ± 0.00085	1727 ± 22	1674 ± 15	–3.2
1	27	23.1	121	66	0.56	–0.001	3.247 ± 0.048	0.10264 ± 0.00090	3.247 ± 0.048	0.10265 ± 0.00090	1731 ± 22	1673 ± 16	–3.5
1	1	1.1	160	139	0.90	0.130	3.248 ± 0.056	0.10376 ± 0.00082	3.252 ± 0.056	0.10264 ± 0.00107	1728 ± 26	1672 ± 19	–3.4
1	3	2.2	173	92	0.55	0.040	3.461 ± 0.049	0.10297 ± 0.00075	3.462 ± 0.049	0.10262 ± 0.00084	1636 ± 20	1672 ± 15	2.2
1	30	26.1	134	112	0.87	0.029	3.296 ± 0.058	0.10285 ± 0.00083	3.297 ± 0.059	0.10260 ± 0.00091	1708 ± 27	1672 ± 16	–2.1
1	25	21.1	199	170	0.88	–0.031	3.427 ± 0.048	0.10212 ± 0.00072	3.426 ± 0.048	0.10239 ± 0.00074	1651 ± 20	1668 ± 13	1.0
1	15	11.1	140	84	0.62	0.166	3.320 ± 0.061	0.10371 ± 0.00081	3.325 ± 0.061	0.10227 ± 0.00112	1695 ± 27	1666 ± 20	–1.8
1	11	8.1	164	135	0.85	0.109	3.331 ± 0.047	0.10283 ± 0.00070	3.335 ± 0.047	0.10188 ± 0.00080	1691 ± 21	1659 ± 14	–1.9
1	32	28.1	113	65	0.59	0.060	3.401 ± 0.050	0.10176 ± 0.00093	3.403 ± 0.050	0.10124 ± 0.00104	1661 ± 22	1647 ± 19	–0.8
1	19	15.1	72	35	0.50	0.194	3.327 ± 0.065	0.10255 ± 0.00117	3.333 ± 0.065	0.10087 ± 0.00137	1691 ± 29	1640 ± 25	–3.1
1	31	27.1	82	42	0.53	0.170	3.427 ± 0.053	0.10219 ± 0.00152	3.433 ± 0.054	0.10072 ± 0.00188	1648 ± 23	1637 ± 35	–0.6
2	29	25.1	98	53	0.56	0.112	3.573 ± 0.054	0.10080 ± 0.00100	3.577 ± 0.054	0.09983 ± 0.00112	1589 ± 21	1621 ± 21	1.9
2	10	7.2	176	149	0.88	0.005	3.425 ± 0.053	0.09948 ± 0.00084	3.425 ± 0.053	0.09943 ± 0.00087	1651 ± 23	1613 ± 16	–2.4
2	22	18.1	188	146	0.80	–0.080	3.645 ± 0.052	0.09785 ± 0.00073	3.643 ± 0.052	0.09855 ± 0.00084	1564 ± 20	1597 ± 16	2.1
2	28	24.1	136	109	0.82	–0.065	3.704 ± 0.054	0.09793 ± 0.00099	3.702 ± 0.054	0.09849 ± 0.00105	1542 ± 20	1596 ± 20	3.4
2	12	9.1	185	162	0.90	0.181	3.434 ± 0.053	0.09991 ± 0.00069	3.440 ± 0.054	0.09835 ± 0.00084	1645 ± 23	1593 ± 16	–3.3
2	23	19.1	126	85	0.70	0.109	3.727 ± 0.055	0.09767 ± 0.00092	3.731 ± 0.055	0.09673 ± 0.00096	1531 ± 20	1562 ± 19	2.0
D	7	5.1	107	57	0.55	0.615	3.613 ± 0.055	0.10446 ± 0.00099	3.635 ± 0.056	0.09915 ± 0.00242	1566 ± 21	1608 ± 46	2.6
D	8	6.1	102	60	0.61	0.673	4.423 ± 0.119	0.09226 ± 0.00224	4.453 ± 0.120	0.08652 ± 0.00357	1306 ± 32	1350 ± 80	3.3
D	5	4.1	133	50	0.39	0.681	4.447 ± 0.066	0.09173 ± 0.00290	4.478 ± 0.068	0.08593 ± 0.00435	1299 ± 18	1337 ± 98	2.8
D	4	3.1	45	0	0.01	0.380	4.746 ± 0.086	0.07961 ± 0.00144	4.764 ± 0.088	0.07642 ± 0.00322	1228 ± 21	1106 ± 84	–11.1
D	13	9.2	35	45	1.35	1.132	4.901 ± 0.117	0.08139 ± 0.00171	4.957 ± 0.122	0.07193 ± 0.00509	1185 ± 27	984 ± 144	–20.4
D	6	4.2	17	0	0.00	3.290	4.968 ± 0.129	0.09912 ± 0.00406	5.137 ± 0.145	0.07163 ± 0.00996	1147 ± 30	976 ± 284	–17.5
D	2	2.1	8	0	0.01	4.694	4.544 ± 0.169	0.10824 ± 0.01296	4.767 ± 0.275	0.06918 ± 0.03904	1228 ± 64	904 ±1163	–35.8
D	9	7.1	31	29	0.97	4.837	4.644 ± 0.108	0.10263 ± 0.00943	4.880 ± 0.198	0.06284 ± 0.02920	1202 ± 45	703 ± 989	–71.0

Table A6. Ion microprobe analytical results for zircons from sample 184310: leucocratic granodiorite, Fisheries Bay headland

Grp no.	Spot no.	Grain .spot	^{238}U (ppm)	^{232}Th (ppm)	$^{232}Th/^{238}U$	f204 (%)	$^{238}U/^{206}Pb$ ±1σ	$^{207}Pb/^{206}Pb$ ±1σ	$^{238}U/^{206}Pb^*$ ±1σ	$^{207}Pb^*/^{206}Pb^*$ ±1σ	$^{238}U/^{206}Pb^*$ date (Ma) ±1σ	$^{207}Pb^*/^{206}Pb^*$ date (Ma) ±1σ	Disc (%)
1	21	17.2	159	165	1.07	0.064	4.768 ± 0.118	0.08097 ± 0.00053	4.771 ± 0.118	0.08043 ± 0.00065	1227 ± 28	1208 ± 16	–1.6
1	16	13.1	133	273	2.12	0.060	4.961 ± 0.124	0.08050 ± 0.00058	4.964 ± 0.124	0.07999 ± 0.00097	1183 ± 27	1197 ± 24	1.1
1	4	3.1	443	276	0.64	0.018	5.032 ± 0.030	0.08010 ± 0.00039	5.033 ± 0.030	0.07995 ± 0.00041	1168 ± 6	1196 ± 10	2.3
1	8	5.1	122	188	1.60	–0.005	5.127 ± 0.127	0.07982 ± 0.00063	5.127 ± 0.127	0.07986 ± 0.00063	1149 ± 26	1194 ± 15	3.8
1	6	4.1	568	256	0.47	0.023	5.049 ± 0.029	0.08002 ± 0.00035	5.050 ± 0.029	0.07983 ± 0.00037	1165 ± 6	1193 ± 9	2.4
1	13	10.1	389	170	0.45	0.061	4.735 ± 0.115	0.08029 ± 0.00034	4.738 ± 0.115	0.07977 ± 0.00039	1234 ± 27	1191 ± 10	–3.6
1	2	2.1	470	207	0.45	0.075	4.973 ± 0.042	0.08039 ± 0.00037	4.977 ± 0.042	0.07976 ± 0.00043	1180 ± 9	1191 ± 11	0.9
1	20	17.1	138	261	1.95	0.015	4.895 ± 0.120	0.07980 ± 0.00057	4.896 ± 0.121	0.07967 ± 0.00073	1198 ± 27	1189 ± 18	–0.8
1	17	13.2	1336	182	0.14	0.022	4.953 ± 0.120	0.07961 ± 0.00018	4.954 ± 0.120	0.07943 ± 0.00020	1185 ± 26	1183 ± 5	–0.2
1	14	10.2	75	75	1.03	0.026	4.499 ± 0.113	0.07961 ± 0.00077	4.500 ± 0.113	0.07939 ± 0.00104	1294 ± 29	1182 ± 26	–9.5
1	15	12.1	1421	129	0.09	0.055	4.519 ± 0.113	0.07984 ± 0.00018	4.521 ± 0.113	0.07938 ± 0.00022	1288 ± 29	1182 ± 5	–9.0
1	18	15.1	657	324	0.51	0.054	4.868 ± 0.118	0.07981 ± 0.00026	4.871 ± 0.118	0.07935 ± 0.00029	1204 ± 27	1181 ± 7	–1.9
1	19	16.1	458	310	0.70	0.017	5.075 ± 0.124	0.07949 ± 0.00031	5.076 ± 0.124	0.07935 ± 0.00034	1159 ± 26	1181 ± 9	1.8
1	1	1.1	479	196	0.42	0.135	5.036 ± 0.029	0.08047 ± 0.00037	5.042 ± 0.029	0.07933 ± 0.00048	1166 ± 6	1180 ± 12	1.2
1	26	22.1	125	127	1.05	0.112	4.870 ± 0.120	0.08019 ± 0.00060	4.875 ± 0.120	0.07925 ± 0.00061	1203 ± 27	1178 ± 15	–2.1
1	30	18.1	1709	76	0.05	0.010	4.831 ± 0.118	0.07925 ± 0.00016	4.832 ± 0.118	0.07917 ± 0.00016	1213 ± 27	1176 ± 4	–3.1
1	25	21.2	572	372	0.67	0.017	4.934 ± 0.120	0.07930 ± 0.00027	4.935 ± 0.120	0.07915 ± 0.00030	1189 ± 26	1176 ± 7	–1.1
1	5	3.2	76	91	1.25	0.155	4.884 ± 0.053	0.08044 ± 0.00094	4.892 ± 0.053	0.07913 ± 0.00125	1199 ± 12	1175 ± 31	–2.0
1	29	14.2	974	32	0.03	0.006	4.736 ± 0.115	0.07907 ± 0.00021	4.736 ± 0.115	0.07902 ± 0.00024	1235 ± 27	1173 ± 6	–5.3
1	23	20.1	347	308	0.92	0.069	5.188 ± 0.128	0.07949 ± 0.00038	5.192 ± 0.128	0.07890 ± 0.00053	1136 ± 26	1170 ± 13	2.9
1	27	11.1	2402	96	0.04	0.013	4.814 ± 0.117	0.07901 ± 0.00014	4.814 ± 0.117	0.07890 ± 0.00014	1217 ± 27	1170 ± 4	–4.0
1	12	9.1	359	118	0.34	0.198	4.726 ± 0.118	0.08057 ± 0.00036	4.735 ± 0.118	0.07890 ± 0.00051	1235 ± 28	1170 ± 13	–5.6
1	9	6.1	119	201	1.76	0.051	4.893 ± 0.121	0.07918 ± 0.00065	4.895 ± 0.121	0.07875 ± 0.00080	1198 ± 27	1166 ± 20	–2.8
1	11	8.1	463	197	0.44	1.337	4.881 ± 0.119	0.08995 ± 0.00034	4.947 ± 0.121	0.07866 ± 0.00106	1187 ± 26	1164 ± 27	–2.0
1	3	2.2	95	138	1.50	0.840	4.949 ± 0.084	0.08575 ± 0.00121	4.991 ± 0.085	0.07866 ± 0.00217	1177 ± 18	1164 ± 55	–1.2
1	10	7.1	75	135	1.86	0.111	4.583 ± 0.115	0.07949 ± 0.00077	4.588 ± 0.115	0.07855 ± 0.00123	1271 ± 29	1161 ± 31	–9.5
1	22	19.1	390	326	0.86	0.055	4.876 ± 0.119	0.07898 ± 0.00034	4.878 ± 0.119	0.07851 ± 0.00041	1202 ± 27	1160 ± 10	–3.6
1	24	21.1	172	168	1.00	0.714	5.177 ± 0.127	0.08372 ± 0.00053	5.214 ± 0.128	0.07771 ± 0.00111	1131 ± 25	1139 ± 28	0.7
1	7	4.2	55	67	1.26	0.496	4.972 ± 0.099	0.08182 ± 0.00116	4.997 ± 0.100	0.07764 ± 0.00191	1176 ± 21	1138 ± 49	–3.4
D	28	14.1	36	32	0.92	0.617	4.702 ± 0.122	0.07985 ± 0.00110	4.731 ± 0.123	0.07467 ± 0.00179	1236 ± 29	1060 ± 48	–16.6

Table A7. Ion microprobe analytical results for zircons from sample 184312: granodioritic gneiss, Short Beach headland

Grp no.	*Spot no.*	*Grain .spot*	^{238}U *(ppm)*	^{232}Th *(ppm)*	$^{232}Th/^{238}U$	*f204 (%)*	$^{238}U/^{206}Pb$ ±1σ	$^{207}Pb/^{206}Pb$ ±1σ	$^{238}U/^{206}Pb^*$ ±1σ	$^{207}Pb^*/^{206}Pb^*$ ±1σ	$^{238}U/^{206}Pb^*$ *date (Ma)* ±1σ	$^{207}Pb^*/^{206}Pb^*$ *date (Ma)* ±1σ	*Disc (%)*
1	3	3.1	94	154	1.69	0.266	3.164 ± 0.057	0.10766 ± 0.00103	3.172 ± 0.057	0.10534 ± 0.00207	1766 ± 28	1720 ± 36	–2.7
1	15	15.1	120	189	1.62	0.058	3.253 ± 0.049	0.10485 ± 0.00091	3.255 ± 0.049	0.10435 ± 0.00092	1727 ± 23	1703 ± 16	–1.4
1	25	25.1	648	44	0.07	0.040	3.240 ± 0.042	0.10465 ± 0.00038	3.241 ± 0.042	0.10431 ± 0.00040	1734 ± 20	1702 ± 7	–1.8
1	6	6.1	199	163	0.85	0.038	3.495 ± 0.068	0.10439 ± 0.00131	3.496 ± 0.068	0.10406 ± 0.00141	1622 ± 28	1698 ± 25	4.5
1	32	32.1	110	166	1.55	0.096	3.255 ± 0.055	0.10484 ± 0.00108	3.258 ± 0.055	0.10401 ± 0.00113	1726 ± 25	1697 ± 20	–1.7
1	34	34.1	86	133	1.60	0.091	3.163 ± 0.049	0.10417 ± 0.00108	3.166 ± 0.049	0.10338 ± 0.00109	1769 ± 24	1686 ± 19	–5.0
1	21	21.1	193	24	0.13	0.237	3.471 ± 0.049	0.10531 ± 0.00075	3.480 ± 0.049	0.10326 ± 0.00108	1628 ± 20	1683 ± 19	3.3
1	26	26.1	46	55	1.23	0.905	3.130 ± 0.076	0.11090 ± 0.00175	3.158 ± 0.077	0.10306 ± 0.00287	1773 ± 38	1680 ± 51	–5.6
1	31	31.1	81	117	1.49	0.343	3.258 ± 0.051	0.10575 ± 0.00109	3.269 ± 0.051	0.10278 ± 0.00160	1720 ± 24	1675 ± 29	–2.7
1	7	7.1	136	106	0.81	0.894	3.376 ± 0.050	0.10946 ± 0.00156	3.407 ± 0.052	0.10172 ± 0.00361	1659 ± 22	1656 ± 66	–0.2
1	23	23.1	129	203	1.62	–0.037	3.360 ± 0.049	0.10135 ± 0.00087	3.358 ± 0.049	0.10167 ± 0.00089	1680 ± 22	1655 ± 16	–1.5
1	9	9.1	498	252	0.52	0.854	3.448 ± 0.049	0.10904 ± 0.00101	3.478 ± 0.049	0.10165 ± 0.00137	1629 ± 20	1654 ± 25	1.5
1	20	20.1	61	57	0.97	0.573	3.308 ± 0.055	0.10650 ± 0.00151	3.327 ± 0.056	0.10154 ± 0.00216	1694 ± 25	1652 ± 40	–2.5
1	4	4.1	119	154	1.33	0.334	3.635 ± 0.060	0.10424 ± 0.00093	3.647 ± 0.061	0.10135 ± 0.00133	1562 ± 23	1649 ± 24	5.3
1	18	18.1	74	71	1.00	0.019	3.266 ± 0.054	0.10119 ± 0.00150	3.266 ± 0.054	0.10102 ± 0.00179	1722 ± 25	1643 ± 33	–4.8
2	30	30.1	124	3	0.02	0.201	4.828 ± 0.071	0.08239 ± 0.00092	4.837 ± 0.072	0.08069 ± 0.00130	1211 ± 16	1214 ± 32	0.2
2	16	16.1	31	58	1.93	0.311	4.906 ± 0.099	0.08215 ± 0.00189	4.921 ± 0.100	0.07952 ± 0.00230	1193 ± 22	1185 ± 57	–0.6
2	19	19.1	85	133	1.62	0.045	4.949 ± 0.079	0.07958 ± 0.00116	4.952 ± 0.079	0.07920 ± 0.00145	1186 ± 17	1177 ± 36	–0.7
2	33	33.1	100	96	1.00	0.562	4.808 ± 0.073	0.08300 ± 0.00105	4.835 ± 0.074	0.07825 ± 0.00184	1212 ± 17	1153 ± 47	–5.1
2	22	22.1	115	268	2.42	0.468	4.956 ± 0.075	0.08202 ± 0.00101	4.979 ± 0.076	0.07807 ± 0.00181	1180 ± 16	1149 ± 46	–2.7
2	11	11.1	53	171	3.30	0.391	4.939 ± 0.083	0.08111 ± 0.00135	4.958 ± 0.084	0.07782 ± 0.00161	1184 ± 18	1142 ± 41	–3.7
2	1	1.1	39	166	4.42	0.562	4.876 ± 0.093	0.08247 ± 0.00166	4.903 ± 0.095	0.07774 ± 0.00339	1196 ± 21	1140 ± 87	–4.9
2	29	29.1	29	54	1.90	0.525	4.775 ± 0.103	0.08185 ± 0.00189	4.800 ± 0.103	0.07743 ± 0.00213	1220 ± 24	1132 ± 55	–7.7
2	27	27.1	193	3	0.02	0.267	4.861 ± 0.068	0.07967 ± 0.00074	4.874 ± 0.069	0.07742 ± 0.00093	1203 ± 15	1132 ± 24	–6.3
2	14	14.1	55	209	3.91	0.663	5.066 ± 0.088	0.08177 ± 0.00140	5.100 ± 0.089	0.07619 ± 0.00168	1154 ± 18	1100 ± 44	–4.9
3	13	13.1	353	154	0.45	0.024	2.277 ± 0.035	0.16541 ± 0.00068	2.277 ± 0.035	0.16520 ± 0.00069	2347 ± 30	2510 ± 7	6.5
3	28	28.1	237	127	0.55	0.079	3.249 ± 0.044	0.11695 ± 0.00067	3.252 ± 0.044	0.11626 ± 0.00071	1728 ± 21	1899 ± 11	9.0
3	12	12.1	69	86	1.29	0.291	3.265 ± 0.052	0.11330 ± 0.00123	3.274 ± 0.053	0.11076 ± 0.00201	1718 ± 24	1812 ± 33	5.2
3	2	2.1	133	162	1.26	0.123	3.278 ± 0.048	0.10794 ± 0.00106	3.282 ± 0.048	0.10687 ± 0.00128	1714 ± 22	1747 ± 22	1.8
4	10	10.1	96	235	2.54	0.164	3.435 ± 0.051	0.10181 ± 0.00097	3.441 ± 0.051	0.10039 ± 0.00121	1645 ± 22	1631 ± 22	–0.8
4	24	24.1	90	85	0.98	0.170	3.624 ± 0.056	0.09802 ± 0.00110	3.630 ± 0.056	0.09655 ± 0.00175	1569 ± 21	1558 ± 34	–0.6
4	8	8.1	78	117	1.56	0.098	4.162 ± 0.064	0.09437 ± 0.00112	4.166 ± 0.065	0.09353 ± 0.00169	1387 ± 19	1499 ± 34	7.4
4	17	17.1	141	399	2.92	0.067	3.950 ± 0.058	0.09166 ± 0.00095	3.953 ± 0.058	0.09108 ± 0.00112	1454 ± 19	1448 ± 23	–0.4
D	5	5.1	41	77	1.96	1.215	4.924 ± 0.096	0.08424 ± 0.00308	4.985 ± 0.101	0.07406 ± 0.00581	1179 ± 22	1043 ± 158	–13.0

Table A8. Ion microprobe analytical results for zircons from sample 184326: pegmatitic leucogranite, Short Beach headland

Grp no.	Spot no.	Grain .spot	^{238}U (ppm)	^{232}Th (ppm)	$^{232}Th/^{238}U$	f204 (%)	$^{238}U/^{206}Pb$ ±1σ	$^{207}Pb/^{206}Pb$ ±1σ	$^{238}U/^{206}Pb^*$ ±1σ	$^{207}Pb^*/^{206}Pb^*$ ±1σ	$^{238}U/^{206}Pb^*$ date (Ma) ±1σ	$^{207}Pb^*/^{206}Pb^*$ date (Ma) ±1σ	Disc (%)
1	50	40.2	62	117	1.97	–0.268	5.036 ± 0.116	0.08369 ± 0.00142	5.023 ± 0.116	0.08597 ± 0.00202	1170 ± 25	1338 ± 45	12.5
1	35	30.1	38	81	2.21	–0.497	4.983 ± 0.124	0.08001 ± 0.00171	4.958 ± 0.124	0.08424 ± 0.00253	1184 ± 27	1298 ± 58	8.8
1	19	16.1	52	93	1.86	–0.184	5.046 ± 0.118	0.08176 ± 0.00146	5.036 ± 0.118	0.08332 ± 0.00179	1168 ± 25	1277 ± 42	8.6
1	30	26.1	52	124	2.45	0.195	5.327 ± 0.125	0.08371 ± 0.00153	5.337 ± 0.126	0.08206 ± 0.00184	1107 ± 24	1247 ± 44	11.2
1	17	15.1	70	108	1.58	–0.077	5.215 ± 0.117	0.08104 ± 0.00124	5.211 ± 0.117	0.08169 ± 0.00127	1132 ± 23	1238 ± 30	8.6
1	33	28.1	116	206	1.84	0.028	5.170 ± 0.109	0.08155 ± 0.00098	5.171 ± 0.109	0.08131 ± 0.00145	1140 ± 22	1229 ± 35	7.3
1	21	17.1	110	173	1.62	–0.085	5.089 ± 0.107	0.08017 ± 0.00100	5.085 ± 0.107	0.08088 ± 0.00104	1157 ± 22	1219 ± 25	5.0
1	29	25.1	126	134	1.10	–0.002	5.135 ± 0.107	0.08078 ± 0.00096	5.135 ± 0.107	0.08080 ± 0.00096	1147 ± 22	1217 ± 23	5.7
1	8	8.1	48	113	2.42	0.158	5.206 ± 0.123	0.08200 ± 0.00153	5.214 ± 0.124	0.08066 ± 0.00237	1131 ± 25	1213 ± 58	6.8
1	34	29.1	121	221	1.89	0.099	5.051 ± 0.133	0.08126 ± 0.00146	5.056 ± 0.133	0.08042 ± 0.00155	1163 ± 28	1207 ± 38	3.6
1	37	32.1	120	176	1.52	–0.042	5.236 ± 0.110	0.07990 ± 0.00099	5.233 ± 0.110	0.08026 ± 0.00102	1127 ± 22	1203 ± 25	6.3
1	38	33.1	288	229	0.82	0.068	5.245 ± 0.104	0.08067 ± 0.00063	5.249 ± 0.104	0.08009 ± 0.00084	1124 ± 20	1199 ± 21	6.3
1	12	11.1	51	103	2.12	0.181	4.967 ± 0.116	0.08140 ± 0.00149	4.976 ± 0.117	0.07987 ± 0.00273	1181 ± 25	1194 ± 67	1.1
1	43	36.2	454	329	0.75	0.005	5.112 ± 0.102	0.07977 ± 0.00051	5.112 ± 0.102	0.07972 ± 0.00053	1152 ± 21	1190 ± 13	3.2
1	39	34.1	110	104	0.98	0.275	5.070 ± 0.107	0.08197 ± 0.00101	5.084 ± 0.107	0.07965 ± 0.00169	1158 ± 22	1188 ± 42	2.6
1	4	4.1	39	87	2.30	–0.158	4.921 ± 0.121	0.07817 ± 0.00166	4.913 ± 0.121	0.07950 ± 0.00184	1194 ± 27	1185 ± 46	–0.8
1	48	39.2	218	204	0.97	0.113	5.142 ± 0.103	0.07977 ± 0.00072	5.148 ± 0.103	0.07882 ± 0.00098	1144 ± 21	1168 ± 25	2.0
1	27	23.1	410	298	0.75	0.107	5.053 ± 0.099	0.07962 ± 0.00056	5.058 ± 0.099	0.07872 ± 0.00061	1163 ± 21	1165 ± 15	0.2
1	44	37.1	364	313	0.89	0.066	5.126 ± 0.100	0.07923 ± 0.00069	5.130 ± 0.100	0.07868 ± 0.00091	1148 ± 21	1164 ± 23	1.4
1	28	24.1	425	327	0.79	0.093	5.167 ± 0.100	0.07944 ± 0.00052	5.172 ± 0.100	0.07865 ± 0.00068	1139 ± 20	1163 ± 17	2.1
1	1	1.1	56	102	1.88	0.588	5.146 ± 0.119	0.08343 ± 0.00143	5.177 ± 0.120	0.07847 ± 0.00191	1139 ± 24	1159 ± 48	1.7
1	52	41.2	88	179	2.09	0.122	5.106 ± 0.111	0.07896 ± 0.00113	5.112 ± 0.112	0.07794 ± 0.00160	1152 ± 23	1145 ± 41	–0.6
1	55	44.1	127	230	1.87	0.212	5.137 ± 0.107	0.07956 ± 0.00095	5.147 ± 0.107	0.07778 ± 0.00103	1144 ± 22	1141 ± 26	–0.3
1	54	43.1	86	155	1.86	0.139	5.099 ± 0.111	0.07878 ± 0.00115	5.106 ± 0.112	0.07761 ± 0.00166	1153 ± 23	1137 ± 43	–1.4
1	22	18.1	111	204	1.90	0.279	5.099 ± 0.107	0.07994 ± 0.00101	5.113 ± 0.108	0.07759 ± 0.00198	1152 ± 22	1136 ± 51	–1.3
1	23	19.1	213	188	0.91	0.278	5.224 ± 0.106	0.07942 ± 0.00073	5.238 ± 0.107	0.07708 ± 0.00095	1126 ± 21	1123 ± 24	–0.3
1	9	9.1	56	72	1.33	0.399	5.264 ± 0.122	0.08043 ± 0.00140	5.285 ± 0.123	0.07708 ± 0.00215	1117 ± 24	1123 ± 56	0.5
1	32	27.1	56	108	2.01	0.301	5.221 ± 0.121	0.07883 ± 0.00138	5.237 ± 0.122	0.07630 ± 0.00245	1127 ± 24	1103 ± 64	–2.1
1	16	14.1	37	84	2.30	0.399	5.153 ± 0.130	0.07926 ± 0.00234	5.174 ± 0.132	0.07591 ± 0.00398	1139 ± 27	1093 ± 105	–4.2
1	53	42.1	51	122	2.48	0.288	5.039 ± 0.119	0.07778 ± 0.00187	5.054 ± 0.119	0.07537 ± 0.00209	1164 ± 25	1078 ± 56	–7.9
1	5	5.1	86	8	0.10	0.800	4.902 ± 0.108	0.08200 ± 0.00121	4.942 ± 0.109	0.07528 ± 0.00172	1188 ± 24	1076 ± 46	–10.4
1	36	31.1	109	203	1.92	0.710	5.087 ± 0.107	0.08073 ± 0.00102	5.123 ± 0.108	0.07477 ± 0.00162	1149 ± 22	1062 ± 44	–8.2
1	14	12.1	53	133	2.56	0.770	5.082 ± 0.152	0.08107 ± 0.00144	5.122 ± 0.155	0.07461 ± 0.00344	1150 ± 32	1058 ± 93	–8.7
1	56	45.1	114	215	1.95	0.259	5.116 ± 0.108	0.07648 ± 0.00097	5.129 ± 0.108	0.07430 ± 0.00148	1148 ± 22	1050 ± 40	–9.4
1	41	35.2	79	125	1.63	0.573	5.188 ± 0.118	0.07893 ± 0.00133	5.218 ± 0.119	0.07413 ± 0.00184	1130 ± 24	1045 ± 50	–8.2
1	46	38.2	37	81	2.25	1.586	5.116 ± 0.127	0.08043 ± 0.00174	5.199 ± 0.130	0.06728 ± 0.00265	1134 ± 26	846 ± 82	–34.0
2	25	21.1	152	130	0.88	0.211	5.382 ± 0.111	0.08028 ± 0.00094	5.394 ± 0.112	0.07850 ± 0.00158	1096 ± 21	1160 ± 40	5.4
3	31	26.2	84	62	0.77	0.149	3.433 ± 0.086	0.10546 ± 0.00113	3.438 ± 0.086	0.10416 ± 0.00148	1646 ± 36	1700 ± 26	3.2
3	49	40.1	142	113	0.83	0.104	3.344 ± 0.068	0.10423 ± 0.00085	3.348 ± 0.069	0.10333 ± 0.00102	1685 ± 30	1685 ± 18	0.0
3	2	2.1	135	78	0.60	0.294	3.531 ± 0.073	0.10567 ± 0.00104	3.542 ± 0.073	0.10312 ± 0.00142	1603 ± 29	1681 ± 25	4.6
3	6	6.1	467	274	0.61	0.088	3.501 ± 0.068	0.10367 ± 0.00047	3.505 ± 0.068	0.10290 ± 0.00054	1618 ± 28	1677 ± 10	3.5
3	13	11.2	212	147	0.71	0.197	3.519 ± 0.070	0.10425 ± 0.00070	3.526 ± 0.070	0.10255 ± 0.00088	1609 ± 28	1671 ± 16	3.7

Table A8. (continued)

Grp no.	*Spot no.*	*Grain .spot*	^{238}U *(ppm)*	^{232}Th *(ppm)*	$^{232}Th/^{238}U$	*f204 (%)*	$^{238}U/^{206}Pb$ ±1σ	$^{207}Pb/^{206}Pb$ ±1σ	$^{238}U/^{206}Pb^*$ ±1σ	$^{207}Pb^*/^{206}Pb^*$ ±1σ	$^{238}U/^{206}Pb^*$ *date (Ma)* ±1σ	$^{207}Pb^*/^{206}Pb^*$ *date (Ma)* ±1σ	*Disc (%)*
3	3	3.1	74	58	0.81	0.448	3.458 ± 0.076	0.10610 ± 0.00158	3.473 ± 0.076	0.10222 ± 0.00194	1631 ± 32	1665 ± 35	2.0
3	15	13.1	216	138	0.66	0.005	3.460 ± 0.069	0.10223 ± 0.00069	3.460 ± 0.069	0.10219 ± 0.00075	1637 ± 29	1664 ± 13	1.7
3	40	35.1	68	52	0.79	0.042	3.735 ± 0.083	0.10253 ± 0.00125	3.737 ± 0.083	0.10217 ± 0.00171	1529 ± 30	1664 ± 31	8.1
3	24	20.1	111	77	0.72	0.189	3.414 ± 0.073	0.10291 ± 0.00118	3.421 ± 0.073	0.10127 ± 0.00149	1653 ± 31	1647 ± 27	–0.3
3	7	7.1	109	66	0.63	0.149	3.486 ± 0.073	0.10226 ± 0.00096	3.491 ± 0.073	0.10097 ± 0.00125	1624 ± 30	1642 ± 23	1.1
3	11	10.1	172	108	0.65	0.778	3.579 ± 0.072	0.10736 ± 0.00081	3.607 ± 0.073	0.10063 ± 0.00164	1578 ± 28	1636 ± 30	3.6
3	26	22.1	121	47	0.40	0.410	3.555 ± 0.074	0.10409 ± 0.00095	3.570 ± 0.074	0.10054 ± 0.00170	1592 ± 29	1634 ± 31	2.6
3	45	38.1	277	235	0.88	0.059	3.585 ± 0.071	0.10083 ± 0.00078	3.587 ± 0.071	0.10032 ± 0.00085	1585 ± 28	1630 ± 16	2.7
3	18	15.2	131	87	0.69	0.273	3.637 ± 0.075	0.10240 ± 0.00088	3.647 ± 0.075	0.10004 ± 0.00130	1562 ± 29	1625 ± 24	3.9
4	10	9.2	261	354	1.40	0.016	3.852 ± 0.076	0.09823 ± 0.00064	3.852 ± 0.076	0.09809 ± 0.00066	1488 ± 26	1588 ± 13	6.3
4	20	16.2	172	94	0.57	0.113	3.837 ± 0.078	0.09883 ± 0.00077	3.842 ± 0.078	0.09786 ± 0.00113	1491 ± 27	1584 ± 22	5.8
4	47	39.1	72	70	1.01	0.266	4.031 ± 0.089	0.09565 ± 0.00159	4.042 ± 0.089	0.09336 ± 0.00243	1425 ± 28	1495 ± 49	4.7
D	42	36.1	168	65	0.40	0.044	4.813 ± 0.098	0.08345 ± 0.00084	4.815 ± 0.098	0.08307 ± 0.00107	1217 ± 23	1271 ± 25	4.3
D	51	41.1	257	189	0.76	0.363	4.981 ± 0.107	0.10449 ± 0.00081	4.999 ± 0.108	0.10135 ± 0.00122	1175 ± 23	1649 ± 22	28.7

Table A9. Ion microprobe analytical results for zircons from sample 184119: monzogranitic gneiss, Point Henry

Grp no.	Spot no.	Grain .spot	^{238}U (ppm)	^{232}Th (ppm)	$^{232}Th/^{238}U$	f204 (%)	$^{238}U/^{206}Pb$ ±1σ	$^{207}Pb/^{206}Pb$ ±1σ	$^{238}U/^{206}Pb^*$ ±1σ	$^{207}Pb^*/^{206}Pb^*$ ±1σ	$^{238}U/^{206}Pb^*$ date (Ma) ±1σ	$^{207}Pb^*/^{206}Pb^*$ date (Ma) ±1σ	Disc (%)
1	30	30.1	115	98	0.88	0.110	3.328 ± 0.099	0.10429 ± 0.00069	3.331 ± 0.099	0.10334 ± 0.00084	1692 ± 44	1685 ± 15	–0.4
1	24	24.1	302	–	–	0.013	3.246 ± 0.090	0.10343 ± 0.00040	3.246 ± 0.090	0.10332 ± 0.00040	1731 ± 42	1685 ± 7	–2.8
1	4	4.1	306	160	0.54	0.014	3.342 ± 0.100	0.10330 ± 0.00039	3.342 ± 0.100	0.10318 ± 0.00040	1687 ± 44	1682 ± 7	–0.3
1	28	28.1	279	92	0.34	0.124	3.369 ± 0.094	0.10378 ± 0.00073	3.373 ± 0.094	0.10271 ± 0.00079	1674 ± 41	1674 ± 14	0.0
1	5	5.1	313	227	0.75	0.018	3.440 ± 0.105	0.10204 ± 0.00053	3.441 ± 0.105	0.10188 ± 0.00054	1645 ± 44	1659 ± 10	0.8
1	12	12.1	351	177	0.52	0.057	3.491 ± 0.105	0.10235 ± 0.00043	3.493 ± 0.105	0.10186 ± 0.00046	1623 ± 43	1658 ± 8	2.1
1	18	18.1	298	209	0.72	0.284	3.504 ± 0.106	0.10422 ± 0.00045	3.514 ± 0.107	0.10176 ± 0.00063	1614 ± 43	1656 ± 12	2.5
1	13	13.1	385	190	0.51	0.000	3.449 ± 0.103	0.10153 ± 0.00048	3.449 ± 0.103	0.10153 ± 0.00048	1641 ± 43	1652 ± 9	0.7
2	2	2.1	1057	7	0.01	0.022	4.832 ± 0.145	0.07999 ± 0.00021	4.833 ± 0.145	0.07980 ± 0.00024	1212 ± 33	1192 ± 6	–1.7
2	29	29.1	715	98	0.14	0.035	4.940 ± 0.137	0.07985 ± 0.00029	4.941 ± 0.137	0.07955 ± 0.00032	1188 ± 30	1186 ± 8	–0.2
2	14	14.1	2016	9	0.00	0.045	4.333 ± 0.129	0.07977 ± 0.00021	4.335 ± 0.129	0.07939 ± 0.00022	1338 ± 36	1182 ± 5	–13.2
2	3	3.1	2342	378	0.17	0.003	4.935 ± 0.147	0.07935 ± 0.00021	4.936 ± 0.147	0.07933 ± 0.00021	1189 ± 32	1180 ± 5	–0.8
2	6	6.1	4563	25	0.01	0.003	4.937 ± 0.147	0.07933 ± 0.00013	4.937 ± 0.147	0.07931 ± 0.00014	1189 ± 32	1180 ± 3	–0.8
2	7	7.1	3963	14	0.00	0.005	4.814 ± 0.143	0.07933 ± 0.00011	4.814 ± 0.143	0.07929 ± 0.00011	1217 ± 33	1179 ± 3	–3.2
2	19	19.1	3017	22	0.01	0.017	4.687 ± 0.129	0.07938 ± 0.00014	4.687 ± 0.129	0.07924 ± 0.00014	1247 ± 31	1178 ± 4	–5.8
2	20	20.1	3334	42	0.01	0.022	4.563 ± 0.126	0.07941 ± 0.00013	4.564 ± 0.126	0.07922 ± 0.00013	1277 ± 32	1178 ± 3	–8.4
2	1	1.1	1973	419	0.22	0.010	4.933 ± 0.147	0.07929 ± 0.00016	4.933 ± 0.147	0.07921 ± 0.00017	1190 ± 32	1177 ± 4	–1.1
2	10	10.1	2714	37	0.01	–0.004	4.973 ± 0.149	0.07915 ± 0.00016	4.973 ± 0.149	0.07919 ± 0.00017	1181 ± 32	1177 ± 4	–0.4
2	22	22.1	1036	342	0.34	0.017	4.971 ± 0.138	0.07916 ± 0.00023	4.972 ± 0.138	0.07902 ± 0.00024	1181 ± 30	1173 ± 6	–0.7
2	26	26.1	4530	100	0.02	0.015	4.330 ± 0.120	0.07914 ± 0.00011	4.330 ± 0.120	0.07901 ± 0.00011	1339 ± 33	1172 ± 3	–14.3
2	15	15.1	962	243	0.26	0.015	5.100 ± 0.152	0.07909 ± 0.00022	5.100 ± 0.152	0.07897 ± 0.00024	1154 ± 32	1171 ± 6	1.5
2	8	8.1	2027	377	0.19	0.002	5.076 ± 0.152	0.07897 ± 0.00019	5.076 ± 0.152	0.07896 ± 0.00019	1159 ± 32	1171 ± 5	1.0
3	34	34.1	494	100	0.21	0.115	3.475 ± 0.097	0.10172 ± 0.00035	3.479 ± 0.097	0.10072 ± 0.00041	1629 ± 40	1637 ± 8	0.5
3	31	31.1	226	100	0.46	0.103	3.490 ± 0.098	0.10150 ± 0.00052	3.494 ± 0.098	0.10061 ± 0.00061	1623 ± 40	1635 ± 11	0.8
3	33	33.1	195	103	0.55	0.248	3.496 ± 0.098	0.10256 ± 0.00055	3.505 ± 0.098	0.10042 ± 0.00098	1618 ± 40	1632 ± 18	0.8
3	27	27.1	226	97	0.44	0.112	3.488 ± 0.098	0.10136 ± 0.00050	3.492 ± 0.098	0.10039 ± 0.00059	1623 ± 40	1631 ± 11	0.5
3	16	16.1	197	139	0.73	0.064	3.780 ± 0.113	0.09975 ± 0.00055	3.782 ± 0.114	0.09920 ± 0.00060	1512 ± 40	1609 ± 11	6.0
3	11	11.1	224	152	0.70	0.142	3.746 ± 0.112	0.09895 ± 0.00043	3.751 ± 0.113	0.09772 ± 0.00055	1524 ± 41	1581 ± 10	3.6
4	21	21.1	11	0	0.02	0.481	4.613 ± 0.197	0.08953 ± 0.00237	4.636 ± 0.198	0.08543 ± 0.00410	1259 ± 49	1325 ± 93	5.0
4	25	25.1	31	0	0.00	–0.112	4.873 ± 0.148	0.08400 ± 0.00140	4.868 ± 0.148	0.08495 ± 0.00140	1204 ± 33	1314 ± 32	8.4
4	9	9.1	134	0	0.00	–0.044	4.876 ± 0.147	0.08110 ± 0.00061	4.874 ± 0.147	0.08147 ± 0.00061	1203 ± 33	1233 ± 15	2.4
5	17	17.1	2214	410	0.19	–0.006	5.217 ± 0.155	0.07866 ± 0.00014	5.217 ± 0.155	0.07870 ± 0.00015	1130 ± 31	1165 ± 4	2.9
5	32	32.1	1713	103	0.06	0.034	4.961 ± 0.137	0.07896 ± 0.00019	4.963 ± 0.137	0.07867 ± 0.00021	1183 ± 30	1164 ± 5	–1.7
D	23	23.1	12	0	0.00	2.113	4.574 ± 0.157	0.09316 ± 0.00240	4.672 ± 0.161	0.07541 ± 0.00292	1250 ± 39	1080 ± 78	–15.8

Table A10. Ion microprobe analytical results for zircons from sample 184307: pegmatitic granodiorite, Point Henry

Grp no.	Spot no.	Grain .spot	^{238}U (ppm)	^{232}Th (ppm)	$^{232}Th/^{238}U$	f204 (%)	$^{238}U/^{206}Pb$ ±1σ	$^{207}Pb/^{206}Pb$ ±1σ	$^{238}U/^{206}Pb^*$ ±1σ	$^{207}Pb^*/^{206}Pb^*$ ±1σ	$^{238}U/^{206}Pb^*$ date (Ma) ±1σ	$^{207}Pb^*/^{206}Pb^*$ date (Ma) ±1σ	Disc (%)
1	27	14.1	543	5	0.01	0.020	4.771 ± 0.117	0.08022 ± 0.00029	4.772 ± 0.117	0.08005 ± 0.00032	1227 ± 27	1198 ± 8	–2.4
1	17	15.1	863	5	0.01	0.020	4.881 ± 0.118	0.08021 ± 0.00024	4.882 ± 0.118	0.08004 ± 0.00026	1201 ± 27	1198 ± 6	–0.3
1	28	23.1	536	24	0.05	0.028	4.884 ± 0.119	0.08025 ± 0.00030	4.886 ± 0.119	0.08001 ± 0.00038	1200 ± 27	1197 ± 9	–0.3
1	33	29.1	675	22	0.03	0.023	5.042 ± 0.202	0.07996 ± 0.00033	5.043 ± 0.202	0.07977 ± 0.00034	1166 ± 43	1191 ± 8	2.1
1	2	2.1	974	6	0.01	0.008	4.910 ± 0.033	0.07984 ± 0.00026	4.910 ± 0.033	0.07977 ± 0.00027	1195 ± 7	1191 ± 7	–0.3
1	31	27.1	661	4	0.01	0.027	4.951 ± 0.120	0.07995 ± 0.00027	4.953 ± 0.120	0.07972 ± 0.00029	1186 ± 26	1190 ± 7	0.4
1	18	16.1	1948	164	0.09	–0.001	5.131 ± 0.124	0.07962 ± 0.00017	5.131 ± 0.124	0.07963 ± 0.00017	1148 ± 25	1188 ± 4	3.4
1	30	26.1	716	8	0.01	–0.006	4.958 ± 0.120	0.07955 ± 0.00027	4.958 ± 0.120	0.07960 ± 0.00027	1184 ± 26	1187 ± 7	0.2
1	8	6.1	2060	342	0.17	0.000	4.858 ± 0.117	0.07944 ± 0.00015	4.858 ± 0.117	0.07944 ± 0.00015	1207 ± 27	1183 ± 4	–2.0
1	29	25.1	1712	95	0.06	0.019	4.865 ± 0.119	0.07934 ± 0.00017	4.866 ± 0.119	0.07918 ± 0.00019	1205 ± 27	1177 ± 5	–2.4
2	20	18.1	95	187	2.04	–0.144	4.892 ± 0.122	0.08014 ± 0.00071	4.885 ± 0.122	0.08136 ± 0.00109	1201 ± 27	1230 ± 26	2.4
2	1	1.1	188	424	2.33	0.038	5.012 ± 0.038	0.08097 ± 0.00061	5.014 ± 0.038	0.08065 ± 0.00065	1172 ± 8	1213 ± 16	3.4
2	10	8.1	142	299	2.18	0.049	4.949 ± 0.125	0.08066 ± 0.00058	4.951 ± 0.125	0.08024 ± 0.00067	1186 ± 27	1203 ± 16	1.4
2	7	5.1	99	236	2.47	0.045	4.885 ± 0.121	0.07987 ± 0.00068	4.888 ± 0.121	0.07949 ± 0.00078	1200 ± 27	1184 ± 19	–1.3
2	22	20.1	174	393	2.33	0.090	4.973 ± 0.122	0.08003 ± 0.00051	4.977 ± 0.122	0.07927 ± 0.00067	1180 ± 26	1179 ± 17	–0.1
2	4	3.1	195	400	2.12	0.063	4.914 ± 0.040	0.07958 ± 0.00060	4.917 ± 0.040	0.07905 ± 0.00078	1194 ± 9	1173 ± 19	–1.7
2	11	9.1	101	231	2.35	0.236	4.693 ± 0.116	0.08066 ± 0.00068	4.704 ± 0.117	0.07866 ± 0.00124	1243 ± 28	1164 ± 31	–6.8
2	15	13.1	132	353	2.77	0.090	4.618 ± 0.114	0.07910 ± 0.00059	4.622 ± 0.114	0.07834 ± 0.00080	1263 ± 28	1155 ± 20	–9.3
2	12	10.1	121	294	2.51	0.211	4.727 ± 0.122	0.08001 ± 0.00061	4.737 ± 0.123	0.07824 ± 0.00102	1235 ± 29	1153 ± 26	–7.1
2	19	17.1	103	219	2.18	0.101	4.790 ± 0.119	0.07892 ± 0.00066	4.795 ± 0.120	0.07807 ± 0.00082	1221 ± 28	1149 ± 21	–6.3
2	6	4.1	203	439	2.23	0.107	4.745 ± 0.035	0.07890 ± 0.00055	4.750 ± 0.035	0.07800 ± 0.00071	1232 ± 8	1147 ± 18	–7.4
2	26	24.1	125	320	2.65	0.215	4.971 ± 0.123	0.07978 ± 0.00060	4.982 ± 0.123	0.07797 ± 0.00104	1179 ± 27	1146 ± 26	–2.9
2	25	22.2	71	112	1.63	0.147	4.734 ± 0.119	0.07899 ± 0.00100	4.741 ± 0.119	0.07775 ± 0.00134	1234 ± 28	1141 ± 34	–8.2
2	14	12.1	149	325	2.25	0.509	4.613 ± 0.114	0.08168 ± 0.00097	4.637 ± 0.114	0.07738 ± 0.00150	1259 ± 28	1131 ± 39	–11.3
2	21	19.1	88	208	2.45	0.250	5.002 ± 0.124	0.07919 ± 0.00071	5.014 ± 0.125	0.07708 ± 0.00103	1172 ± 27	1123 ± 27	–4.4
2	23	21.1	119	199	1.73	0.197	5.004 ± 0.124	0.07863 ± 0.00061	5.014 ± 0.124	0.07698 ± 0.00127	1172 ± 27	1121 ± 33	–4.6
3	5	3.2	553	424	0.79	0.123	3.627 ± 0.022	0.09808 ± 0.00053	3.631 ± 0.022	0.09702 ± 0.00057	1568 ± 9	1568 ± 11	0.0
3	3	2.2	247	134	0.56	0.111	4.024 ± 0.032	0.09573 ± 0.00049	4.029 ± 0.032	0.09477 ± 0.00060	1429 ± 10	1524 ± 12	6.2
4	24	22.1	3428	255	0.08	0.005	4.824 ± 0.117	0.07862 ± 0.00011	4.824 ± 0.117	0.07858 ± 0.00012	1214 ± 27	1162 ± 3	–4.5
4	32	28.1	1853	350	0.20	0.051	4.979 ± 0.121	0.07887 ± 0.00023	4.982 ± 0.121	0.07843 ± 0.00024	1179 ± 26	1158 ± 6	–1.9
4	9	7.1	3433	613	0.18	0.502	5.362 ± 0.130	0.07772 ± 0.00012	5.389 ± 0.131	0.07352 ± 0.00033	1097 ± 24	1028 ± 9	–6.7
D	13	11.1	1	0	0.38	3.365	4.836 ± 0.503	0.11178 ± 0.00885	5.005 ± 0.562	0.08320 ± 0.03730	1174 ± 121	1274 ± 874	7.8
D	16	13.2	6	3	0.53	3.798	4.903 ± 0.226	0.09100 ± 0.00411	5.097 ± 0.254	0.05994 ± 0.01639	1155 ± 53	601 ± 592	–92.1

Table A11. Ion microprobe analytical results for zircons from sample 184123: garnet-bearing monzogranitic gneiss, Plum Pudding Rocks

Grp no.	Spot no.	Grain .spot	^{238}U (ppm)	^{232}Th (ppm)	$^{232}Th/^{238}U$	f204 (%)	$^{238}U/^{206}Pb$ ±1σ	$^{207}Pb/^{206}Pb$ ±1σ	$^{238}U/^{206}Pb^*$ ±1σ	$^{207}Pb^*/^{206}Pb^*$ ±1σ	$^{238}U/^{206}Pb^*$ date (Ma) ±1σ	$^{207}Pb^*/^{206}Pb^*$ date (Ma) ±1σ	Disc (%)
1	2	2.1	123	56	0.47	0.141	3.355 ± 0.096	0.10638 ± 0.00443	3.360 ± 0.096	0.10516 ± 0.00453	1679 ± 42	1717 ± 79	2.2
1	23	23.1	178	63	0.37	0.118	3.354 ± 0.044	0.10604 ± 0.00115	3.358 ± 0.044	0.10501 ± 0.00126	1680 ± 19	1715 ± 22	2.0
1	19	19.1	250	162	0.67	0.016	3.487 ± 0.045	0.10490 ± 0.00066	3.487 ± 0.045	0.10477 ± 0.00071	1625 ± 18	1710 ± 13	5.0
1	18	18.1	178	94	0.55	–0.006	3.436 ± 0.046	0.10456 ± 0.00089	3.436 ± 0.046	0.10461 ± 0.00089	1647 ± 20	1707 ± 16	3.6
1	37	37.1	350	64	0.19	0.019	3.426 ± 0.052	0.10445 ± 0.00074	3.427 ± 0.052	0.10429 ± 0.00076	1651 ± 22	1702 ± 13	3.0
1	33	33.1	138	53	0.40	–0.194	3.345 ± 0.045	0.10245 ± 0.00239	3.338 ± 0.045	0.10413 ± 0.00249	1689 ± 20	1699 ± 44	0.6
1	39	39.1	130	66	0.52	–0.034	3.443 ± 0.047	0.10374 ± 0.00093	3.442 ± 0.047	0.10404 ± 0.00094	1644 ± 20	1697 ± 17	3.1
1	29	29.1	246	55	0.23	0.124	3.304 ± 0.042	0.10422 ± 0.00071	3.308 ± 0.042	0.10314 ± 0.00074	1703 ± 19	1681 ± 13	–1.3
1	42	42.1	129	47	0.38	0.043	3.339 ± 0.046	0.10308 ± 0.00093	3.341 ± 0.046	0.10271 ± 0.00104	1688 ± 21	1674 ± 19	–0.9
1	36	36.1	329	162	0.51	0.037	3.417 ± 0.043	0.10291 ± 0.00110	3.419 ± 0.043	0.10259 ± 0.00112	1654 ± 18	1671 ± 20	1.0
1	17	17.1	177	106	0.62	0.059	3.388 ± 0.076	0.10296 ± 0.00122	3.390 ± 0.076	0.10245 ± 0.00126	1666 ± 33	1669 ± 23	0.2
1	35	35.1	171	80	0.48	0.246	3.487 ± 0.054	0.10427 ± 0.00159	3.495 ± 0.054	0.10214 ± 0.00173	1622 ± 22	1663 ± 31	2.5
1	34	34.1	98	42	0.44	0.234	3.323 ± 0.066	0.10408 ± 0.00105	3.330 ± 0.066	0.10205 ± 0.00145	1693 ± 30	1662 ± 26	–1.9
1	40	40.1	222	92	0.43	0.023	3.372 ± 0.046	0.10185 ± 0.00193	3.372 ± 0.046	0.10165 ± 0.00194	1674 ± 20	1654 ± 35	–1.2
1	22	22.1	141	55	0.40	0.164	3.340 ± 0.045	0.10259 ± 0.00267	3.346 ± 0.045	0.10117 ± 0.00278	1686 ± 20	1646 ± 51	–2.4
1	10	10.1	166	62	0.39	0.048	3.637 ± 0.048	0.10158 ± 0.00081	3.639 ± 0.048	0.10116 ± 0.00098	1565 ± 18	1645 ± 18	4.9
2	25	25.1	2462	33	0.01	0.013	4.743 ± 0.056	0.08180 ± 0.00036	4.744 ± 0.056	0.08169 ± 0.00036	1233 ± 13	1238 ± 9	0.4
2	16	16.1	2170	7	0.00	0.023	4.790 ± 0.058	0.08174 ± 0.00024	4.792 ± 0.058	0.08154 ± 0.00027	1222 ± 14	1234 ± 7	1.0
2	26	26.1	1098	62	0.06	0.030	4.764 ± 0.056	0.08156 ± 0.00032	4.766 ± 0.056	0.08131 ± 0.00035	1228 ± 13	1229 ± 9	0.1
2	32	32.1	972	7	0.01	0.052	4.809 ± 0.056	0.08175 ± 0.00034	4.812 ± 0.056	0.08131 ± 0.00038	1217 ± 13	1229 ± 9	0.9
2	20	20.1	390	4	0.01	0.221	4.835 ± 0.059	0.08310 ± 0.00052	4.846 ± 0.059	0.08123 ± 0.00080	1209 ± 13	1227 ± 19	1.4
2	15	15.1	1504	11	0.01	0.008	4.737 ± 0.056	0.08093 ± 0.00032	4.737 ± 0.056	0.08086 ± 0.00032	1235 ± 13	1218 ± 8	–1.4
2	9	9.1	1184	21	0.02	0.027	4.741 ± 0.055	0.08094 ± 0.00030	4.742 ± 0.055	0.08070 ± 0.00033	1233 ± 13	1214 ± 8	–1.6
2	14	14.1	1403	18	0.01	0.202	4.785 ± 0.060	0.08227 ± 0.00057	4.794 ± 0.060	0.08056 ± 0.00083	1221 ± 14	1211 ± 20	–0.9
2	44	44.1	658	5	0.01	0.083	4.828 ± 0.067	0.08122 ± 0.00042	4.832 ± 0.067	0.08052 ± 0.00048	1213 ± 15	1210 ± 12	–0.2
2	27	27.1	521	10	0.02	0.039	4.836 ± 0.060	0.08061 ± 0.00046	4.838 ± 0.060	0.08028 ± 0.00048	1211 ± 14	1204 ± 12	–0.6
3	7	7.1	226	148	0.68	0.124	3.499 ± 0.045	0.10142 ± 0.00077	3.503 ± 0.045	0.10034 ± 0.00115	1619 ± 18	1630 ± 21	0.7
3	38	38.1	84	38	0.46	0.239	3.625 ± 0.126	0.10234 ± 0.00117	3.634 ± 0.127	0.10027 ± 0.00164	1567 ± 48	1629 ± 30	3.8
3	1	1.1	120	75	0.65	–0.061	3.655 ± 0.110	0.09958 ± 0.00133	3.653 ± 0.110	0.10010 ± 0.00135	1560 ± 42	1626 ± 25	4.1
3	24	24.1	117	33	0.29	–0.007	3.606 ± 0.081	0.09959 ± 0.00141	3.606 ± 0.081	0.09966 ± 0.00141	1578 ± 31	1618 ± 26	2.5
3	13	13.1	175	65	0.38	0.121	3.453 ± 0.055	0.10045 ± 0.00158	3.457 ± 0.055	0.09940 ± 0.00167	1638 ± 23	1613 ± 31	–1.6
3	31	31.1	418	147	0.36	0.029	3.489 ± 0.058	0.09924 ± 0.00096	3.490 ± 0.058	0.09899 ± 0.00099	1624 ± 24	1605 ± 19	–1.2
3	5	5.1	118	61	0.53	0.068	3.468 ± 0.055	0.09925 ± 0.00093	3.470 ± 0.055	0.09866 ± 0.00119	1632 ± 23	1599 ± 23	–2.1
3	12	12.1	162	88	0.56	–0.017	3.650 ± 0.058	0.09791 ± 0.00079	3.650 ± 0.058	0.09806 ± 0.00079	1561 ± 22	1588 ± 15	1.7
4	21	21.1	1851	9	0.00	–0.005	4.652 ± 0.054	0.08239 ± 0.00024	4.652 ± 0.054	0.08244 ± 0.00024	1255 ± 13	1256 ± 6	0.1
4	41	41.1	1601	7	0.00	0.032	4.694 ± 0.057	0.08265 ± 0.00054	4.695 ± 0.057	0.08238 ± 0.00054	1245 ± 14	1255 ± 13	0.8
4	11	11.1	996	4	0.00	0.047	4.652 ± 0.054	0.08234 ± 0.00033	4.654 ± 0.054	0.08195 ± 0.00041	1255 ± 13	1244 ± 10	–0.8
4	28	28.1	2088	20	0.01	0.002	4.759 ± 0.057	0.08194 ± 0.00023	4.759 ± 0.057	0.08192 ± 0.00023	1229 ± 13	1244 ± 6	1.1
5	8	8.1	97	1	0.01	0.159	4.591 ± 0.074	0.08594 ± 0.00108	4.598 ± 0.074	0.08458 ± 0.00130	1269 ± 18	1306 ± 30	2.9
D	43	43.1	67	31	0.48	0.448	3.736 ± 0.143	0.09463 ± 0.00147	3.753 ± 0.144	0.09079 ± 0.00260	1523 ± 52	1442 ± 55	–5.6
D	30	30.1	132	107	0.84	0.048	3.042 ± 0.044	0.10737 ± 0.00113	3.044 ± 0.044	0.10695 ± 0.00120	1831 ± 23	1748 ± 20	–4.8
D	4	4.1	753	31	0.04	–0.043	4.850 ± 0.057	0.08213 ± 0.00039	4.848 ± 0.057	0.08250 ± 0.00042	1209 ± 13	1257 ± 10	3.9
D	6	6.1	2646	14	0.01	0.083	11.292 ± 0.131	0.06092 ± 0.00027	11.301 ± 0.131	0.06024 ± 0.00029	547 ± 6	612 ± 10	10.7
D	3	3.1	1658	11	0.01	0.186	5.921 ± 0.069	0.07968 ± 0.00028	5.932 ± 0.069	0.07812 ± 0.00043	1004 ± 11	1150 ± 11	12.7

Table A12. Ion microprobe analytical results for zircons from sample 184122: metamorphosed quartz sandstone, Plum Pudding Rocks

Grp no.	Spot no.	Grain .spot	^{238}U (ppm)	^{232}Th (ppm)	$^{232}Th/^{238}U$	f204 (%)	$^{238}U/^{206}Pb$ ±1σ	$^{207}Pb/^{206}Pb$ ±1σ	$^{238}U/^{206}Pb^*$ ±1σ	$^{207}Pb^*/^{206}Pb^*$ ±1σ	$^{238}U/^{206}Pb^*$ date (Ma) ±1σ	$^{207}Pb^*/^{206}Pb^*$ date (Ma) ±1σ	Disc (%)
1	4	4.1	800	24	0.03	0.002	4.807 ± 0.078	0.08176 ± 0.00023	4.807 ± 0.078	0.08174 ± 0.00024	1218 ± 18	1239 ± 6	1.7
1	6	6.1	511	22	0.04	0.020	4.797 ± 0.077	0.08190 ± 0.00029	4.798 ± 0.077	0.08173 ± 0.00032	1221 ± 18	1239 ± 8	1.5
1	16	16.1	443	19	0.04	0.002	4.912 ± 0.080	0.08135 ± 0.00035	4.912 ± 0.080	0.08133 ± 0.00037	1195 ± 18	1230 ± 9	2.8
1	20	20.1	608	27	0.05	0.020	4.872 ± 0.077	0.08138 ± 0.00031	4.873 ± 0.077	0.08122 ± 0.00033	1203 ± 17	1227 ± 8	1.9
1	18	18.1	611	29	0.05	–0.003	4.830 ± 0.077	0.08112 ± 0.00026	4.830 ± 0.077	0.08115 ± 0.00026	1213 ± 18	1225 ± 6	1.0
1	41	28.1	737	30	0.04	0.010	4.821 ± 0.077	0.08122 ± 0.00025	4.822 ± 0.077	0.08114 ± 0.00027	1215 ± 18	1225 ± 6	0.8
1	12	12.1	468	25	0.06	0.021	4.847 ± 0.077	0.08114 ± 0.00029	4.848 ± 0.077	0.08096 ± 0.00032	1209 ± 18	1221 ± 8	0.9
1	2	2.1	566	22	0.04	0.023	4.809 ± 0.077	0.08105 ± 0.00029	4.810 ± 0.077	0.08085 ± 0.00031	1218 ± 18	1218 ± 7	0.0
1	40	27.1	546	25	0.05	0.028	4.841 ± 0.084	0.08102 ± 0.00042	4.843 ± 0.084	0.08078 ± 0.00043	1210 ± 19	1216 ± 11	0.5
1	19	19.1	557	31	0.06	0.015	4.894 ± 0.078	0.08075 ± 0.00027	4.895 ± 0.078	0.08062 ± 0.00029	1198 ± 18	1212 ± 7	1.1
1	5	5.1	502	21	0.04	0.028	4.915 ± 0.078	0.08080 ± 0.00033	4.916 ± 0.078	0.08057 ± 0.00036	1194 ± 17	1211 ± 9	1.4
2	31	14.2	62	62	1.03	0.201	3.038 ± 0.077	0.10924 ± 0.00214	3.044 ± 0.077	0.10749 ± 0.00230	1831 ± 41	1757 ± 39	–4.2
3	35	19.2	100	113	1.17	0.107	2.635 ± 0.045	0.12532 ± 0.00075	2.638 ± 0.045	0.12437 ± 0.00084	2072 ± 30	2020 ± 12	–2.6
3	50	37.1	424	302	0.74	0.045	2.743 ± 0.045	0.12536 ± 0.00048	2.744 ± 0.045	0.12497 ± 0.00050	2003 ± 28	2028 ± 7	1.3
3	55	42.1	404	120	0.31	0.044	2.468 ± 0.060	0.12596 ± 0.00051	2.469 ± 0.060	0.12557 ± 0.00054	2192 ± 45	2037 ± 8	–7.6
3	26	5.2	370	109	0.30	0.021	2.436 ± 0.039	0.12917 ± 0.00144	2.436 ± 0.039	0.12898 ± 0.00145	2217 ± 30	2084 ± 20	–6.4
3	62	49.1	76	120	1.63	0.034	2.613 ± 0.046	0.13108 ± 0.00111	2.614 ± 0.046	0.13079 ± 0.00118	2088 ± 31	2109 ± 16	1.0
3	73	60.1	235	160	0.70	0.017	2.437 ± 0.040	0.13528 ± 0.00140	2.437 ± 0.040	0.13513 ± 0.00141	2216 ± 31	2166 ± 18	–2.3
3	52	39.1	177	55	0.32	0.111	2.419 ± 0.040	0.14370 ± 0.00122	2.422 ± 0.041	0.14271 ± 0.00128	2228 ± 32	2260 ± 15	1.4
3	57	44.1	95	113	1.23	0.021	2.234 ± 0.038	0.14428 ± 0.00320	2.235 ± 0.038	0.14410 ± 0.00320	2384 ± 34	2277 ± 38	–4.7
3	37	22.2	267	67	0.26	0.105	2.445 ± 0.040	0.14647 ± 0.00303	2.447 ± 0.040	0.14554 ± 0.00305	2209 ± 31	2294 ± 36	3.7
3	34	18.2	59	33	0.59	0.094	2.147 ± 0.049	0.14926 ± 0.00156	2.149 ± 0.049	0.14842 ± 0.00166	2463 ± 47	2328 ± 19	–5.8
3	66	53.1	261	39	0.15	0.030	2.192 ± 0.056	0.15104 ± 0.00176	2.192 ± 0.056	0.15077 ± 0.00177	2423 ± 52	2355 ± 20	–2.9
3	47	34.1	379	40	0.11	0.009	2.251 ± 0.036	0.15167 ± 0.00132	2.251 ± 0.036	0.15159 ± 0.00132	2369 ± 32	2364 ± 15	–0.2
3	61	48.1	172	64	0.39	0.150	2.327 ± 0.040	0.15547 ± 0.00558	2.331 ± 0.040	0.15414 ± 0.00560	2301 ± 33	2392 ± 62	3.8
3	68	55.1	234	37	0.17	0.011	2.060 ± 0.034	0.15572 ± 0.00136	2.060 ± 0.034	0.15562 ± 0.00136	2551 ± 35	2409 ± 15	–5.9
3	23	2.2	149	56	0.39	0.167	2.243 ± 0.037	0.16281 ± 0.00173	2.247 ± 0.037	0.16132 ± 0.00178	2373 ± 33	2470 ± 19	3.9
3	36	20.2	334	57	0.18	0.008	2.341 ± 0.046	0.16512 ± 0.00832	2.341 ± 0.046	0.16504 ± 0.00832	2293 ± 38	2508 ± 85	8.6
3	65	52.1	100	43	0.44	–0.024	2.141 ± 0.054	0.16713 ± 0.00107	2.140 ± 0.054	0.16734 ± 0.00107	2471 ± 52	2531 ± 11	2.4
3	46	33.1	75	63	0.87	–0.026	2.009 ± 0.036	0.17035 ± 0.00335	2.009 ± 0.036	0.17058 ± 0.00335	2604 ± 38	2563 ± 33	–1.6
3	54	41.1	316	166	0.54	0.001	1.994 ± 0.032	0.17615 ± 0.00086	1.994 ± 0.032	0.17614 ± 0.00086	2620 ± 35	2617 ± 8	–0.1
3	27	6.2	367	70	0.20	0.022	2.111 ± 0.034	0.17700 ± 0.00119	2.111 ± 0.034	0.17680 ± 0.00119	2500 ± 33	2623 ± 11	4.7
3	44	31.1	116	119	1.06	0.048	1.973 ± 0.034	0.17772 ± 0.00156	1.974 ± 0.034	0.17729 ± 0.00159	2642 ± 37	2628 ± 15	–0.5
3	70	57.1	288	96	0.34	0.042	1.884 ± 0.031	0.17776 ± 0.00206	1.885 ± 0.031	0.17739 ± 0.00206	2744 ± 37	2629 ± 19	–4.4
3	49	36.1	424	270	0.66	0.001	1.984 ± 0.039	0.17753 ± 0.00115	1.984 ± 0.039	0.17752 ± 0.00115	2631 ± 42	2630 ± 11	0.0
3	28	8.2	420	226	0.56	0.002	1.918 ± 0.032	0.17847 ± 0.00173	1.918 ± 0.032	0.17845 ± 0.00173	2705 ± 36	2639 ± 16	–2.5
3	67	54.1	320	152	0.49	0.001	2.053 ± 0.039	0.17957 ± 0.00081	2.053 ± 0.039	0.17956 ± 0.00081	2558 ± 40	2649 ± 7	3.4
3	63	50.1	162	70	0.45	–0.021	2.001 ± 0.033	0.18010 ± 0.00083	2.000 ± 0.033	0.18029 ± 0.00083	2613 ± 36	2656 ± 8	1.6
3	53	40.1	166	71	0.44	0.041	1.901 ± 0.032	0.18190 ± 0.00188	1.901 ± 0.032	0.18153 ± 0.00189	2724 ± 37	2667 ± 17	–2.2
3	56	43.1	169	154	0.94	–0.015	1.973 ± 0.066	0.18282 ± 0.00537	1.973 ± 0.066	0.18295 ± 0.00537	2643 ± 73	2680 ± 49	1.4
3	58	45.1	117	124	1.09	–0.026	1.977 ± 0.034	0.18677 ± 0.00102	1.976 ± 0.034	0.18700 ± 0.00108	2639 ± 37	2716 ± 10	2.8
3	30	11.2	72	51	0.74	0.063	1.877 ± 0.086	0.18788 ± 0.00339	1.878 ± 0.086	0.18732 ± 0.00341	2752 ± 103	2719 ± 30	–1.2

Table A12. (continued)

Grp no.	Spot no.	Grain .spot	^{238}U (ppm)	^{232}Th (ppm)	$^{232}Th/^{238}U$	f204 (%)	$^{238}U/^{206}Pb$ ±1σ	$^{207}Pb/^{206}Pb$ ±1σ	$^{238}U/^{206}Pb^*$ ±1σ	$^{207}Pb^*/^{206}Pb^*$ ±1σ	$^{238}U/^{206}Pb^*$ date (Ma) ±1σ	$^{207}Pb^*/^{206}Pb^*$ date (Ma) ±1σ	Disc (%)
3	71	58.1	47	26	0.57	0.102	2.060 ± 0.053	0.19358 ± 0.00166	2.062 ± 0.053	0.19268 ± 0.00170	2549 ± 54	2765 ± 15	7.8
3	69	56.1	115	47	0.42	0.036	1.985 ± 0.034	0.19751 ± 0.00623	1.986 ± 0.034	0.19719 ± 0.00624	2629 ± 37	2803 ± 52	6.2
3	25	24.1	137	101	0.76	0.008	1.756 ± 0.029	0.21282 ± 0.00073	1.756 ± 0.029	0.21274 ± 0.00074	2906 ± 38	2927 ± 6	0.7
3	24	23.1	44	15	0.36	–0.008	1.698 ± 0.063	0.25582 ± 0.00513	1.698 ± 0.063	0.25590 ± 0.00513	2985 ± 88	3222 ± 32	7.3
3	33	16.2	283	228	0.83	–0.002	1.578 ± 0.026	0.25806 ± 0.00100	1.578 ± 0.026	0.25808 ± 0.00100	3164 ± 41	3235 ± 6	2.2
3	64	51.1	317	239	0.78	0.002	1.477 ± 0.024	0.28528 ± 0.00088	1.477 ± 0.024	0.28526 ± 0.00088	3332 ± 42	3392 ± 5	1.8
4	10	10.1	627	27	0.04	0.075	4.740 ± 0.078	0.08118 ± 0.00025	4.743 ± 0.078	0.08054 ± 0.00033	1233 ± 18	1210 ± 8	–1.9
4	13	13.1	746	42	0.06	0.123	5.149 ± 0.082	0.08148 ± 0.00035	5.155 ± 0.082	0.08044 ± 0.00041	1143 ± 17	1208 ± 10	5.4
4	7	7.1	543	23	0.04	0.003	4.824 ± 0.077	0.08045 ± 0.00028	4.824 ± 0.077	0.08043 ± 0.00028	1214 ± 18	1207 ± 7	–0.6
4	45	32.1	477	45	0.10	0.048	4.901 ± 0.079	0.08082 ± 0.00045	4.903 ± 0.079	0.08042 ± 0.00047	1197 ± 18	1207 ± 12	0.9
4	42	29.1	485	21	0.04	0.084	5.035 ± 0.081	0.08112 ± 0.00032	5.040 ± 0.081	0.08041 ± 0.00040	1167 ± 17	1207 ± 10	3.3
4	8	8.1	602	33	0.06	0.140	4.897 ± 0.081	0.08149 ± 0.00026	4.904 ± 0.081	0.08030 ± 0.00036	1196 ± 18	1204 ± 9	0.7
4	39	26.1	449	21	0.05	0.139	5.041 ± 0.081	0.08141 ± 0.00033	5.048 ± 0.081	0.08023 ± 0.00046	1165 ± 17	1203 ± 11	3.1
4	1	1.1	495	22	0.05	0.127	4.922 ± 0.079	0.08112 ± 0.00031	4.928 ± 0.079	0.08005 ± 0.00040	1191 ± 17	1198 ± 10	0.6
4	21	21.1	517	17	0.03	0.294	5.065 ± 0.081	0.08245 ± 0.00048	5.080 ± 0.081	0.07997 ± 0.00059	1158 ± 17	1196 ± 15	3.1
4	38	25.1	447	18	0.04	0.010	4.930 ± 0.089	0.08002 ± 0.00064	4.931 ± 0.089	0.07994 ± 0.00065	1190 ± 20	1196 ± 16	0.4
4	22	22.1	477	25	0.05	0.050	4.971 ± 0.080	0.08015 ± 0.00029	4.974 ± 0.081	0.07973 ± 0.00035	1181 ± 17	1190 ± 9	0.8
4	43	30.1	408	16	0.04	0.048	4.834 ± 0.077	0.08010 ± 0.00034	4.837 ± 0.078	0.07969 ± 0.00044	1212 ± 18	1189 ± 11	–1.9
4	15	15.1	708	47	0.07	0.023	4.899 ± 0.079	0.07978 ± 0.00023	4.900 ± 0.079	0.07958 ± 0.00026	1197 ± 18	1187 ± 6	–0.9
4	11	11.1	693	22	0.03	0.025	5.168 ± 0.085	0.07963 ± 0.00028	5.170 ± 0.086	0.07941 ± 0.00033	1140 ± 17	1182 ± 8	3.6
4	14	14.1	446	34	0.08	0.043	5.049 ± 0.081	0.07973 ± 0.00029	5.051 ± 0.081	0.07936 ± 0.00038	1165 ± 17	1181 ± 9	1.4
4	9	9.1	477	18	0.04	0.098	5.352 ± 0.085	0.07991 ± 0.00030	5.357 ± 0.085	0.07908 ± 0.00038	1103 ± 16	1174 ± 10	6.0
5	3	3.1	461	17	0.04	0.206	4.740 ± 0.077	0.08482 ± 0.00043	4.750 ± 0.077	0.08308 ± 0.00056	1232 ± 18	1271 ± 13	3.1
D	32	15.2	313	74	0.24	–0.026	2.408 ± 0.040	0.12503 ± 0.01541	2.407 ± 0.040	0.12525 ± 0.01541	2240 ± 32	2032 ± 218	–10.2
D	48	35.1	265	58	0.23	–0.024	3.063 ± 0.051	0.12799 ± 0.00442	3.062 ± 0.051	0.12820 ± 0.00442	1822 ± 27	2073 ± 61	12.1
D	29	10.2	145	72	0.51	0.033	2.762 ± 0.047	0.14696 ± 0.00739	2.763 ± 0.047	0.14667 ± 0.00739	1991 ± 29	2307 ± 87	13.7
D	51	38.1	101	88	0.90	0.371	2.311 ± 0.040	0.18841 ± 0.00113	2.320 ± 0.040	0.18510 ± 0.00134	2311 ± 34	2699 ± 12	14.4
D	72	59.1	255	87	0.35	0.048	3.054 ± 0.050	0.13802 ± 0.00321	3.055 ± 0.050	0.13759 ± 0.00322	1825 ± 26	2197 ± 41	16.9
D	59	46.1	197	65	0.34	0.047	3.019 ± 0.050	0.14245 ± 0.00358	3.021 ± 0.050	0.14204 ± 0.00359	1843 ± 27	2252 ± 44	18.2
D	60	47.1	141	83	0.61	0.017	2.018 ± 0.035	0.28703 ± 0.02226	2.018 ± 0.035	0.28688 ± 0.02226	2594 ± 37	3401 ± 121	23.7
D	17	17.1	390	62	0.16	–0.013	3.881 ± 0.062	0.12047 ± 0.00446	3.881 ± 0.062	0.12058 ± 0.00446	1478 ± 21	1965 ± 66	24.8

Table A13. Ion microprobe analytical results for zircons from sample 184125: orthopyroxene-bearing dioritic gneiss, Observatory Point

Grp no.	Spot no.	Grain .spot	^{238}U (ppm)	^{232}Th (ppm)	$^{232}Th/^{238}U$	f204 (%)	$^{238}U/^{206}Pb$ ±1σ	$^{207}Pb/^{206}Pb$ ±1σ	$^{238}U/^{206}Pb^*$ ±1σ	$^{207}Pb^*/^{206}Pb^*$ ±1σ	$^{238}U/^{206}Pb^*$ date (Ma) ±1σ	$^{207}Pb^*/^{206}Pb^*$ date (Ma) ±1σ	Disc (%)
1	3	3.1	138	73	0.55	–0.188	4.437 ± 0.071	0.08575 ± 0.00092	4.429 ± 0.071	0.08736 ± 0.00114	1312 ± 19	1368 ± 25	4.1
1	11	11.1	209	111	0.55	–0.113	4.361 ± 0.056	0.08619 ± 0.00072	4.356 ± 0.056	0.08715 ± 0.00093	1332 ± 16	1364 ± 21	2.3
1	8	8.1	130	66	0.53	–0.086	4.441 ± 0.062	0.08576 ± 0.00091	4.437 ± 0.062	0.08649 ± 0.00118	1310 ± 16	1349 ± 26	2.9
1	13	13.1	168	118	0.72	–0.001	4.492 ± 0.060	0.08615 ± 0.00081	4.492 ± 0.060	0.08616 ± 0.00081	1296 ± 16	1342 ± 18	3.4
1	17	17.1	170	87	0.53	0.021	4.479 ± 0.066	0.08614 ± 0.00081	4.480 ± 0.066	0.08596 ± 0.00086	1299 ± 17	1337 ± 19	2.9
1	16	16.1	193	162	0.87	–0.111	4.347 ± 0.057	0.08498 ± 0.00076	4.343 ± 0.057	0.08593 ± 0.00091	1336 ± 16	1337 ± 21	0.0
1	2	2.1	193	98	0.52	–0.082	4.348 ± 0.068	0.08518 ± 0.00078	4.345 ± 0.068	0.08588 ± 0.00088	1335 ± 19	1336 ± 20	0.0
1	10	10.1	188	95	0.52	–0.047	4.414 ± 0.058	0.08545 ± 0.00076	4.412 ± 0.058	0.08584 ± 0.00086	1317 ± 16	1335 ± 19	1.3
1	19	19.1	198	100	0.52	–0.049	4.362 ± 0.058	0.08537 ± 0.00080	4.360 ± 0.058	0.08579 ± 0.00085	1331 ± 16	1333 ± 19	0.2
1	14	14.1	148	74	0.51	0.215	4.485 ± 0.061	0.08697 ± 0.00086	4.495 ± 0.061	0.08514 ± 0.00127	1295 ± 16	1319 ± 29	1.8
1	25	25.1	154	79	0.53	–0.045	4.317 ± 0.058	0.08471 ± 0.00084	4.315 ± 0.058	0.08509 ± 0.00094	1344 ± 16	1318 ± 21	–2.0
1	40	40.1	168	84	0.51	0.065	4.388 ± 0.058	0.08558 ± 0.00102	4.391 ± 0.059	0.08502 ± 0.00112	1323 ± 16	1316 ± 25	–0.5
1	34	34.1	180	99	0.57	0.086	4.420 ± 0.071	0.08570 ± 0.00117	4.424 ± 0.071	0.08497 ± 0.00126	1314 ± 19	1315 ± 29	0.1
1	7	7.1	133	69	0.54	0.095	4.473 ± 0.084	0.08575 ± 0.00093	4.478 ± 0.084	0.08494 ± 0.00105	1299 ± 22	1314 ± 24	1.1
1	20	20.1	161	79	0.51	0.026	4.361 ± 0.058	0.08478 ± 0.00081	4.362 ± 0.058	0.08456 ± 0.00084	1330 ± 16	1306 ± 19	–1.9
1	35	35.1	158	84	0.55	0.134	4.430 ± 0.060	0.08549 ± 0.00084	4.436 ± 0.060	0.08434 ± 0.00102	1310 ± 16	1300 ± 23	–0.8
1	38	38.1	237	182	0.79	0.039	4.517 ± 0.058	0.08458 ± 0.00075	4.519 ± 0.058	0.08425 ± 0.00100	1289 ± 15	1298 ± 23	0.7
1	9	9.1	123	55	0.46	–0.012	4.377 ± 0.061	0.08390 ± 0.00092	4.377 ± 0.061	0.08401 ± 0.00092	1327 ± 17	1293 ± 21	–2.6
1	12	12.1	263	165	0.65	0.074	4.461 ± 0.059	0.08457 ± 0.00064	4.464 ± 0.059	0.08394 ± 0.00075	1303 ± 16	1291 ± 17	–0.9
1	1	1.1	198	107	0.56	0.240	4.348 ± 0.061	0.08556 ± 0.00090	4.359 ± 0.061	0.08353 ± 0.00142	1332 ± 17	1282 ± 33	–3.9
1	33	33.1	132	62	0.49	0.216	4.401 ± 0.064	0.08487 ± 0.00155	4.410 ± 0.064	0.08303 ± 0.00178	1317 ± 17	1270 ± 42	–3.7
1	21	21.1	191	110	0.59	0.282	4.528 ± 0.059	0.08497 ± 0.00076	4.541 ± 0.060	0.08258 ± 0.00135	1283 ± 15	1259 ± 32	–1.9
2	4	4.1	899	156	0.18	–0.010	4.973 ± 0.059	0.08027 ± 0.00035	4.973 ± 0.059	0.08035 ± 0.00036	1181 ± 13	1206 ± 9	2.0
2	44	43.1	2091	46	0.02	0.165	4.881 ± 0.056	0.08165 ± 0.00032	4.889 ± 0.056	0.08026 ± 0.00040	1200 ± 13	1203 ± 10	0.3
2	26	26.1	2524	128	0.05	0.008	4.828 ± 0.055	0.08021 ± 0.00021	4.828 ± 0.055	0.08014 ± 0.00022	1213 ± 13	1200 ± 5	–1.1
2	15	15.1	1013	197	0.20	0.031	4.957 ± 0.058	0.08038 ± 0.00033	4.959 ± 0.058	0.08012 ± 0.00034	1184 ± 13	1200 ± 8	1.3
2	27	27.1	1634	141	0.09	–0.016	4.940 ± 0.058	0.07995 ± 0.00026	4.939 ± 0.058	0.08008 ± 0.00028	1189 ± 13	1199 ± 7	0.9
2	28	28.1	1366	249	0.19	–0.003	5.010 ± 0.058	0.08002 ± 0.00029	5.010 ± 0.058	0.08005 ± 0.00029	1173 ± 12	1198 ± 7	2.1
2	23	23.1	748	138	0.19	–0.002	4.959 ± 0.070	0.07999 ± 0.00039	4.959 ± 0.070	0.08000 ± 0.00039	1184 ± 15	1197 ± 10	1.1
2	22	22.1	2224	102	0.05	0.047	4.952 ± 0.057	0.08040 ± 0.00024	4.954 ± 0.057	0.08000 ± 0.00027	1185 ± 12	1197 ± 7	1.0
2	6	6.1	1721	183	0.11	0.088	5.169 ± 0.060	0.08053 ± 0.00025	5.174 ± 0.060	0.07979 ± 0.00030	1139 ± 12	1192 ± 7	4.4
2	29	29.1	1476	234	0.16	–0.013	4.950 ± 0.057	0.07944 ± 0.00027	4.950 ± 0.057	0.07955 ± 0.00028	1186 ± 13	1186 ± 7	0.0
2	41	41.1	1034	181	0.18	0.048	4.969 ± 0.065	0.07991 ± 0.00035	4.971 ± 0.065	0.07950 ± 0.00039	1182 ± 14	1185 ± 10	0.3
2	37	37.1	1230	202	0.17	0.012	4.995 ± 0.058	0.07949 ± 0.00030	4.996 ± 0.058	0.07938 ± 0.00031	1176 ± 13	1182 ± 8	0.5
2	39	39.1	538	168	0.32	0.076	4.997 ± 0.060	0.07977 ± 0.00045	5.001 ± 0.060	0.07913 ± 0.00049	1175 ± 13	1175 ± 12	0.0
3	43	42.1	1195	201	0.17	0.012	5.139 ± 0.063	0.07904 ± 0.00033	5.140 ± 0.063	0.07894 ± 0.00034	1146 ± 13	1171 ± 8	2.1
3	24	24.1	1761	210	0.12	0.069	5.314 ± 0.064	0.07940 ± 0.00027	5.317 ± 0.064	0.07881 ± 0.00032	1111 ± 12	1167 ± 8	4.8
3	36	36.1	1570	132	0.09	0.025	4.935 ± 0.057	0.07902 ± 0.00027	4.937 ± 0.057	0.07880 ± 0.00029	1189 ± 13	1167 ± 7	–1.9
3	5	5.1	1518	232	0.16	0.042	5.071 ± 0.059	0.07908 ± 0.00027	5.073 ± 0.059	0.07873 ± 0.00032	1160 ± 12	1165 ± 8	0.5
3	32	32.1	870	141	0.17	0.059	4.972 ± 0.058	0.07899 ± 0.00036	4.975 ± 0.058	0.07849 ± 0.00042	1181 ± 13	1159 ± 11	–1.8
D	18	18.1	82	38	0.47	0.220	4.321 ± 0.065	0.08395 ± 0.00112	4.331 ± 0.066	0.08208 ± 0.00196	1339 ± 18	1248 ± 47	–7.4
D	42	41.2	301	21	0.07	0.444	5.480 ± 0.069	0.08279 ± 0.00112	5.504 ± 0.070	0.07904 ± 0.00146	1076 ± 13	1173 ± 37	8.3
D	31	31.1	2138	188	0.09	0.139	6.021 ± 0.069	0.07793 ± 0.00033	6.030 ± 0.070	0.07676 ± 0.00039	989 ± 11	1115 ± 10	11.3
D	30	30.1	2123	328	0.16	0.189	7.130 ± 0.082	0.07417 ± 0.00026	7.144 ± 0.083	0.07259 ± 0.00038	845 ± 9	1003 ± 10	15.8

RECORD 2009/10

INTERPRETED BEDROCK GEOLOGY OF THE SOUTH YILGARN AND CENTRAL ALBANY–FRASER OROGEN, WESTERN AUSTRALIA

SPAGGIARI ET AL.

This Record is published in digital format (PDF) and is available online at:
www.dmp.wa.gov.au/GSWApublications.
Laser-printed copies can be ordered from the Information Centre for the cost of printing and binding.

Further details of geological publications and maps produced by the Geological Survey of Western Australia can be obtained by contacting:

Information Centre
Department of Mines and Petroleum
100 Plain Street
EAST PERTH, WESTERN AUSTRALIA 6004
Phone: (08) 9222 3459 Fax: (08) 9222 3444
www.dmp.wa.gov.au/GSWApublications